Industrial Ni-Based Catalyst Development for Carbon Dioxide Reforming of Methane

A Thesis Submitted to the College of

Graduate and Postdoctoral Studies

in Partial Fulfilment of the Requirements for

the Degree of Doctor of Philosophy in the

Department of Chemical and Biological Engineering

University of Saskatchewan

Saskatoon, Saskatchewan

By

Mohsen Shakouri

Permission to Use

In presenting this thesis in partial fulfillment of the requirements for a Doctor of Philosophy Degree from the University of Saskatchewan, I agree that the libraries of this University may make this thesis freely available for inspection. I further agree that permission for copying of this thesis in any manner, in whole or in part, for scholarly purpose may be granted by the professors who supervised my thesis work or, in their absence, by the Head of the Department or the Dean of the College of Graduate Research and Studies in which the thesis work was complete. It is understood that any copying or publication or use of this thesis or parts thereof for financial gain shall not be allowed without my written permission. It is also understood that due recognition shall be given to me and to the University of Saskatchewan in any scholarly use which may be made of any material in my thesis.

Requests for permission to copy or to make other use of material in this thesis in whole or parts shall be addressed to:

Head
Department of Chemical and Biological Engineering
University of Saskatchewan
Saskatoon, Saskatchewan
S7N 5A9, Canada
or
Dean
College of Graduate and Postdoctoral Studies
University of Saskatchewan
116 Thorvaldson Building, 110 Science Place
Saskatoon, Saskatchewan
S7N 5C9, Canada

Abstract

This research work was conducted in three main phases. In the first phase, Ni and Co monometallic and Ni-Co bimetallic catalysts were prepared by using both co-precipitation and impregnation methods. Cylindrical and spherical shaped catalysts were made using the Ni-Co bimetallic catalyst with and without the addition of Boehmite as the binding material. The shaped catalysts were comparably as strong as the commercial spherical alumina ones. The catalysts were also stable and active for carbon dioxide reforming of methane (CRM) reaction in the range of 800 to 900 °C. However, the mass transfer could limit the performance of the spherical catalyst for CRM reaction. Study showed that the external mass transfer limitation could be neglected at high superficial velocity. However, the internal mass transfer was still restricting the performance of the spherical catalyst. Temperature gradients within the spherical catalyst radius were negligible. In the second phase, performance of the Ni-Co bimetallic, Ni monometallic, Co monometallic, and Co-Op commercial catalysts in powder form for steam carbon dioxide reforming of methane (SCRM) reaction at 850 °C were evaluated with various biogas feed compositions. Steam content in the feed gas was the key factor affecting the catalytic performance. The Ni-Co bimetallic, Ni monometallic, and Co monometallic catalysts could not handle a biogas feed composition with more than 12, 15, and 6 mol% of steam content, respectively. The Ni-Co bimetallic catalyst was the most stable than the other evaluated catalysts in a certain range of the steam content. The Ni-Co catalyst and biogas feed 5, which contains about 33% of CH_4, 21.5 mol% of CO_2, 12 mol% of H_2O, 3.5 mol% of H_2 and 30 mol% of N_2, represent the best combination, not only to produce syngas with the desired H_2/CO ratio (1.8 to 2) but also to convert more than 70% of CO_2 of the biogas feed. In the third phase, to understand the sulfur poisoning mechanism, CRM reaction over Ni and Co catalysts in the presence of SO_2 was studied. CH_4 and CO_2 conversions increased and H_2 and CO along with the by-products of H_2S, elemental sulfur and water were produced as soon as SO_2 was added to the CRM feed. Mg-Al-O_x support plays a key role in the SO_2 poisoning period by providing additional active sites for methane dissociation. Ni, Co, and S K-edges XAS (X-ray Absorption Spectroscopy) of the catalysts showed that species such as sulfide (S^{2-}), sulfite (S^{4+}) and sulfate (S^{6+}) could be formed during the SO_2 poisoning. Produced H_2S during CRM in the presence of SO_2, is likely from the reaction between S^{2-} and H^+ intermediates on the catalysts' surface. When CH_4 also dissociated on the metallic sites or sulfur-support intermediates, hydrogen-intermediates reacted with sulfide to produce H_2S. Also, when CO_2 dissociated on the

support, the produced O-intermediate could have reacted with SO_2 to form sulfite or sulfate. Monometallic and bimetallic sites and catalyst preparation methods have different impacts on the poisoning mechanism. Co-containing catalysts facilitated sulfate formation while Ni-monometallic catalysts facilitated sulfide formation.

Acknowledgement

I would like to express my sincere appreciation to my supervisor, Dr. Hui Wang for his patience, guidance and encouragement during the research and writing of the thesis. His deep understanding of situation and providing financial support are greatly valued and highly appreciated.

I would like to extend my great gratitude to my advisory committee: Dr. Yongfeng Hu, Dr. Venkatesh Meda, Dr. Robert W.J. Scott, and Dr. Jafar Soltan at the University of Saskatchewan for compassion and coaching they have given me throughout my doctorate program. I believe their valuable advice and suggestions helped me to improve the quality of my work.

Furthermore, I would like to acknowledge the Natural Science and Engineering Research Council of Canada (NSERC), the Department of Chemical and Biological Engineering at the University of Saskatchewan, Greenfield Specialty Ethanol Inc., Government of Saskatchewan's Innovative & Opportunity Scholarship, Petroleum Technology Research Centre (PTRC) 10^{th} Anniversary Graduate Student Scholarship, and The Bruce J. Milne Memorial Graduate Student Award for the financial support.

I am also thankful to all the staff in the Department of Chemical and Biological Engineering. My special thanks goes to Ms. Kelly Bader, Mr. Richard Blondin, Ms. Paul Meghan, and Mr. RLee Prokopishyn for their support during my graduate study in this department. You are such wonderful and understandable personalities.

Many thanks to Soft X-ray Microcharacterization Beamline (SXRMB) staff at the Canadian Light Source: Dr. Yongfeng Hu., Ms. Aimee MacLennan, Mr. Qunfeng Xia, for their support and assistance during the X-ray Absorption Spectroscopy analysis and result interpretations.

My sincere thanks go to the other members of Dr. Wang's research group for their assistant and valuable advice at every stage of this work.

My special thanks also go to my lovely friends who supported me with endless love and words of encouragements during the adversity period of my life. Sarvenaz Amini, Parisa Ashtijoo, Farhad Fathieh, Sepehr Khatir, Amirhosein Rajabi, Mohsen Sanayei, and especially Homa

Mostaghimi. I appreciate you guys and value your support during the toughest time of my program. I love you all.

I must not forget to mention the most especial people in my life; my family. My beloved mother, father and sisters. Thank you all for your support and love.

Dedication

Every challenging work needs self efforts as well as guidance

of elders especially, who are very close to our heart.

This dissertation is dedicated:

To My Mum, Kobra Najafi, who I loved and cherished more than life itself (Rest in Peace Mum),

To My Dad, Behrouz Shakouri, for being a great source of motivation and inspiration,

To My Sisters, Mahboubeh and Mansoureh, who are the best sisters in the word,

And to My Sweet Niece, Niki.

Table of Contents

List of Tables

List of Figures

Nomenclature

$\langle R \rangle$	average reaction rate per unit catalyst particle volume, $mol/m^3/s$
A	Frequency constant or Arrhenius factor
b.c.c.	body-centered cubic
C_{AS}	concentration of reactant A at the external surface of catalyst, mol/m^3
C_{WP}	dimensionless Weisz-Prater
D	diameter of the specimen, mm or in
D_e	effective diffusivity, m^2/s
d_p	average catalyst particle diameter, m
DW	weight of samples put into the cell
E_0	edge energy of an element
E_a	apparent activation energy, J/mol
F	force necessary to crush the specimen, N or lb_f
f.c.c.	face-centered cubic
F_{in}, i	flow rate of component i in the reactor inlet, mL/min
F_{out}, i	flow rate of component i in the reactor outlet, mL/min
FW	weight percent fines
k	reaction rate constant
K-edge	binding energy in which the excitation of 1s electron of an element occurs
L	length or diameter of the specimen along the horizontal axis, mm or in
Me	metal
pH	power of hydrogen, a measure of acidity or basicity
PW	weight of fines after sieving
R	universal gas constant, 8.314 $Pa.m^3/mol/K$
r_A	reaction rate based on reactant or product A, mol g^{-1} s^{-1}
T_s	surface temperature of the catalyst particle, K
wt%	weight percent
x	crush strength for one specimen, N/mm or lb_f/mm
Xi	volume of component i / total volume
ΔH_r	reaction enthalpy, kJ/mol

λ_p thermal conductivity of catalyst particle, W/m/K

ρ_C catalyst density, g/m^3

σ_t splitting tensile strength, MPa or psi

Abbreviations

ASAP	Accelerated Surface Area and Porosimetry
ASTM	American Society for Testing and Materials
B	Boehmite
BCS	Bulk Crushing Strength
BET	Brunauer–Emmett–Teller
BJH	Barret-Joyner-Halenda
C	Ni-Co/AlMgO_x catalyst
CC	Co-precipitation Catalyst
CLS	Canadian Light Source
CRM	Carbon Dioxide Reforming of Methane
EXAFS	Extended X-ray Absorption Fine Structure
Ext	Extrudate/Cylindrical
FLY	Fluorescence Yield
GC	Gas Chromatograph
GHG	Greenhouse Gas
GHSV	Gas Hour Space Velocity
IC	Impregnation Catalyst
ICP-MS	Inductively Coupled Plasma Mass Spectroscopy
ID	Inner Diameter
IPCC	Intergovernmental Panel on Climate Change
LCF	Linear Combination Fitting
PFPD	Pulsed Flame Photometric Detector
PU	Polyurethane
RPM	Revolutions Per Minute
RWGS	Reverse Water Gas Shift
SCRM	Combined Steam and Carbon Dioxide Reforming of Methane
SD	Standard Deviation
SE	Standard Error
Sph	Spherical

SRM	Steam Reforming of Methane
SXRMB	Soft X-Ray Microcharacterization Beamline
TCD	Thermal Conductivity Detector
TEM	Transmission Electron Microscopy
TEY	Total Electron Yield
TOF	Turnover Frequency
TOS	Time on Stream
US	United States
WGS	Water Gas Shift
XANES	X-ray Absorption Near Edge Structure
XAS	X-ray Absorption Spectroscopy
XRD	X-ray Diffraction

CHAPTER 1

Introduction

1.1 Overview

With the industrial revolution around 1750's, demand for energy sources to sustain the industrial development have raised. This forces human beings to consume the fossil fuels as the most practical available energy sources. The sustained consumption of these carbon-based energy sources, especially during the last few decades, led to dramatic growth in emissions of greenhouse gases (GHGs) into the atmosphere. The increased concentrations of GHGs in the atmosphere accelerated the climate change on Earth. The National Oceanic and Atmospheric Administration (NOAA) reported that the average global land and ocean surface temperature for the period of January to April, 2017, was about 0.95 °C above the 20th century average of 13.7 °C (National Centers for Environmental Information: Global Climate Report, 2017). Carbon dioxide (CO_2) and methane (CH_4) are the most significant GHGs coming from human activities. As a result, research interest has been growing on CH_4 and CO_2 disposal, removal, and utilization to minimize the threat that these gases pose to our environmental security. Tribal Energy and Environmental Information Clearinghouse (TEEIC) reported three primary methods which have been used to reduce the amounts of CH_4 and CO_2 emissions to the atmosphere: (1) engaging energy efficiency and preservation practices (such as insulation upgrades, using high efficiency furnaces, etc.); (2) using carbon-free or reduced-carbon energy sources (solar power, wind power, nuclear power, biomass energy sources, etc.); and (3) carbon capture and sequestration (collection and storage of CO_2 in soil, underground, etc.). Consequently, there were several efforts to develop technologies to convert the GHGs to value-added products. Successful development of such technologies could

not only reduce the emission of GHGs but could also profit the industries from the value-added products.

The study of CO_2 reforming of CH_4 (CRM), also known as dry reforming of methane compared with steam reforming of methane (SRM), is important in the development of gas-to-liquid (GTL) fuel technology. CRM can convert both CH_4 and CO_2 into value-added product, a mixture containing hydrogen and carbon monoxide which is commonly known as synthesis gas or syngas, in locations where CO_2 and CH_4 coexist (Usman et al., 2015). The situations could include biogas from biomass or bio-waste degradation, cogeneration from the mixture of coal gasification gas and oven gas, low-grade natural gas reservoirs when carbon dioxide content is significant, and petroleum fields where methane is now flared. Moreover, CRM reaction provides a short-term CO_2 mitigation when the synthesized hydrocarbons are used for fuel again (Hu & Ruckemstein, 2004; Fan et al., 2009). The conversion of natural gas to transportable fuels such as gasoline, diesel, and methanol has also attracted much attention from both industrial and environmental players. Natural gas, which mainly contains CH_4, is in direct competition with oil and coal as a source of energy in many applications. Besides, some low grades of natural gas contain significant amounts of CO_2 as compared to its CH_4 content. CO_2 is also generated as a waste by-product in processes like fossil fuel combustion, synthesis fuels manufacturing, and chemical production plants. Considering all these sources, significant amounts of CO_2 and CH_4 are readily available to produce syngas using CRM technologies. Many liquid hydrocarbon fuels could be then synthesized from syngas through the catalytic Fischer–Tropsch process (reaction 1.1) by varying the H_2/CO ratio of the syngas in the feed. Thus, different individual methane reforming reactions (SRM, CRM, autothermal reforming of methane, etc.) or their combinations have been broadly studied to produce syngas with a desired H_2/CO ratio.

$$(2n+1)H_2 + nCO \rightleftharpoons C_nH_{(2n+2)} + nH_2O \text{ ; exothermic : } \Delta H^{\circ}_{298K} < 0 \qquad (1.1)$$

CRM, like other catalytic reactions, requires a stable, highly active, and product-selective catalyst. Despite the significant environmental potentials of CRM, it is not considered as a mature industrial process due to the lack of a stable catalyst. CRM catalysts could suffer from deactivation due to sintering, poisoning (such as sulfur sintering), metal oxidation, and most significantly, severe carbon deposition (Ashcroft et al., 1991; Bradford & Vannice, 1999; Rostrup-Nielsen, 1997; Slagtern, et al., 1997). Both noble and non-noble, metal-based catalysts have been studied

for CRM reaction (Ertl et al., 2008; Wang & Ziadi, 2013). Non-noble metals attract more attentions because of their competitive activity and availability. On the other hand, noble metals (Rh and Rd) show superiority in terms of resisting carbon deposition (Bradford et al., 1996, 1997; Wang & Ziadi, 2013). However, considering the high cost and restricted availability of the noble metals, scale-up towards commercialization is not economically feasible.

Our research group at the University of Saskatchewan has developed a Ni-Co/$AlMgO_x$ bimetallic catalyst with a Ni/Co ratio of one, prepared by co-precipitation method, which is highly active and stable for CRM reaction (Zhang et al., 2007, 2008, 2012). 2000 hours of time-on-stream (TOS) testing at bench-top scale at the University of Saskatchewan (0.05 g catalyst) and 500 hours TOS at pilot-plant scale at the Carbon Science Inc. facility (1 g catalyst) have shown that (a) the conversion of CO_2 and CH_4 is close to the equilibrium values, (b) the selectivity of H_2 and CO is between 90 and 100 %, and (c) the deactivation due to carbon formation and structural change is negligibly small. It is notable that the Ni-Co/$AlMgO_x$ bimetallic catalyst was awarded a patent in July 2011 as a catalyst for production of synthesis gas (US Patent 7,985,710). Carbon Science Inc. (Santa Barbara, USA) also acknowledged, in December 2010, a two-year worldwide exclusive licence agreement with the University of Saskatchewan for the Ni-Co bimetallic catalyst.

1.2 Motivation and Outline of the Work

Based on the best available knowledge about previous research on the Ni-Co catalyst (Gomez, 2016; Shakouri, 2012; Tian, 2013; Xi & Wang, 2009; Zhang, 2008), it has great potential for commercialization for industrial applications.

To make the Ni-Co catalyst ready for industrial use, a shaped catalyst made from the loose powder form is required. Moreover, Greenfield Specialty Ethanol Inc. (Ontario, Canada) has shown an interest in using the catalyst for industrial gas to liquid fuel (GFL) technology to produce methanol. In such a process, a synthesis gas with a H_2/CO ratio of 1.8 to 2 is required as a feedstock. A possible route to produce a syngas with such a composition is to perform both SRM and CRM reactions in a single reactor using a biogas feed that contains CO_2, CH_4, and steam to some extent. Furthermore, industrial feed-stocks may contain sulphur compounds, which can deactivate the reforming catalysts. Therefore, the work of this research comprises three major

phases: **Phase I** focuses on development of shaped catalysts and evaluation of their performance for CRM reaction. Mechanical strength of the shaped catalysts, instrumental characterizations that could aim to understand the relationships between influential factors and catalytic performance, and the effects of mass and heat transfer on catalytic performances were investigated in this phase as well. In **Phase II**, Ni-Co bimetallic, Ni monometallic and Co monometallic catalysts were prepared. Then their performances in various biogas feed compositions were compared with the performances of commercial catalysts. Based on the experimental results, the most effective catalyst as well as a possible biogas feed composition to produce a syngas with a H_2/CO ratio between 1.8 and 2 are suggested. **Phase III** addresses the effect of SO_2, introduced to the feed of CRM reaction, on the performance of Ni-Co bimetallic, Ni monometallic and Co monometallic catalysts. X-ray absorption spectroscopy (XAS) characterization technique, which could aim to understand the relationships between influential factors and catalytic performance in the presence of SO_2, were conducted.

1.3 Organization of Thesis

This thesis is organized in 8 chapters. Following this chapter, Chapter 2 presents relevant literature reviews for various catalytic methane-reforming reactions. It also includes different preparation methods and types of shaped catalysts for methane-reforming reactions. In addition, the knowledge gaps and objectives of this work are presented. Chapter 3 describes the experimental set-up and procedures, which were used for catalyst preparation and catalytic performance tasting. The material characterization techniques, which have been used in this research, are also highlighted in this chapter. Chapter 4 addresses the mechanical strength test, statistical analysis and characterization results of the prepared shaped catalysts. Chapter 5 includes the performance of the shaped catalysts for CRM reaction. The effects of mass and heat transfer on the catalytic performance of shaped catalysts for CRM are also presented. Chapter 6 contains the performance of different catalysts in various biogas feed compositions. Chapter 7 is devoted to the performance of different monometallic and bimetallic catalysts for CRM reaction in the presence of SO_2. Chapter 8 highlights major conclusions as well as recommendations and suggestions for future studies. References and Appendices are presented at the end of this thesis.

CHAPTER 2

Literature Review

2.1 Greenhouse Gas

Greenhouse gas (GHG) emissions are known as one of the major threats to the environment. A decrease of environmental sustainability and its impact on human lives has been a great concern in the past few decades. GHGs trap the heat in the Earth's atmosphere, which leads to warming the air inside the atmosphere and therefore an increase in global average temperature. Carbon dioxide (79%), methane (14%) and nitrous oxides (5%) are known as the main GHGs emitted by human activities (Intergovernmental Panel on Climate Change, 2014). In May 2017, Environment and Climate Change Canada reported the greenhouse gas emissions from the Canadian economic sector per year from 1990 to 2015. As shown in Figure 2.1 (a), the total of GHGs emitted in 2015, expressed as CO_2 equivalent, was as large as 722 megatons, while as late as 1990 it was 611 megatons. This growth was primarily driven by increased emissions from the oil and gas industries (76%) and transportation (42%). Moreover, over 100 nations have agreed on reduction of GHG emissions to limit the temperature increase of global warming to less than 2 °C (IPCC, 2014; United Nations, 2015). Figure 2.1 (b) also reveals that carbon dioxide and methane are the most significant GHGs coming from human activities. As a result, several actions and researches are underway in oil and gas processes, waste-water treatments, electricity production, agricultural industries, and many other areas to reduce the amount of CO_2 and CH_4 emissions (Solomon et al., 2009; Varga et al., 2015; Ma et al., 2017; Quiros et al., 2017). The research theme "Greenhouse Gas" yields about 4200 papers through the online database of published journal articles from January, 2000 to October, 2017 (www.sciencedirect.com). Figure 2.2 clearly reveals that research interests in reduction of GHGs have increased significantly during the past few years.

2.2 Synthesis Gas (Syngas)

Synthesis gas, also abbreviated as syngas, is the name given to a mixture of hydrogen and carbon monoxide because of its use as an intermediate in the production of synthetic natural gas. Syngas has been widely used as the main feedstock in fuel cells and many downstream processes including synthesis of ammonia and methanol, production of fuels through the Fischer–Tropsch (F–T) process, H_2 production, and as a source of power/heat for gas and steam turbines (Abatzoglou & Fauteux-Lefebvre, 2015; Lavoie, J. M., 2014). Many processes have been developed for syngas production with various H_2/CO ratios as shown in Table 2.1. On the other hand, conversion of natural gas, coal gas and shale gas to value-added products has been of great interest from both industrial and environmental point of views.

Since (a) CH_4 is the main component of natural gas, coal gas and shale gas, and (b) its chemistry has the potential for production of H_2 and CO in the presence of an oxidizing agent, therefore various reactions and processes have been studied to produce syngas from CH_4. Table 2.2 summarizes the most common methane-reforming reactions for syngas production such as (1) partial oxidization of methane; (2) steam reforming of methane (SRM); (3) carbon dioxide reforming of methane (CRM) also known as dry reforming; and (4) auto-thermal reforming of methane. The water gas shift (WGS) reaction is the major side reaction that could affect the ratio of H_2/CO produced from most of these methane-reforming reactions. Hypothetically speaking, in order to obtain a desired H_2/CO ratio, a combination of these reactions could be used. For instance, equimolar SRM and CRM reactions produce a theoretical H_2/CO ratio of 3 and 1, respectively. Thus, an equimolar combination of SRM and CRM reactions could possibly produce a syngas with H_2/CO ratio of 2.

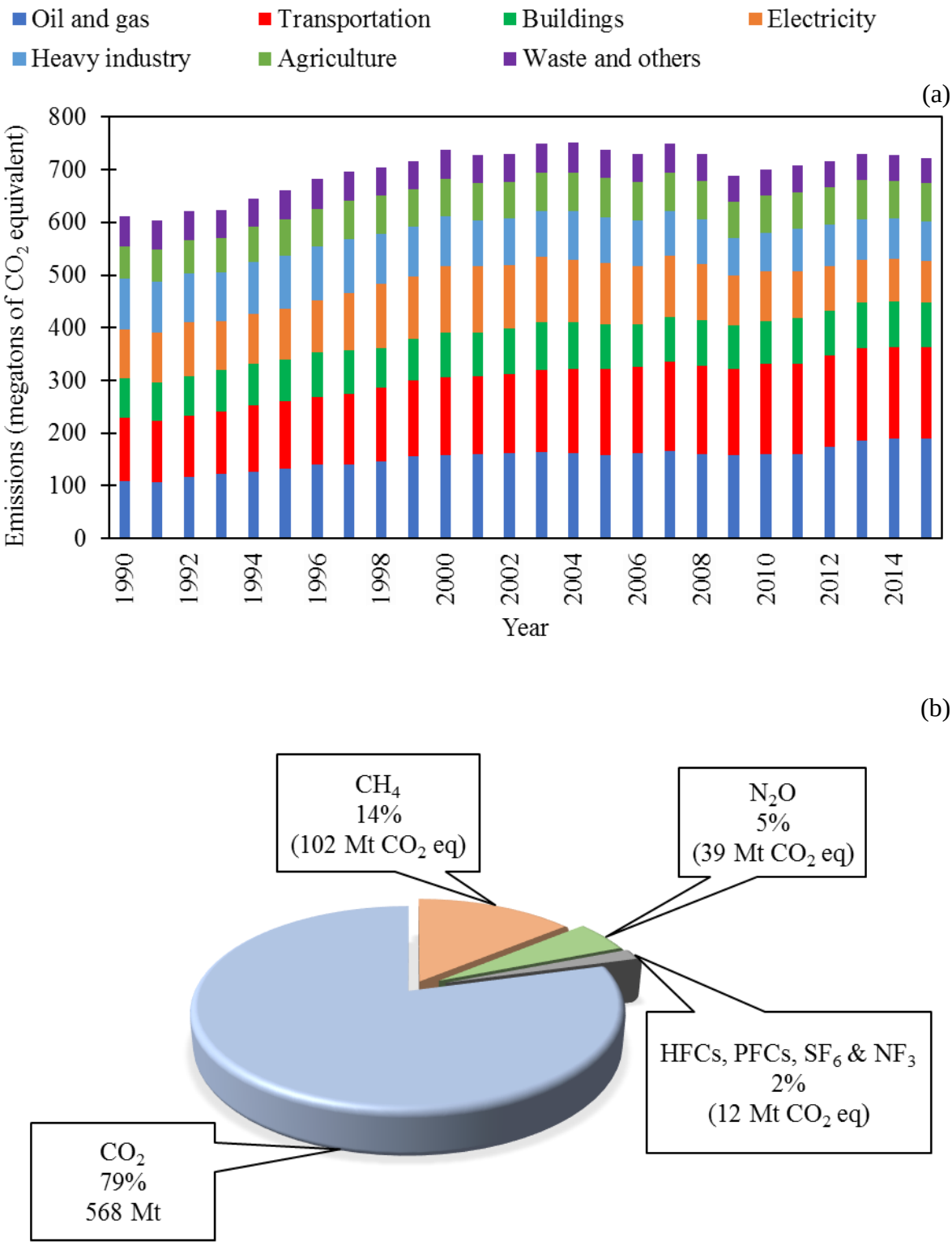

Figure 2.1 (a) Greenhous gas emissions by Canadian economic sector, 1990 to 2015. (b) Canada's emissions' breakdown by GHGs (2015). Source: Environment and Climate Change Canada (May, 2017), National Inventory Report 1190–2015

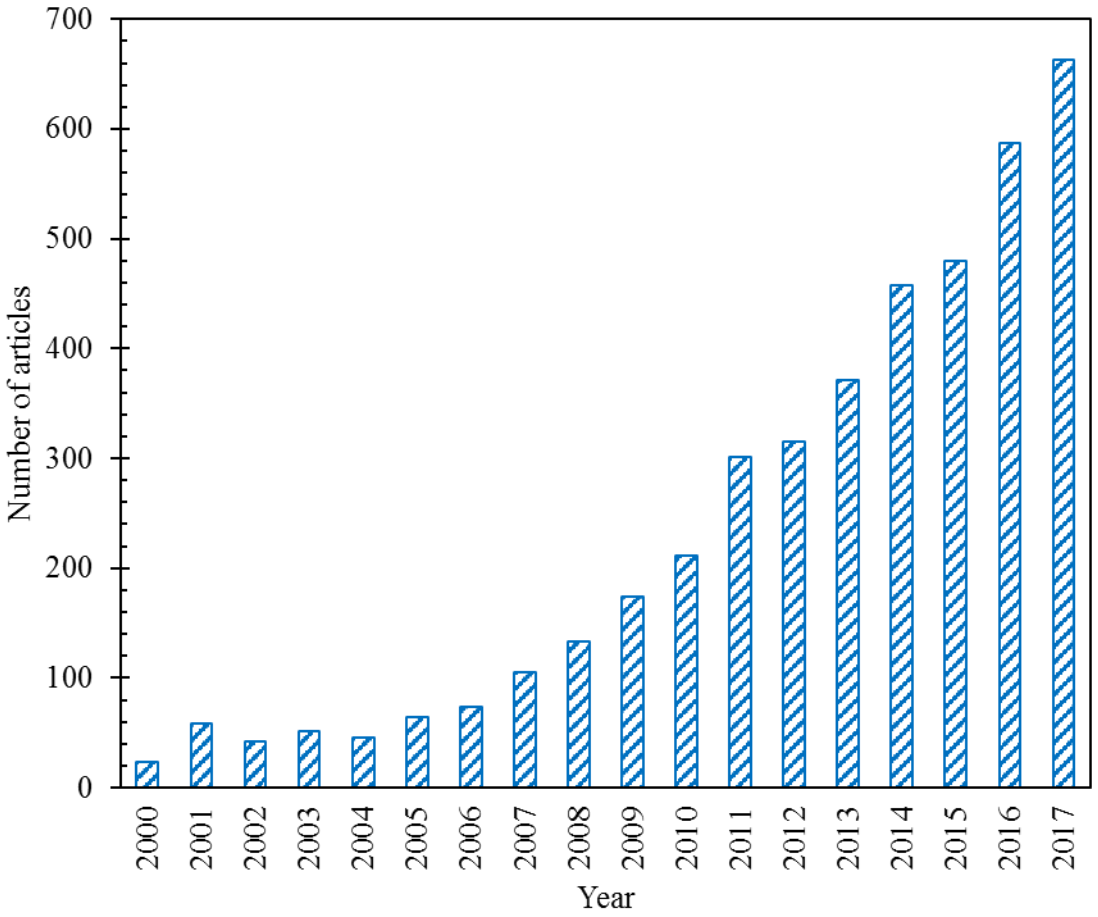

Figure 2.2 Statistical analysis on "Greenhouse Gas" as a keyword in research publications from January, 2000 to October, 2017 (www.sciencedirect.com)

Table 2.1 Typical applications of syngas in industrial processes

H_2/CO	Application
>3	Hydrogen, Ammonia production
2-2.5	High temperature Fischer−Tropsch (gasoline and light olefins)
1.7-2	Low temperature Fischer−Tropsch (Waxes or diesel)
1.5	Aldehydes, Isobutane, Isobutanol, Higher alcohols (C_1-C_6)
1	Acetic acid
<1	Polycarbonates

2.3 Synthesis Gas Production Processes via Reforming of Methane

Catalytic methane reforming reactions have been widely studied over the past decade. To enhance the hydrogen production and obtain a desired H_2/CO ratio in the syngas, many researchers investigated methane reforming reactions under various operating conditions (e.g. temperature, pressure, feed compositions, flow rates, etc.) using several types of catalysts and reactors (e.g. packed beds, fluidized beds, membrane reactors, etc.). A statistical analysis using "reforming of methane or reforming of CH_4" as the key phrase resulted in over 3200 manuscript titles available online at www.sciencedirect.com for the last decade alone. Figure 2.3 clearly reveals that research interests in methane reforming reactions have been greatly increased in recent years.

2.3.1 Steam Reforming of Methane (SRM)

SRM is the well-developed and dominant industrial process to produce hydrogen. Motay and Marechal in1868 developed a process for the conversion of hydrocarbons to hydrogen in the presence of steam and SRM was initially used in an industrial process in the 1930s (Adris et al., 1996). SRM is an endothermic reaction with $\Delta H°_{298K}$ of 206 kJ/mol at 101.3 kPa. Simultaneously, the water gas shift reaction (WGS) could occur between produced CO and unreacted steam ($\Delta H°_{298K}$ = -41 kJ/mol at 101.3 KPa). The reactions governing SRM and WGS are:

$$CH_4 + H_2O \rightleftharpoons CO + 3H_2 \text{ (SRM)} \quad (2.1)$$

$$CO + H_2O \rightleftharpoons CO_2 + H_2 \text{ (WGS)} \quad (2.2)$$

SRM reaction is an endothermic reaction, which makes it thermodynamically unfavourable at low temperatures. Equilibrium compositions for equimolar SRM reaction at various temperatures, calculated using the HSC Chemistry software, are shown in Figure 2.4 and clearly indicate that SRM is thermodynamically feasible at high temperatures (e.g.: 22% of steam and 11 % of CH_4 would be converted at 500 °C while the conversion of CH_4 and steam are about 85% and 87%, respectively, at 900 °C). Many researchers have investigated the influences of operating conditions and feed compositions on the equilibrium conversions and the equilibrium product compositions (Li et al., 2008; Tabrizi et al., 2015; Wang et al., 2014). A review by Barelli et al. (2008) summarizes that the typical operating temperatures and pressures for SRM reaction, to obtain a reasonable conversion of CH_4 and a H_2/CO ratio of 3, are in a range of 800–1000 °C and 14-20 bar. They also reported that at high temperatures the effect of WGS reaction would be minimal.

Table 2.2 Processes that produce syngas

Process	Reaction Equation	H_2/CO ratio	$\Delta H°_{298K}$ (kJ/mol)
Partial oxidation	$CH_4 + 0.5O_2 \rightleftharpoons CO + 2H_2$	2	-36
Steam reforming	$CH_4 + H_2O \rightleftharpoons CO + 3H_2$	>3	+206
Water gas shift	$CO + H_2O \rightleftharpoons CO_2 + H_2$		-41
Dry reforming	$CH_4 + CO_2 \rightleftharpoons 2CO + 2H_2$	<1	+247
Reversed water gas shift	$CO_2 + H_2 \rightleftharpoons CO + H_2O$		+41
Auto-thermal reforming	$CH_4 + 2O_2 \rightleftharpoons CO_2 + 2H_2O$	1 to 3	-802
	(Methane in excess)		
	$CH_4 + CO_2 \rightleftharpoons 2CO + 2H_2$		+247
	$CH_4 + H_2O \rightleftharpoons CO + 3H_2$		+206
	$CO + H_2O \rightleftharpoons CO_2 + H_2$		-41

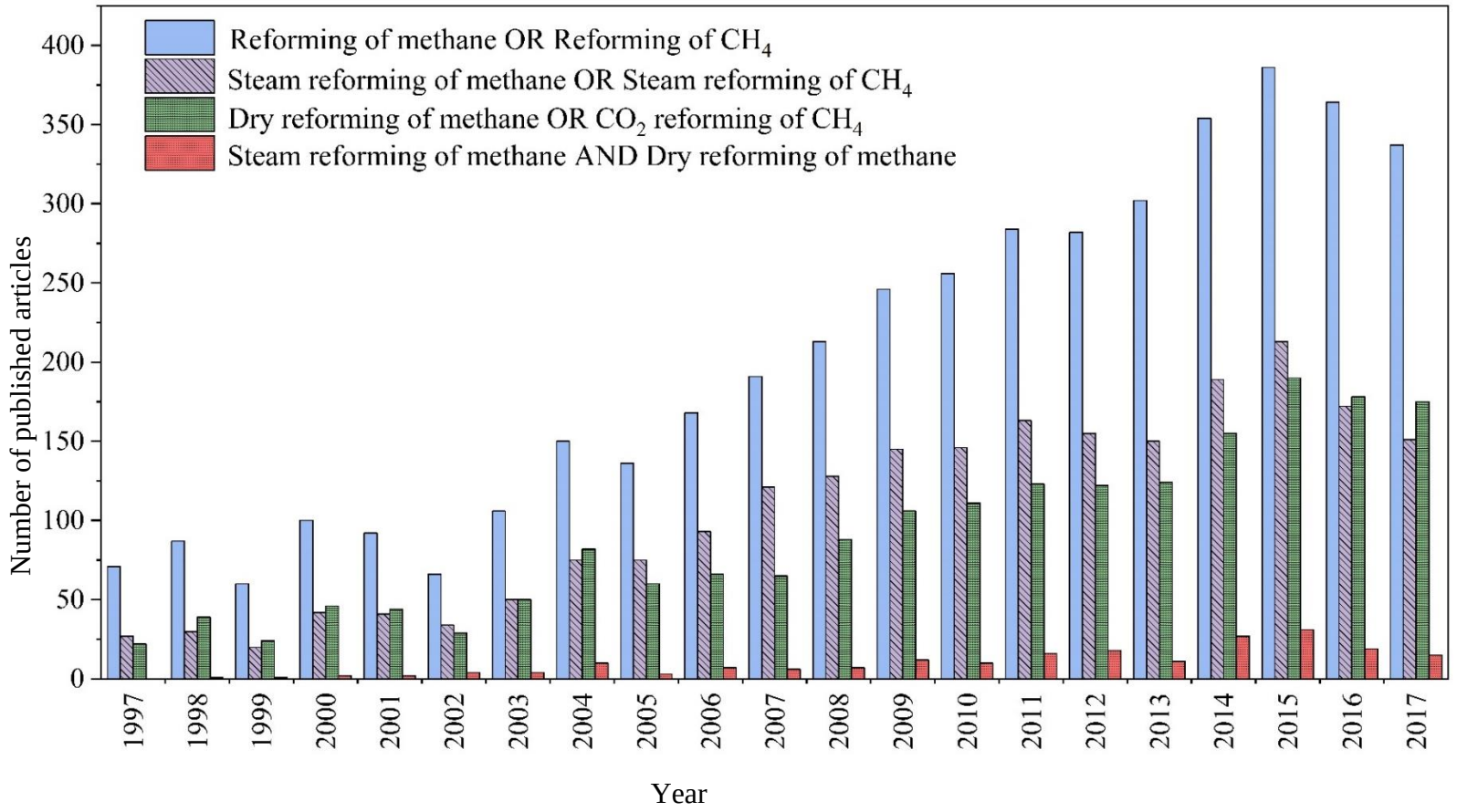

Figure 2.3 Statistical analysis on reforming of methane reactions in research publications from January, 2000 to October, 2017 (www.sciencedirect.com)

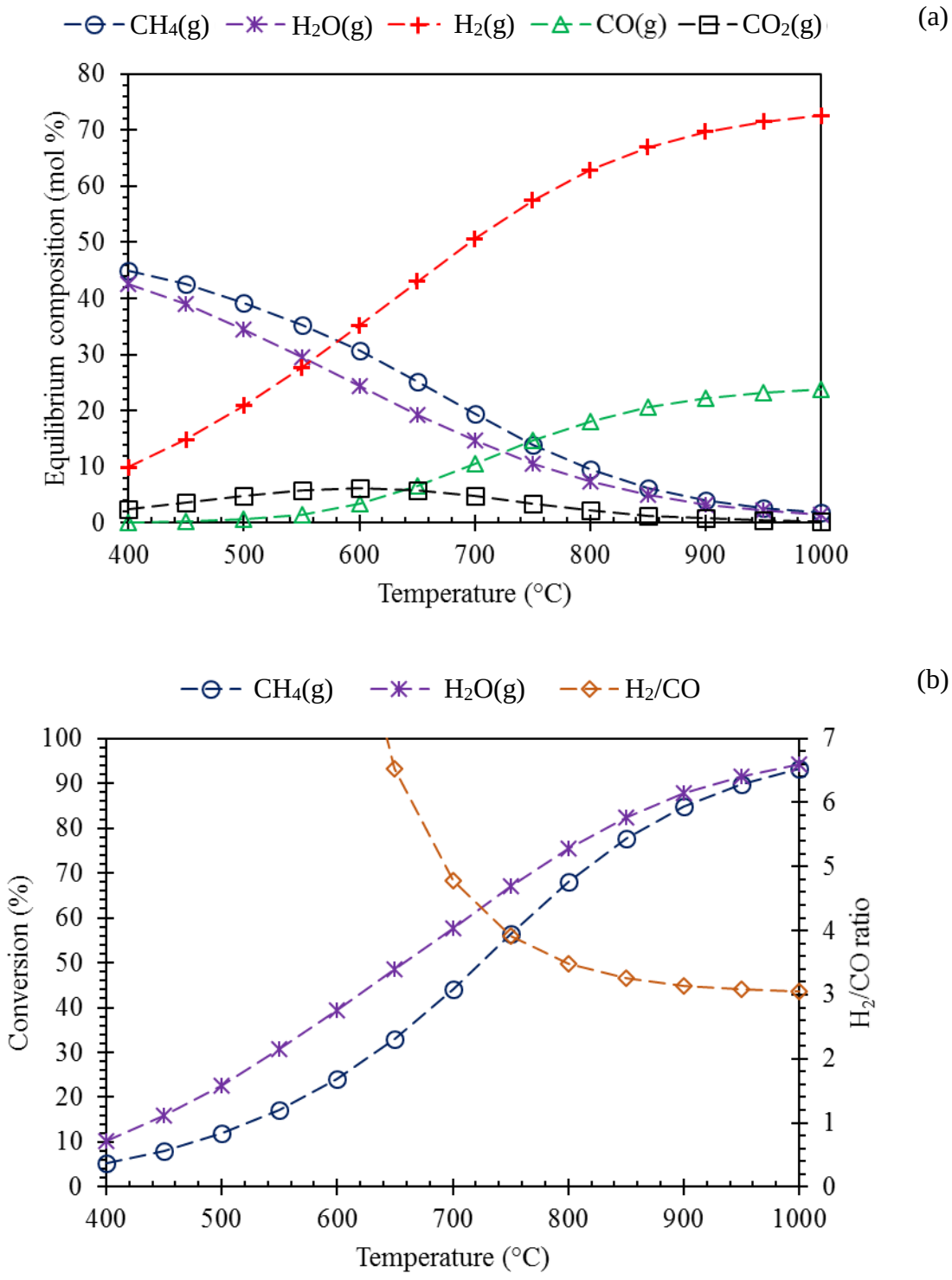

Figure 2.4 (a) Equilibrium compositions (mol %) and (b) theoretical reactant conversions as well as the H_2/CO ratio in the product gas for SRM reaction. Reaction conditions: 1 bar, equimolar reactants (CH_4 = H_2O), temperature range: 400–1000 °C

2.3.2 Carbon Dioxide Reforming of Methane (CRM)

Carbon dioxide reforming of methane (CRM) has attracted tremendous research interest in the last decade. The reaction is capable of converting the most environmentally problematic GHGs (CO_2 and CH_4) to a value-added product (syngas). The CRM reaction is an endothermic reaction with $\Delta H°_{298K}$ = 247 kJ/mol at 101.3 kPa. Concurrently, the reversed water gas shift reaction (RWGS) could occur between produced H_2 and unreacted CO_2 ($\Delta H°_{298K}$ = 41 kJ/mol at 101.3 KPa).

$$CH_4 + CO_2 \rightleftharpoons 2CO + 2H_2 \text{ (CRM)} \quad (2.3)$$

$$H_2 + CO_2 \rightleftharpoons CO + H_2O \text{ (RWGS)} \quad (2.4)$$

In the reaction environment, CRM together with RWGS advance toward the equilibrium conversions and equilibrium product compositions of the system. Figure 2.5 shows a preliminary equilibrium consideration for CRM reaction with an equimolar reactant ratio (CH_4 = CO_2) in a temperature range of 400–1000 °C. Figure 2.5 clearly reveals that, at low temperature, the thermodynamic barrier is unfavourable and obtaining a high conversion of CH_4 and CO_2 and a H_2/CO ratio of one is a challenging task. Comprehensive studies on the thermodynamic equilibrium compositions of CRM reaction at various operating conditions and feed compositions are found in many literatures (Aparicio et al., 2002; Zhang et al., 2008). Yaw and Saidina Amin (2005) reported that temperatures above 1000 K should be used to achieve a high conversion of CH_4 and CO_2. They also suggested using a feed with a CO_2/CH_4 ratio lower than one to minimize the effect of the RWGS reaction and therefore enhance the selectivity of H_2 production. Tsai and Wang (2008) studied CRM reaction in a temperature range of 500–1150 °C, and CO_2/CH_4 ratio in a range of 0.5 to 2. They found that a reaction temperature of 850 °C and a CO_2/CH_4 ratio of 0.8 were an optimum condition, thermodynamically favourable for a CRM reaction. Zhang et al. (2012) also found that CH_4 conversion and H_2 yield were enhanced and the effect of RWGS on CRM reaction was decreased at lower pressures. In summary, literature reviews show that at temperatures above 800 °C, the CRM reaction is thermodynamically more favourable and the effect of RWGS reaction would be minimal.

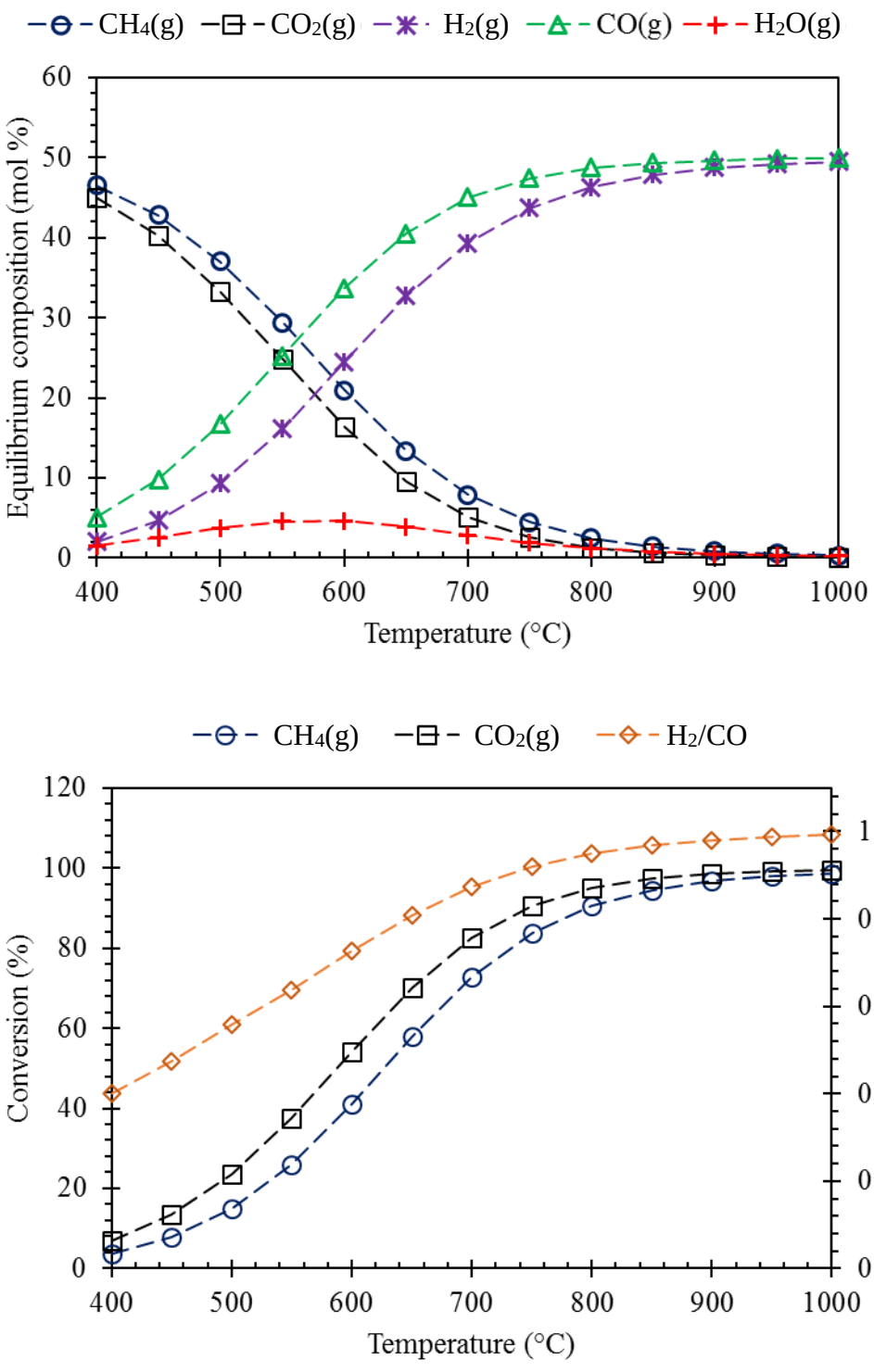

Figure 2.5 (a) Equilibrium compositions (mol %) and (b) theoretical reactant conversions as well as the H_2/CO ratio in the product gas for CRM reaction. Reaction conditions: 1 bar, equimolar reactants (CH_4 = CO_2), temperature range: 400–1000 °C

2.3.3 Combined Reforming of Methane Reactions

In recent years, there has been significant commercial interest in gas to liquid conversion's technologies, especially in methanol synthesis and the F–T process. Both processes desire a syngas feed with a H_2/CO ratio in a range of 1.8-2.2 (Froment, 2000). On the other hand, SRM is broadly commercialized as a traditional process of syngas production with H_2/CO >3 (Barelli et al., 2008; Twigg, 1989). The produced syngas from SRM could be modified with the produced syngas from other methane reforming reactions to obtain the desired H_2/CO ratio. Combination of partial oxidation of methane or auto thermal reforming of methane with steam reforming of methane have been widely investigated (Al-Nakoua & El-Naas, 2012; Tsang et al., 1995; York, et al., 2003; Zhu et al., 2004).

Amin and Yaw (2007) analyzed thermodynamic equilibrium in combined carbon dioxide and partial oxidation of methane. They reported that the optimum equilibrium conditions for CH_4: CO_2: O_2 were in a range of 1:0.8–1:0.1–0.2 and a minimum temperature of 1000 K. Li et al., (2008) also conducted a thermodynamic analysis of autothermal steam reforming of methane. They suggested that for a good reaction performance, a minimum temperature of 700 °C, O_2/CH_4 ratios > 0.4 and H_2O/CH_4 ratios> 1.2 would be required.Huang and T-Raissi (2007) performed a thermodynamic analysis on the equilibrium compositions of the autothermal steam reforming of methane reaction. The results show that a pressure of 1 atm, temperatures greater than 850 °C, and a CH_4: H_2O: O_2 ratio in the range of 1:1–2: 0.375 were the optimum conditions for steam autothermal steam reforming.

Simultaneous SRM and CRM, as a potential route for production of syngas with an adjustable H_2/CO ratio in a range of 1.8 to 2.2, has recently attracted great interest from both environmental and industrial stakeholders. From an environmental point of view, the reaction system could convert the most damaging carbon emission sources (CO_2 and CH_4). From an industrial perspective, the reaction has the potential to produce a syngas which is a suitable feedstock for methanol synthesis and F-T process. A few studies have been reported on the combined steam and carbon dioxide reforming of methane (SCRM) reaction. Demidov et al. (2011) used the Gibbs free energy minimization as a method to find the optimum condition for producing a syngas with a H_2/CO ratio in a range of 2.1–2.2 using combined steam and CO_2 reforming of methane. They reported that at various temperature and pressure conditions, the key

factor was the ratio of steam to CO_2 in the feed. They also found that to maintain the desired H_2/CO ratio, at higher temperatures, pressure should be increased as well. For example, using an identical feed composition, the desired H_2/CO ratio could be obtained at 800 °C and 5 atm while if the temperature rises to 900 °C, a pressure of 20 atm would then be required. Aydinoglu & Aksoylu (2010) analyzed the thermodynamic equilibrium of combined SRM and CRM to produce syngas. They found that with a feed composition of CH_4: CO_2: H_2O = 3:1:2 at 850 °C and 1 bar, a syngas with H_2/CO ratio of 1.94 could be obtained. He also reported that with an increase in pressure, both CH_4 and CO conversions as well as the H_2/CO ratio decreased.

2.4 Catalysts for CRM and SRM Reactions

Activation of methane molecules is a challenging task in methane reforming reactions. The main reason is the high CH_3–H(g) bond dissociation energy, which is about 439 kJ/mol (Enger et al., 2008; Lide, 2005). Therefore, heterogeneous catalysts are used to overcome the methane dissociation challenge. Researchers have developed several types of catalysts for CRM reaction using different preparation methods such as co-precipitation, wet impregnation, dry impregnation, and sol-gel methods (Wang & Zaidi, 2013). Transition, noble, and non-noble metals, as the active metal sites for methane dissociation, have been commonly used in the catalyst development for CRM reaction. On the other hand, aluminum oxide (alumina), silicon dioxide (silica), and rare earth oxides are the most common catalyst support materials in methane reforming catalysts (Abatzoglou & Fauteux-Lefebvre, 2016; Alvarez-Galvan et al., 2008; Usman et al., 2015).

Because of their low cost, availability and competitive activity, Ni-based catalysts have attracted tremendous research interest for methane reforming reactions. Published papers under keywords “Ni catalyst” and “reforming of methane” have increased from about 300 during 1997–2007 to over one thousand during 2007–2017. Table 2.3 reviews some of Ni-based catalysts which have been recently developed for methane reforming reaction. Despite considerable activity of Ni-based catalysts for these reactions, the major problem is carbon deposition which leads to a rapid catalyst deactivation. Noble metal catalysts have showed high activity, selectivity and resistance to coke deposition; however industrial use of these catalysts was not considered, because of their high cost and limited availability (Aramouni et al., 2018).

Table 2.3 Developed Ni-based catalysts for methane reforming reactions

Catalyst	Reference
Rh–Ni-MCM-41; Ni-MCM-41	Arbag et al., 2010
Rh–Ni/CeO_2–Al2O_3 catalysts	Ocsachoque et al., 2011
Au-Ni/$MgAl_2O_4$	Horvath et al., 2013
Ni/$La_{0.7}/Sr_{0.3}AlO_{3-\delta}$	Sugiura et al., 2013
Ni-Ce/SiO_2	Zhu et al., 2013
Ni-K/α-Al_2O_3	Borowiecki et al., 2014
Ni-Au-La/γAl_2O_3	Palma et al., 2014
Ni-Pr/Al_2O_3	Wang et al., 2014
Ni-Pt/γ-Al_2O_3/CeO_2	Wang et al., 2014
Ni-Me (Me = Au or Pt) /Al_2O_3-MO_x (M = Ce or Mg)	Wu et al., 2014
Ni-MO_x/Ni-foam (M = Al, Zr or Y)	Chai et al., 2015
Ni/SBA-15	Gil et al., 2015
Me/CeO_2 (Me = Rh, Pt, Ni)	Vita et al., 2015
Ni/CaO/ZrO_2	Wang et al., 2015
Ni/$CaFe_2O_4$	Anwar Hossain et al., 2016
NiMo_2C/Al_2O_3	Duan et al., 2016
Ni/$Y_2Zr_2O_7$	Fang, et al., 2016
$LaNi_xFe_{1-x}O_3$	Song et al., 2016
Ni/$Ce_{1-x}Pr_xO_{2-\delta}$	Vasiliades et al., 2016
Ni/$Ce_{0.95}M_{0.05}O_{2-d}$ (M = Zr, Pr, La)	Iglesias et al., 2017

Table 2.3 (*Continued*)

$Ni/Ce_{0.95}M_{0.05}O_{2-d}$ (M = Zr, Pr, La)	Iglesias et al., 2017
$Ni_X/Mg_{6-X}Al_2$	Dahdah et al., 2017
Carbon-Ni/MgO-Al_2O_3	Jin et al., 2017
$Ce_{0.70}La_{0.20}Ni_{0.10}O_2$	Pino et al., 2017
Ni/ZrO_2	Silveira et al., 2017
Ni-B/SBA-15	Siang et al., 2018

Although there are controversial arguments about the mechanism of carbon formation during catalytic methane reforming reactions, CH_4 decomposition (reaction 2.5), Boudouard reaction (reaction 2.6), and CO Reduction (reaction 2.7) are believed to be the main reasons (Bradford & Vannice, 1999).

$$CH_4(g) \rightleftharpoons C(s) + 2H_2(g) \quad (2.5)$$

$$2CO(g) \rightleftharpoons C(s) + CO_2(g) \quad (2.6)$$

$$CO(g) + H_2 \rightleftharpoons C(s) + H_2O \quad (2.7)$$

Reactions 2.5, 2.6, and 2.7 reveal that if the carbon-catalyst intermediates (C(s)) from methane dissociation do not react with either CO_2 or H_2O, carbon could stay on the catalyst's surface resulting in catalyst deactivation. Therefore, there have been tremendous research interests in modification of Ni-based catalysts to mitigate carbon formation. Both active metal sites and support materials have been subjected to modifications.

Heterogeneous catalysts could also lose their activity in the presence of poisonous gases. Sulfur compounds are the most common poisonous gases in industrial feeds which could deactivate Ni-based reforming catalysts. Sulfur atoms could adsorb strongly to the nickel surface, as shown in reaction 2.8. Consequently, these Ni sites will lose their ability to activate CH_4 molecules resulting in catalyst deactivations (Rostrup-Nielsen et al., 1984; 2004).

$$S + Ni_{surface} \rightleftharpoons Ni_{surface}{-}S \quad (2.8)$$

Sintering is another common challenge which could deactivate reforming catalysts. In heterogeneous catalysis, sintering is defined as a process where small catalyst particles grow in sizes. Literature declares that sintering of Ni-based becomes more sever at high temperature and high steam content in a feed. At theses conditions, Ni metal particles could grow larger and subsequently are more likely to be deactivated by carbon formation, oxidation or sulfur poisoning. Thus, it is essential to balance the steam content in the feed to avoid catalyst sintering (Morales-Cano et al., 2015; Sehested, 2006).

Wang and Zaidi (2013) precisely reviewed the published manuscripts on Ni-based catalyst modifications for CRM reaction from 2000 to 2010. They stated that due to its high surface area, alumina was most commonly used as the support material in development of Ni-based catalysts. They also reported that MgO, CaO, ZrO_2, and CeO_2 were used to modify the Ni-based alumina-supported catalysts. On the other hand, various metals such as Rh, Ru, Mo, Ca, Ce, Co, Cu have

been used as promoters to (a) improve the performance of both metal active sites and support of a catalyst and (b) enhance the resistance toward carbon formation.

2.5 Development of Ni-Co/$AlMgO_x$ catalyst for CRM in U of S

To begin development of a catalyst for CRM reaction in our research group, comprehensive analyses of thermodynamics, stoichiometry, and the reaction mechanism of CRM system together with literature reviews revealed that a good catalyst must have: (a) relatively high surface area, (b) thermal stability at elevated temperatures, (c) small and stable Ni sites, and (d) acceptable metal dispersion and strong support-metal interaction (Wang & Ziadi, 2013; Zhang et al., 2012). In addition, the availability and cost of the catalyst's components as well as the simplest preparation procedures were considered in selection of the materials. Considering these factors, Ni-Me/$AlMgO_x$ bimetallic catalysts (Me = Co, Fe, Cu, and Mn) were produced by the co-precipitation method from the corresponding nitrite solutions. The Ni-Co catalyst had not only a higher activity but also, because of its resistance to carbon deposition, a better stability compared to the other Ni-Me bimetallic catalysts (Me = Fe, Cu, and Mn). In addition, the Ni-Co catalyst had a higher surface area and lower pore diameter in contrast to the other Ni-Me bimetallic catalysts (Zhang et al., 2007). They found that the size of reduced metal sites was the key factor which could affect the catalyst resistance toward carbon formation. It was also reported that the reduced metal sites of smaller than 10 nm could improve the catalyst carbon resistant. To investigate the stability of the catalyst, the Ni-Co bimetallic catalyst (0.05 g) was reduced in a 20% H_2 and 80% N_2 mixture, and then CRM reaction was carried out for 2000 hours at 750 °C and GHSV of 110 L g^{-1} hr^{-1}. The results show competitive conversion of CH_4 and CO_2 to the equilibrium values, selectivity of 90 to 100% for H_2 and CO, and negligible carbon formation on the catalyst after the reaction (Zhang et al., 2007).

Shakouri (2012) investigated the effect of preparation method (co-precipitation and impregnation) and Ni/Co ratio of Ni-Co/$AlMgO_x$ bimetallic catalyst for CRM reaction. He found that due to the lack of metal-metal interactions in catalysts prepared by the impregnation method, the obtained Ni/Co and Al/Mg ratios were closer to the intended ratios as compared to the catalysts prepared by the co-precipitation method. He also found that the Ni-Co bimetallic catalyst, which was prepared by the co-precipitation method with a Ni/Co ratio of 0.6, facilitated CRM reaction

toward the theoretical values and showed the highest selectivity and lowest effect of side reaction (reverse water gas shift reaction). This catalyst was stable for CRM reaction at 710 °C near 1000 hr TOS with average CH_4 and CO_2 conversions of 80% and 88%, respectively. When the reaction temperature was raised to 760 °C, the catalyst activity was improved and was stable for about 550 hr TOS with CH_4 and CO_2 conversions of 92% and 95%, respectively. Moreover, an in-situ XAS (X-ray Absorption Spectroscopy) study on the reduced Ni-Co bimetallic, Ni monometallic and Co monometallic catalysts reveals higher reduction of Ni than Co, but there was a Ni-Co interaction in the bimetallic catalyst during the reduction process. Ni improved the Co reduction, but Co supressed Ni reduction. TEM images of the reduced catalysts also reveal a more uniform metal dispersion in the Ni-Co bimetallic catalyst (Wang et al., 2013).

Shakouri (2012) also studied the effect of the presence of 30 ppm H_2S on the performance of Ni monometallic, Co monometallic and Ni-Co bimetallic catalysts prepared with both co-precipitation and impregnation methods for CRM reaction. It was found that the catalysts with higher Ni than Co content showed better H_2S resistance regardless of the preparation method. Moreover, Ni-Co bimetallic impregnated catalysts were regenerated faster than the co-precipitated ones, due to the higher reduced metal content on the catalyst surface of the impregnated. In case of Ni monometallic catalysts, similar regeneration behaviour after H_2S poisoning was observed regardless of the preparation method.

2.6 Shaped Catalyst Preparation Methods

The literature review has reveled that significant efforts have been made to develop carbon resistant and active Ni-based catalysts for CRM reaction. These researches have yielded to excellent Ni-based catalysts that could facilitate a stable operation of CRM reaction and prevent carbon formation. However, there is still lack of an industrial catalyst which could be used in CO_2 reforming of CH_4 technology (Wang & Zaidi, 2013). To form a catalyst for industrial use, two major methods could be considered. One is randomly packing the powdered catalyst into forms such as pellets or extrudates of different shapes and geometries. An alternate method is making a structure from the powdered catalyst like ceramic foams, metallic foams or honeycomb-shaped monolithic structures (Liang et al., 2010; Tronconi et al., 2014; Twigg and Richardson, 1995). Figure 2.6 shows some examples of commercial catalysts with different shapes and geometries.

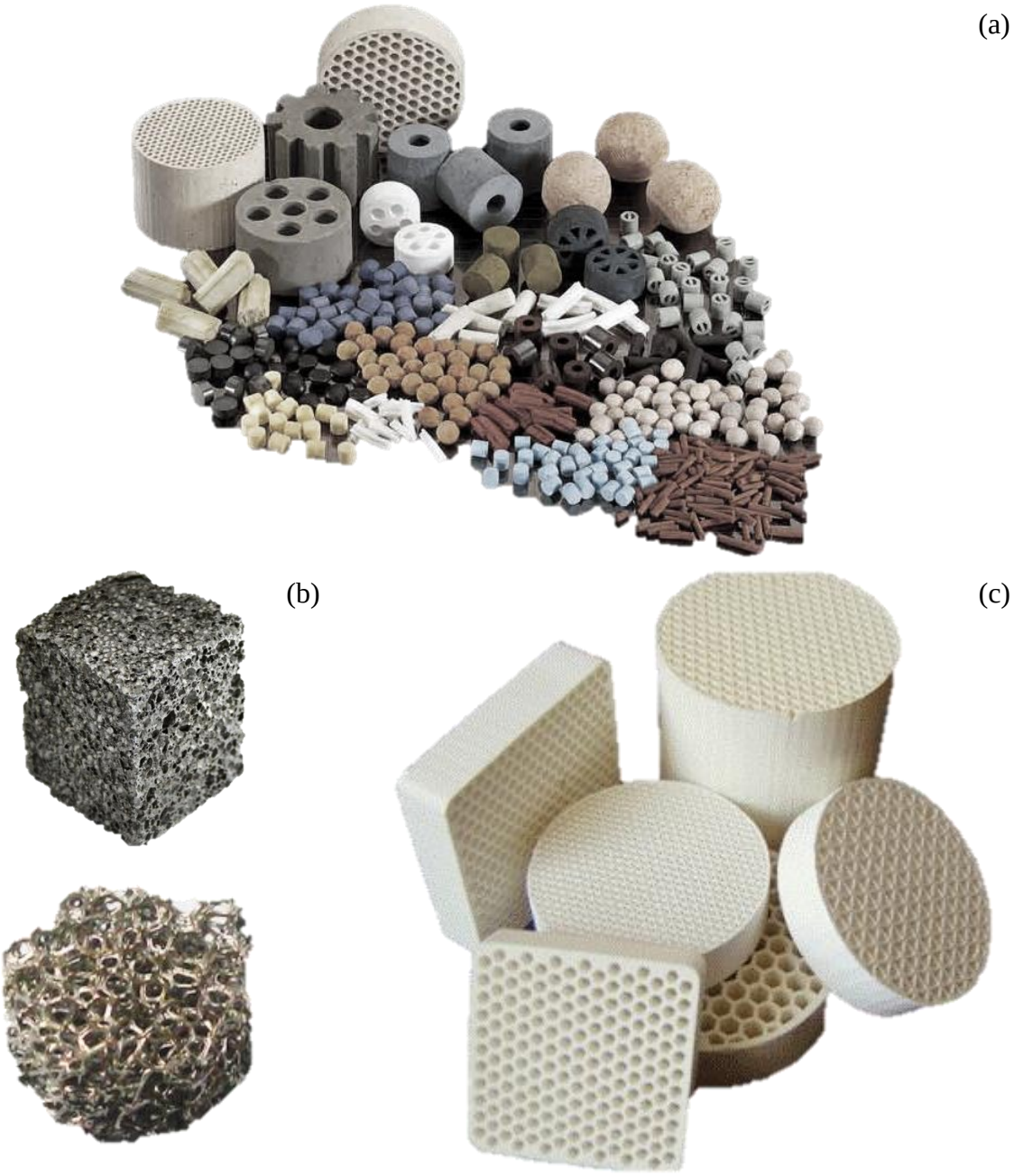

Figure 2.6 (a) Various commercial shaped catalysts (www.arabianoilandgas.com) (b) metallic foam structure (www.villainousvoodoo.com), and (c) monolithic structure (www.diytrade.com)

2.6.1 Impregnation Method Using the Commercial Support

A common method to make a shaped catalyst is to impregnate the metal part (active sites) of the catalyst on the surface of an available support (dry impregnation method). Tian (2013) used commercial BASF CSS-350 alumina spheres (BASF Catalyst LLC) as the support to make the spherical Ni-Co/$AlMgO_x$ bimetallic catalyst. The required amount of Ni, Co and Mg metallic solution was impregnated on the alumina balls followed by the calcination with various cycles. Liang et al. (2017) found that Ni-Co bimetallic catalyst, made by using 4 impregnation-calcination cycles, showed the best performance among the others for 160 hr TOS at 750°C. They also reported that the methane conversion dropped slightly from 66.7% at the beginning to 52.8% after the 160 hours. However, the performance of powdered catalyst was significantly higher than the spherical one for CRM reaction (Liang et al., 2017).

2.6.2 Pellets

The simplest way to make a shaped catalyst is to form pellets from the loose powder. The common procedure is to combine the powdered catalyst with binding material(s) and lubricants in a press to obtain a desired shape such as spheres, disks, rings, and cylinders. The key point in this process is to choose a proper binding material that (a) does not significantly affect the performance of the catalyst and (b) improves the mechanical resistance of the pellet. Pellets of various shapes and dimensions could be obtained with this method.

Jenness (1938) made disk shape pellets from Ni-base catalyst. He reported that the catalyst pellets made through this method are suitable for catalytic reaction in gaseous phase and high temperature. He also found that the fine powder catalyst should be mixed in a range of 40 to 60 wt% with the finely divided powder of a binder. Then the mixture was compressed, dried and finally calcined (600 – 800 °C) to obtain the catalyst pellet. Jenness also emphasized that calcination at high temperature caused the active metal oxide to diffuse into the particles of the binder and then form an alloy, which resulted in a porous and metallic skeleton structure. The presence of this alloy increased the mechanical strength of the catalyst pellet compared to its loose powdered form.

2.6.3 Structured Catalysts

Structured catalysts with different geometries could be made from various pre-shaped structures such as ceramic, metallic or monolithic substrates.

2.6.3.1 Ceramic Foams

Ceramic foams were developed to reduce the common disadvantages of using catalyst pellets for hydrocarbon reforming reactions: pressure drop and heat and mass transfer limitations. In addition, ceramic foams are known as materials with high temperature resistance, low bulk density and high porosity (Gibson and Ashby, 1988). Despite all the advantages, ceramic foams are relatively weak compared with other structures. These sponge-like porous structures are usually prepared from organic polymer precursors, such as polyurethane or polyolefins, which have porosity the same as the required final product (Lang et al., 1987. Twigg & Sengelow 1989).

Twigg & Richardson (1995) prepared a ceramic alumina foam as the support material to make Rh and Pt catalysts for steam reforming reaction. They initially filled the pores of organic precursor with a low viscosity aqueous slurry of alumina using wet impregnation method. The excess amount of slurry was removed by blowing air through the foam or by compressing it. The foams then dried at 100 °C and calcined at a temperature above 1000 °C. The high temperature calcination removed organic precursor through evaporation and combustion resulting in a ceramic copy of the plastic foam skeleton. Twigg & Richardson (1995) also suggested that alumina silicate, α-alumina, magnetite, haematite and calcium aluminate are examples of suitable ceramics for foam production which could be fabricated in different shapes and dimensions like cylinders, rings or rods.

Faure et al. (2010; 2011) developed foam-supported catalysts for industrial steam reforming processes. They prepared alumina ceramic foams as the catalyst support material using polyurethane (PU) precursors. PU precursors were immersed in an alumina slurry solution to coat the structure with layers of alumina and then left at room temperature in the presence of air to dry. The immersion and drying cycles were repeated to achieve the desired product. At this point the foams were calcined in two steps: The first step was to heat the foam up in order to remove the PU template; the second step was to calcine the alumina body. They reported that while the resulting

alumina ceramic foam had a structure like the PU precursor, its mechanical properties were weaker than the PU template.

2.6.3.2 Metallic Foams

Because of their uniform thermal dispersion, high thermal conductivity and remarkable mechanical strength, the metallic foam catalysts have recently attracted great interest. The metallic foams are porous metal structure and are classified in two types: closed cell, when the internal cell are not interconnected and open cell, when the internal pores are connected. Thus, a fluid could easily go trough open cell metallic foams. As the general procedure to make a metallic foam catalyst, a porous catalyst material should be wash−coated on the surface of the foam by using either sol-gel or wet impregnation (slurry) method. In the sol-gel method, the catalyst can be coated on the surface layer by layer to obtain the desired catalyst loading. In the wet-impregnation method, the metallic foams are dipped into the slurry solution of the desired catalyst. It is reported that the foam prepared with sol-gel method could develop a more uniform wash-coated layer of the catalyst than the ones prepared with wet-impregnation method (Liang et al., 2010; Zhao, 2012).

Park et al. (2014) prepared $Ni/Al_2O_3/Ni$ foam by wash-coating the $Ni\text{-}Al_2O_3$ powdered catalyst on Ni metallic foam. They reported that the $Ni/Al_2O_3/Ni$ foam had a good thermal stability compared with the commercial pellet catalysts. Also, the metallic foam catalyst could uniformly maintain the temperature distribution even at high space velocity values. Moreover, the catalyst showed a good activity and selectivity for steam-CO_2 reforming of methane with 99.7% and 44% conversions of CH_4 and CO_2, respectively, and a produced syngas with a H_2/CO ratio of 2.

2.6.3.3 Monolith Structure

In recent decades, an alternate way to make a shaped catalyst is using the monolith structure. Compared to the other catalyst forms (such as powders, pellets, foams, etc.), monolithic catalysts offer a lower ratio of pressure drop to a given geometric surface area. Consequently, the monolithic catalysts could be an excellent choice in industrial catalytic processes where large volumetric flow rate often have to be used. Although, fabrication of monolithic catalysts are more expensive than that of other shapes such as pellets or powders. The process of making these types

of catalysts is fairly similar to the procedure of making metallic foam catalyst. In this process, the desired support layers are usually wash-coated on the monolith structure followed by drying and calcination steps. Then, the active site will be uploaded onto the aforesaid structure by dipping the support into an aqueous solution containing the active metal precursor. Several cycles of immersion / drying / calcination could be repeated until the desired catalyst composition is obtained. There is a variety of different geometrics of monoliths available, which can be used to obtain the desired catalyst shape (Boger et al., 2004; Cybulski et al., 1994; Irandoust & Andersoon, 1988; Kapteijn et al., 2001).

Kohn et al. (2010) prepared an $Rh/\gamma Al_2O_3$ wash-coated monolith obtained from BASF Catalysts. The catalyst was used for both CO_2 reforming of CH_4 and autothermal reforming reactions using a compact quartz reactor, temperature range of 150 °C to 800 °C, a gas hour space velocity of 8000 hr^{-1}, and various CH_4:CO_2:O_2 ratios in the feed. They reported that (a) the pressure drop was not significant using the catalyst and (b) the catalyst achieved equilibrium conversions of CH_4 and CO_2 at the tested reaction conditions.

Vita et al. (2014) prepared 1.5 wt% Ru/γ-Al_2O_3 catalysts on commercial structured cordierite monoliths (obtained from Applied Ceramics Inc.) for methane oxy-steam reforming (OSR) reaction. For 80 hr TOS, the catalyst showed high conversion of CH_4 (98%) as well as absence of carbon deposition and by-product formation. They also found that the use of monolith structure catalyst aimed to improve the catalytic performance toward the OSR reaction, especially at high flow rates. Moreover, they reported that the prepared monolith catalyst offered a high surface area to volume ratio, good heat and mass transfer characteristics as well as a low pressure drop which could minimize the traditional problems associated with packed bed reactors.

2.7 Knowledge Gap and Objectives

Considering the high catalytic activity, stability, selectivity and more importantly the coke resistance of the developed Ni-Co/$AlMgO_x$ catalyst, it has an exciting potential for use in industrial CRM technologies. Therefore, in this study, shaped catalyst development from the loose powder form of Ni-Co/$AlMgO_x$ catalyst is investigated to move it forward to the commercialization and industrial applications. Furthermore, in industrial Gas to Liquid Fuel technology, synthesis gas with a H_2/CO ratio of 1.8 to 2 is required (Greenfield Specialty Ethanol Inc.). Therefore, the performance of the Ni and Co catalysts for a combination of CO_2 and steam reforming of methane should be investigated to find out whether production of a syngas with the desired ratio using the catalysts is feasible. Moreover, in industrial applications, methane from landfill or coal-delivered gas or natural gas may contain sulfur compounds, which can deactivate the reforming catalysts. Thus, the performance of Ni and Co catalysts for CRM reaction in the presence of sulfur compounds should also be studied.

To address the mentioned goals, the following objectives have been considered:

- Preparation of the shaped catalyst (cylindrical and spherical); investigation of the catalysts' mechanical strength as well as characterization of the catalysts.
- Performance of the shaped catalysts for CRM reaction and effects of mass and heat transfer limitations on performance of shaped catalysts.
- Performance of Ni and/or Co catalysts using various biogas feed compositions for combine steam reforming and dry reforming of methane reactions.
- To understand the sulfur poisoning mechanism, CRM reaction over Ni and Co catalysts for CRM in the presence of SO_2 is going to be explored in this work.

CHAPTER 3

Experimental Set-up and Procedure

This chapter includes the experimental set-ups and procedures used for catalyst preparation, characterization and performance tests.

3.1 Experimental Set-Up and Procedure for Catalyst Preparation

Ni-Co bimetallic, Ni monometallic and Co monometallic catalysts were prepared using co-precipitation and impregnation procedures. Then, the powdered catalysts were used for shaped catalyst preparation.

3.1.1 Powder Form Catalyst Preparation

The powdered Ni and/or Co catalysts supported by $AlMgO_x$ were synthesized by both co-precipitation and impregnation methods. In the co-precipitation method, the following steps were used to synthesize the catalysts in our laboratory:

1- **Solution preparation:** The solution containing various metal salts was prepared through dissolving of metal nitrite precursors using de-ionized water. Nickel (II) nitrate hexahydrate (98 to 102% purity; Alfa Aesar), cobalt (II) nitrate hexahydrate (98 to 102% purity; Alfa Aesar), magnesium nitrate hexahydrate (98 to 102% purity; Alfa Aesar) and aluminum nitrate nonahydrate (98 to 102% purity; Alfa Aesar) were used as the metal precursors. The selection of metals and their amount were varied depending on the desired catalyst composition.

2- Precipitation: The precipitation of metal was made through adjusting the pH value of the solution to 8.5-8.7 by adding the ammonium hydroxide (28 to 30 w/w%; Fisherbrand) as the precipitating reagent. The precipitation set-up is shown in Figure 3.1.

3- **Filtration and washing:** A Buchner vacuum filtration unit was used to remove most of the unwanted ions and water. Then, the filtrate cake was washed to remove unwanted ions at room temperature until the pH value of the washing flow reached 7.

4- **Drying:** Since the precipitated cake held a significant amount of water, it was dried at 120 °C overnight to remove the water.

5- **Calcination:** This step is known as one of the most important pre-treatment steps in catalyst preparations. A high temperature calcination process could generate strong interaction between metals and support material leading to formation of stable catalysts (Somorjai, 1994). Also, catalyst calcination at a temperature slightly higher than the reaction temperature is a common practice in catalyst preparation. Thus, the catalysts were calcined at 850 °C for 6 hours.

6- **Sieving:** The calcined catalyst was ground and sieved to obtain the desired size (between No. 45 and 60 US sieve sizes).

In the impregnation method, which is also called the dry impregnation method, the $AlMgO_x$ support was prepared by a co-precipitation procedure, and then the metal solution was added to it. Several ways are available to find the appropriate amount of metal solution to be added to the support to obtain the desired catalyst. In this research, the required volume of the metal solution was determined to correspond to that beyond which catalyst support starts to look wet. To determine the solution volume, de-ionized water was added to the support (particle size between No. 45 and 60 US sieve sizes) until the first drop of water appeared on its surface indicting the catalyst support was saturated. This condition was indicative of the amount of metal solution required by the support. As an example, for each gram of prepared support 1.2 mL of de-ionized water was added. Based on the desired metal (Ni and/or Co) content in the catalyst, the metal solution was prepared and sprayed onto the surface of the prepared support. The mixtures were then dried and calcined to obtain the desired catalyst.

Ni and Co monometallic and Ni-Co bimetallic catalysts were prepared using both co-precipitation and impregnation methods as summarized in Table 3.1.

Table 3.1 Names and descriptions of prepared loose powder catalysts.

Name	Preparation Method	Description
CC-Co6	Co-precipitation	Cobalt monometallic
CC-Ni2Co4		Nickel-Cobalt bimetallic
CC-Ni4		Nickel monometallic
IC-Co5	Impregnation	Cobalt monometallic
IC-Ni2Co3		Nickel-Cobalt bimetallic
IC-Ni5		Nickel monometallic

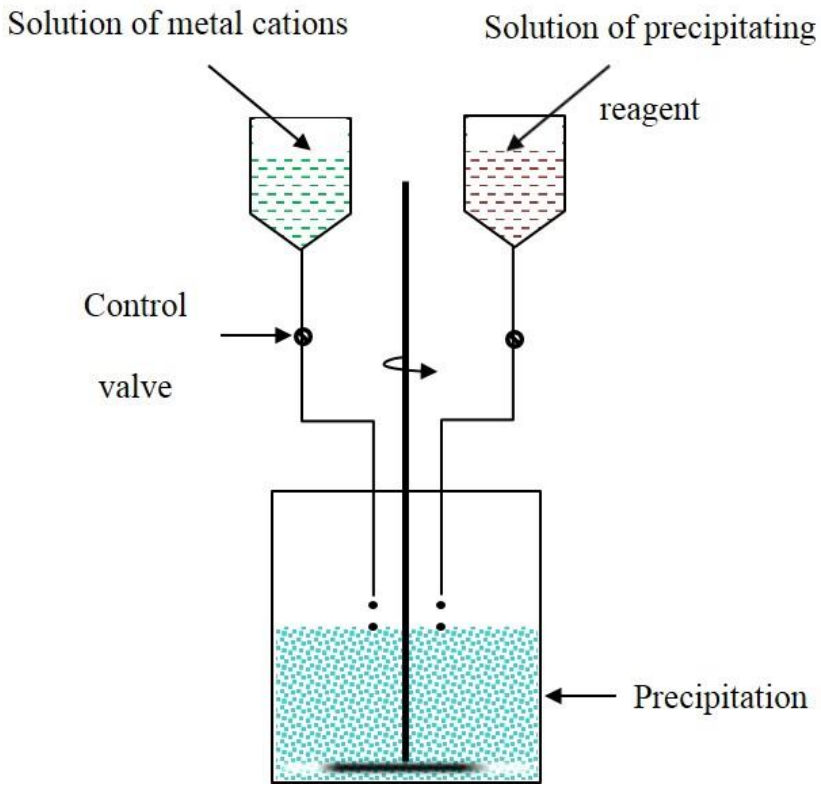

Figure 3.1 Schematic of the precipitation set-up used for catalyst preparation

3.1.2 Shaped Catalyst Preparation

Spherical and cylindrical shaped catalysts were made from the loose powders using a Multi-Lab Extruder and Spheronizer manufactured by Caleva Process Solutions Ltd., shown in Figure 3.2. Moreover, Boehmite (Capital B Alumina; SASOL) was chosen as the binding material to make the shaped catalysts.

The following steps were used to make the shaped catalysts with the Caleva Multi-Lab Extruder and Spheronizer:

1- Ground the catalyst powder under 250 µm (No. 60 US sieve size).

2- Mixed the powder thoroughly using mixer attachment (added desired amount of binder, when required).

3- Made a paste from the solid particles by adding de-ionized water.

4- Loaded the obtained paste into the extruder attachment to obtain cylindrical shapes as shown in Figure 3.2.

5- For spherical shape (as shown in Figure 3.2), loaded the cylindrical shapes (extrudates) in the spheronizer attachment and set the RPM to achieve the desired sphere size.

6- Dried the obtained catalysts at 120 °C overnight and then calcine them at 850 °C for 6 hr.

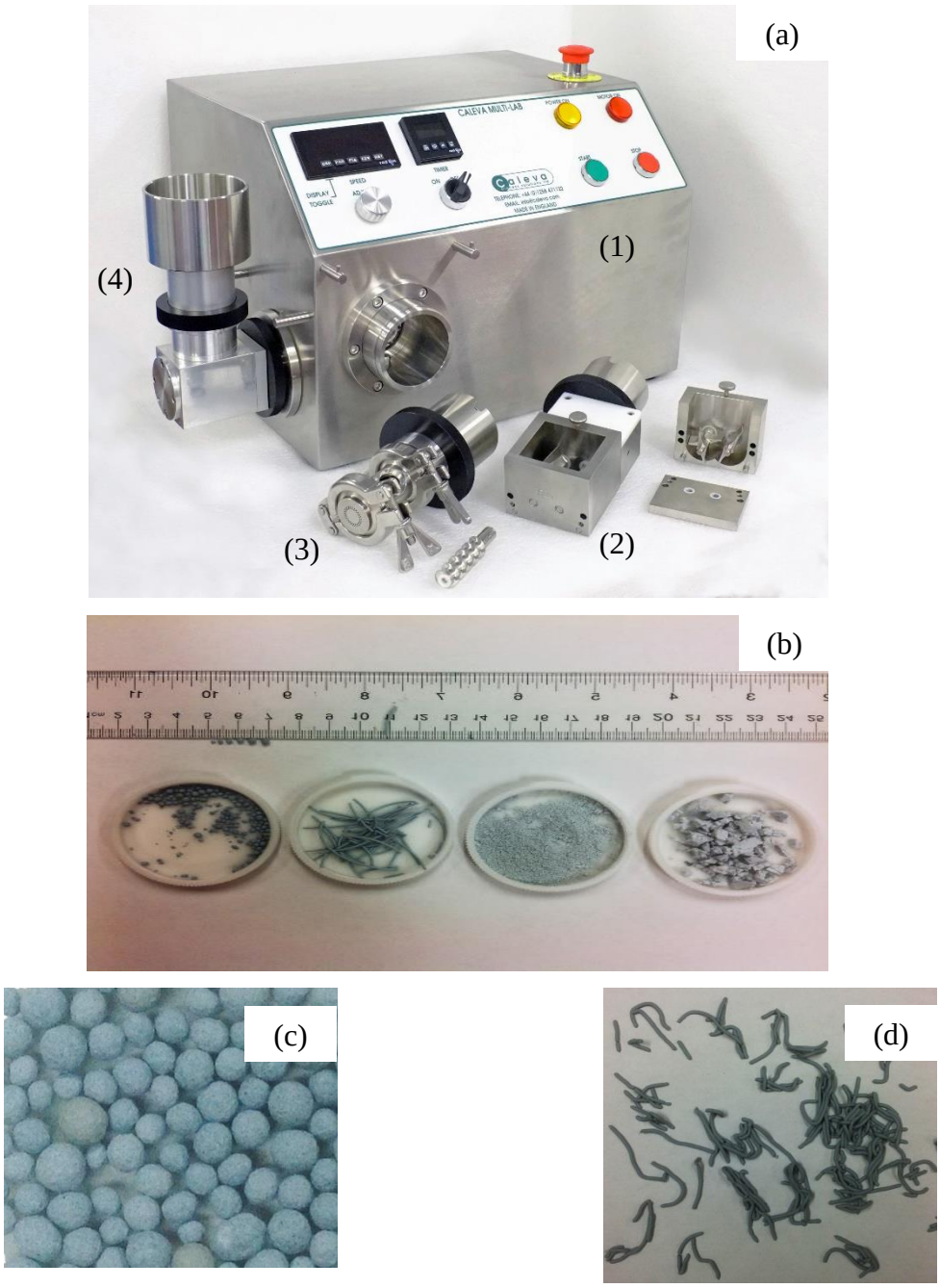

Figure 3.2 Schematic of the mechanized experimental set-up for catalyst preparation; (a) Caleva Multi-Lab instrument: (a-1) main machine, (a-2) mixer attachment, (a-3) extruder attachment, (a-4) spheronizer attachment; (b) prepared catalysts; (c) spherical shape, and (d) cylindrical shape.

3.2 Catalyst Characterization Analysis and Techniques

3.2.1 Brunauer–Emmett–Teller (BET) Surface Area Analysis

BET surface area is an important property for many kinds of materials and especially solid catalysts. B.E.T. (or BET) stands for Brunauer, Emmett, and Teller, the scientists who proposed the theory for measuring the surface area (Brunauer et al., 1938). BET surface area, pore sizes and pore volumes of the prepared catalysts were measured by N_2 adsorption at -196 °C using a Micromeritics ASAP 2000. Approximately 0.2 g of catalyst was used for each analysis. A degassing temperature of 200 °C was used to remove the moisture and other adsorbed gases from the catalyst's surface.

3.2.2 X-ray Diffraction (XRD) Technique

The X-Ray Diffraction (XRD) analysis was used for phase identification of the prepared catalysts. XRD patterns of the catalyst samples were collected using a Rigaku diffractometer instrument with a cobalt target (Kα = 1.79Å). The voltage and current were set to 30 kV and 20 mA, respectively. A digital hydraulic press (Pike CrushIR) was used to compress 0.5 grams of ground catalyst into disks. The disk samples were then loaded into the analysis chamber. Each sample was scanned at a rate of 4°/min with 2-Theta varying from 30 to 100 degrees.

3.2.3 X-ray Absorption Spectroscopy (XAS) Technique

To investigate the electronic arrangement, local geometry, and reduction extent of the catalysts before or after any treatment, an X-ray Absorption Spectroscopy (XAS) technique was used. X-ray Absorption Near Edge Structure (XANES) and Extended X-ray Absorption Fine Structure (EXAFS) analyses were conducted using the Soft X-Ray Microcharacterization Beamline (SXRMB) at the Canadian Light Source. The SXRMB is a bending magnet-based beamline. This beamline is capable to tune the photon energy in the range of 2 to 10 keV. The Ni, Co, and S K-edge spectra of the catalysts and reference samples were recorded using the Solid

State Endestation which was equipped with fluorescence yield (FLY) and total electron yield (TEY) detectors. Athena software was used to analyze the XANES spectra.

For XAS experiments, about 10 mg of catalyst sample, ground to very fine powder, was packed and pressed into a die in the sample holder, called six-hole shooter because it could hold up to 6 samples a time. The shooter with catalyst samples was installed in a quartz tube reactor with window material at both ends. Depending on the purpose of the experiment, the required treatment (such as reduction, CRM, SRM, poisoning, etc.) was conducted. After the treatment, the reactor was cooled down to room temperature while N_2 gas passed through to protect the samples from being re-oxidized. The reactor was then taken to the SXRMB beamline for XAS scan.

3.2.4 Raman Spectroscopy Technique

Raman spectroscopy technique was used to observe whether carbon was deposited on the spent catalyst support. Raman Spectroscopy was conducted on the spent support using Renishaw 2000 micro-Raman system, operated with an argon laser with a wavelength of 514.5 nm. Approximately 0.1 g of sample was used for each analysis.

3.2.5 CO Chemisorption Analysis

0.3 g of catalyst was loaded into the instrument's sample holder. The catalyst was reduced in a 30 mL/min flow of 10% H_2 mixed with 90% Ar. The temperature was ramped from room temperature to 800 °C at 10 °C/min and maintained at 800 °C for 4 hr. Then the sample was purged in He for 40 min at 800 °C, and naturally cooled to 35 °C. CO was adsorbed at 35 °C for 40 min, then switched to H_2 to purge for 40 min. Then, the temperature was ramped at a rate of 10 °C/min to 800 °C while H_2 purging was continued. The exhausted gas was measured by a TCD after water was removed with a cold trapper.

3.2.6 Single and Bulk Crushing Strength Analysis

Single pellet and bulk crush strength of the shaped catalysts were tested following the procedures of ASTM-D4179-11 and ASTM-D7084-04 standard test methods. A texture analyzer

instrument manufactured by Texture Technologies Corporation and Dual Column Testing System (model # 5966) manufactured by INSTRON® were used to investigate the single pellet crush strength and the bulk crush strength of the shaped catalysts, respectively. The schematic of the instruments used for mechanical strength tests is shown in Figure 3.3.

Each shaped catalyst, commercial alumina sphere and commercial alumina cylinder, was positioned at the centre of the lower compression plate for the single crush test (shown in Figure 3.3 (a)). The compression strength was measured 10 times for each sample and the force necessary (F) to crush each sample was recorded. The crush strength (x) and splitting tensile strength (σt) of each sample were calculated using ASTM- C 496-96 standard method (equations 3.1 and 3.2).

$$x = F/L \tag{3.1}$$

where:

x = crush strength for one specimen per millimetre, N/mm (lb_f/mm),

F = force necessary to crush the specimen, N (lb_f),

L = length or diameter of the specimen along the horizontal axis, mm.

$$\sigma_t = 2F/(\pi DL) \tag{3.2}$$

where:

σ_t = splitting tensile strength, MPa (psi),

F = force necessary to crush the specimen, N (lbf),

L = length of the specimen, mm (in),

D = diameter of the specimen, mm (in).

The bulk crushing strength of a spherical catalyst and commercial alumina sphere were tested. Spherical catalysts of 0.5 grams with an average diameter of 4 mm were placed into the cell (shown in Figure 3.3 (b)), which has an inner diameter of 6 mm. 100 N was applied and held on the samples for 30 s. Then the crushed samples were carefully sieved to a fine powder using US No. 16 sieve size and then weighed. The procedure was repeated with fresh load of catalysts for 200 N and 300 N. Fines weight (FW) percent was then determined using equation 3.3.

$$FW = PW/DW \times 100 \quad (3.3)$$

where:

FW = weight percent fines,

PW = weight of fines after sieving,

DW = weight of samples put into the cell.

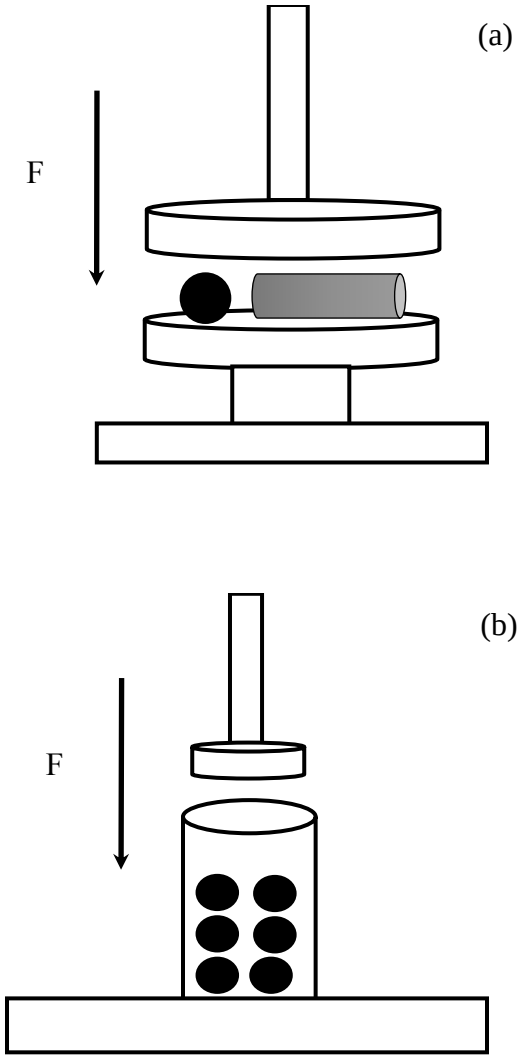

Figure 3.3 Schematic diagram of (a) single pellet and (b) bulk crushing strength test instruments.

3.3 Experimental Set-up and Procedure of Catalyst Evaluation Tests

Carbon dioxide reforming of methane (CRM), steam reforming of methane (SRM), steam carbon dioxide reforming of methane (SCRM), and CRM in the presence of SO_2 over Ni and Co catalysts were performed using the experimental set-up shown in Figure 3.4. Either an Inconel tube with 3/8-inch ID and 30-inch length or a quartz tube with 1/8-inch ID and 15-inch length were used as the reactors. It should be noted that in all the experiments catalysts were reduced in an Inconel reactor unless otherwise stated. The catalyst size and purity of the gases used for the evaluation tests are summarized in Table 3.2 and Table 3.3, respectively.

3.3.1 Carbon Dioxide Reforming of Methane (CRM)

In most of the CRM experiments, unless otherwise mentioned, 0.1 g of catalyst was mixed with 0.4 g of silica carbide then reduced in an Inconel reactor in a mixture of H_2 (50%) and N_2 (50%) for 4 h. Then the CRM reaction was carried out at the desired reaction temperature with an equimolar ratio of reactant ($CH_4/CO_2 = 1$) balanced with N_2. The product gas was then analyzed every 18 minutes using an online Agilent 6890N GC, equipped with a TCD (Thermal Conductivity Detector) and a ShinCarbon ST100/12 packed column (RESTEK) with 2 m of length and 1 mm of inner diameter for permanent gas analysis. After each CRM reaction was tested during the desired time-on-stream, the reactor was cooled down to room temperature in the presence of N_2. The spent catalysts were collected for further analysis.

3.3.2 Steam Carbon Dioxide Reforming of Methane (SCRM)

Powder catalyst (0.4 g mixed with 3.6 g of silica carbide) was reduced in an Inconel reactor at 900 °C in a H_2 (50%) and N_2 (50%) mixture for 4 hr. Then SCRM reaction was carried out at 850 °C with a GHSV of 110 L g^{-1} hr^{-1} using various feed compositions, which contain CH_4, CO_2 and H_2O. After removal of unreacted/produced water, using the steam tap shown in Figure 3.4, the product gas was analyzed using the online GC every 18 minutes.

3.3.3 CRM in the Presence of SO_2

Catalyst or support (0.1 g) was reduced in a quartz reactor in a mixture of H_2 (20%) and N_2 (80%) at 800 °C for 4 hr. Next, each CRM reaction with a gas feed of an equimolar ratio of CH_4, CO_2, and N_2 and GHSV of 60 L g^{-1} hr^{-1} was carried out at 800 °C for 1 hr. Then, 500 ppm of SO_2 was introduced to the feed and the reaction continued for 3 hr followed by 2 hr more without the SO_2. The product gas was analyzed using two online gas chromatographs: an Agilent 6890N (described in section 3.3.1) and a Varian 3800 equipped with a PFPD (Pulsed Flame Photometric Detector) detector and a CP-Sil 5 CB capillary column (Agilent) with 50 m in length and 0.32 mm of inner diameter for sulfur analysis. After the reaction was completed, the reactor was cooled down to room temperature in the presence of N_2. The spent catalysts were collected for further analysis.

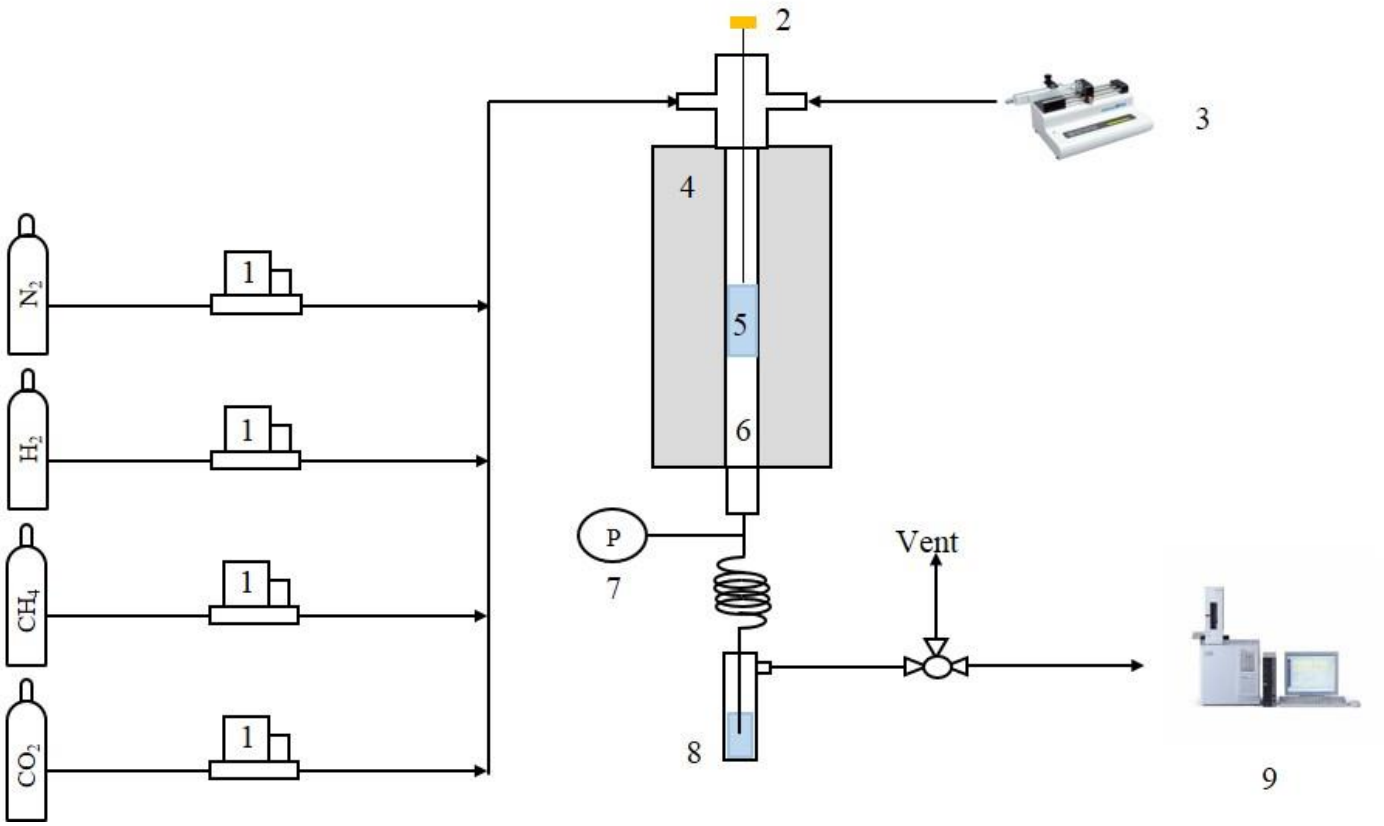

1: MFC
2: Thermocouple
3: Syringe pump
4: Furnace
5: Catalyst bed
6: Reactor
7: Pressure gauge
8: Water trap
9: GC – MS

Figure 3.4 Schematic of the experimental set-up used for catalyst performance evaluation.

Table 3.2 Average size of the catalysts used for evaluation tests.

Catalyst	Average Diameter	Average Length
Loose powder form	0.3 mm	-
Cylindrical (extruded) shape	1.30 (±0.05) mm	5.0 (±0.1) mm
Spherical shape	4.00 (±0.05) mm	-

Table 3.3 Purity of the gases used for the catalyst evaluation tests.

Gas	Grade*
N_2	>99.0 %, Industrial grade
H_2	>99.0%, Industrial grade
He	99.9%, Ultra High Purity 5.0
CH_4	>99.0%, Industrial grade
CO_2	>99.0%, Industrial grade
SO_2	1.04 (±0.01) % balanced with N_2

* All the gases were purchased from PRAXAIR Inc.

3.4 Data Analysis Procedure

The conversion of reactants and yield of the products were calculated using the following procedure:

Consider X_i (volume of component i / total volume) as the GC value

$$X_i = \frac{F_{out},i}{\sum_j F_{out},i} \tag{3.4}$$

where:

F_{out}, i = flow rate of component "i" after the reaction (mL/min)

j = CO_2, CH_4, N_2, H_2, CO

The flow rate of each component exiting from the rector could be calculated based on N_2 flow rate which was kept constant during the reaction. As an inert gas, N_2 did not react with the other gases during reactions.

For example, the flow rate of methane in the product stream could be calculated by the following procedure:

$$X_{N_2} = \frac{F_{out},N_2}{\sum_j F_{out},j}, \; j = CO_2, CH_4, N_2, H_2, CO \tag{3.5}$$

$$X_{CH_4} = \frac{F_{out},CH_4}{\sum_j F_{out},j} \; j = CO_2, CH_4, N_2, H_2, CO \tag{3.6}$$

Dividing equation 3.10 by equation 3.9:

$$\frac{F_{out},CH_4}{F_{out},N_2} = \frac{X_{CH_4}}{X_{N_2}} \rightarrow F_{out}, CH_4 = F_{out}, N_2 \times \frac{X_{CH_4}}{X_{N_2}} \tag{3.7}$$

So, as with the above procedure, equation 3.8 could be developed for all the gases in the reactor outlet stream.

$$F_{out}, i = F_{out}, N_2 \times \frac{X_{N_2}}{X_i} \; i = CO_2, CH_4, N_2, H_2, CO \tag{3.8}$$

Since N_2 was inert during the reaction(s), therefore F_{out}, N_2 is equal to F_{in}, N_2. The values of X_i are obtained from the GC calibration curves; therefore F_{out}, i can be calculated from equation 3.8. The reactant conversion could be calculated using the following equations:

$$Methane\ (CH_4) conversion, \% = \frac{(F_{in,CH_4} - F_{out,CH_4})}{F_{in,CH_4}} \times 100 \quad (3.9)$$

$$Carbon\ Dioxide\ (CO_2) conversion, \ \% = \frac{(F_{in,CO_2} - F_{out,CO_2})}{F_{in,CO_2}} \times 100 \quad (3.10)$$

where:

F_{out}, i = the flow rate of component "i" in the reactor outlet (mL/min)

F_{in}, i = the flow rate of component "i" in the reactor inlet (mL/min)

To calculate the consumption rate of reactants and the formation rate of products, the following equations could be used:

$$-r_{reactant} = \frac{(F_{in,reactant} - F_{out,reactant})}{m_{catalyst}}, \text{ mol } g^{-1}\ hr^{-1} \quad (3.11)$$

$$r_{product} = \frac{F_{out,product}}{m_{catalyst}}, \text{ mol } g^{-1}\ hr^{-1} \quad (3.12)$$

where flow rates were used with the unit of mol/hr

Athena (version 0.9.26) software was used for processing X-ray Absorption Spectroscopy data such as normalization of the spectra, linear combination fittings, etc. Also, Origin Lab pro (2016 version) and Microsoft Office Excel (2013 version) were used to prepare the figures.

Mass Flow Controller calibration curves, GC method and calibration curves as well as the repeatability of some data obtained from characterization analysis and experimental tests are presented in the Appendixes.

3.5 Statistical Analysis Procedure

Mean (m), standard deviation (SD) and standard error (SE) of the mechanical strength test measurements were calculated using equations 3.13, 3.14, and 3.15, respectively. Also, size

distribution of the pellet catalysts was investigated using the descriptive statistics module of Microsoft Office Excel 2016.

$$m = \frac{\sum_{i=1}^{n} x_i}{n} \tag{3.13}$$

where:

m = mean/average of the measurements

x_i = value of i^{th} measurement

n = number of measurements

$$SD = \sqrt{\frac{\sum_{i=1}^{n}(x_i - m)^2}{n-1}} \tag{3.14}$$

where:

SD = standard deviation of the measurements

and

m, xi, and n are as defined in equation 3.17.

$$SE = \frac{SD}{\sqrt{n}} \tag{3.15}$$

where:

SE = standard error of the measurements

and

SD and n are as defined in equation 3.18.

CHAPTER 4

Development of Shaped Catalysts for CRM

4.1 Shaped Catalyst Preparation

Ni-Co bimetallic catalysts supported with $AlMgO_x$ were made by a co-precipitation method as described in section 3.1.1. Then, Spherical catalysts, noted as Sph, and cylindrical/extrudate catalysts, noted as Ext, were made using the procedure in section 3.1.2. Also, Boehmite was chosen as the binding material and used in preparation of the shaped catalysts. To indicate the content, shaped catalysts were named in the general form of CmBn where C, B and m/n ratio stand for Ni-Co bimetallic catalyst, Boehmite, and Ni-Co catalyst to Boehmite weight ratio, respectively. The description of the prepared catalysts is reported in Table 4.1.

The actual Ni and Co (wt%) loading in the Ni-Co bimetallic catalyst was determined by Inductively Coupled Plasma Mass Spectroscopy (ICP-MS) analysis in our previous work (Shakouri, 2011). The results indicated 2.73 wt% and 4.83 wt% for Ni and Co content, respectively. Therefore, equations 4.1 and 4.2 could be developed to calculate the Ni and Co (wt%) loading in the prepared catalyst with the general form of CmBn, respectively.

$$Ni\ (wt\%) = \frac{m}{m+n} \times 2.73 \tag{4.1}$$

$$Co\ (wt\%) = \frac{m}{m+n} \times 4.83 \tag{4.2}$$

The cylindrical catalysts had diameter of 1.3 mm, while their lengths could be varied. Moreover, the diameter of the spherical catalysts could be varied using different rpm (revolutions per minutes) in the spheronizing step. In general, a higher the rpm rate yielded a smaller diameter sphere.

4.2 Statistical Analysis on Shaped Catalyst Sizes and Distribution

Pellet size is a key factor in engineering the properties of a solid catalyst (Fulton, 1986). Therefore, size distribution of shaped catalysts should be investigated in the initial steps of such development. As mentioned before, the cylindrical diameters of shaped catalysts, using each procedure described in section 3.1.2, were fixed. However, as the diameter of the spherical shapes could be varied, to investigate their size distribution, 2 and 5 batches of Sph-C catalyst prepared using 500 and 2000 rpm in the spheronization step, respectively. Then, the dimeters of 10 random samples from each batch were measured to the hundredth of a millimetre using a Mastercraft electronic digital caliper. Statistical analysis on the measured Sph-C sizes was performed using the descriptive statistics module of Microsoft Office Excel 2016. Statistical analysis and distribution of spherical catalyst sizes are summarized in Table 4.2 and Figure 4.1, respectively.

Table 4.2 shows that a spheronization speed of 2000 rpm created a larger range of sphere diameters distributed than 500 rpm. Also, the smaller standard deviation in sphere sizes prepared with 500 rpm indicates better size distribution than 2000. However, comparing the statistical parameters within each group reveals that the prepared Sph-C sizes in each batch were well distributed and reproducible. In addition, Figure 4.1 indicates that the diameter distribution of Sph-C catalyst pellets follows the normal distribution.

The conclusion is that average sphere sizes were about 4 mm when made at 500 rpm and 3.1 mm at 2000 rpm. Also, sphere diameters of the prepared catalysts were well distributed regardless of the spheronization speed.

Table 4.1 Name and description of the prepared shaped catalysts

Catalyst*	Description
C	Ni-Co/AlMgO_x powder catalyst prepared with precipitation procedure
Sph-C	spherical Ni-Co/AlMgO_x catalyst
Sph-CmBn	spherical catalyst with catalyst to Boehmite weight ratio of m/n
Ext-C	cylindrical Ni-Co/AlMgO_x catalyst
Ext-CmBn	cylindrical catalyst with catalyst to Boehmite weight ratio of m/n
Ext-A	Commercial cylindrical alumina
Sph-A	Commercial spherical alumina

* The catalysts were shaped using a mechanized procedure unless otherwise noted.

Table 4.2 Descriptive statistics analysis on the size distribution of Sph-C catalysts prepared with 500 and 2000 rpm

Spheronizer rate	500 rpm		2000 rpm				
Batch	1	2	1	2	3	4	5
Mean (mm)	3.92	3.97	3.10	3.10	3.15	3.07	3.10
Standard Error (mm)	0.11	0.11	0.19	0.15	0.21	0.20	0.23
Standard Deviation (mm)	0.35	0.34	0.61	0.46	0.66	0.63	0.71
Sample Variance	0.12	0.12	0.37	0.21	0.44	0.39	0.51
Median (mm)	3.78	3.92	3.15	3.15	3.25	3.11	2.83
Confidence Level (95%)	0.25	0.24	0.43	0.33	0.47	0.45	0.51
Number of samples	10	10	10	10	10	10	10

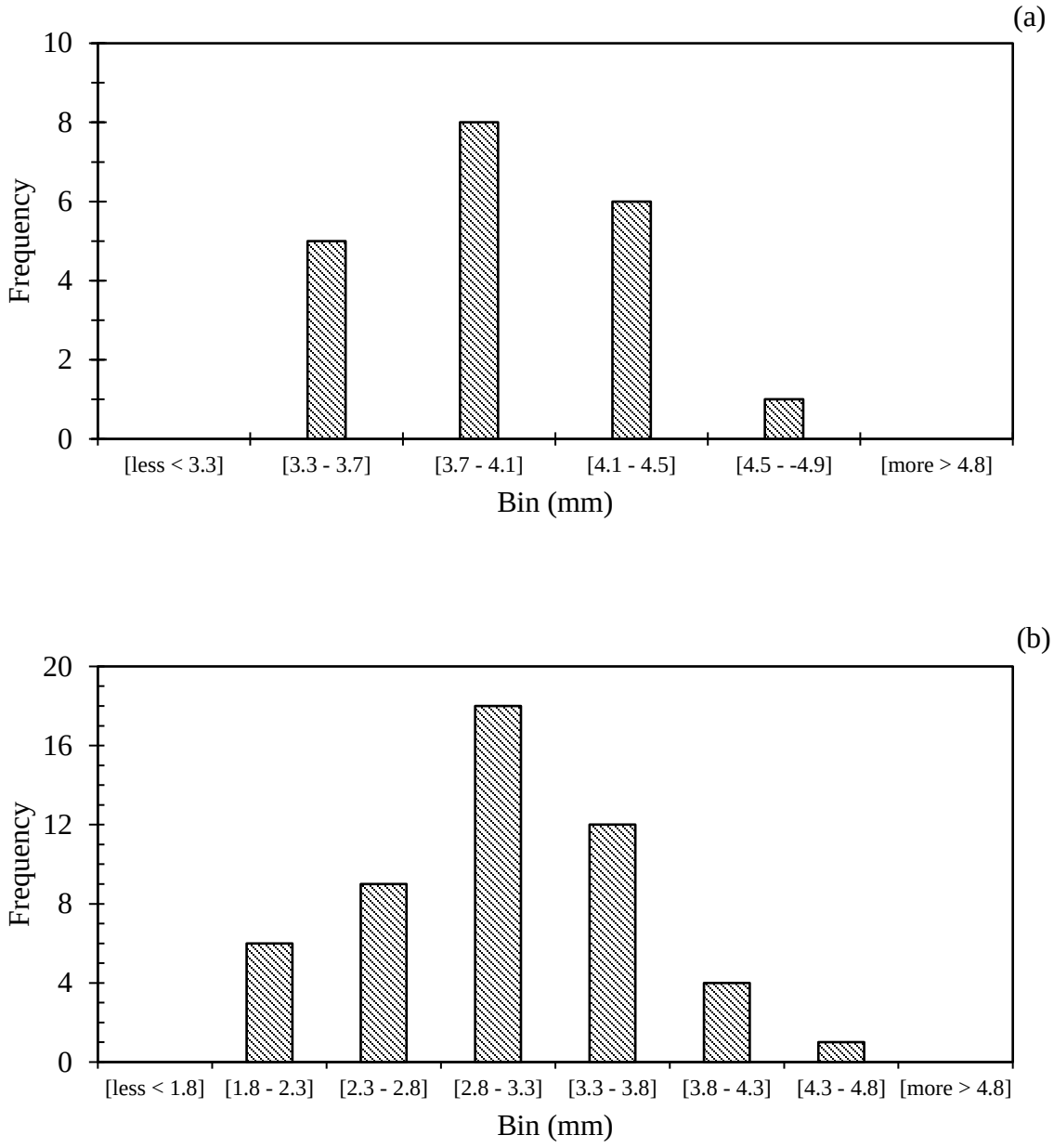

Figure 4.1 Diameter distribution histogram of Sph-C catalysts prepared with (a) 500 rpm, and (b) 2000 rpm

4.3 Mechanical Strength of the Shaped Catalyst

It is well-known that an effective catalyst requires not only a good catalytic performance such as good stability and selectivity toward the desired reaction products, but also a good physical property such as mechanical strength (Wu et al., 2006). In industrial fixed-bed reformers, solid catalysts could fracture when they are loaded into the reactor or during operation due to the weight of the catalysts' bed. The mechanical fracture could cause various problems such as large pressure drops, uneven fluid flow distribution, blockage of the reactor, and variation in heat and mass fluxes. Therefore, mechanically strong catalyst pellets are essential to achieve reliable performance in fixed-bed reactors (Gallei and Schwab, 1999; Staub et al., 2014). Thus single pellet and bulk crush strength tests, based on the ASTM standards, were performed to investigate the mechanical strength of the prepared shaped catalysts.

4.3.1 Single Pellet Crush Strength

Single pellet crush strengths of the shaped catalysts, commercial spherical alumina (Sph-A) and commercial cylindrical alumina (Ext-A) were tested following the procedure described in section 3.2.6. The average compressive load (F) and splitting tensile strength (σ_t) of each sample with their associated error bars are shown in Figure 4.2. Also, mean (m) and standard deviations (SD) of measured F and calculated x and σ_t, generated using the descriptive statistics module of Microsoft Office Excel 2016, are summarized in Table 4.3. It is assumed that the compressive strength of the commercial products, spherical and cylindrical alumina, is acceptable for industrial use. It should also be mentioned that the mechanical strength of cylindrical catalysts made by using Caleva Multi-Lab instrument was too weak and not in the operational range of the instrument and therefore their mechanical strengths are not reported.

Table 4.3 and Figure 4.2 (a) reveal that the Ext-A could withstand more compressive force than the spherical ones. Heffner and Pfost (1973) reported that different geometry of the cylindrical shape could explain their higher strength than the spherical pellets. The contact area between pellet and the lower compression plate (Figure 3.3 (a)) in cylindrical shapes are larger than the spherical shapes. Therefore, more force was required to crush the cylindrical than the spherical ones. In case of the spherical shapes, the higher the diameter of a sphere, the higher the force required to crush

the sample. The higher measured compressive loads in commercial spherical catalysts are likely because of their larger sizes.

The splitting tensile strength, which considers size and geometry of pellets, could be a better parameter to compare the mechanical strength. Figure 4.2 (b) shows that, similar to the compressive load results, the tensile strengths of Ext-A were significantly more than the spherical catalysts. The splitting tensile strength of Sph-C and Sph-C1B1 catalysts were comparable to that of commercial spherical alumina (Sph-A).

Comparing mechanical strength of Sph-C and Sph-C1B1 also reveals that, the addition of Boehmite as the binding material did not significantly change the strength of the spherical catalysts. The presence of alumina as the major content of both Boehmite and the Ni-Co/$AlMgO_x$ catalysts, could be the possible explanation for these observations. Considering the shaped catalyst geometries and compositions, it is reasonable to conclude that, they were comparably as strong as the commercial ones.

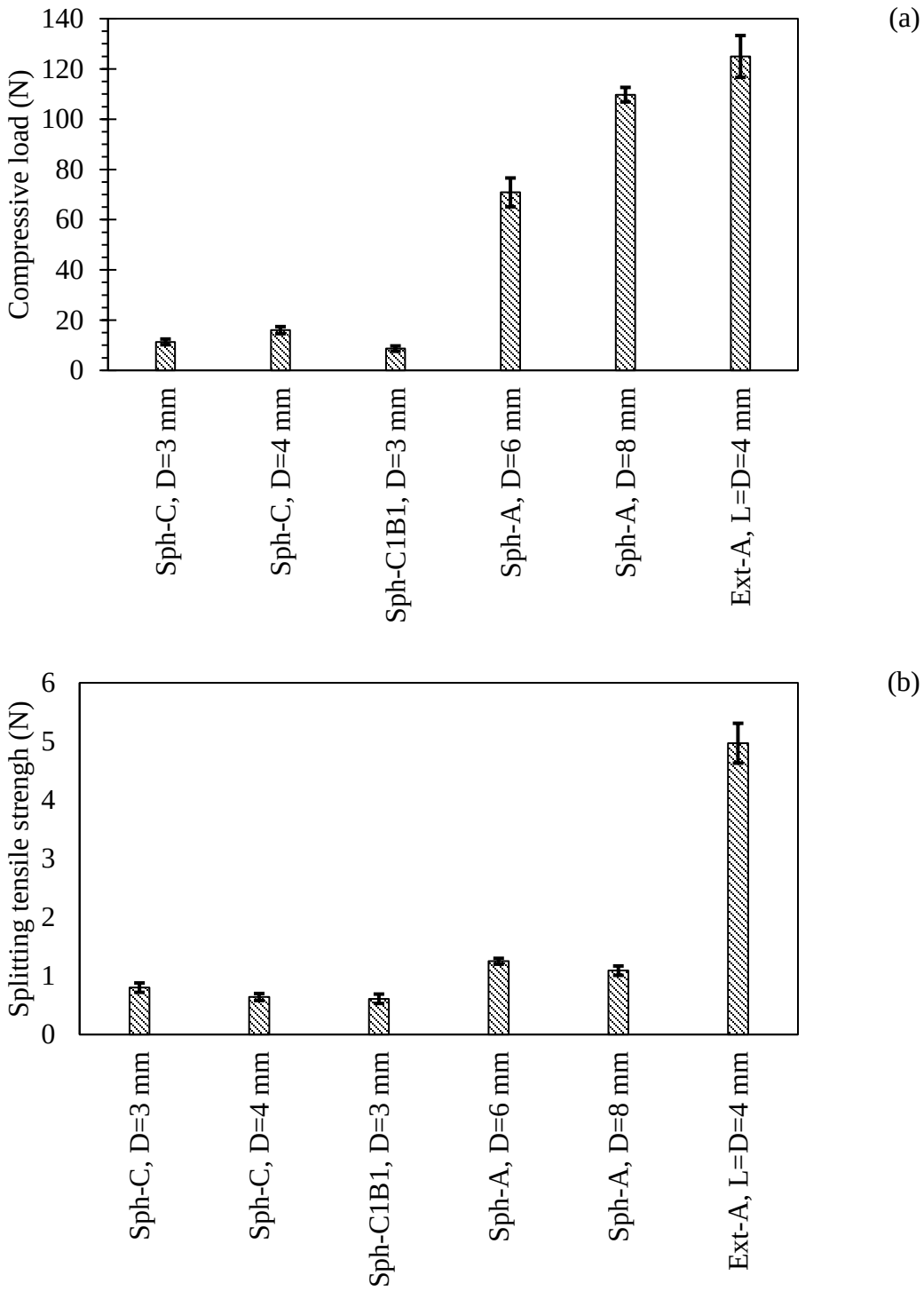

Figure 4.2 (a) Compressive load and (b) splitting tensile strength of spherical and cylindrical shaped catalysts obtained from single-pellet crush strength tests

Table 4.3 Descriptive statistical analysis on compressive load, crush strength and splitting tensile strength of cylindrical and spherical shaped catalysts

Catalyst	L (mm)	D (mm)	F (N)		x (N/mm)		σ_t (Mpa)	
			m	SD	m	SD	m	SD
Sph-C	-	3	11.34	1.14	3.78	0.38	0.80	0.08
Sph-C	-	4	16.01	0.91	4.00	0.12	0.64	0.06
Sph-C1B1	-	3	8.67	1.07	2.89	0.36	0.61	0.08
Sph-A	-	6	70.85	2.90	11.81	0.48	1.25	0.05
Sph-A	-	8	109.75	8.33	13.72	1.04	1.09	0.08
Ext-A	4	4	124.97	8.63	31.24	2.16	4.97	0.34

4.3.2 Bulk Crush Strength Test

The mechanical strength of bulk spherical solid catalysts for industrial application is commonly investigated by bulk crushing strength (BCS) tests. Thus, a BCS test of the spherical catalysts (Sph-C) was performed as described in section 3.2.6. Sph-C catalysts totaling 0.5 grams were placed into a cell. 100 N was applied and held on the samples for 30 s. The crushed samples were carefully weighed and then sieved using US No. 16 sieve size; the fine powders after sieving were then weighed. The procedure was repeated with a fresh load of catalysts for 200 N and 300 N. To compare, the tests were performed on commercial spherical alumina (Sph-A), as well. Then, the weight percent fines (FW) for each load (100, 200, and 300 N) were calculated using equation 3.3. Average size, weight and density of the Sph-C and Sph-A used for these BSC tests are summarized in Table 4.4. Also, crushing pressure was calculated using the load amount and the area of the pellets and plotted versus weight percent fines as shown in Figure 4.3. The correlation in Figure 4.3 was used to calculate the crush strengths for 1% fines generation, which are summarized in Table 4.5.

As reported in Table 4.4 spherical catalysts with an average diameter of 4 mm were chosen for the BSC tests. Also, the density of the Sph-C samples (1.6 g/cm^3) was more than that of Sph-A samples (1.5 g/cm^3). This slight difference is easily explained since the Sph-A samples were made of alumina while the Sph-C catalysts also contained Ni, Co and Mg oxides which are heavier oxides than alumina. Moreover, Table 4.5 reveals that the required pressure to produce 1% fines of Sph-C was almost 7 times that of Sph-A.

The results from both single and bulk crush strength tests indicate the mechanical strength of the prepared spherical Ni-Co bimetallic catalysts (Sph-C) compared favourably with available commercial ones and could be further investigated for the catalytic performance tests.

Table 4.4 Properties of spherical shaped catalysts and commercial spherical alumina used for bulk crush strength tests

	Sph-C			Sph-A		
BSC test load	diameter (mm)	weight (mg)	density (g/cm^3)	diameter (mm)	weight (mg)	density (g/cm^3)
100 N	4.01(±0.02)	55.22(±2.50)	1.63(±0.06)	4.02(±0.01)	50.21(±1.23)	1.48(±0.03)
200 N	4.01(±0.02)	55.00(±3.17)	1.63(±0.08)	4.02(±0.02)	49.50(±1.97)	1.45(±0.05)
300 N	4.01(±0.02)	54.47(±2.00)	1.62(±0.05)	4.02(±0.01)	50.63(±1.86)	1.49(±0.04)

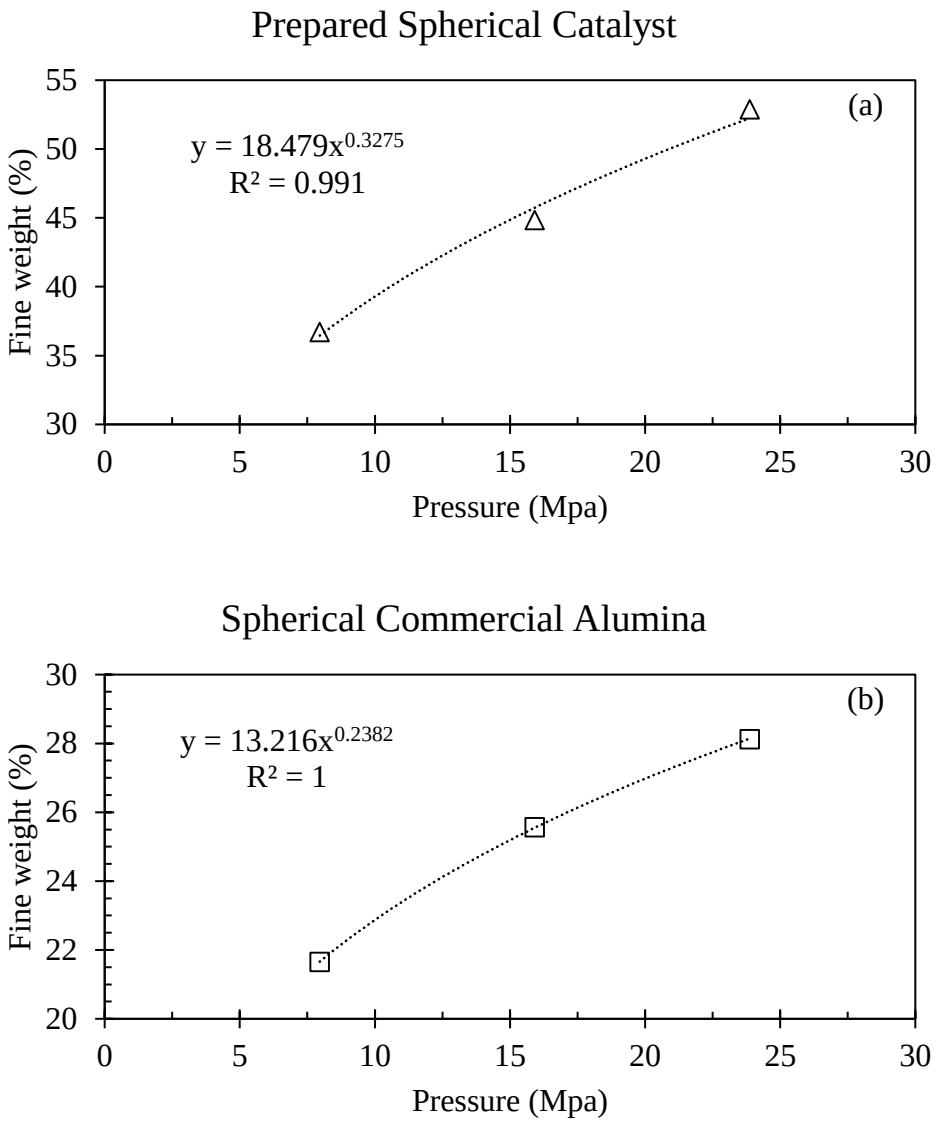

Figure 4.3 Crushing pressure versus fine weight percent of (a) Sph-C, and (b) Sph-A, obtained from bulk crush strength tests

Table 4.5 Pressure which was required for crushing bulk sample of spherical pellets to produce 1 weight% fine powder (smaller than US sieve size No. 16) calculated from bulk crush strength tests

Sample	Crush pressure to produce 1% fines (Pa)
Sph-C (spherical catalyst)	135
Sph-A (commercial spherical alumina)	20

4.4 BET Surface Area of the Prepared Catalysts

N_2 sorption analyzer was used to obtain the specific surface area, porous volume, and average pore size of the prepared catalysts. The results are summarized in Table 4.6. The pore size distribution is shown in Figure 4.4, which was obtained from the adsorption branch of the N_2 isotherm by the Barret-Joyner-Halenda (BJH) method (Rostrup-Neilsen and Hansen, 1993; Barret et al., 1951).

Table 4.6 reveals that, unlike pore volume and pore size, a significant difference in BET area of the prepared catalysts was not observed. This indicates that the addition of Boehmite to the Ni-Co powder catalyst as well as the physical shaping process did not significantly affect the BET surface area. The pore volume and the average pore size diameter followed the same order of Ext-C1B1 > Sph-C2B1 > C > Sph-C. In addition, Figure 4.4 clearly depicts that the samples containing Boehmite had higher pore volume and pore area than the others. Moreover, the greater the Boehmite content, the larger the pore diameter of the maxima peak. As an example, the average pore volume and pore size increased from 0.317 cm^3/g and 82.1 Å in Ni-Co loose powder catalyst (C) to 0.491 cm^3/g and 117.6 Å in Ext-C1B1. It is reported that at temperatures higher than 500 °C, the aluminum oxide hydrate in Boehmite will be dehydrated in the form of γ-alumina with an average pore volume and pore size of 0.5 cm^3/g (Boehmite description from manufacturer; SASOL). Since all the prepared catalysts were calcined at 850 °C, formation of γ -alumina could explain the pore volume and pore size of the Boehmite-containing catalysts (Ext-C1B1 and Sph-C2B1) being higher than the others (C and Sph-C). On the other hand, the Sph-C catalyst showed smaller pore volume and pore size than C. This observation could be explained by the calcination step being performed twice for Sph-C catalyst but only once for the C catalyst (Liang et al., 2017; Tian, 2013).

Table 4.6 N_2-chemisorption analysis results for Ni-Co bimetallic powder catalyst (C), cylindrical catalyst with Ni-Co powder catalyst to Boehmite ratio of 1 (Ext-C1B1), cylindrical catalyst with Ni-Co powder catalyst to Boehmite ratio of 2 (Sph-C2B1), spherical Ni-Co catalyst (Sph-C), and Boehmite (B). All samples were calcined at 850 °C in air for 6 hr.

Catalyst	(Catalyst/Boehmite) ratio	BET area (m^2/g)	Pore volume (cm^3/g)	Average pore size (Å)
B	0	173 (±3%)	0.578	132.8
Ext-C1B1	1	169 (±3%)	0.491	117.6
Sph-C2B1	2	160 (±3%)	0.462	115.4
C	-	154 (±3%)	0.317	82.1
Sph-C	-	166 (±3%)	0.267	65.6

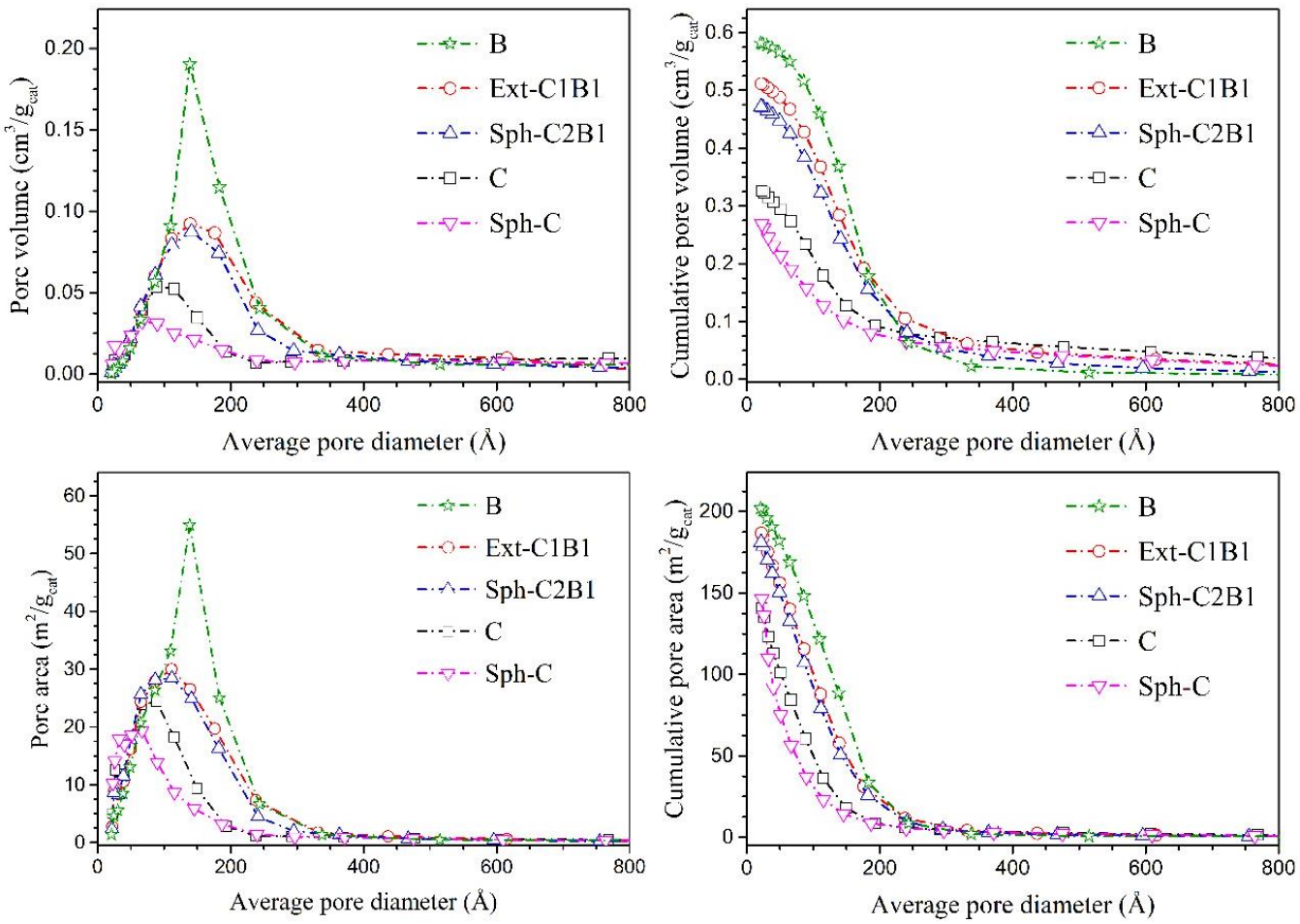

Figure 4.4 Pore volume and area distribution obtained from the adsorption branch of the N_2 isotherm by BJH method for Ni-Co bimetallic powder catalyst (C), cylindrical catalyst with Ni-Co powder catalyst to Boehmite ratio of 1 (Ext-1C1B), cylindrical catalyst with Ni-Co powder catalyst to Boehmite ratio of 2 (Sph-2C1B), spherical Ni-Co catalyst (Sph-C), and Boehmite (B). All samples were calcined at 850 °C in air for 6 hr.

4.5 X-ray Diffraction Patterns of the Prepared Catalysts

The phase structure of calcined catalysts was identified with X-ray diffraction analysis (XRD). XRD patterns of the calcined catalysts and support as well as Boehmite (B) before and after calcination are shown in Figure 4.5.

Figure 4.5 (a) indicates that the Boehmite bulk structure was altered after the calcination. Prior to calcination, the diffraction peaks at 33°, 45°, 58°, 65°, 76°, 80°, and 85° correspond to an aluminum oxide hydrate (Boehmite) phase with body-centered cubic (bcc) orthorhombic structure (Pdf No. 00-001-1283). After calcination, the diffraction peaks at 38°, 44°, 46°, 54°, 72° and 79° are more likely characteristics of a γ-alumina phase with face-centered cubic (fcc) structure. The observed phase change in Boehmite from aluminum oxide hydrate (before calcination) to γ-alumina (after calcination) is also in agreement with the Boehmite manufacturer's report (SASOL).

As shown in Figure 4.5 (b), spinel and MgO were the two main phases found in the $AlMgO_x$ catalyst support as well as the prepared catalyst precursors. The diffraction peaks at 50.5° and 74° represent the magnesium oxide phase with fcc structure (Pdf No. 00-045-0946). In addition, diffraction peaks at 39°, 43°, 45°, 53°, 71°, and 77.5° degrees were found, which might correspond to the spinel phase with fcc structure (Pdf No. 00-003-0901) and a phase with cubic structure (Pdf No. 00-003-1162). In the case of calcined catalyst support, the spinel phases could be assigned to the structure of $MgAl_2O_4/MgO.Al_2O_3$ (Pacurariu et al., 2007). On the other hand, in the calcined catalysts, the XRD patterns of $MgAl_2O_4$, $NiAl_2O_4$, and $CoAl_2O_4$ were found from literature (Coq et al., 2000; Tichit et al., 1997; Yadav et al., 2007). Due to overlaps, it is hard to distinguish the spinel phase among $MgAl_2O_4$, $NiAl_2O_4$, $CoAl_2O_4$ and Co_2AlO_4 phases. It is observed that MgO oxide phase content followed the order of C > C1B1> C1B2 > C1B3 while the spinel phase followed the reverse order. It seems that the Mg from the MgO phase interacted with the added alumina from Boehmite to form additional spinel phase. Therefore, the higher the Boehmite content, the higher the spinel phase and the lower the MgO phase.

The XRD patterns in Figure 4.5 (c) show that MgO and spinel phases, like Ni-Co bimetallic catalyst (C) and $AlMgO_x$ support, are the major phases in the bulk structure of the shaped catalysts. As an example, no apparent difference was observed between the diffraction patterns of C, Ext-C, and Sph-C catalysts. It is also clear that increase of Boehmite content resulted in weakening the MgO phase and strengthening the spinel phase. Therefore, it could be concluded that the physical

process used to shape the catalysts into cylinders or spheres, did not significantly change their structure.

4.6 Metal Dispersion

Dispersion of metals in catalysts prepared with and without Boehmite was measured using CO-chemisorption analysis; results are presented in Table 4.7. The metal dispersions were calculated based on the total Ni and Co content in the samples, which were obtained earlier through ICP-MS analysis. Table 4.7 clearly shows that the metal dispersion was improved with an increase of Boehmite content following the order of C1B2 > C1B1 > C. In other words, metal dispersions increased with the decrease of Ni-Co content, which is in agreement with the earlier study on the Ni-Co/$AlMgO_x$ catalyst by Zhang et al. (2008). It seems that the increase of Boehmite (alumina) content could assist the scattering of metals during the calcination. The XRD results also revealed that with the addition of the Boehmite, spinel phase was increasing while the MgO phase was decreasing within the catalyst structure.

Zhang (2012) reported that an increase of spinel phase content in the catalyst structure could improve Ni and Co metal dispersions in the Ni-Co/$AlMgO_x$ catalyst. It is also observed that metal dispersion in Sph-C was comparable with C. This could suggest that shaping the catalyst as well as a second calcination did not significantly change the metal dispersion.

○ : γ-alumina phase □ : aluminum oxide hydrate phase

◊ : MgO phase ❋: spinel phase

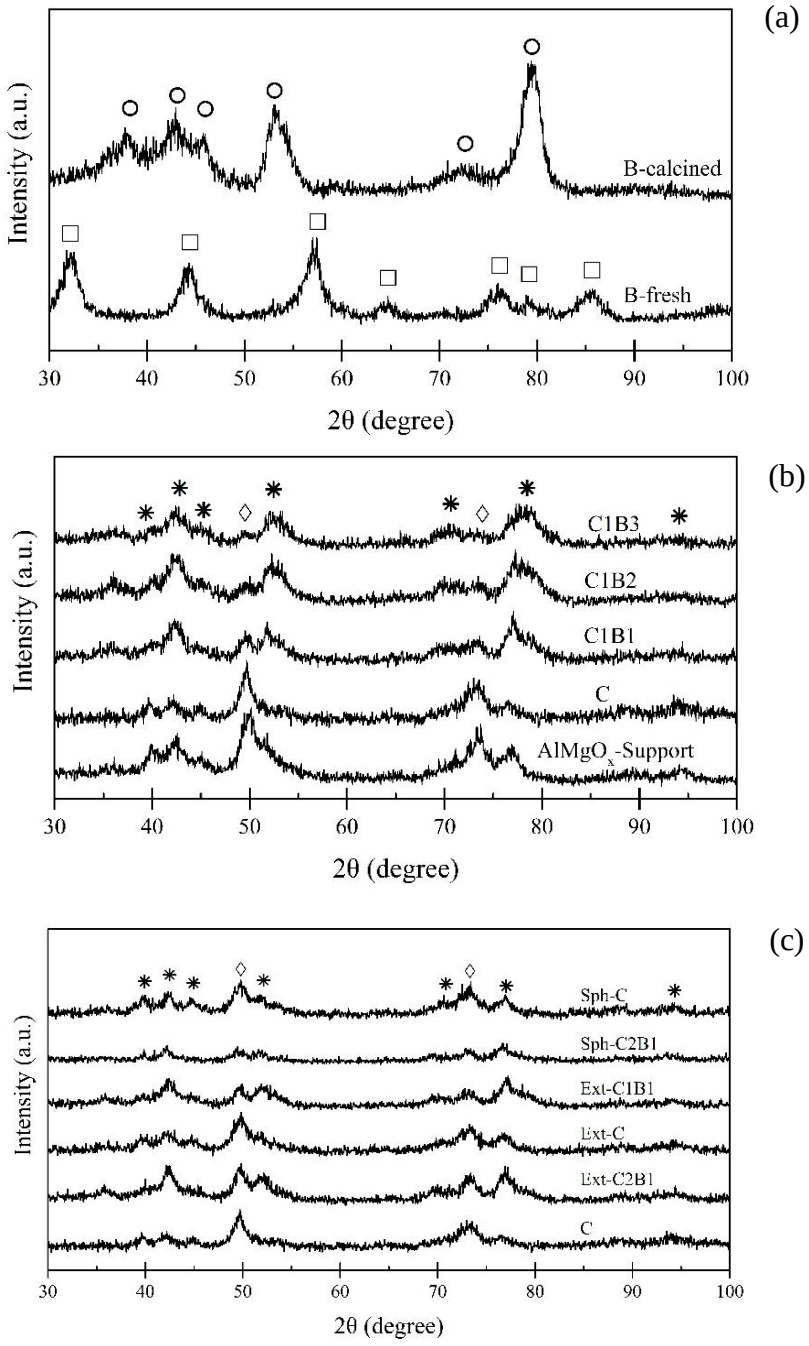

Figure 4.5 XRD diffraction patterns of (a) Boehmite before and after calcination, (b) calcined catalysts prepared with various Boehmite to catalyst ratios, and (c) calcined shaped catalysts. Calcination was done in air at 850 °C for 6 hr.

Table 4.7 Metal dispersion of Sph-C and Ni-Co/$AlMgO_x$ catalysts with or without addition of Boehmite

Catalyst	Adsorbed CO (mL/g)	Dispersion (%)	Ni content (wt %)	Co content (wt %)
C	2.0	7.3	2.7	4.8
C1B1	1.6	11.4	1.4	2.4
C1B2	1.6	17.2	0.9	1.6
Sph-C	2.0	7.3	2.7	4.8

4.7 Effect of Addition of Boehmite on Metal Reducibility of Ni-Co Bimetallic Catalysts

A portion of about 10 mg of each of C (Ni-Co/$AlMgO_x$), Sph-C, C1B1, C1B1-M and C2B1 catalysts was loaded in the six-hole shooter and installed in a quartz tube reactor as described in section 3.2.3. Catalysts were reduced in a mixture of H_2 (20%) and N_2 (80%) at 800 °C for 4 hr. The reactor was then cooled down to room temperature in the presence of N_2 to protect samples from being re-oxidized. The reactor was then taken to the SXRMB beamline for XAS analysis. The Ni and Co K-edges spectra were measured for the catalyst samples before and after reduction. Also, XAS scans for standard samples of Ni foil, Co foil, NiO and CoO were recorded. After collecting the data, Athena software was used to calibrate, normalize and fit the XAS data. Normalized Ni and Co XANES (X-ray Absorption Near Edge Structure) spectra of the reduced and calcined samples as well as the metal foil spectra are shown in Figures 4.6 and 4.7, respectively. Results clearly show that after H_2 treatment, both Ni and Co are partially reduced. In other words, both Ni and Co K-edge near edge spectra for each reduced catalyst are located between the metal foil and the calcined catalyst spectra.

XANES linear curve fitting of an unknown sample with the standard samples (metal foil and metal oxide) is a common procedure to provide more quantitative results of the extent of metal reduction. Therefore, Athena software was used to perform the linear combination fitting (LCF) in the range of -20 to +30 eV of the edge jump for each spectrum. The LCF results are summarized in Table 4.8. It must be noted that in LCF fitting of Co K-edge spectra, only CoO was used as cobalt the oxide standard. Co_2O_3 was not considered because it reduces to CoO at much lower temperature than 800 °C (Wang et al., 2013).

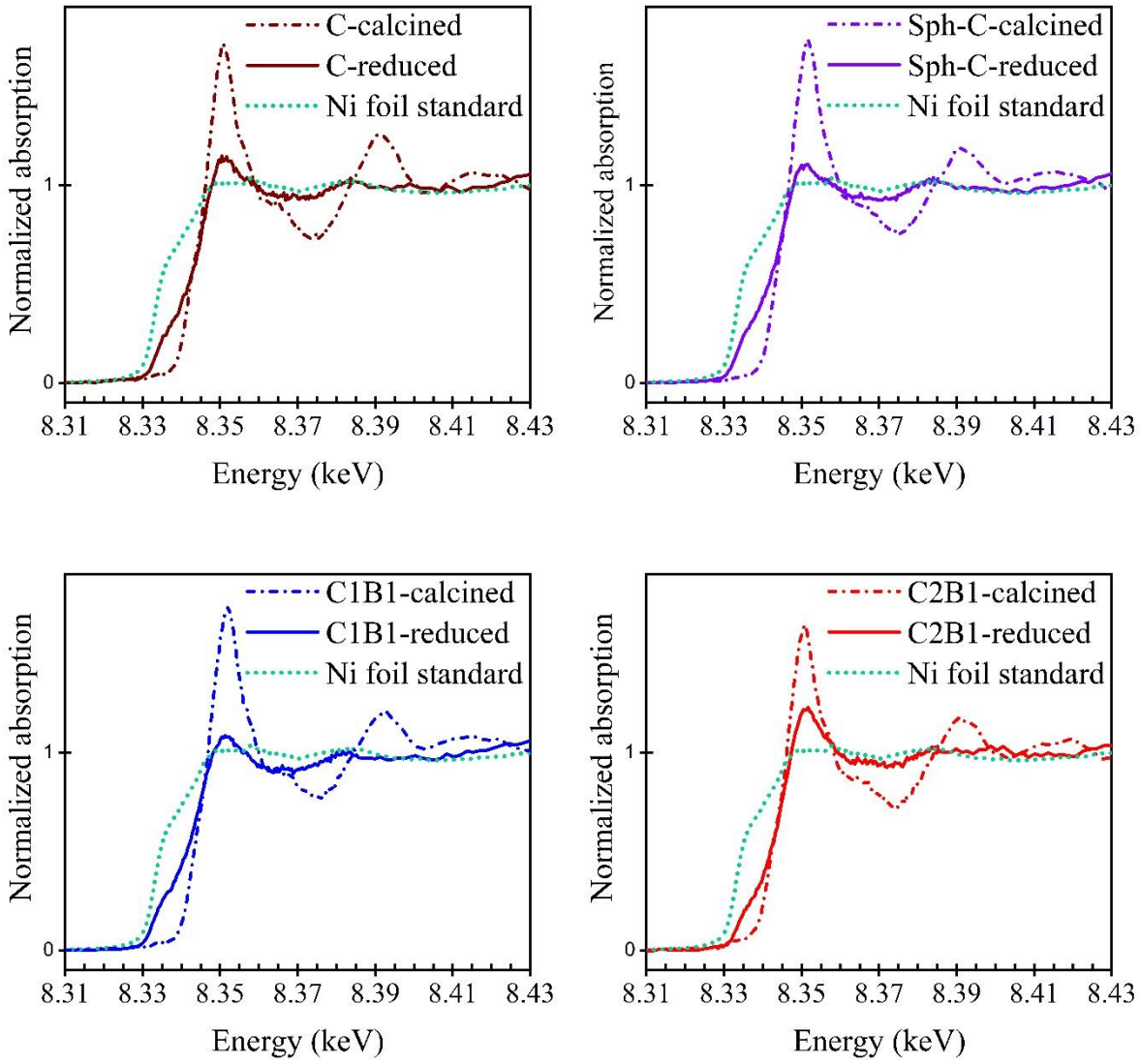

Figure 4.6 Ni K-edge XANES from 8.31 to 8.43 keV of metal foil, calcined catalysts, and catalyst samples reduced at 800 °C for 4 hr in 20% H_2/N_2

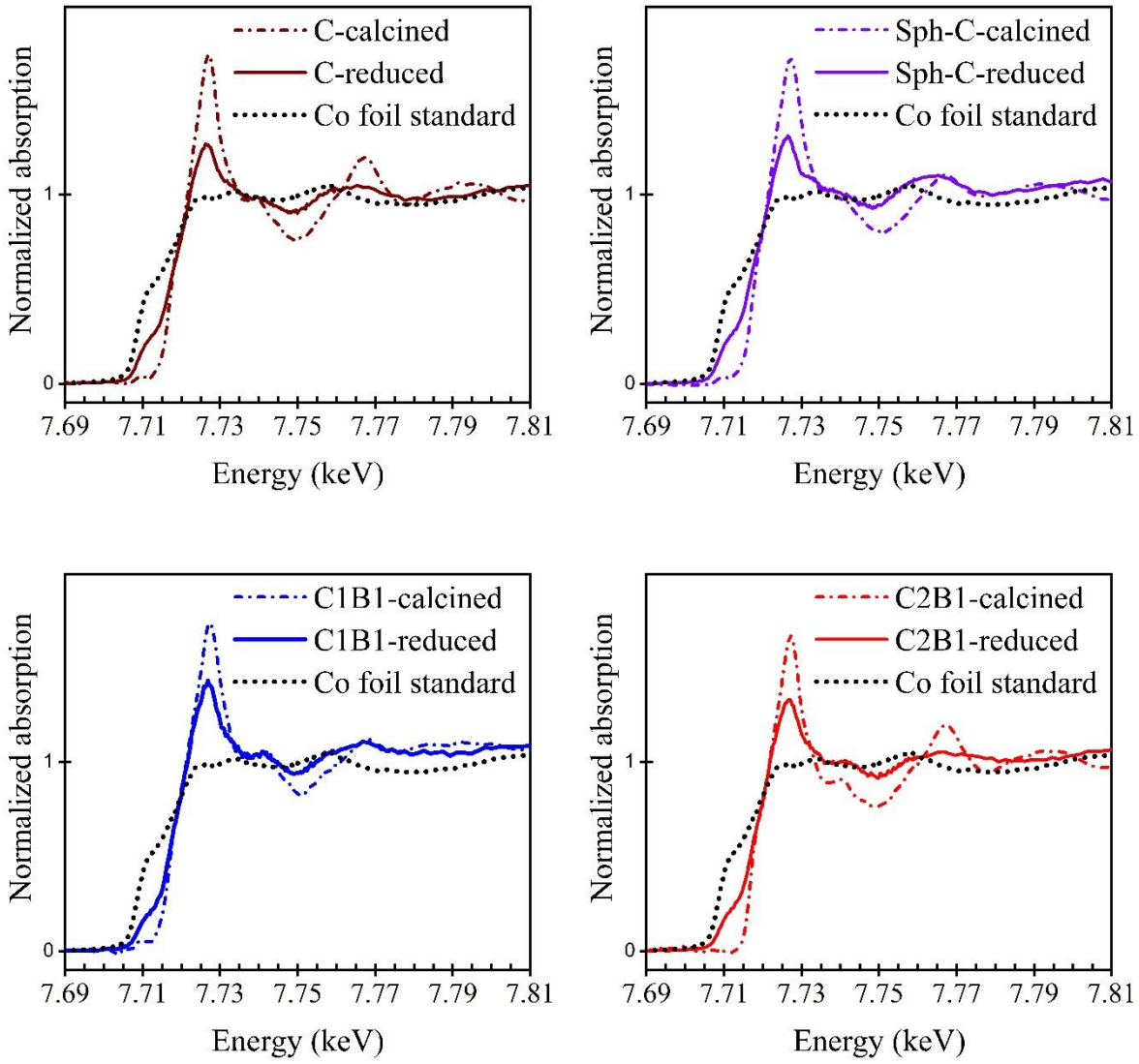

Figure 4.7 Co K-edge XANES from 7.69 to 7.81 keV of metal foil, calcined catalysts, and catalyst samples reduced at 800 °C for 4 hr in 20% H_2/N_2

Table 4.8 Metal oxide and metal extent in reduced catalysts calculated by linear combination fitting of XANES in the range of -20 to +30 eV of edge jump. Catalysts were reduced at 800 °C for 4 hr in 20% H_2/N_2

Catalyst	Catalyst to Boehmite ratio	Ni	NiO	Co	CoO
		%			
C1B1	1	80	20	17	83
C2B1	2	83	17	18	82
C	-	77	23	23	77
Sph-C	-	79	21	24	76

Table 4.8 reveals that Ni and Co reduction were in a range of 75–83 % and 17–24 %, respectively. It is clear that Ni was significantly reduced more than Co in all the catalyst samples. It is known that in the Ni-Co bimetallic catalyst, Co is more stable in oxide form than metallic form and therefore it is harder to reduce. This could explain the lower extent of reduction of Co than Ni (Wang et al., 2013). A closer look at the Ni and Co reduction in C, 1C1B, and 2C1B reveals that the addition of Boehmite has not significantly changed the reducibility of the catalysts (e.g., Ni and Co reduction in 1C1B were 80% and 17% and in 2C1B were 83% and 18%, respectively). Moreover, the LCF results show similar reduction of Ni and Co in C and Sph-C catalyst samples. This suggests that shaping the catalyst did affect its reducibility.

4.8 Conclusions

The prepared spherical catalysts, unlike the cylindrical ones, with and without the addition of Boehmite as binding material were comparably as strong as the commercial ones. Pore volume and average pore size of the shaped catalysts with the addition of Boehmite were larger than those of the Ni-Co bimetallic powder catalyst. However, the BET surface area (about 160 m^2/g) was not significantly changed. Formation of γ -alumina in Boehmite-containing samples at 850 °C calcination temperature could explain the higher pore volume and pore size of those samples. XRD patterns reveal that the higher the Boehmite content, the higher the aluminum-magnesium spinel phase and the lower the MgO phase. It seems that the Mg from the MgO phase interacted with the added alumina from Boehmite to form more spinel phase. The addition of Boehmite also provides extra support-metal interactions which could improve the metal dispersions in the prepared shaped catalysts. The physical process used to make cylindrical or spherical shapes, did not significantly change the catalyst's XRD patterns or metal dispersions. Finally, Ni and CO K-edge XANES reveals that the addition of Boehmite, shaping the catalyst, and catalyst geometry did not significantly affect the catalysts' reducibility. Ni and Co reduction extents of the shaped catalysts at 800 °C were about 80% and 20%, respectively.

CHAPTER 5

Performance of the Shaped Catalysts

Performance of cylindrical and spherical shaped catalysts for use in carbon dioxide reforming of methane reaction was investigated and compared with that of powdered Ni-Co/AlMgO_x bimetallic catalyst using the reactor set-up described in section 3.3. To compare, the performance of two different reforming catalysts (noted as catalysts X, and Y) from other resources were investigated under the same condition. Also, the catalytic performance compared with the equilibrium composition of the CRM reaction was calculated by using the HSC Chemistry software developed by Outotec.

5.1 Carbon Dioxide Reforming of Methane (CRM)

It should be noted that in all the experiments, unless mentioned, the catalysts were reduced in an Inconel reactor in a mixture of H_2 (50%) and N_2 (50%) for 4 hr. Then the CRM reaction was carried out with an equimolar ratio of reactant (CH_4/CO_2 = 1) balanced with N_2 and GHSV of 110 L g^{-1} hr^{-1}. The product gas was then analyzed using an online GC every 18 minutes. It also, should be restated that "C" stands for the powder form of the Ni-Co bimetallic catalyst prepared with a co-precipitation method.

5.1.1 Performance of Powder Catalyst

A mixture of 0.1 g of catalyst C and 4 g of silica carbide was reduced at 800 °C for 4 hr and CRM reaction was then carried out at 800 °C, 850 °C, and 900 °C. The consumption rate of

reactants and H_2/CO ratio in the product gas at 800 °C, 850 °C, and 900 °C are shown in Figure 5.1. Regardless of the reaction temperature, a stable catalytic performance for the CRM reaction was observed. It is well known that the CRM reaction is highly endothermic and more favourable at high temperatures (Wang et al., 1996). This could explain both higher activity and selectivity of the catalyst for CRM at higher temperatures (900 °C > 850 °C > 800 °C). Also, a larger difference between consumption rate of reactants and a lower H_2/CO ratio at 800 °C than 850 °C and 900 °C was observed. The occurrence of the reverse water-gas shift (RWGS) reaction can explain these phenomena (Ghoneim et al., 2016). Figure 5.1 (d) also indicates that the H_2/CO ratio in the product gas was oscillating versus time-on-stream at all the temperatures. A periodic cycle of carbon deposition and elimination on catalysts during the CRM reaction could be the possible explanation for this phenomenon (Wei et al., 2000). Richardson (1989) also suggested that this periodic carbon deposition and elimination could be effective to stabilize the catalytic performance for methane reforming reactions.

The catalytic performance of two other reforming catalysts (noted as X and Y) for the CRM reaction was investigated at various temperatures. The CRM experimental conditions were the same as those used for catalyst C (Ni-Co bimetallic), as described earlier in this section. The reaction results in terms of CH_4 and CO_2 conversions and H_2/CO ratio in the product gas for catalysts X, Y, and C are summarized in Table 5.1. It reveals that both catalysts X and C showed higher CH_4 and CO_2 conversions (7% more for each reactant) than those for catalyst Y at 800 °C. It is also clear that every catalyst showed higher conversion of CO_2 than CH_4 and a lower H_2/CO ratio than unity at 800 °C. The occurrence of the RWGS reaction can explain these phenomena (Ghoneim et al., 2016). Table 5.1 also indicates that the catalysts facilitated similar activity for CRM at 850 °C and 900 °C. At higher temperatures, the differences between CO_2 and CH_4 conversion became insignificant and the produced H_2/CO ratio was closer to one. These imply a lower effect of RWGS reaction at 900 °C for all the catalysts. It could be concluded that the Ni-Co bimetallic catalyst (C) facilitates CRM reaction similar to catalysts X and Y.

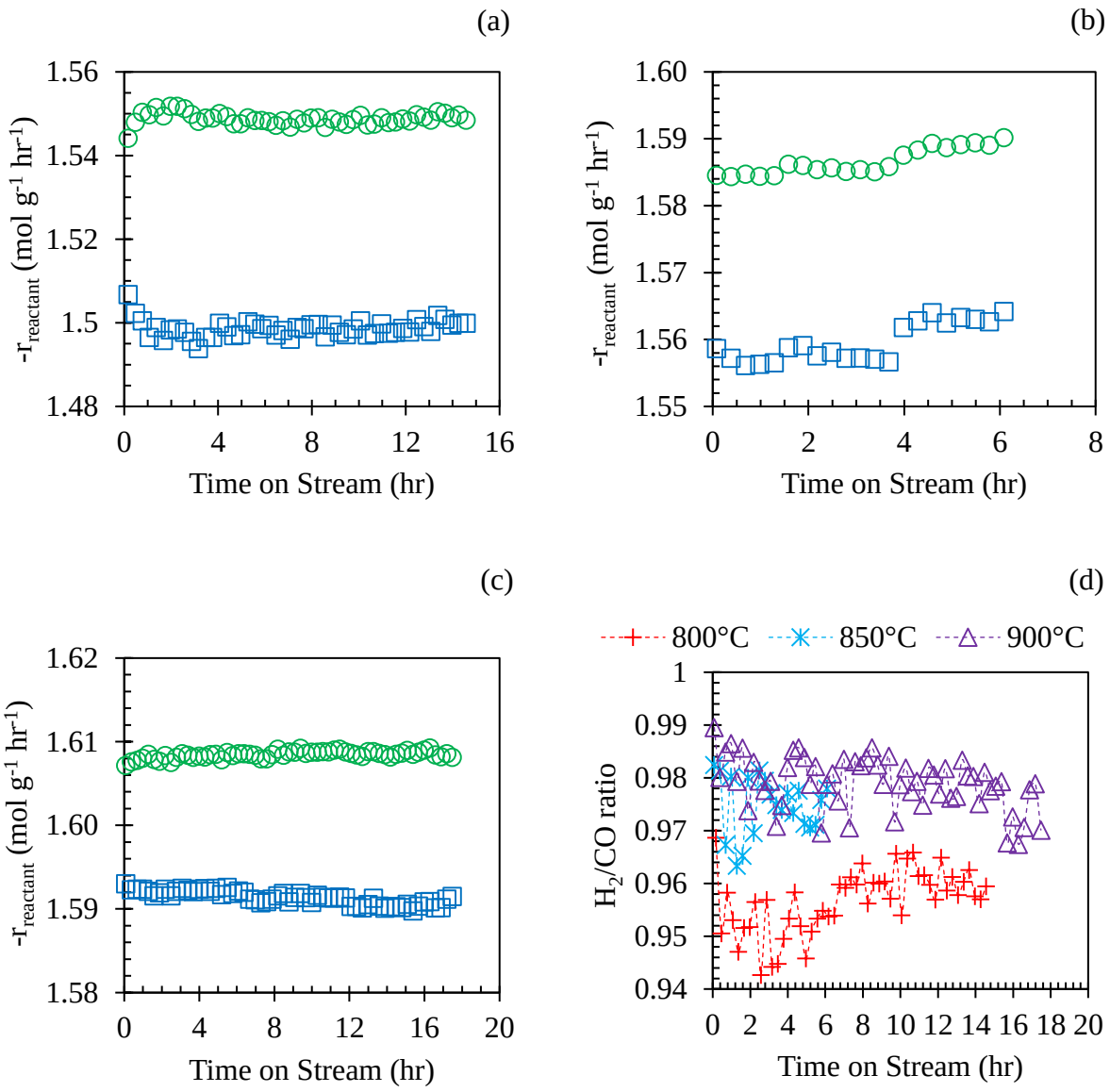

Figure 5.1 Consumption rate of reactants (CO_2 ○ and CH_4 □) using Ni-Co bimetallic powder catalyst for CRM reaction at (a) 800 °C, (b) 850 °C, (c) 900 °C, and (d) H_2/CO ratio of the product gas. Reaction conditions: 0.10 g catalyst, temperatures: 800 °C, 850 °C and 900 °C, 1atm, GHSV of 110 L g^{-1} hr^{-1}, $CH_4/CO_2/N_2$ = 1/1/1

Table 5.1 CRM test results over catalysts C, X and Y. Reaction conditions: 0.10 g catalyst, temperatures: 800 °C, 850 °C and 900 °C, 1atm, GHSV of 110 L g^{-1} hr^{-1}, $CH_4/CO_2/N_2$ = 1/1/1

Temperature	800 °C			850 °C		900 °C		
Catalyst	X	Y	C	Y	C	X	Y	C
CH_4 Conversion (%)	90.5	83.2	91.2	95.3	94.9	96.7	97.8	96.8
CO_2 Conversion (%)	93.1	87.4	93.5	95.9	95.8	97.0	97.4	97.1
(H_2/CO) ratio	0.92	0.93	0.95	0.99	0.97	0.95	0.98	0.98
TOS (hr)	10	50	14	18	6	10	23	17

To further investigate the catalytic performances for CRM, HSC chemistry software was used to simulate the equilibrium composition of CRM with conditions identical to these experiments. Then, theoretical CH_4 and CO_2 conversions as well as H_2/CO ratio in the product gas for the CRM reaction were calculated. Figure 5.2 compares the calculated theoretical values with obtained experimental values for CRM reaction over catalysts C, X, and Y. If the products are not removed within the catalyst bed, the theoretical conversions are the maximum values that could be achieved in an experiment. The results show that regardless of the catalyst used, reactant conversions are close to, but never exceed, the theoretical values for CRM reaction at all the temperatures. Moreover, a higher value of H_2/CO ratio in catalyst Y suggests that catalyst Y facilitates the RWGS reaction more than the other catalysts.

5.1.2 Performance of Extrudate Catalyst

The performance of extrudate catalysts, Ext-C, Ext-C1B1, Ext-C1B2, and Ext-X, for CRM reaction was investigated and compared to catalytic performance of Ni-Co powered catalyst (catalyst C). In each experiment, a mixture of 0.1 g of catalyst sample and 2 g of silica carbide was reduced in an Inconel reactor followed by CRM reaction carried out at 800 °C. The consumption rate of CO_2 and CH_4 as well as the selectivity in terms of H_2/CO ratio are shown in Figure 5.3. To facilitate comparison, Ni and Co content of the catalysts, overall reactant conversions, X_{CH_4}/X_{CO_2} and H_2/CO ratios in the product gases along with the theoretical calculated values for CRM reaction at 800 °C are given in Table 5.2.

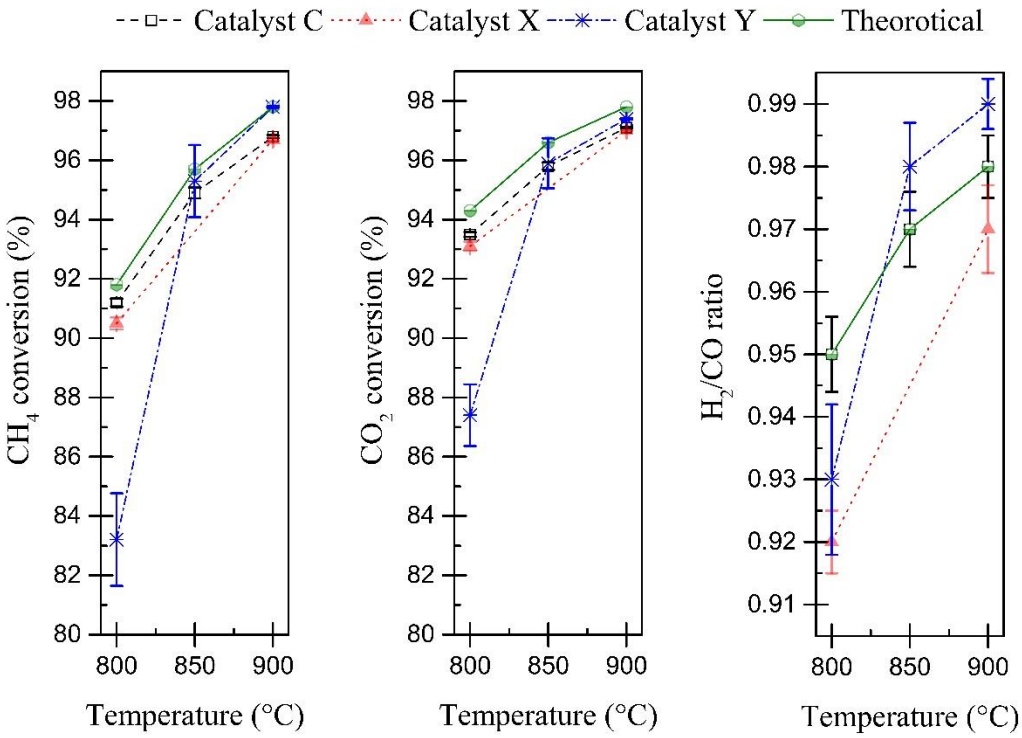

Figure 5.2 Theoretical and experimental values for CH_4 and CO_2 conversions as well as H_2/CO ratio in the product for CRM reaction over C, X, and Y catalysts. Reaction conditions: 0.10 g catalyst, temperatures: 800 °C, 850 °C and 900 °C, 1atm, GHSV of 110 L g^{-1} hr^{-1}, $CH_4/CO_2/N_2$ = 1/1/1. Error bar shows the 95 % confidence intervals.

Figure 5.3 illustrates that catalytic performances of all the catalysts for CRM were stable and that the consumption rate of CO_2 was higher than that of CH_4. The occurrence of RWGS reaction could explain this phenomenon. CO_2 and CH_4 consumption rates as well as H_2/CO ratios in the product gases followed the order of C > Ext-C ≈ Ext-C1B1 > Ext-C1B2 ≈ Ext-X. Reaction results, shown in Table 5.2 and Figure 5.3, indicate that catalyst C facilitated the highest activity, for which the CO_2 and CH_4 conversions were steadily at 91.2 % and 93.5 % for 14 hr TOS, respectively. Ext-C and Ext-C1B1 catalysts showed comparable activity (82.4 % CH_4 and 87.3 % CO_2 conversions) and remained at this level for 13 hr and 15 hr TOS, respectively. Ext-C1B2 and Ext-X catalysts facilitated CRM similarly, while showing the lowest CH_4 and CO_2 conversions at 77.8 % and 84.3 %, respectively. It should be noted that the cylindrical catalysts' reactant conversions for CRM were 10% to 15% lower than those of theoretical values and they facilitated lower CH_4 and CO_2 conversions than the loose powder catalyst (catalyst C). Mass transfer limitations could be a possible explanation for this phenomenon however it is yet to be further investigated.

The selectivity results indicate that the average ratio of H_2 to CO for the tested catalysts ranged from 0.86 to 0.95 which suggests the occurrence of RWGS reaction. The lowest X_{CH_4}/X_{CO_2} ratio and a closer H_2/CO ratio to one in the product gas for catalyst C could also indicate the lower effect of RWGS reaction over this catalyst than the cylindrical ones.

To further investigate the effect of Boehmite on the performance of the catalysts for CRM reaction, Figure 5.4 compares the activity of the cylindrical catalysts made with various Boehmite to powder catalyst (B/C) ratios. Both Ext-C and Ext-C1B1 catalysts facilitated similar activity for CRM reaction, suggesting that the addition of Boehmite to Ext-C catalyst did not significantly change the activity. However, when the B/C ratio rose to 2 in Ext-C1B2, a 5% drop in both CO_2 and CH_4 conversions were obtained. In catalytic reactions, all the active catalyst sites may not be used by reactants. On the other hand, for robust catalyst activity, the presence of a certain number of active sites is necessary. For these reasons, the lower activity level of Ext-C1B2, as compared with Ext-C1B1 and Ext-C, could be explained by the decrease in number of available active sites.

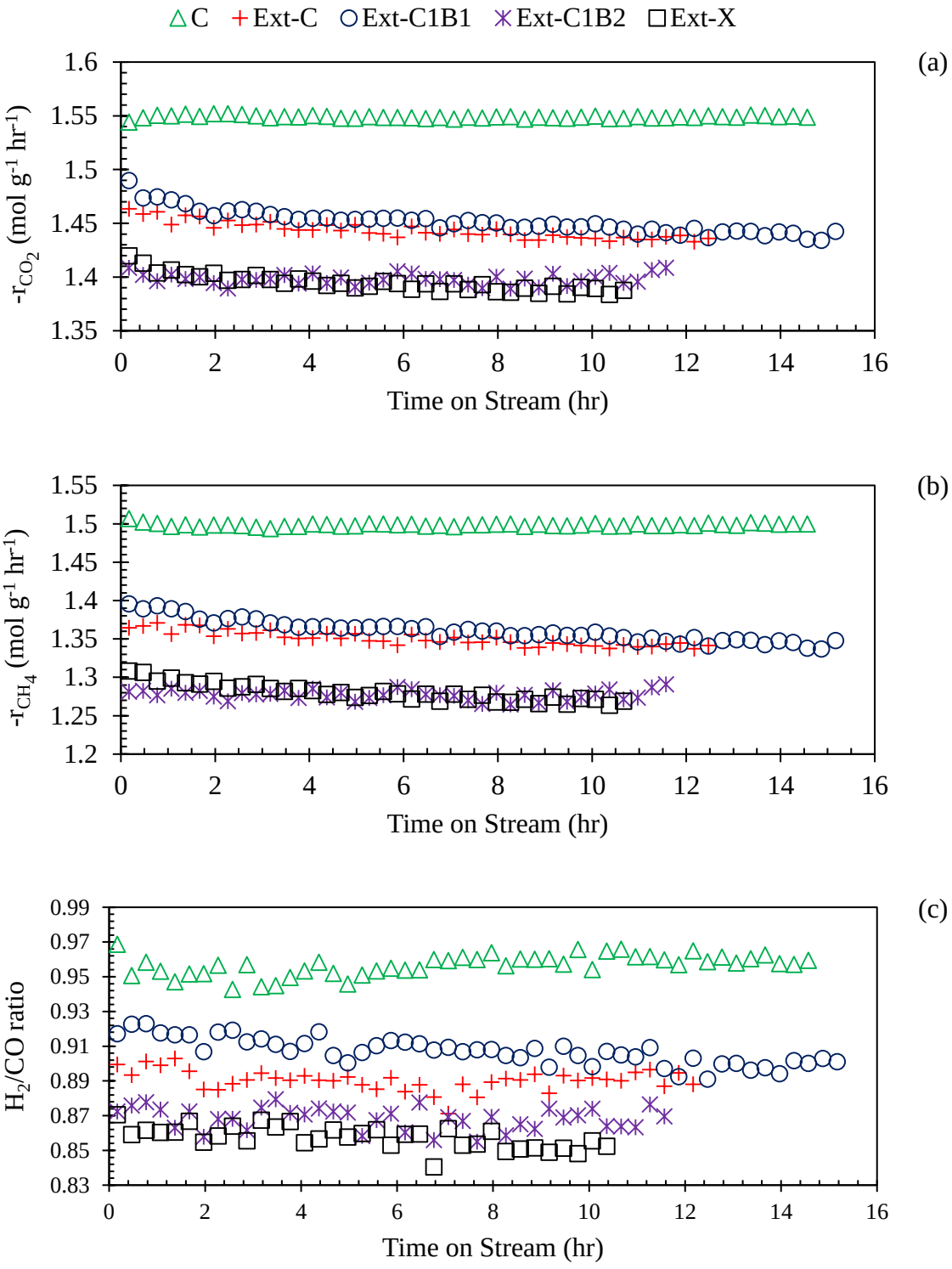

Figure 5.3 (a) CO_2 consumption rate, (b) CH_4 consumption rate, and (c) produced H_2/CO ratio from CRM reaction over cylindrical catalysts. Reaction conditions: 0.10 g catalyst, 800 °C, 1atm, GHSV of 110 L g^{-1} hr^{-1}, $CH_4/CO_2/N_2$ = 1/1/1

Table 5.2 CRM reaction results over C, Ext-C, Ext-C1B1, Ext-C1B2 and Ext-X catalysts. Reaction conditions: 0.10 g catalyst, 800 °C, 1atm, GHSV of 110 L g^{-1} hr^{-1}, $CH_4/CO_2/N_2$ = 1/1/1

Catalyst	C	Ext-C	Ext-C1B1	Ext-C1B2	Ext-X	Theoretical*
CH_4 Conversion (%)	91.2	82.3	82.5	77.7	77.9	91.8
CO_2 Conversion (%)	93.5	87.3	87.4	84.4	84.2	94.3
TOS (hr)	14	13	15	12	11	-
(X_{CH_4}/X_{CO_2}) ratio in product gas	1.35	1.39	1.39	1.42	1.39	-
Produced (H_2/CO) ratio	0.95	0.89	0.90	0.87	0.86	0.95
Ni content (wt%)**	2.7	2.7	1.4	0.9	-	-
Co content (wt%)**	4.8	4.8	2.4	1.6	-	-

* Theoretical values were calculated from equilibrium compositions using the HSC Chemistry software.

** Calculated from ICP results given in section 4.1 using equations 4.1 and 4.2

We know that with the addition of Boehmite, the Ni and Co contents were decreased however, the observed reaction rates were not significantly changed. To investigate the performance of the catalysts based on the site activity, Turnover Frequency (TOF) could be used (Boudrat, 1995). TOF is defined as the total number of moles of reactant converted through reaction by one mole of active catalyst site per unit of time. Therefore, TOF could be calculated from equation (5.1).

$$TOF = \frac{-r_A}{total\ mole\ of\ active\ sites\ per\ gram\ of\ catalyst} \quad (5.1)$$

where, $-r_A$ is reaction the rate in terms of reactant A (mol g^{-1} (unit of time)$^{-1}$). Consequently, one TOF unit would be (unit of time)$^{-1}$.

It is believed that in the Ni-Co bimetallic catalyst, both metallic Ni and Co sites are the active sites for CRM reaction (Zhang et al., 2007). The total mole of active sites in equation 5.1 could be calculated using two approaches: (1) the Ni and Co metal contents and their corresponding reduction extents, and (2) the amount of CO adsorbed by the catalysts obtained from CO chemisorption analysis. In the first approach the assumptions are that all the reduced sites equally takes part in facilitation of the reaction. In the second approach, it was assumed that the adsorption of CO molecules on the active sites was linear and the CO adsorption at STP condition (standard condition for temperature and pressure) was followed the monolayer adsorption model. Therefore, the number of adsorbed CO molecules could be used to estimate the number of available active sites (Ni and/or Co metallic sites) on the catalyst's surface. Moreover, in both approaches, it was assumed that the size of active sites (Ni and Co metallic sites) were the same in all the catalysts and all sites had similar activity toward CRM reaction. Thus, TOF_{red} (first approach) and TOF_{CO} (second approach) could be calculated using equations 5.2 and 5.3, respectively.

$$TOF_{red} = \frac{-r_A}{(moles\ of\ Ni\ content) \times (Ni\ reduction\ extent) + (moles\ of\ Co\ content) \times (Co\ reduction\ extent)} \quad (5.2)$$

where, metal contents and their reduction extent obtained from ICP-MS and XANES of the reduced catalysts, respectively (sections 4.1 and 4.6).

$$TOF_{CO} = \frac{-r_A}{(moles\ of\ adsorbed\ CO\ on\ the\ catalyst\ surafce)} \quad (5.3)$$

where, moles of adsorbed CO for each catalysts were obtained from CO chemisorption analysis (section 4.6).

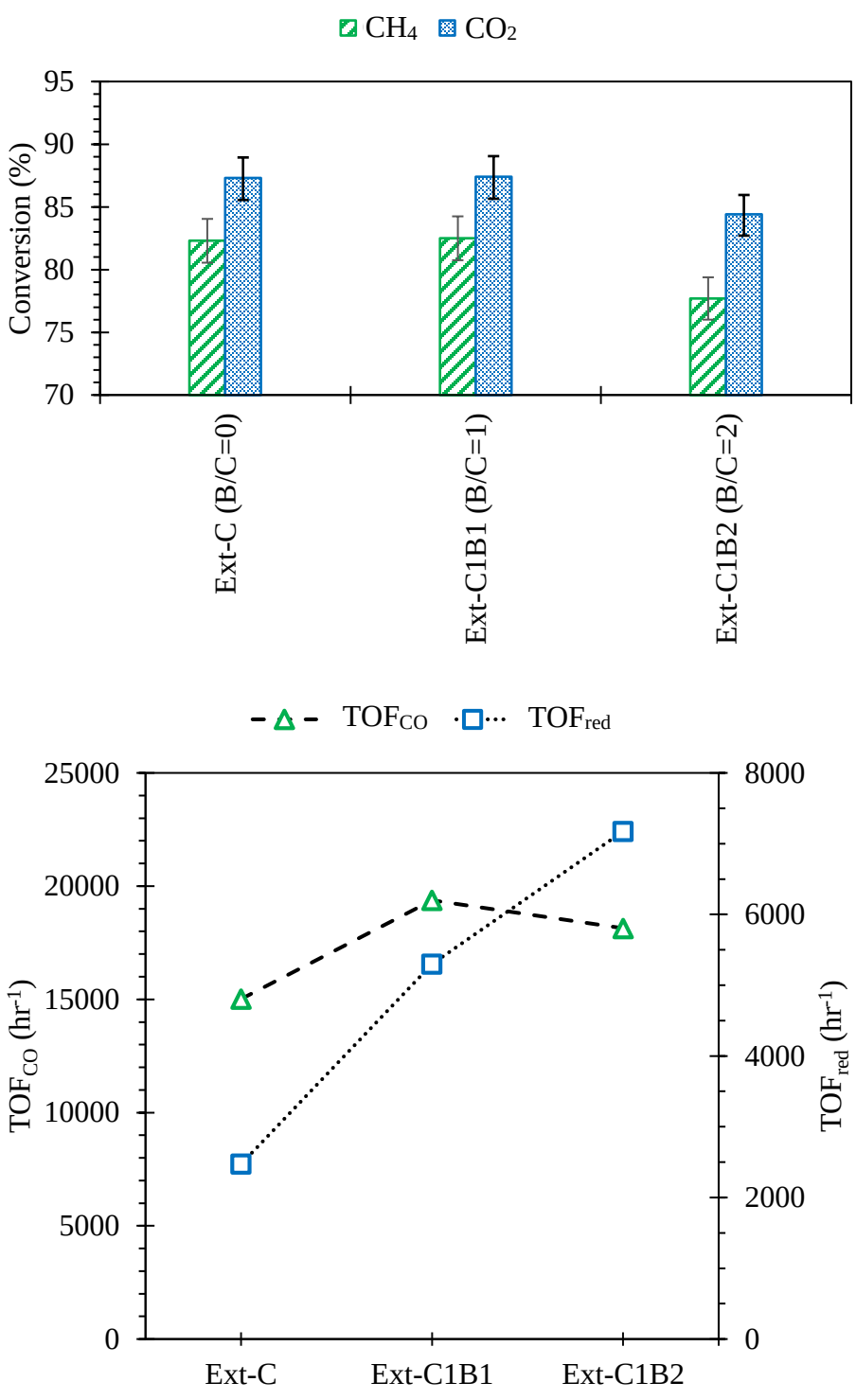

Figure 5.4 (a) Activity and (b) TOF_{CO} and TOF_{red} of cylindrical catalysts for CRM over Ext-C (B/C=0), Ext-C1B1 (B/C=1), and Ext-C1B2 (B/C=2). Reaction conditions: 0.10 g catalyst, 800 °C, 1atm, GHSV of 110 L g^{-1} hr^{-1}, $CH_4/CO_2/N_2$ = 1/1/1. Error bar shows the 95 % confidence intervals.

TOF_{red} and TOF_{CO} for each cylindrical catalyst were calculated and are summarized in Table 5.3 and Figure 5.4 (b). The results reveal that both TOF_{red} and TOF_{CO} were enhanced with the addition of Boehmite from Ext-C to Ext-C1B1. Although the TOF_{CO} was slightly decreased when more Boehmite was added (Ext-C1B2). Lower Ni and Co content, similar metal reduction extents, a better dispersion of active sites, and comparable reaction rates in the catalysts with higher Boehmite content could explain the increase of TOF_{red} in these catalysts. Also, TOF_{red} was always about 20 to 30 times smaller than the TOF_{CO} for each catalyst. This is likely because all the reduced metals (active sites) were not presented on the surface therefore, the denominator in equation 5.2 was always greater than that in equation 5.3 leading to higher calculated value of TOF_{CO} than that of TOF_{red}.

An increase of TOF_{CO} in the Boehmite containing catalysts (Ext-C1B1 and Ext-C1B2) implies that the available metallic sites on the surface of these catalysts were different than the ones on the Ext-C catalysts. It seems that the earlier sites were more active toward CH_4 dissociation. Zhang (2008) reported that CH_4 dissociation on the metallic sites is the rate limiting step of CRM reaction over Ni-Co bimetallic catalyst. In our previous work, it was also found that the Ni sites are more active toward CH_4 dissociation and bimetallic catalysts with higher Ni content than Co could better facilitate CRM reaction (Shakouri, 2012; Zhang, 2008). Putting the parcels together, it seems that more Ni sites, in presence of Boehmite and during the second calcination, could be presented on the reduced catalyst's surface resulting in more effective performance of active sites for CRM reaction and a higher TOF_{CO} in Ext-C1B1 and Ext-C1B2 than Ext-C catalyst.

In summary, cylindrical catalysts facilitated CRM reaction similarly and the addition of Boehmite (to some extent); (a) did not significantly change the catalytic performance, (b) enhanced the metal sites dispersion, (c), improved the efficiency of the metal-active sites for CRM reaction and (d) a smaller amount of Ni-Co catalysts would be required to prepare an industrial cylindrical pellet. However, a cost estimation for large scale production of Ni-Co/$AlMgO_x$ catalyst and Boehmite should be conducted prior commercialization.

Table 5.3 Turnover Frequency of Ext-C, Ext-C1B1, and Ext-C1B2 catalysts for CRM reaction. Reaction conditions: 0.10 g catalyst, 800 °C, 1atm, GHSV of 110 L g^{-1} hr^{-1}, $CH_4/CO_2/N_2$ = 1/1/1.

	Ext-C	Ext-C1B1	Ext-C1B2
$-r_{CH_4}$ (mmol g^{-1} hr^{-1})	1352	1356	1277
Ni content (mmol/g)	0.47	0.23	0.16
Co content (mol/g)	0.82	0.41	0.27
Ni reduction extent (%)	77	80	83
Co reduction extent (%)	23	17	18
Total reduced metal content (mmol/g)	0.55	0.26	0.18
TOF_{red} (hr^{-1})	2500	5300	7200
CO adsorbed (mmol/g)	0.09	0.07	0.07
TOF_{CO} (hr^{-1})	15000	19400	18100

5.1.3 Performance of Spherical Catalyst

A mixture of 0.1 g Sph-C (spherical catalyst made from Ni-Co/$AlMgO_x$ powder), with average diameter of 3.5 mm (standard error = 0.15 mm), and 0.4 g of silicon carbide sand was reduced in an Inconel reactor and then used for CRM reactions with equimolar reactants at 800 °C, 850 °C, and 900 °C. The consumption rate of CO_2 and CH_4 and the H_2/CO ratio in the product gases are shown in Figure 5.5. CH_4 and CO_2 conversions as well as the CH_4/CO_2 ratio in the product gases are summarized in Table 5.4. Also, to further investigate the performance of Sph-C catalyst, Figure 5.6 compares experimental CRM reaction results over Sph-C and C catalysts with those of calculated theoretical values.

Figure 5.5 reveals that the performance of Sph-C was stable at all reaction temperatures while the catalytic activity and selectivity were improved at elevated reaction temperatures. It was also observed that like catalyst C (powder catalyst), CO_2 was consumed more than CH_4 at all reaction temperatures. However, the higher the reaction temperature, the higher the difference between CO_2 and CH_4 consumption rates. For instance, the observed difference between CO_2 and CH_4 consumption rates was about 0.11 mol g^{-1} hr^{-1} at 800 °C while it raises to about 0.17 mol g^{-1} hr^{-1} at 900 °C. Moreover, Table 5.4 indicates that the higher the reaction temperature the higher the H_2/CO and CH_4/CO_2 ratios in the product gas. On the other hand, Figure 5.6 shows that the catalytic performance of Sph-C was significantly lower than that of C and theoretical values under identical reaction conditions. Putting the parcels together, the occurrence of RWGS reaction could be one possible explanation for these phenomena. However, the weak catalytic activity of Sph-C compared with that of powder catalyst implies that mass transfer limitations are suspected when using the spherical shaped catalysts, which needs to be further investigated.

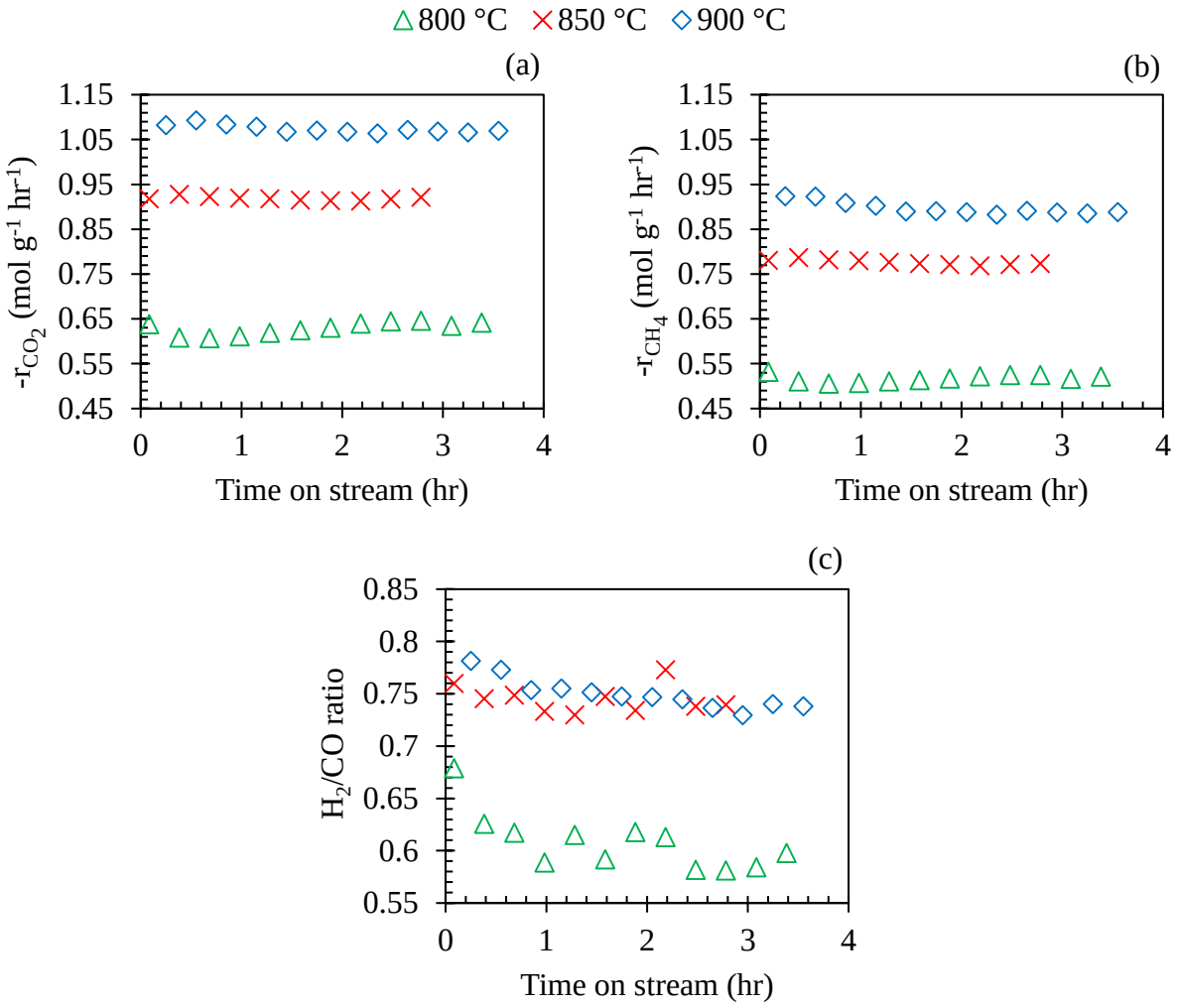

Figure 5.5 Consumption rate of (a) CO_2, (b) CH_4, and (c) H_2/CO ratio in the product gas using Sph-C catalyst for CRM reaction. Reaction conditions: 0.10 g catalyst, 800 °C, 850 °C and 900 °C, 1atm, GHSV of 110 L g^{-1} hr^{-1}, $CH_4/CO_2/N_2$ = 1/1/1

Table 5.4 CRM reaction results over Sph-C catalysts. Reaction conditions: 0.10 g catalyst, 800 °C, 850 °C and 900 °C, 1atm, GHSV of 110 L g^{-1} hr^{-1}, $CH_4/CO_2/N_2$ = 1/1/1

Temperature	800 °C	850 °C	900 °C
CH_4 Conversion (%)	31.5	47.2	54.7
CO_2 Conversion (%)	37.9	55.4	64.7
TOS (hr)	3.5	3	3.5
(X_{CH_4}/X_{CO_2}) ratio in product gas	1.10	1.18	1.28
Product (H_2/CO) ratio	0.61	0.74	0.75

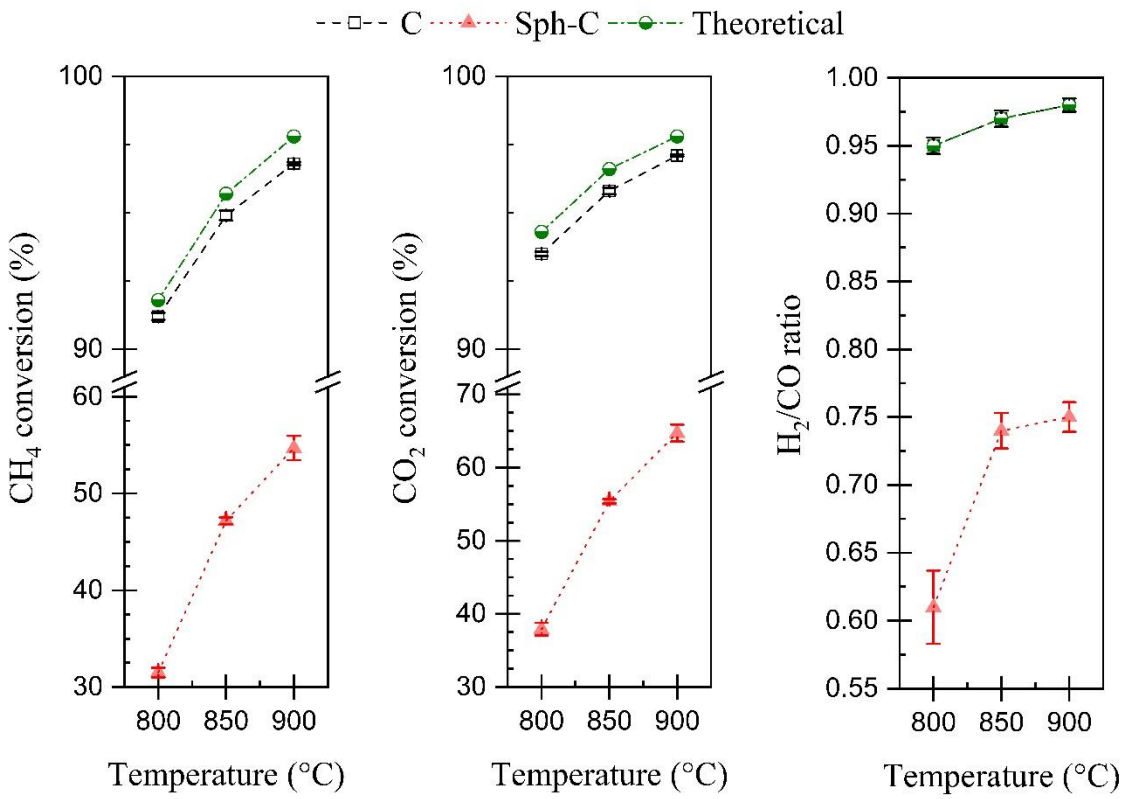

Figure 5.6 Theoretical and experimental values for CH_4 and CO_2 conversions as well as H_2/CO ratio in the product for CRM reaction over C, and SC catalysts. Reaction conditions: 0.10 g catalyst, 800 °C, 850 °C and 900 °C, 1atm, GHSV of 110 L g^{-1} hr^{-1}, $CH_4/CO_2/N_2$ = 1/1/1. Error bar shows the 95 % confidence intervals.

5.2 Effect of Flow Rate and Partial Pressure of Reactants on Performance of Shaped Catalysts for CRM

It was observed that the addition of Boehmite to shape the catalyst did not significantly affect their (a) extent of reduction (section 4.6), (b) mechanical strength (section 4.3), and (c) the catalytic performance for CRM reaction (section 5.1). Thus, cylindrical and spherical catalysts (Ext-C and Sph-C) without Boehmite, prepared from Ni-Co/$AlMgO_x$ catalyst, were chosen for further investigation.

5.2.1 Effect of Gas Hour Space Velocity (GHSV) on Performance of Shaped Catalysts for CRM

The catalytic activities of Ext-C (cylindrical) and Sph-C (spherical) for CRM reaction were tested at 800 °C with equimolar reactant ratios using various GHSVs. Figure 5.7 displays both CH_4 and CO_2 consumption rates and conversions as a function of GHSV over the Ext-C catalyst sample. Results show that under the given conditions when the GHSV elevated, the increase of reaction rates and decrease of reactant conversions were coupled. Moreover, a larger difference between CO_2 and CH_4 consumption rates as well as a lower H_2/CO ratio in the product gas at higher GHSV suggest that the effect of RWGS becomes more significant at higher GHSV.

A closer look at the results indicates that the increase of consumption rates did not follow the same order as the GHSV. As an example, when GHSV doubled from 110 to 220 L g^{-1} hr^{-1}, the CH_4 rate was only raised from 1.35 to 1.90 mol g^{-1} hr^{-1}. A lower residence time of the reactants in the catalyst bed as well reduced accessibility of the reactants to the constant number of active catalyst sites at higher GHSV could be possible explanations for these phenomena. Consequently, CH_4 and CO_2 conversions were decreased while the GHSV was increased for CRM reaction over Ext-C catalyst.

In the case of Sph-C catalyst, it was earlier observed that under the same reaction conditions, Sph-C facilitated CRM reaction much less than Ext-C and powder catalysts (Table 5.2 and Table 5.4). Therefore, for Sph-C tests, smaller values of GHSV, as shown in Figure 5.8, were chosen than for Ext-C catalysts. Figure 5.8 indicates that the effect of GHSV on the performance of Sph-C catalyst was similar to that of Ext-C catalyst. With the increase of GHSVs from 36.7 to

110 L g^{-1} hr^{-1}, reactant consumption rates improved while the conversions decreased. Results also show that both CH_4 and CO_2 were similarly consumed at GHSV of 36.7 L g^{-1} hr^{-1} while at higher GHSVs, more CO_2 were consumed than CH_4. This could suggest that the effect of the RWGS reaction was minimal at GHSV of 36.7 L g^{-1} hr^{-1}. On the other hand, the H_2/CO ratio in the product gas was decreasing when GHSV values were increasing. This observation could further support the possibility of reduced occurrence of RWGS reaction at 36.7 L g^{-1} hr^{-1} than at the higher values.

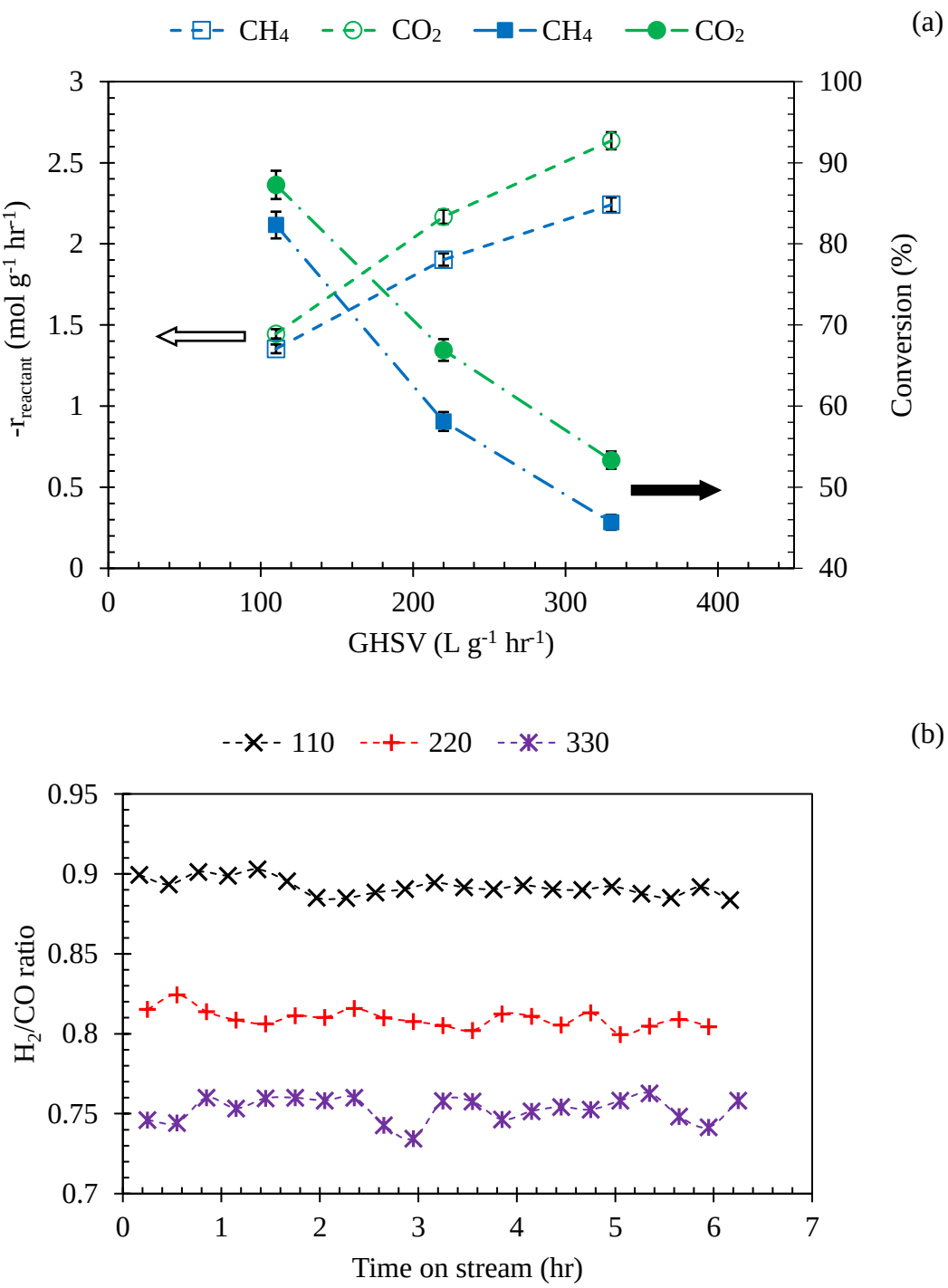

Figure 5.7 Effect of GHSV on the (a) reaction rates and conversions of CH_4 and CO_2 and (b) produced H_2/CO ratio over Ext-C catalyst for CRM. Reaction conditions: 0.10 g catalyst, temperature: 800 °C, 1atm, $CH_4/CO_2/N_2$ = 1/1/1, GHSV 110, 220 and 330 L g^{-1} hr^{-1}. Error bar shows the 95 % confidence intervals.

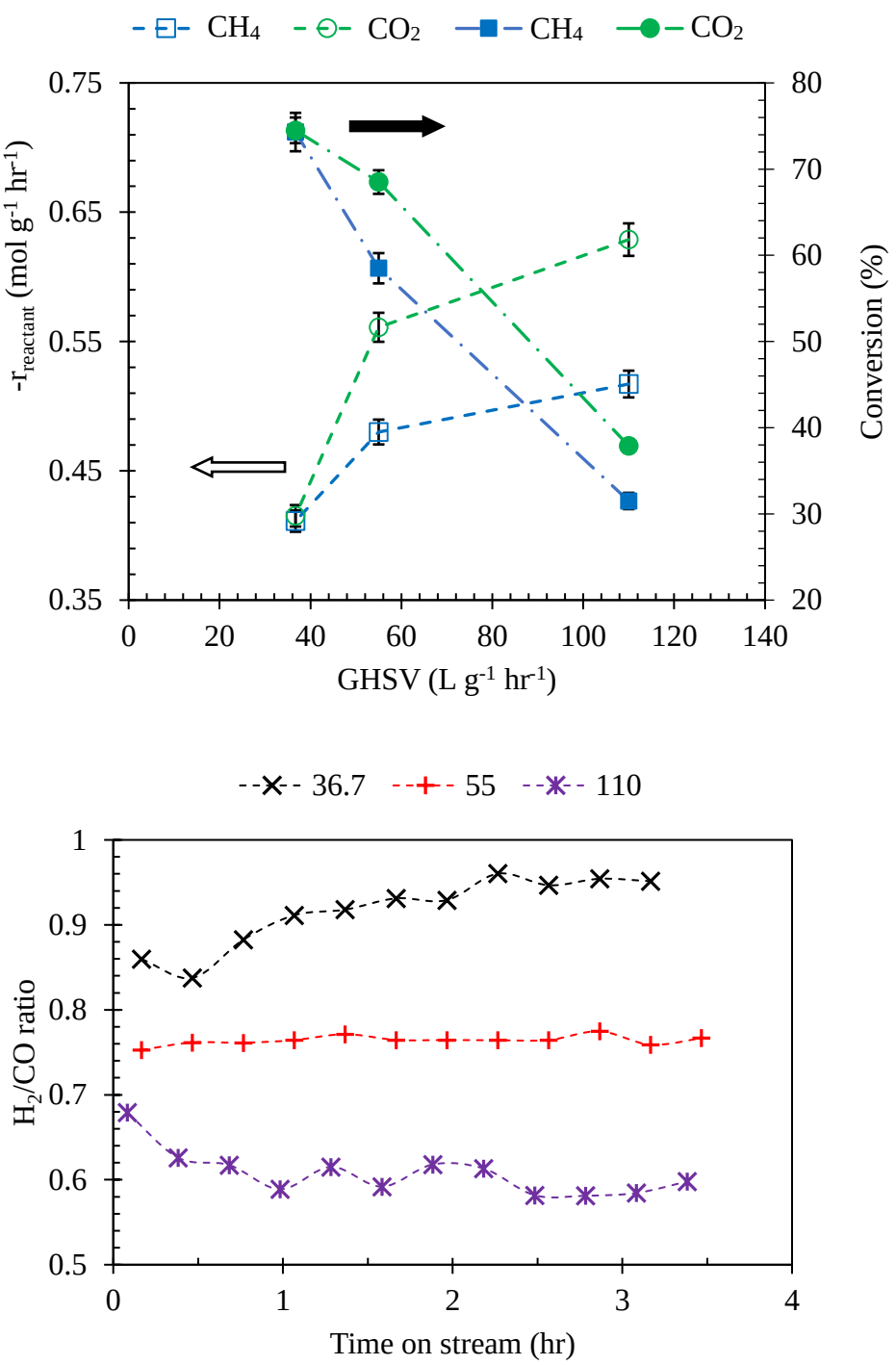

Figure 5.8 Effect of GHSV on the (a) reaction rates and conversions of CH_4 and CO_2 and (b) produced H_2/CO ratio over Sph-C catalyst for CRM. Reaction conditions: 0.10 g catalyst, temperature: 800 °C, 1atm, $CH_4/CO_2/N_2$ = 1/1/1 GHSV 36.7, 55 and 110 L g^{-1} hr^{-1}. Error bar shows the 95 % confidence intervals.

5.2.2 Effect of CH_4/CO_2 on Performance of Sph-C Catalyst for CRM

A 0.15 g of Sph-C catalysts with average diameter of 3.5 mm mixed with 0.4 g of silicon carbide sand was reduced in a quartz reactor (ID = 0.125 inch). CRM reaction at 800 °C was then carried out with various CH_4/CO_2 ratios in the feed and GHSV of 110 L g^{-1} hr^{-1}. Literature suggested that the effect of RWGS reaction on CRM reaction over Ni-based catalysts could be minimized by operating with a lower than stoichiometric CH_4/CO_2 ratio (Luyben, 2014; Lavoie, 2014; Tsai and Wang, 2008). Moreover, an industrial partner of this project requested the catalyst be tested with a CH_4/CO_2 ratio of 1.35 for CRM reaction. Therefore, CH_4/CO_2 ratios of 0.8, 1 and 1.35 were used for the performance tests. Figure 5.9 shows that with each increase of methane content, CH_4 conversions followed the order of $CH_4/CO_2 = 0.8 > 1 > 1.35$ while conversion of CO_2, which was always higher than that of CH_4, followed the reverse order. In other words, the higher the CH_4/CO_2 ratio the lower the CH_4 conversion and the higher the CO_2 conversion. Availability of more CH_4 and therefore more chance of CH_4 molecules to react with CO_2 through the CRM reaction could be one possible explanation for these observations. It was also observed that with each increase of CH_4/CO_2 ratio in the feed, H_2/CO ratio enhanced in the product gas as well. The main possible side reactions that could produce H_2 during CRM are (a) Water Gas Shift reaction (WGS) and (b) CH_4 dissociation to carbon and H_2. Since both CO_2 and H_2 production increased with each increase of the CH_4/CO_2 ratio, therefore the likelihood of WGS could discounted. It seems that in a feed with higher a CH_4/CO_2 ratio, an excess amount of CH_4 dissociated to form H_2, leading to an increase of the H_2/CO ratio, and carbon which could later deactivate the catalyst. It is reasonable to conclude that over Sph.-C catalyst, a CH_4/CO_2 feed ratio of 0.8 could lower the effect of side reaction(s) during CRM reaction at 800 °C.

Over Sph-C catalyst for 6 hours' TOS, 73% (±1) CH_4 conversion, 81% (±1) CO_2 conversion and 0.98 (±0.02) H_2/CO ratio were observed (as shown in Figure 5.9) for CRM reaction with CH_4/CO_2 ratio of 0.8 at 800 °C. To study whether the catalytic performance could be improved, the performance was tested for the effect of GHSV using values of 110, 73, 55, and 37 L g^{-1} hr^{-1}. As shown in Figure 5.10, when GHSV dropped to 73 L g^{-1} hr^{-1}, both CH_4 and CO_2 conversions were improved from 73% to 78% and from 81% to 85%, respectively. However more decreases of GHSV did not significantly affect the catalytic performance. Using the lowest GHSV of 37 L g^{-1} hr^{-1}, the maximum conversion of CH_4 (82%) and CO_2 (86%) was observed. These results further suggest that mass transfer could limit the performance of Sph-C catalyst for CRM.

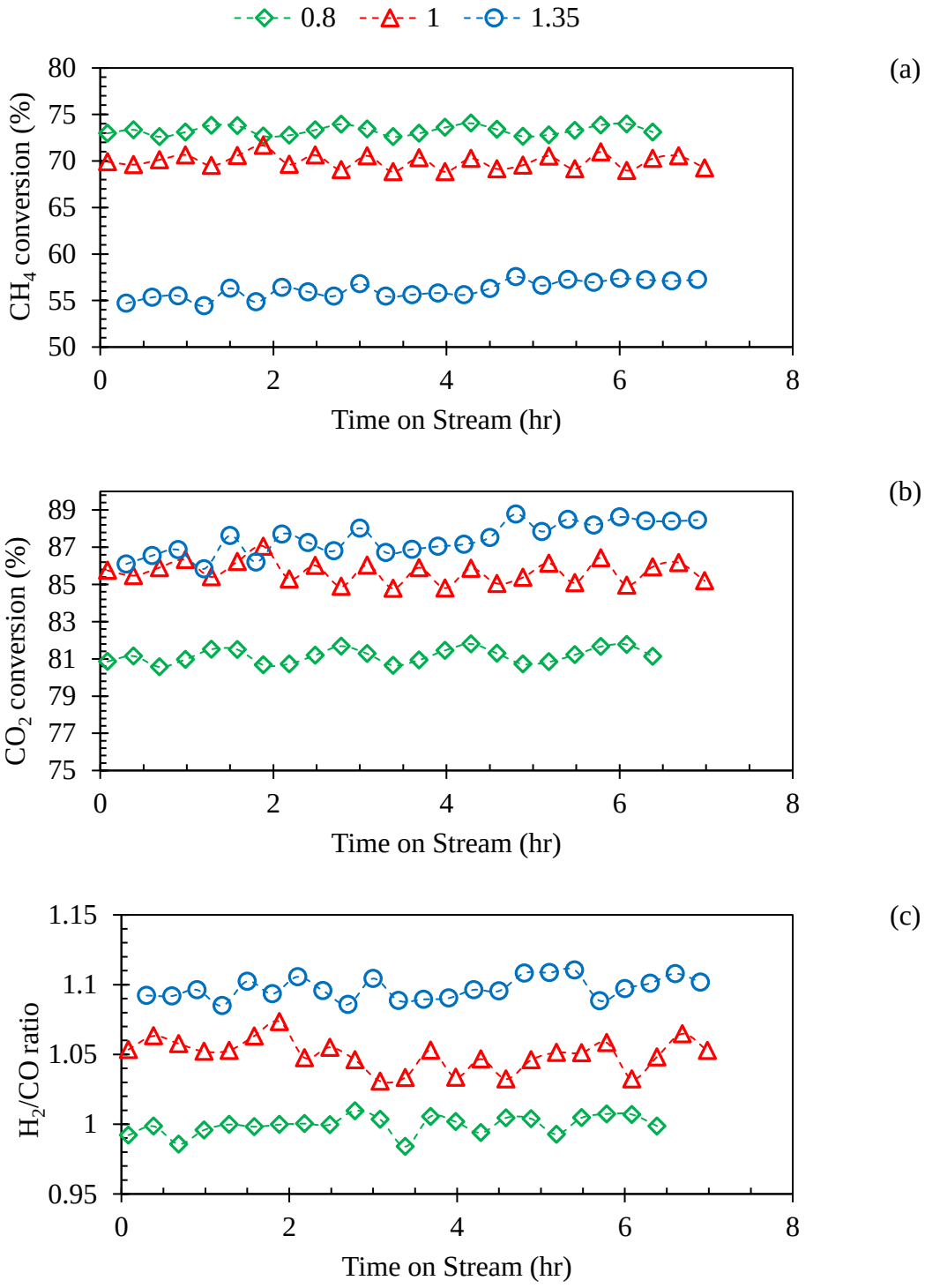

Figure 5.9 (a) CO_2 and (b) CH_4 conversions as well as (c) H_2/CO ratio in the product gas using Sph-C catalyst for CRM reaction with CH_4/CO_2 ratios of 0.8 (green), 1 (red), and 1.35 (blue). Reaction conditions: 0.15 g catalyst, 800 °C, GHSV of 110 L g^{-1} hr^{-1}

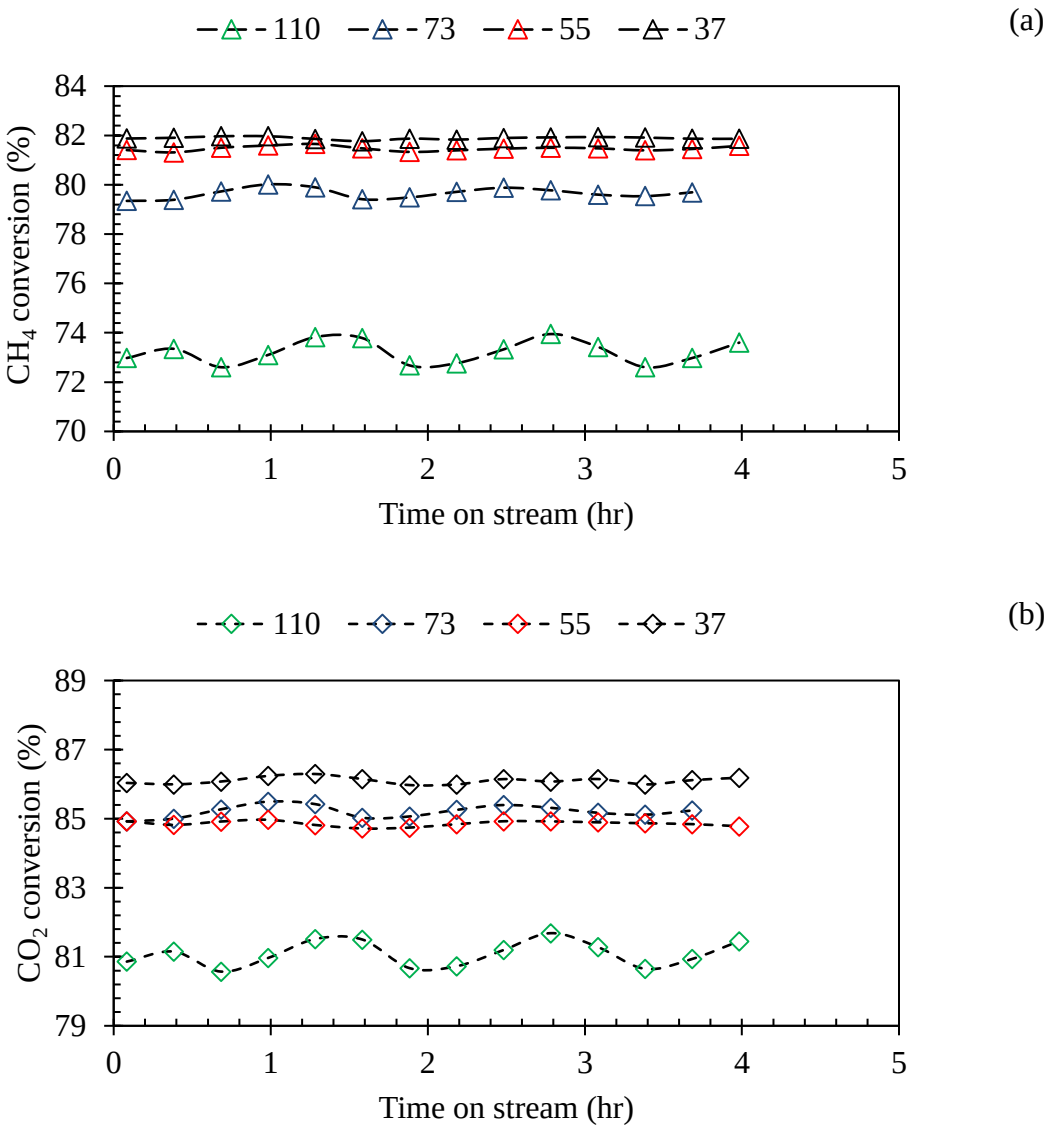

Figure 5.10 Effect of GHSV on conversions of (a) CH_4 and (b) CO_2 for CRM over Sph-C catalyst. Reaction conditions: 0.15 g catalyst, 800 °C, 1atm, $CH_4/CO_2/N_2$ = 0.8/1/1, GHSV of 37, 55, 73 and 110 L g^{-1} hr^{-1}

5.2.3 Effect of Reactant Partial Pressure on Sph-C Catalytic Performance for CRM

The influences of partial pressure of CH_4 and CO_2 on the CRM reaction rate were investigated over Sph-C at 1 atm, 800 °C and W/F of 0.02 g s mL^{-1}. The effect of CO_2 partial pressure was tested by introducing a constant CH_4 partial pressure of 10 kPa and varying the partial pressure of CO_2 in the range of 10 to 20 kPa. Figure 5.11 summarizes the effect of partial pressure of CO_2 on the reforming rate of reactants and the formation rate of CO. It should be mentioned that since the CH_4 and CO_2 conversions were intentionally kept lower than 10%, the GC could not identify the small amount of produced H_2 and therefore it is not presented in this part.

Figure 5.11 illustrates that the reforming rates amplified with an increase in the partial pressure of CO_2. However, the reforming acceleration rate was slower at higher partial pressures. The relatively constant reaction rate at CO_2 partial pressure of 20 kPa could be ascribed to the restriction of thermodynamic equilibrium due to the limited availability of CH_4 (10 kPa). The formation rate of CO also followed the same trend as the reforming rate.

The effect of CH_4 partial pressure was also investigated at a constant CO_2 partial pressure of 10 kPa as shown in Figure 5.12. It is clear that both CO_2 and CH_4 reforming rates and the CO formation rate were affected by the partial pressure of CH_4. The acceleration of the rates became faster at higher CH_4 partial pressures. Moreover, comparing the results in Figures 5.11 and 5.12 reveals that reforming rates were more sensitive to CH_4 partial pressure than that of CO_2. This behaviour is likely explained by the weaker adsorption of CO_2 than CH_4 to the catalyst's surface at higher CH_4 partial pressures (Zhang et al., 2009). The results also indicate that both CO_2 reforming rate and CO formation rate are larger than the reforming rate of CH_4. The occurrence of RWGS reaction could be the possible explanation for this phenomenon.

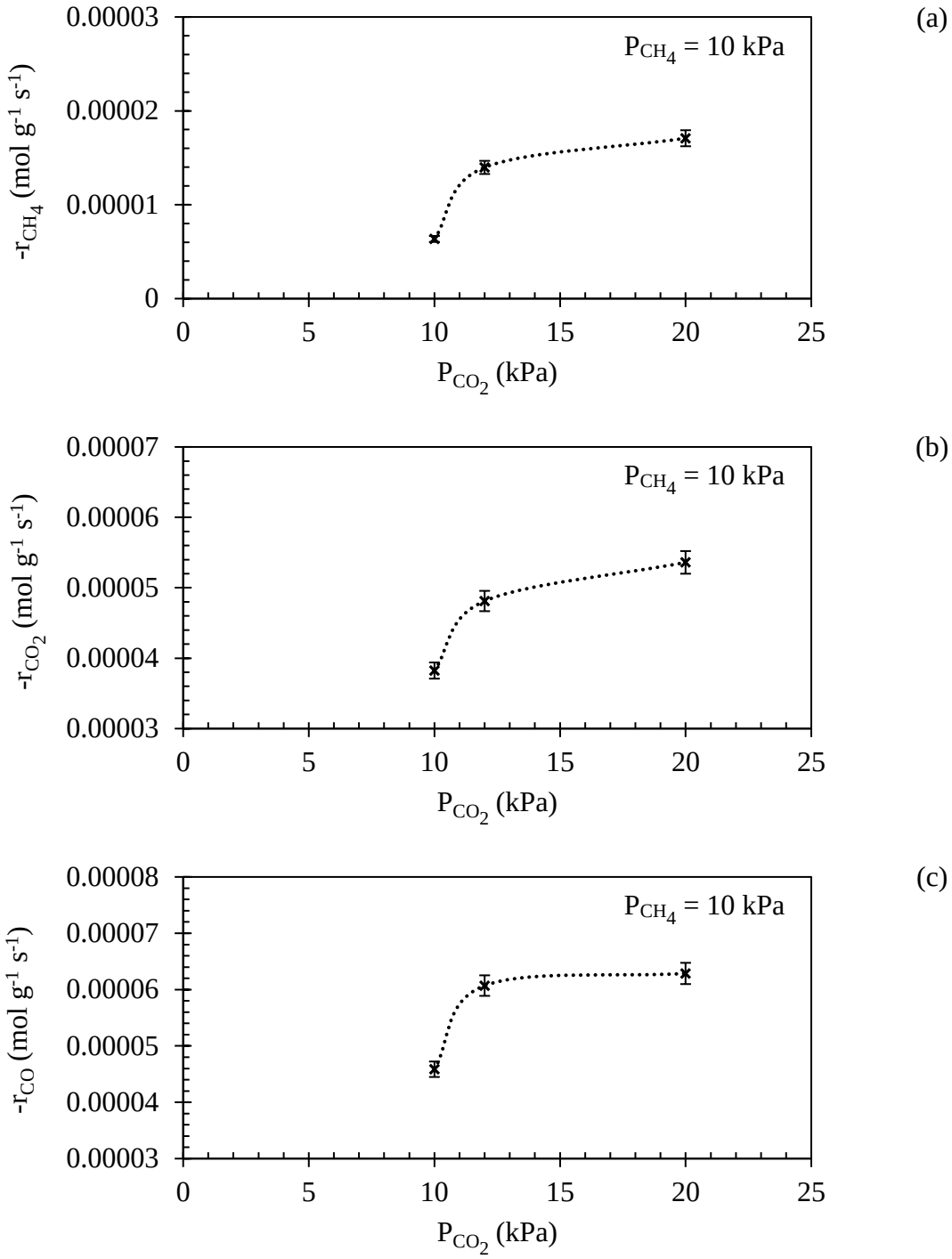

Figure 5.11 Effects of CO_2 partial pressure on consumption rate of (a) CH_4 and (b) CO_2 and formation rate of (c) CO. CRM reaction over Sph-C catalyst at 100 kPa, 800 °C and W/F of 0.02 g s mL^{-1}. Error bar shows the 95 % confidence intervals.

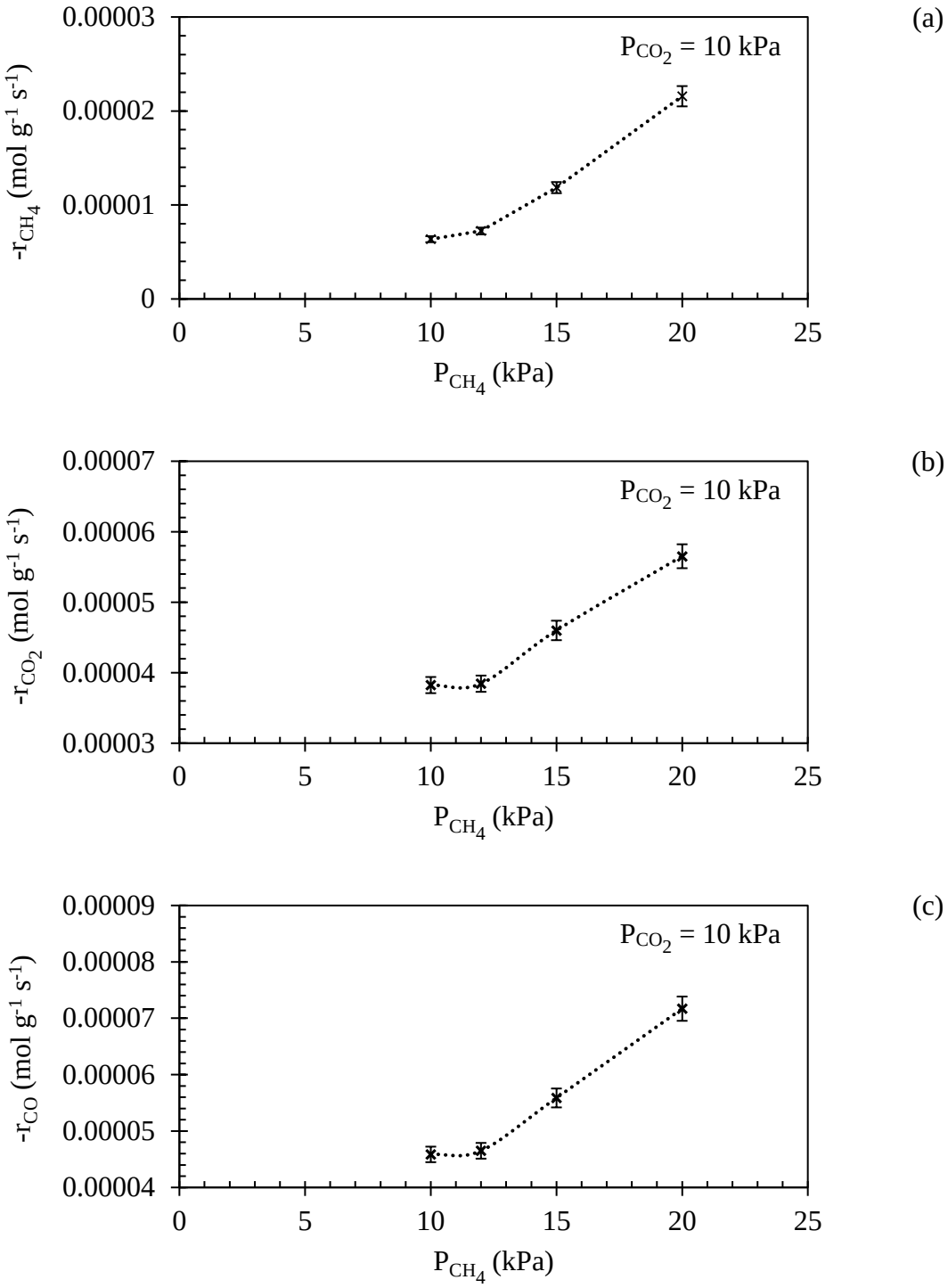

Figure 5.12 Effects of CH_4 partial pressure on consumption rate of (a) CH_4 and (b) CO_2 and formation rate of (c) CO. CRM reaction over Sph-C catalyst at 100 kPa, 800 °C and W/F of 0.02 g s mL^{-1}. Error bar shows the 95 % confidence intervals.

5.3 Heat Transfer Limitation in Performance of Sph-C for CRM

5.3.1 Anderson Criterion

Zhang et al. (2009) reported that heat transfer limitation did not affect the performance of Ni-Co/AlMgO_x catalyst in powder form for CRM reaction. To investigate whether the performance of Sph-C catalyst for CRM reaction is limited by heat transfer, Anderson criterion (equation 5.4) was used (Anderson, 1963).

$$\frac{|-\Delta H_r|\langle R\rangle d_p^2}{4\lambda_p T_s} < 0.75\frac{T_s R}{E_a} \tag{5.4}$$

where ΔH_r is reaction enthalpy (estimated using HSC Chemistry software), $\langle R\rangle$ is average reaction rate per unit catalyst particle volume (obtained from the experimental data), d_p is the average catalyst particle diameter, λ_p is the thermal conductivity of catalyst particle (estimated using the thermal conductivity of Al_2O_3 and MgO, considered as the dominant catalyst content), T_s is the surface temperature of the catalyst particle, R is the gas constant, and E_a is the apparent activation energy (estimated from the experimental data).

One 0.034 g Sph-C catalyst with a diameter of 3.6 mm was reduced in a mixture of 50% H_2 and 50% N_2 at 800 °C for 4hr. Then the CRM reaction was carried out in a temperature range of 800–900 °C, $CH_4/CO_2/N_2$ = 1/1/8, 1atm and W/F = 0.02 g s mL^{-1}. Since the activity of the catalyst was stable during the 5 hr TOS, the consumption rate of CH_4 was used to study the effect of heat transfer using the Anderson criterion. Table 5.5 summarizes the estimated values for the Anderson criterion (Slifka et al., 1998; Zhang et al., (2009).

Table 5.5 clearly shows that the values of the left-hand side of Anderson Criterion (equation 5.4) are far less than those of the right-hand side at each temperature. Thus, the Anderson criterion is valid and the effects of heat transfer limitations were ruled out indicating that the Sph-C catalyst could perform at isothermal condition under the given reaction condition.

Table 5.5 Estimated values for the Anderson criterion

Estimated parameters	Temperature (°C)		
	800	850	900
ΔH_r (kJ/mol)	259.6	259.4	259.0
$\langle R \rangle$ (mol m^{-3} s^{-1})	4.73	8.48	18.55
d_p (m)	3.6e-03	3.6e-03	3.6e-03
λ_p (W/m/K)	9.5	9.0	8.5
T_s (K)	1073	1123	1173
R (Pa.m^3/mol/K)	8.314	8.314	8.314
E_a (kJ/mol)	142.7	142.7	142.7
Left- hand side	3.9e-07	7.1e-07	1.5e-06
Right-hand side	4.7e-02	4.9e-02	5.1e-02

5.3.2 Estimation of Apparent Activation Energy

The apparent activation energy (E_a), which is strongly dependent on the reaction temperature, could be estimated using the Arrhenius Equation (equation 5.5).

$$k = Ae^{\frac{-E_a}{RT}} \tag{5.5}$$

where, k is the rate constant of a reaction, A is the frequency constant or Arrhenius factor, E_a is activation energy, R is the gas constant and T is temperature in Kelvin.

Taking the natural log of both sides of equation 5.5 yields the following:

$$ln\, k = ln\, A - \frac{E_a}{RT} \tag{5.6}$$

The reaction rate for the CRM reaction could be expressed using the Power-Law model:

$$-r_{CH_4} = kP_{CH_4}^{\alpha} P_{CO_2}^{\beta} \tag{5.7}$$

where, $-r_{CH_4}$ is the reaction rate in terms of CH_4, k is the reaction rate constant, P_{CH_4} and P_{CO_2} are partial pressures of CH_4 and CO_2, and α and β order of reactions in respect to CH_4 and CO_2, respectively.

Taking the natural log from both side of equation 5.7:

$$ln\left(-r_{CH_4}\right) = ln\, k + \alpha\, ln\, P_{CH_4} + \beta\, ln\, P_{CO_2} \tag{5.8}$$

Substituting equation 5.6 in 5.8 and rearranging the terms yields the following:

$$ln\left(-r_{CH_4}\right) = -\frac{E_a}{RT} + [\underbrace{ln\, A + \alpha\, ln\, P_{CH_4} + \beta\, ln\, P_{CO_2}}_{\text{constant}}] \tag{5.9}$$

Equation 5.9 indicates that by keeping the partial pressure constant while varying the temperature, E_a could be estimated by plotting the natural log of $-r_{CH_4}$ versus 1/T. Using the same

procedure, CO_2 consumption and CO formation rates from the experiment could be used to estimate E_a for CO_2 and CO. Therefore, reaction results were plotted in the form of equation 5.6 in terms of the reforming rate of CH_4 and CO_2 and the formation rate of CO as shown in Figure 5.13. Then, using the fitted lines, apparent activation energies were estimated to be 142.7 kJ/mol for CH_4, 72.9 kJ/mol for CO_2 and 82.5 kJ/mol for CO. The estimated values are in agreement with those suggested in literature. Bradford and Vannice (1999) reported in a review that apparent activation energies for CRM are typically between 30 to 160 kJ/mol depending on the catalyst. On the other hand, it was observed that for the Sph-C catalyst, the estimated E_a of CO_2 is much lower than that of CH_4. The presence of MgO as a strong Lewis base in the catalyst support, which could facilitate the CO_2 activation, might be the possible explanation for the lower E_a of CO_2 than CH_4 using Sph-C catalyst (Li et al., 1994; Zhang et al., 2009).

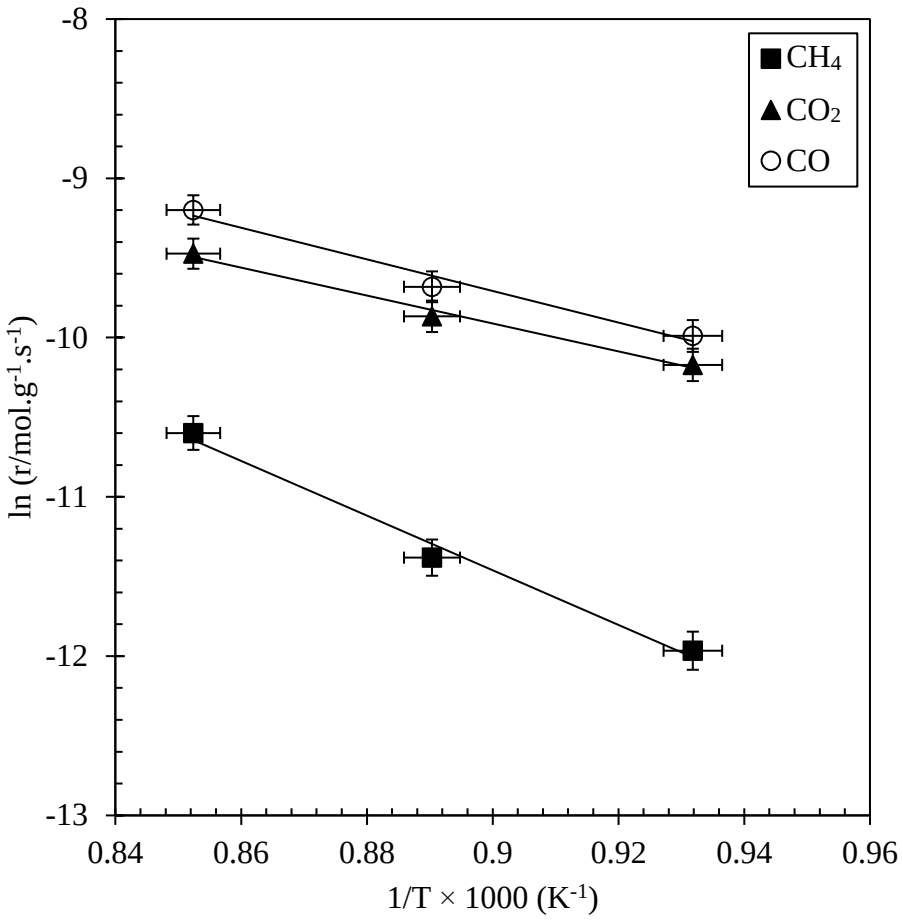

Figure 5.13 Effect of temperatures on the reaction rates of CRM over Sph-C catalyst at 100 kPa, $CH_4/CO_2/N_2$ = 1/1/8, 800 – 900 °C, and W/F of 0.02 g s mL^{-1}. Error bar shows the 95 % confidence intervals.

5.4 Mass Transfer Limitation in Performance of Sph-C for CRM

5.4.1 External Mass Transfer Effect

In catalytic reactions, the external mass transfer limitation could be experimentally examined through variation of the feed flow rate over a fixed residence time. It is reported that at a fixed residence time gained through maintaining a constant W/F ratio (weight of catalyst load/flow rate), increasing the superficial velocity results in a higher mass transfer rate. When the reactant conversions will not significantly change with the change of flow rate, limitation of the external mass transfer can be neglected (Nandini et al., 2006; Perego & Peratello, 1999; Tsipouriari & Verykios, 2001).

To investigate the mass transfer limitation, consecutive CRM reaction tests were carried out at 800 °C using the Sph-C catalysts (with average size of 3.5 mm). Catalyst loadings of 0.1, 0.2, 0.3, and 0.5 g were reduced and CRM was carried out at 800 °C and $CH_4/CO_2/N_2$ = 1/1/1. Both reactant flow rates and catalyst loading were increased to keep a constant of GHSV of 110 L g^{-1} hr^{-1}. A non-dimensional value of Z was calculated for each experiment using Equation 5.10.

Z = total feed flow rate of each experiment / F (5.10)

where, F (~43 m/s) is superficial velocity used for the test with a catalyst loading of 0.1 g.

Figure 5.14 shows the reactant conversions versus Z and the overall reactant conversions are summarized in Table 5.6. Figure 5.14 reveals that the reactant conversions raised while the superficial velocity was increasing and therefore the catalytic performance was limited by external mass transfer diffusion. However, such a phenomenon was not significant when the superficial raised to 215 m/s (Z = 5). It is reasonable to conclude that the external diffusion limitation could be neglected with higher superficial velocity than 129 m/s (Z = 3).

Table 5.6 clearly shows that the reactant conversions for CRM reaction over powder form catalyst C (average diameter of 0.3 mm and loading of 0.1 g) were about 20% greater than those for Sph-C (average diameter of 3.6 mm loading of 0.5 g are). This suggests that while the external mass transfer limitations could be neglected using large catalyst loading, the internal mass transfer could still limit the performance of Sph-C catalysts.

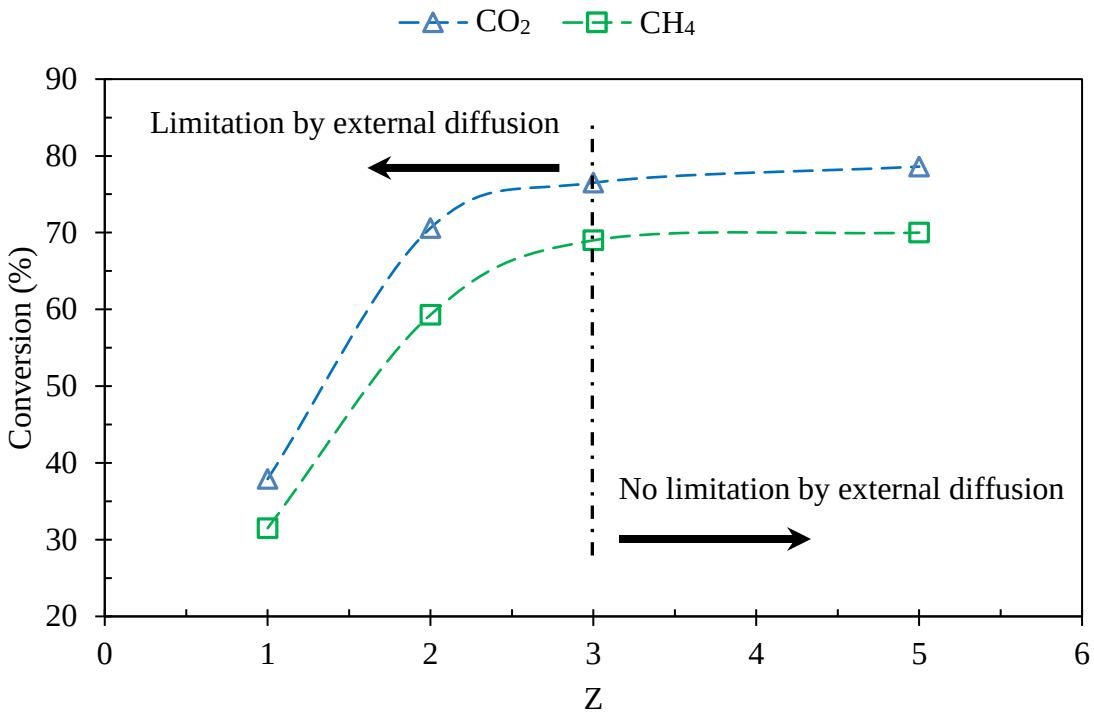

Figure 5.14 Effect of flow rate on reactant conversions at a constant space velocity (GHSV of 110 110 L g^{-1} hr^{-1}) using the Sph-C catalysts for CRM reaction. Reaction conditions: 800 °C, $CH_4/CO_2/N_2$ = 1/1/1, catalyst loadings of 0.1, 0.2, 0.3, and 0.5 g

Table 5.6 Overall reactant conversions of C and various Sph-C loadings for CRM reaction at 800 °C. Reaction conditions: 800 °C, $CH_4/CO_2/N_2$ = 1/1/1, GHSV of 36.7, 55 and 110 L g^{-1} hr^{-1}

Catalyst	C	Sph-C			
Catalyst loading (g)	0.1	0.1	0.2	0.3	0.5
CH_4 Conversion (%)	91.2	31.5	59.3	69.1	70
CO_2 Conversion (%)	93.5	59.3	70.6	76.2	78.6
TOS (hr)	14	4	23	21	20

5.4.2 Internal Mass Transfer Effect

As previously mentioned, because of larger size of Sph-C catalysts as the powder form catalyst (catalyst C), the performance of Sph-C catalysts for CRM was more likely restricted by internal mass transfer diffusion. To further investigate whether internal diffusion is limiting the spherical catalysts' performance, the Weisz-Prater Criterion, given in Equation 5.11, was used.

$$C_{WP} = \frac{-r_A(obs)\rho_c R^2}{D_e C_{AS}} \tag{5.11}$$

where, C_{WP} is the dimensionless Weisz-Prater parameter also known as the experimental Thiele module, $-r_{A(obs)}$ is the observed (actual) reaction rate of reactant A, ρ_C is the catalyst density, R is the catalyst radius, D_e is the effective diffusivity, and C_{AS} is the concentration of reactant A at the external surface of the pellet.

If $C_{WP} \ll 1$ there are no diffusion limitations. On the other hand, if $C_{WP} \gg 1$ then internal diffusion limits the reaction. However, this approach should be carefully used and is valid only when the external diffusion limitation has previously been determined to be absent. Therefore, the CRM reaction results for 0.5 g of Sph-C catalyst loading, where the external diffusion limitation was negligible, were used to estimate the parameters as summarized in Table 5.7. Results clearly reveal that the calculated C_{WP} (893) is much greater than one and consequently internal diffusion is severely limiting the Sph-C performance for CRM reaction.

Table 5.7 Estimated parameters for the Weisz-Prater Criterion. CRM reaction conditions: 0.5 g Sph-C catalyst, reaction temperature: 800 °C, 1atm, GHSV of 110 L g^{-1} hr^{-1}, $CH_4/CO_2/N_2$ = 1/1/1

Parameter	Estimated value	Unit
$-r_{CH_4(obs)}$	3.1e-04	mol g^{-1} s^{-1}
ρ_C	1.39e05	g/m^3
R	1.8e-03	m
D_e	5.0e-07	m^2/s
C_{CH_4S}	3.8	mol/m^3
C_{WP}	893	

5.5 Conclusions

The cylindrical catalysts facilitate CRM reaction similarly. The addition of Boehmite (to some extent) did not significantly change the catalytic performance. On the other hand, the added Boehmite could improve the efficiency of the active metal sites in the catalyst toward the CRM reaction and consequently a decreased amount of Ni-Co catalysts would be required to prepare an industrial pellet. Economically speaking, the cost of preparation of Ni-Co/AlMgO_x catalyst and Boehmite should be considered toward commercialization. In the case of spherical catalysts (D = 3.6 mm), the temperature gradient within the diameter of the spherical catalyst was negligible and the catalyst could perform under isothermal condition for CRM reaction at a temperature range of 800 to 900 °C. However, the mass transfer limitations affected the performance of the catalysts for the CRM reaction. It was found that increasing the superficial velocity to greater than 129 m/s could avoid the external mass transfer limitation. However, the internal mass transfer was still restricting the performance of spherical catalyst.

CHAPTER 6

Catalytic Performance Using Industrial Feed Compositions

Synthesis gas or syngas, a mixture of H_2 and CO, has been widely used in diverse chemical and petrochemical industries. Various forms of catalytic reforming of methane are known to be one of the main routes to produce syngas (Ghoneim et al., 2016; Pena et al., 1996). In theory with the use of an ideal feed (stoichiometric feed composition), steam reforming of methane (SRM) and carbon dioxide reforming of methane (CRM) could theoretically produce synthesis gas with H_2/CO ratios of 3 and 1, respectively. The H_2/CO ratio in the produced syngas from SRM could be adjusted with that of CRM to obtain a H_2/CO ratio between 1 and 3. On of the major challenges in such a procedure is that an ideal feed for both CRM and SRM reactions would be required. As an industrial point of view, purification of feeds is not preferred due to the high cost of the process. Thus, production of syngas from combined steam-carbon dioxide reforming of methane (SCRM) has attracted great attentions in recent years. The industrial partner of this research requires the production of a syngas with H_2/CO ratio in a range of 1.8 to 2 from a biogas feed that contains steam, CO_2, CH_4 and a few percentage of H_2. It is reported that catalysts with alumina and/or MgO as supports with ceramic structure are good choices for the SRM reaction (Bitter et al., 1997; Simakov et al., 2015). Ni and Co are also known to be active sites for both steam and CO_2 reforming of methane reactions (Rostrup-Nielsen, 1997; San-Jose-Alonso et al., 2009; Zhang et al., 2007). Therefore, the performance of Ni-Co bimetallic, Ni monometallic and Co monometallic catalysts on $AlMgO_x$ support using various biogas feed compositions were investigated in this study. To study the effect of steam to carbon ratio in the feed gas for a SCRM reaction, various biogas feed compositions, as summarized in Table 6.1, were selected.

6.1 Equilibrium Compositions Using Various Biogas Feed Compositions

Several chemical reactions could occur in the presence of a biogas feed containing steam, CO_2, CH_4, H_2. The major reactions, which affect the equilibrium compositions, are steam reforming of methane (SRM), carbon dioxide reforming of methane (CRM) and water gas shift (WGS) reactions (Annesini et al., 2007; Snoek et al., 2003; Wang et al., 1996).

$$CH_4 + CO_2 \rightleftharpoons 2H_2 + 2CO \text{ (CRM)} \quad (6.1)$$

$$CH_4 + H_2O \rightleftharpoons 3H_2 + CO \text{ (SRM)} \quad (6.2)$$

$$CO + H_2O \rightleftharpoons CO_2 + H_2 \text{ (WGS)} \quad (6.3)$$

SRM and CRM are the desired reactions but WGS or its reverse are undesired while using the biogas feed. Callaghan (2006) reported that the equilibrium reaction constant of WGS approaches to one at 850 °C, thus the effect of WGS reaction could be minimized. Moreover, reactions 6.1 to 6.3 indicate that at higher total pressures, the equilibrium composition of CRM and SRM shifts to the left-hand side leading to less reactant conversions. In addition to the reaction condition, equilibrium composition of SCRM reaction depends on the feed composition. With biogas feed compositions given in Table 6.1, the equilibrium composition of the reaction environment at 850 °C and 1 bar were calculated using HSC Chemistry software. Figure 6.1 shows the equilibrium composition as a function of initial H_2O/CO_2 ratio in the biogas feed.

As shown in Figure 6.1, the equilibrium composition of CH_4 does not significantly change while varying the H_2O/CO_2 ratio, because CH_4 is theoretically consumed in both CRM and SRM reactions. However, the equilibrium composition of H_2O increases while that of CO_2 decreases due to the increase of H_2O/CO_2 ratio and the occurrence of WGS reaction. Moreover, Figure 6.1 clearly shows that when H_2O/CO_2 increases, the equilibrium composition of H_2 becomes significantly more than that of CO leading to increase of produced H_2/CO ratio. The reason is that with more steam content in the feed, occurrence of SRM is dominant leading to higher production of H_2 than CO. Besides, the equilibrium composition of N_2, as an inert gas, does not change while carrying steam content in the feed.

Table 6.1 Biogas feed compositions used for combined steam and carbon dioxide reforming of methane reaction. Gas contents are reported in mole/volume percent.

Feed #	CH_4 (%)	H_2 (%)	N_2 (%)	H_2O (%)	CO_2 (%)	H_2O/CO_2*
1	33.3	3.4	30	2.8	30.5	0.1
2	33.3	3.4	30	5.6	27.7	0.2
3	33.3	3.4	30	7.8	25.5	0.3
4	33.3	3.4	30	9.8	23.5	0.4
5	33.3	3.4	30	11.9	21.4	0.55
6	33.3	3.4	30	14.7	18.6	0.8
7	33.3	3.4	30	17.5	15.8	1.1
8	33.3	3.4	30	20.3	13.0	1.55
9	33.3	3.4	30	23.1	10.2	2.25
10	33.3	3.4	30	25.9	7.4	3.5
SRM	33.3	-	33.4	33.3	-	-
CRM	33.3	-	33.4	-	33.3	-

* CO_2+H_2O content was constant and equal to CH_4 content.

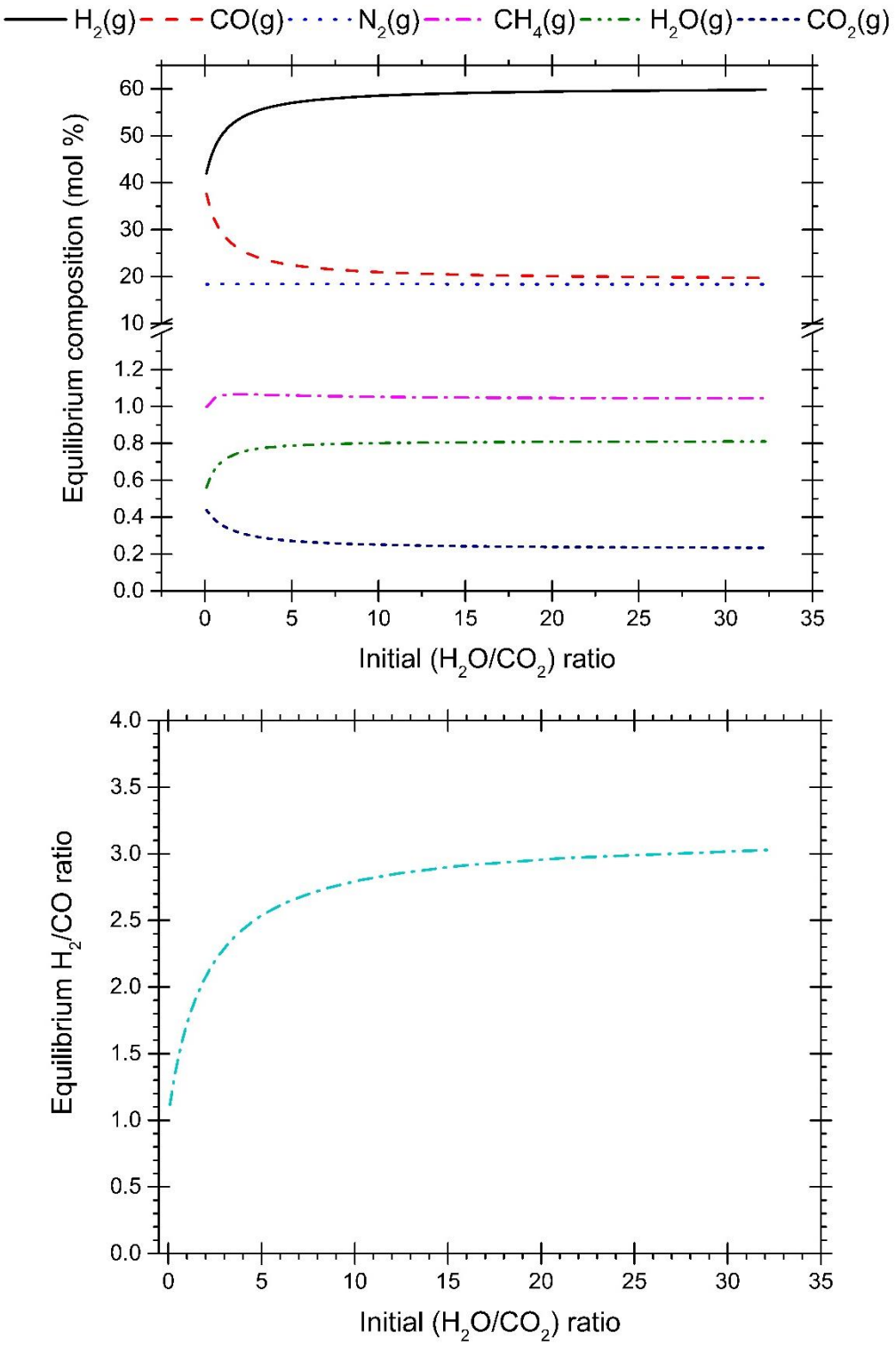

Figure 6.1 (a) Equilibrium compositions (mol %) and (b) equilibrium H_2/CO ratio for combined steam and carbon dioxide reforming of methane (SCRM). Biogas feed compositions: CH_4 = 33.3 mol, N_2 = 30 mol, H_2 = 3.8 mol and H_2O/CO_2 ratio varies from 0.1 to 32 while total amount of CH_4, CO_2, H_2O, H_2 and N_2 kept constant and is equal to 100 mol. Reaction conditions: 850 °C and 1 bar

The equilibrium calculations show that production of syngas with H_2/CO ratio in a range of 1.8 to 2 from biogas feed is thermodynamically possible. In addition to the thermodynamics limitations, the experimental results in catalytic reactions also depend on the nature of the catalysts. In addition to the main reactions (6.1 to 6.3) using biogas feed, other most possible side reactions are given in reactions 6.4 to 6.7.

$$CH_4 \rightleftharpoons C + 2H_2 \text{ } (CH_4 \text{ dissociation/cracking}) \quad (6.4)$$

$$2CO \rightleftharpoons CO_2 + C \text{ (Boudouard reaction)} \quad (6.5)$$

$$CO + H_2 \rightleftharpoons C + H_2O \quad (6.6)$$

$$C + H_2O \rightleftharpoons H_2 + CO \quad (6.7)$$

The extent of occurrence of side reactions depends on both experimental conditions and nature of catalysts (compositions, structures, etc.), which could affect the reactant conversions as well as the H_2/CO ratio in the product stream.

6.2 Steam Carbon Dioxide Reforming of Methane (SCRM) Using Biogas Feed Composition

In each experiment, 0.4 g of catalyst (mixed with 3.6 g of silica carbide) was reduced in an Inconel reactor at 900 °C in a mixture of H_2 (50%) and N_2 (50%) for 4 hours. The reaction was then carried out at 850 °C with a GHSV of 110 L g^{-1} hr^{-1}. As shown in Table 6.1, the CO_2/H_2O ratio was varied while the total amounts of H_2O and CO_2 and the ratio of (H_2O+CO_2) to CH_4 were kept constant. To compare, Ni and Co monometallic catalysts, a commercial reforming catalyst from Federated Co-operatives Limited (FCL) Inc., as well as two other industrial catalysts (X and Y) were also tested for SCRM.

6.2.1 Performance of Bimetallic and Monometallic Catalysts for SCRM

The performance of Ni-Co bimetallic catalyst, Ni monometallic and Co monometallic for SCRM reaction at 850 °C using various biogas feed compositions (Table 6.1) are presented in Figures 6.2, 6.3 and 6.4, respectively.

Figure 6.2 indicates that for the first three feed compositions (1, 2, and 3), methane was almost totally consumed over the Ni-Co catalyst (98% of CH_4 conversion). An increase in the steam content in the feed (feeds 4 and 5) led to oscillation of the CH_4 conversion in a small range, between 90 and 98% for feed 4 and between 96 and 98% for feed 5. It is interesting to note that feed 4, which had less steam, resulted in oscillation of a larger magnitude than feed 5. The CO_2 conversions, which never reached 100%, decreased as the steam content increased in feed. Feed 4 led to even more intensive oscillation between 65 and 98%. The CO_2 conversion with feed 5 began with a couple of oscillations but came to a relatively low value around 70 to 74%. It appears that CO_2 and steam were competing over CH_4 in CRM and SRM (reactions 6.2 and 6.3) and that more steam content in the feed favoured more steam reforming and led to a lower CO_2 conversion. Therefore, the more the steam content in the feed, the more the occurrence of SRM than CRM, leading to the higher H_2/CO ratio in the product. In feed 6, with steam content of 14.7%, quick deactivation of the catalyst within one hour of time on stream was observed. Oxidation of the active metallic sites with steam could explain the catalyst deactivation. A closer look at the results for feed 4 reveals that extremum values of CH_4 and H_2/CO occurred at the same time while those of CO_2 were shifted about 1 hour. It seems that carbon initially accumulated on the catalyst's surface from CH_4 dissociation (reaction 6.4), which resulted in more H_2 production. Meanwhile O-intermediates from steam and CO_2 were competing to react with the C-intermediate from CH_4 dissociation. CO_2 could periodically win the competition every one hour and oxidize the deposited carbon (reaction 6.6), leading to higher conversion of CO_2 and production of CO. Researchers have addressed this phenomena as a periodic cycle of carbon deposition and elimination on the catalyst's surface which could improve the stability of the catalyst's performance (Richardson, 1989; Wei et al., 2000; Zhang, et al., 2007).

For the Ni monometallic catalyst, oscillation in CH_4 conversion was observed for feeds 2 to 6, as shown in Figure 6.3. As steam content in feed increases from 5.6% in feed 2 to 14.7% in feed 6, the oscillation magnitude changes from between 88 and 98% for feed 2–4 , to between 60 and 96% for feed 5 and between 30 and 96% for feed 6. Like the bimetallic catalyst, the CO_2 conversion dropped as the steam content increased in the feed. It was also observed that, like CH_4, the CO_2 conversion was intensively oscillating in feeds 5 and 6. It seems that CO_2 and steam were competing over CH_4 and increasing the steam content in feed favoured more SRM than CRM, which led to a lower CO_2 conversion. In addition, the increase of steam content in feeds 5 and 6

could possibly increase the occurrence of WGS reaction leading to a lower conversion of CO_2. Therefore, the more the steam content in the feed the higher the H_2/CO ratio in the product. Moreover, increasing steam content to 17.5% in feed 7 led to deactivation of the Ni monometallic catalyst within a couple of hours possibly due to oxidization of active metallic sites.

In the case of Co monometallic catalyst, Figure 6.4 reveals that within the first hour of the reaction, CH_4 and CO_2 conversions dropped from 25 to 15% and 44 to 16%, respectively. Higher CO_2 conversion than CH_4, and H_2/CO ratios lower than one in the first hour of the reaction could indicate the occurrence of the RWGS reaction. However, it seems that Co monometallic catalyst favoured SRM more after the first hour of time on stream. It was also observed that the cobalt monometallic catalyst, unlike Ni-Co bimetallic and Ni monometallic catalysts, deactivated badly when the content of steam reached 7.8% in feed 3. In our earlier work, it was discovered that Co was more stable in oxide form and it was harder to reduce. Thus, the number of active metallic sites in the reduced Co monometallic catalyst could be less than those in the reduced Ni containing catalysts (Wang et al., 2013). Lower number of active sites in Co monometallic catalyst than the Ni containing ones, could possibly explain why the Co monometallic catalyst was deactivated with lower steam content in the feed than the Ni-Co bimetallic and Ni monometallic catalysts.

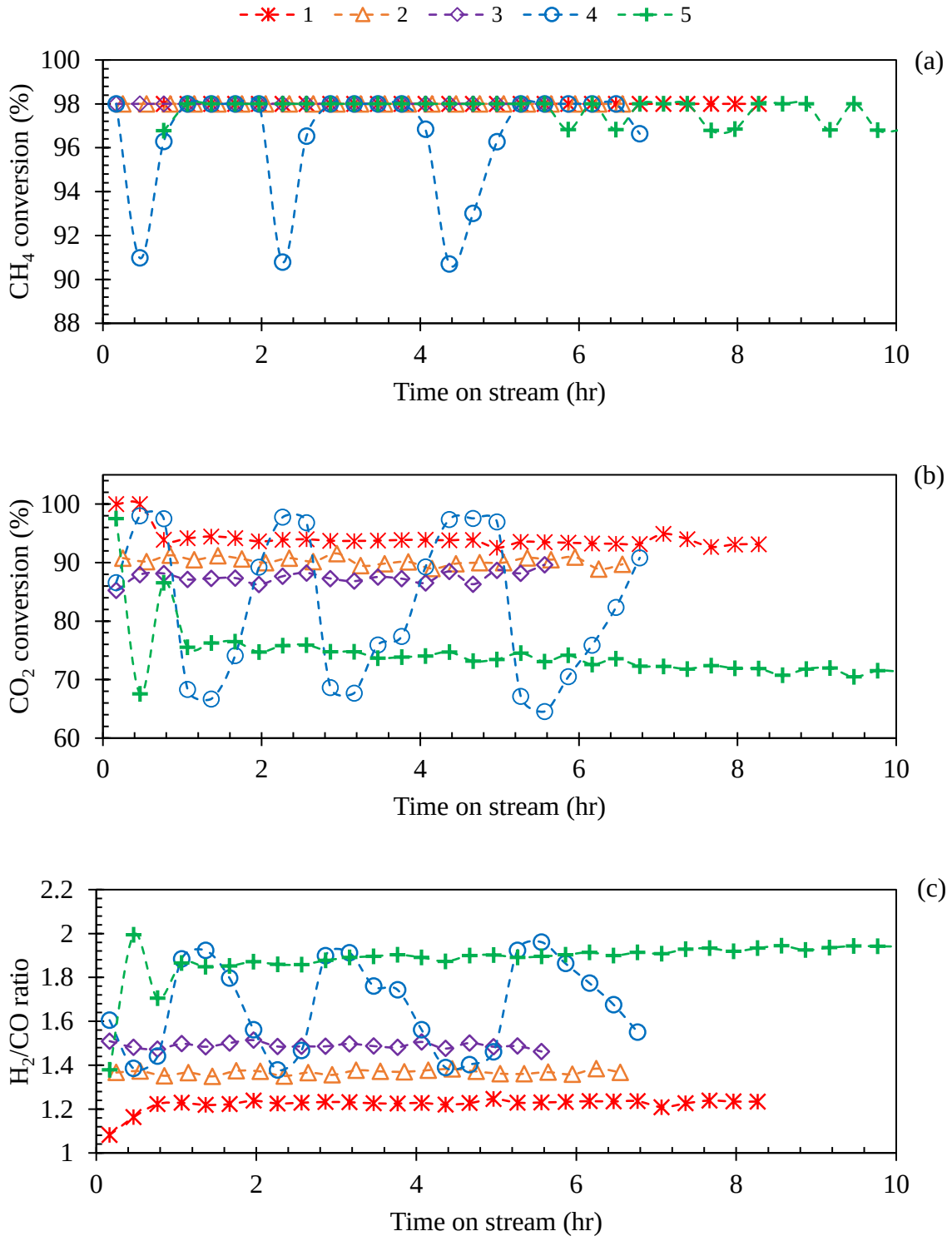

Figure 6.2 (a) CH_4 conversion, (b) CO_2 conversion, and (c) H_2/CO ratio of SCRM over Ni-Co bimetallic catalyst at 850 °C using various biogas feed compositions, GHSV = 110 L g^{-1} hr^{-1}. Legends show the feed numbers

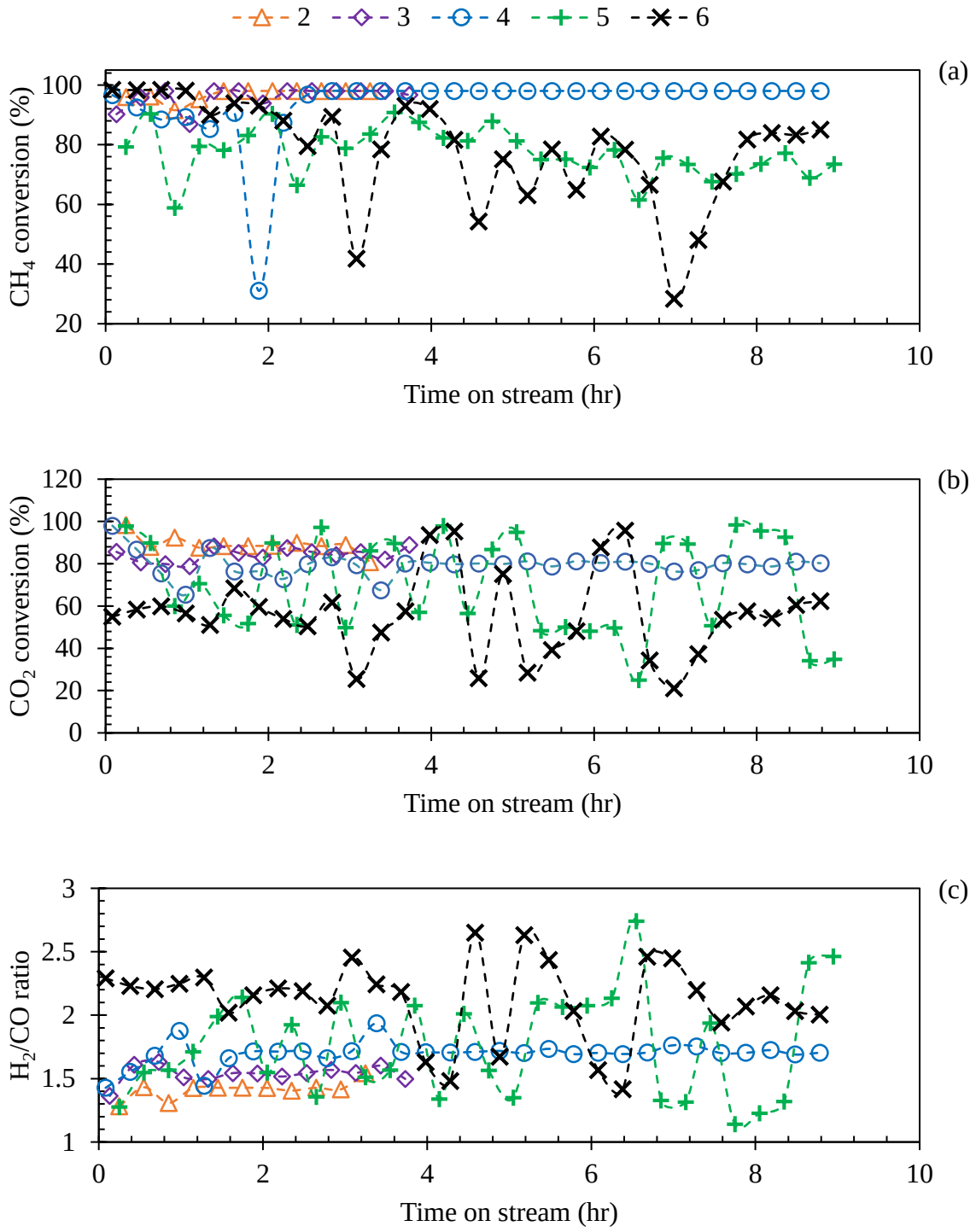

Figure 6.3 (a) CH_4 conversion, (b) CO_2 conversion, and (c) H_2/CO ratio of SCRM over Ni monometallic catalyst at 850 °C using various biogas feed compositions, GHSV = 110 L g^{-1} hr^{-1}. Legends show the feed numbers.

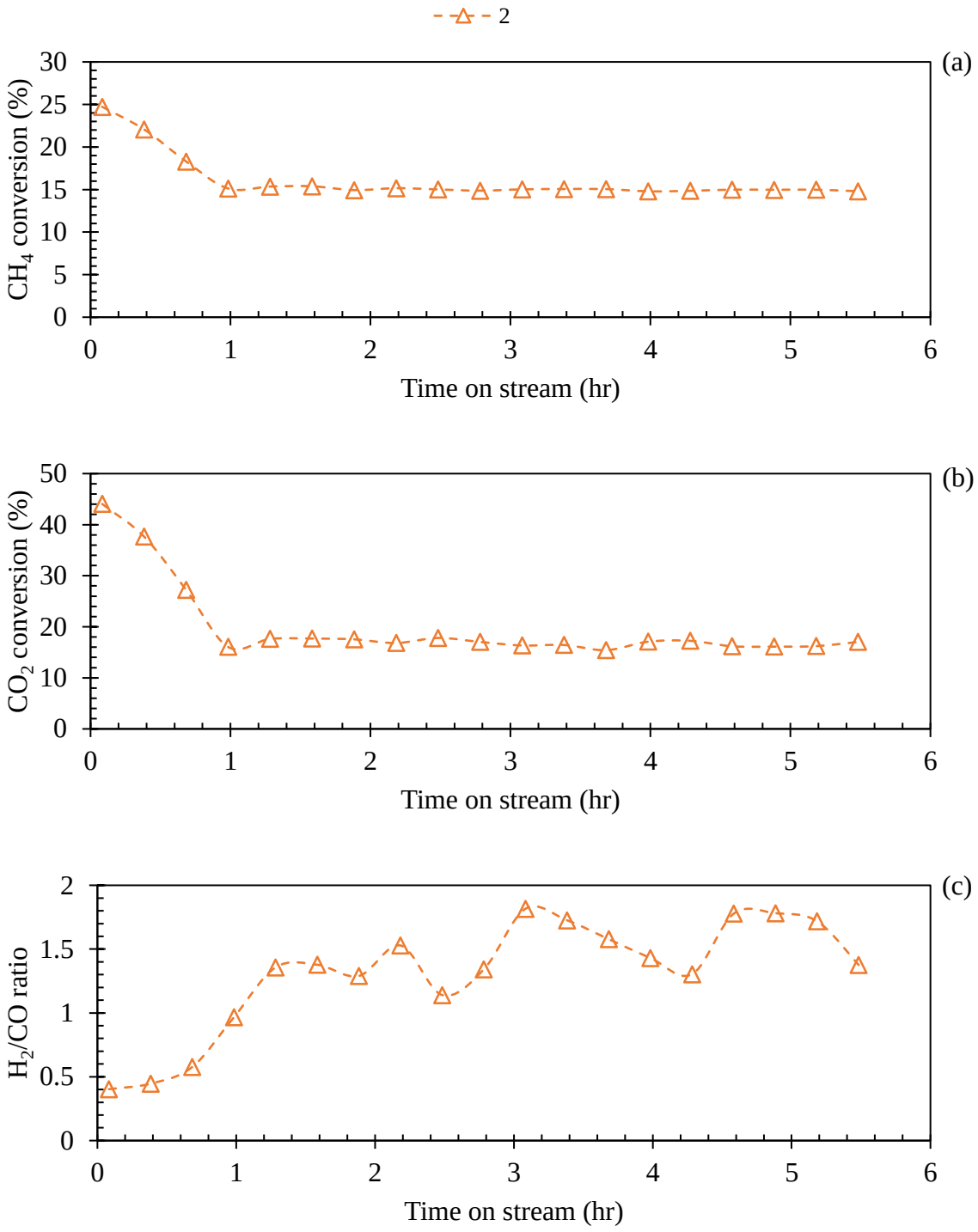

Figure 6.4 (a) CH_4 conversion, (b) CO_2 conversion, and (c) H_2/CO ratio of SCRM over Co monometallic catalyst at 850 °C using various biogas feed compositions, GHSV = 110 L g^{-1} hr^{-1}. Legends show the feed numbers.

6.2.2 Performance of Industrial Reforming Catalyst for SCRM

Three industrial reforming catalysts (X, Y and Co-Op) were tested for SCRM reaction at 850 °C using various biogas feed compositions (Table 6.1). The results for catalyst X, catalyst Y and Co-Op reforming catalyst are presented in Figures 6.5, 6.6, and 6.7, respectively.

As shown in Figure 6.5, for the first three feed compositions (feeds 2, 3 and 4), catalyst X facilitated relatively high and stable methane conversion between 94 and 97%. The increase in the steam content in feeds 4 to 9 led to both decrease and oscillation of CH_4 conversions, in the range of 78 to 95%. In feed that did not contain CO_2, the conversion of CH_4 further dropped and oscillated between 66 and 91% indicating that catalyst X was more active for CRM than SRM. CO_2 conversions decreased and oscillated, too, as the steam content increased in feeds. CO_2 conversions over catalyst X had greater oscillation magnitude with the feed gases having H_2O/CO_2 ratio close to one (feeds 4, and 5). For example, CO_2 conversion in feed 1 oscillated between 75 and 95% while it oscillated between 0 and 90% in feed 5. In feed 6 (H_2O/CO_2 =1.1), the CO_2 conversion dropped dramatically and oscillated between 0 and 22%. A further increase of steam content in feeds 7 to 10 led to higher CO_2 content in the product gases than in the feed gas, meaning the CO_2 production rate was higher than its consumption rate. The occurrence of water gas shift (WGS) reaction could explain production of CO_2 in feeds containing H_2O/CO_2 ratios larger than one. Figure 6.5 (c) reveals that increasing the steam content in the feed raised the H_2/CO ratio in the produced syngas. For the first three feeds (feeds 1, 2 and 3), the H_2/CO ratio in the product was relatively stable while it fluctuated for the rest of the feeds with higher steam content. The higher the steam content in the feed, the larger the oscillation range of H_2/CO ratio in the produced syngas. Moreover, the highest H_2/CO ratio in the product gas was observed for SRM feed has an average of 4.2 for 5 hours TOS, which is higher than the equilibrium value of SRM reaction. This could indicate that catalyst X favoured more SRM than WGS.

Figure 6.6 shows that for feeds 2 and 3, catalyst Y facilitated the similar CH4 conversion in SCRM as our Ni-Co catalyst did. However, larger oscillation magnitude was observed for CO_2 conversions. When the steam content was raised to 9.8% in feed 4, stable catalytic performance was observed. This could indicate that the competition for CH_4 became more stable in this feed. Increasing the steam content in feeds led to CO_2 conversion decrease while the H_2/CO ratio increase. The oscillation of CO_2 conversion became more significant and severe. With an increase

of steam content to 14.7% in feed 6, CO_2 conversion was dramatically oscillating between 0% and 100% for 12 hours TOS while CH_4 conversion was relatively high and stable. The H_2/CO ratio oscillated between 1.5 and 3.8. This might be the result of the swing of CRM and WGS reactions over the catalyst.

Figure 6.7 shows the Co-Op catalyst activity and selectivity for the SCRM reaction. In CRM feed, the average CH_4 and CO_2 conversions as well as H_2/CO ratio are 90%, 91%, and 0.97, respectively. Addition of steam to the feed led to increased methane conversion and higher H_2/CO in the product gas, while CO_2 conversion decreased. Moreover, CH_4 conversion for all the feeds was high and in the range of 90% to 98%, while the CO_2 conversion dramatically decreased. As an example, CO_2 conversion for feed 2 with steam content of 2.8% was about 97%, while increasing the steam content to 11.9% in feed 5 resulted in 20% CO_2 conversion. Putting these observations together, we can see that the Co-Op catalyst favoured SRM reaction more than CRM reaction. When the steam content was increased to 20.3% in feed 8, more CO_2 was observed in product than in feed. This indicates that SRM overwhelmed and CO_2 was produced over the Co-Op catalyst.

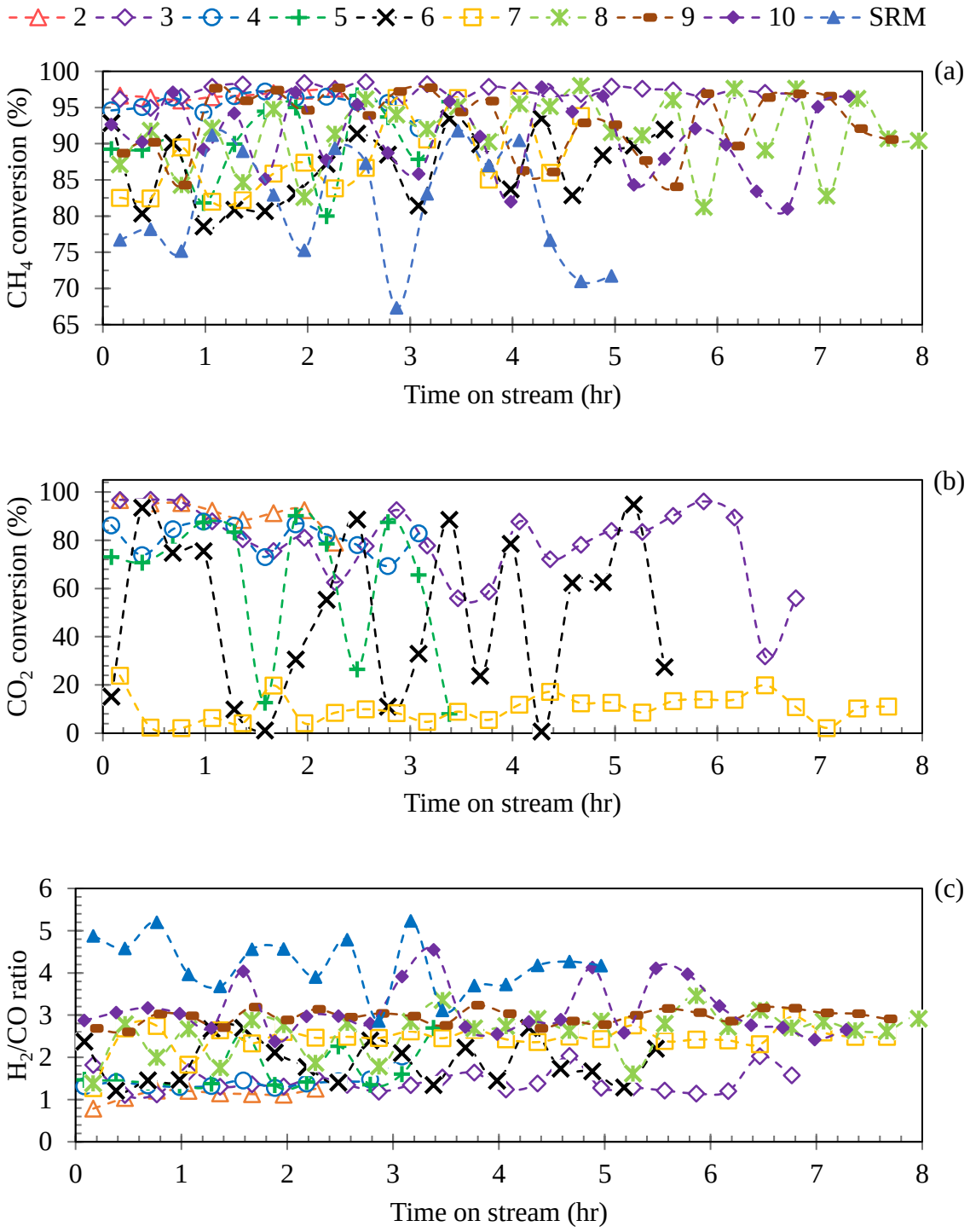

Figure 6.5 (a) CH_4 conversion, (b) CO_2 conversion, and (c) H_2/CO ratio of SCRM over catalyst X at 850 °C using various biogas feed compositions, GHSV = 110 L g^{-1} hr^{-1}. Legends show the feed numbers

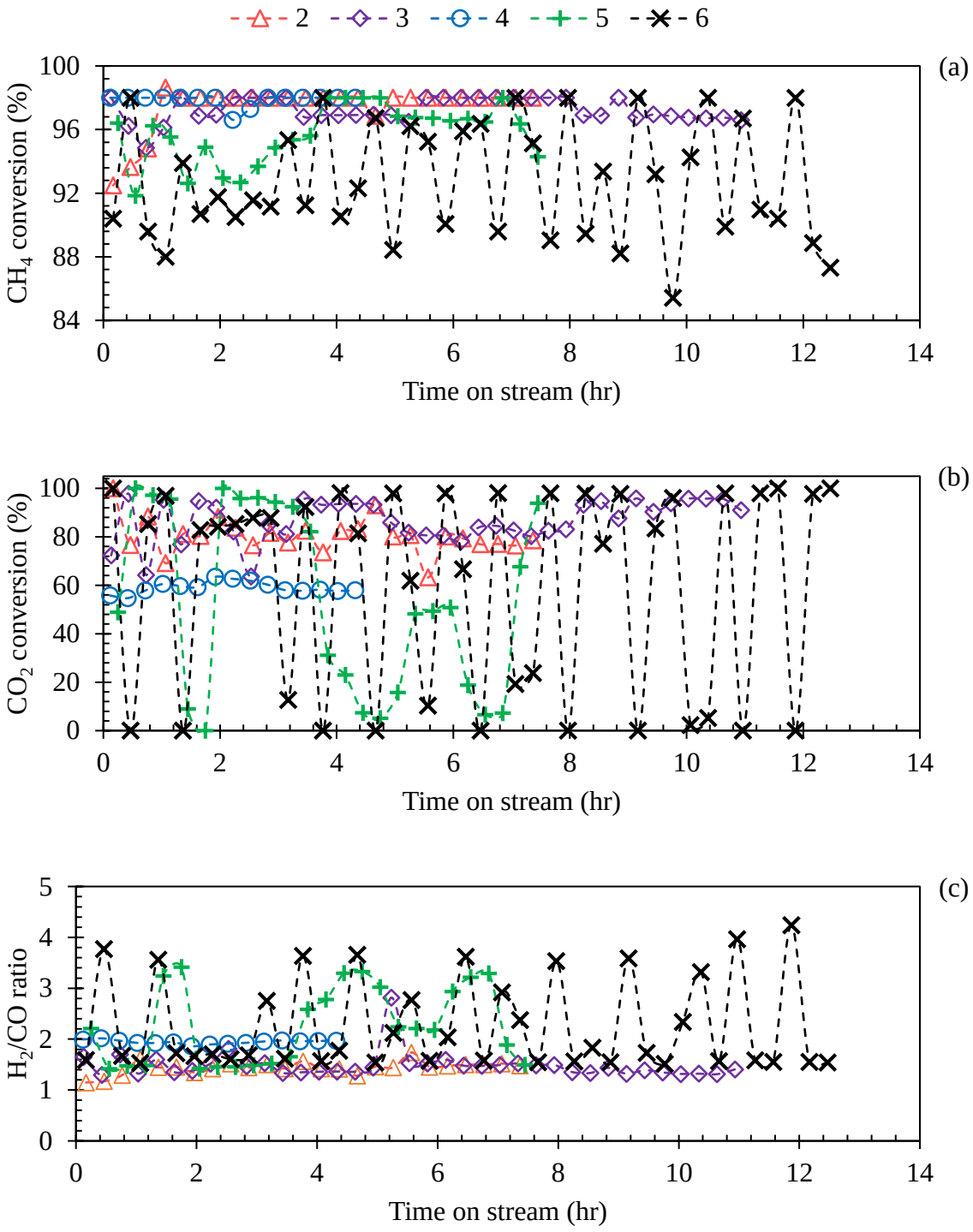

Figure 6.6 (a) CH_4 conversion, (b) CO_2 conversion, and (c) H_2/CO ratio of SCRM over catalyst Y at 850 °C using various biogas feed compositions, GHSV = 110 L g^{-1} hr^{-1}. Legends show the feed numbers

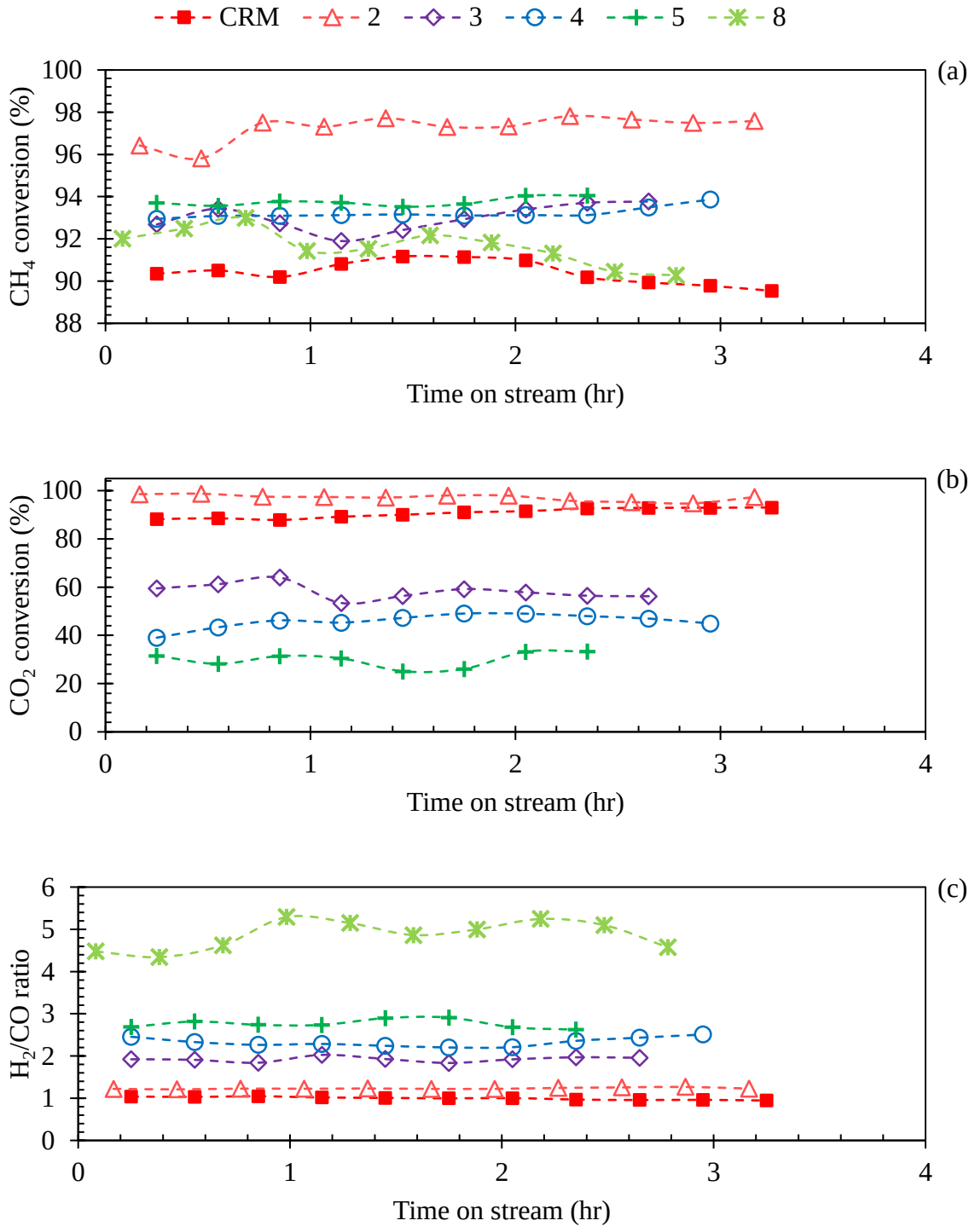

Figure 6.7 (a) CH_4 conversion, (b) CO_2 conversion, and (c) H_2/CO ratio of SCRM over Co-Op reforming catalyst at 850 °C using various biogas feed compositions, GHSV = 110 L g^{-1} hr^{-1}. Legend show the feed numbers

6.2.3 Comparison of Catalysts for SCRM under Accepted Feed Compositions

Discussion in sections 6.2.1 and 6.2.2 has shown that the steam content in feed was the key factor affecting the catalytic performance during SCRM reaction. The Ni-Co bimetallic, Ni monometallic and Co monometallic catalysts could not work properly when a feed contains more than 12, 15, and 6% mol of steam, respectively. During SCRM reactions, catalyst X, catalyst Y and the Co-Op reforming catalyst begin to cause net CO_2 production when the feed contains more than 20, 17, and 15% mol of steam, respectively. On the other hand, the industrial partner requires; (a) that the produced H_2/CO ratio in the syngas is in the range of 1.8 to 2, and (b) CO_2 is consumed through the process to some extent. Considering these criteria and our experimental results, feed 5 is minimal accepted feed composition for catalyst X, Ni-Co bimetallic catalyst and Ni monometallic catalyst; feed 4 is the one for catalyst Y; and feed 3 is the one for the Co-Op reforming catalyst. Figure 6.8 compares the catalysts' performances for SCRM reaction and theoretical conversions of CO_2 and CH_4 at the accepted feed compositions, where the equilibrium conversions were calculated from the equilibrium compositions given in section 6.1.

Figure 6.8 reveals that CH_4 and CO_2 conversions with the accepted feeds never exceed the maximum possible conversions (equilibrium or theoretical conversions). For all the catalysts with accepted feeds, CO_2 conversions were significantly less than the possible theoretical values while CH_4 conversions were closer to the theoretical values. The occurrence of WGS reaction, when there is steam in feed, could explain the low conversion of CO_2. Results also show that the performance of the Ni-Co catalyst, Co-Op catalyst and catalyst Y were more stable than catalyst X and the Ni monometallic catalyst (smaller range for 95% confidence intervals). On the other hand, the Co-Op catalyst with feed 3 and catalyst Y with feed 4 could produce syngas with higher H_2/CO ratios than the Ni-Co catalyst with feed 5. Coupling these with the facts (a) that feed 5 had higher steam content than feeds 3 and 4, and (b) that the Ni-Co catalyst showed the highest CO_2 conversion, it seems that Co-Op and Y catalysts favoured SRM over CRM while the Ni-Co catalyst facilitated CRM more than SRM. It could be concluded that the Ni-Co bimetallic catalyst and biogas feed composition 5 represent the optimum combination, not only to produce syngas with the desired H_2/CO ratio (1.8 to 2) but also to convert more than 70 % of CO_2 of the biogas feed.

(a)

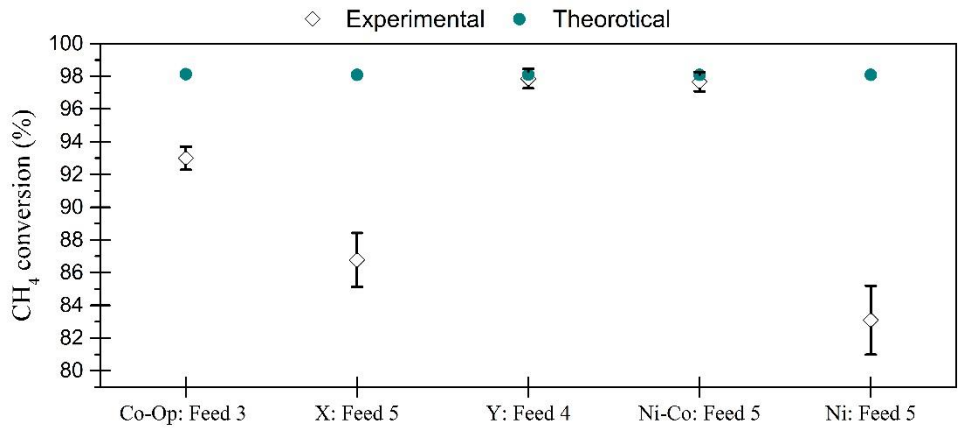

(b)

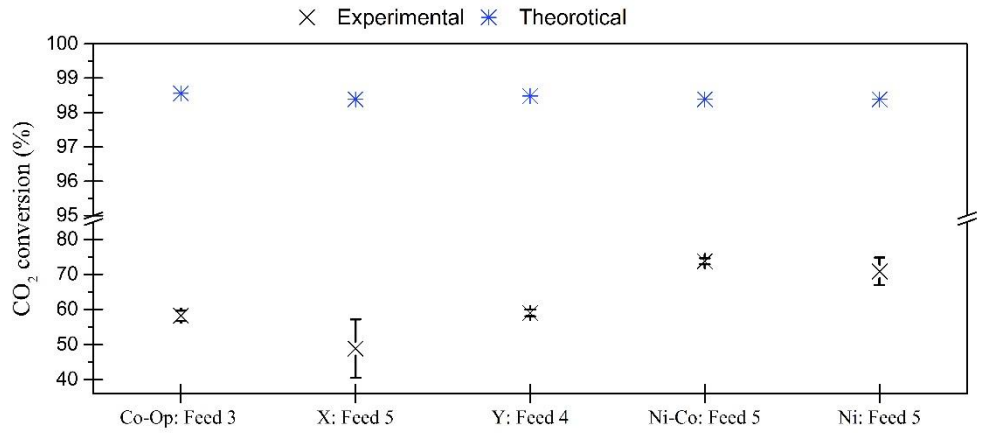

(c)

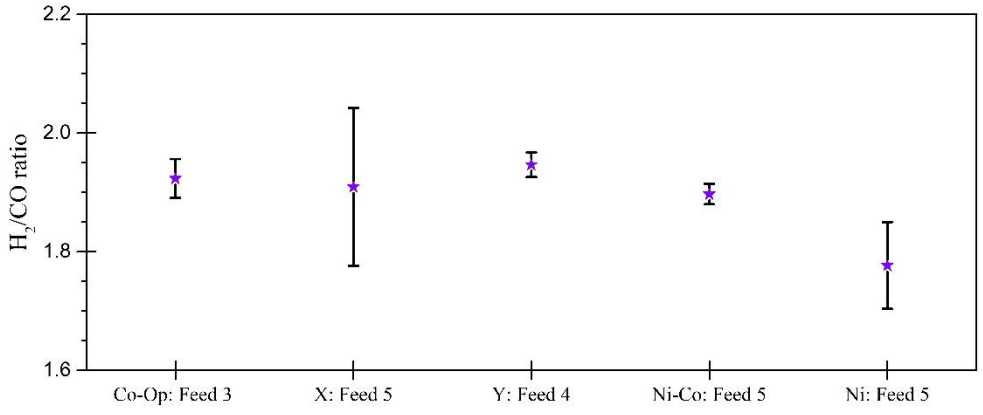

Figure 6.8 Experimental and theoretical (a) CH_4 conversion, (b) CO_2 conversion, and (c) H_2/CO ratio of SCRM over different catalysts at 850 °C, GHSV = 110 L g^{-1} hr^{-1}. Error bars shows the 95% confidence intervals.

6.3 Performance of Catalyst Mixture for SCRM

It was found that none of the catalysts can handle a biogas feed containing more than 12% mol of steam to meet the industrial partner's requirements in H_2/CO ratio and CO_2 conversion. To overcome this challenge, one more trial was attempted with two catalysts working together. Therefore, 0.2 g Ni-Co bimetallic catalyst and 0.2 g Co-Op steam reforming catalyst were loaded with two different arrangements in an Inconel reactor. In arrangement A, the Ni-Co catalyst was loaded above the Co-Op reforming catalyst (each portion of the catalysts was mixed with 1.8 g of silica carbide). In arrangement B, both Ni-Co and Co-Op catalysts were mixed with 3.6 g of silica carbide loaded in the reactor. The catalysts were reduced at 900 °C in a mixture of H_2 (50%) and N_2 (50%) for 4 hr. The SCRM reaction was then carried out with the feed compositions in Table 6.1 at 850 °C with a GHSV of 110 L g^{-1} hr^{-1}. The performance of the catalysts over SCRM reaction for arrangements A and B are shown in Figures 6.9 and 6.10, respectively.

The results indicate that over the mixture of catalysts with either arrangements, high conversion of CH_4 (95%) and CO_2 (96%) was observed for the CRM reaction. Adding steam to the feed (feed 3) led to oscillation of both CH_4 and CO_2 conversions. The oscillation was more intensive in arrangement A than B. Since such a performance was observed for the Ni-Co bimetallic catalyst (Figure 6.2), the oscillation was more likely due to the presence of this catalyst in the reactor. Competition between CRM and SRM over active catalyst sites as well as periodic cycling of carbon deposition and elimination could explain this behaviour (Wei et al., 2000; Zhang et al., 2007). However, with more steam content in feed 5, the CH_4 and CO_2 conversion oscillations were eliminated. It seems that there is a certain range of steam to CH_4 ratio in the feed (between 2 and 3), where the oscillation and therefore, the competition between SRM and CRM reactions over the catalysts becomes dominant. Moreover, in feed 5, CH_4 was almost consumed in both catalyst arrangements while the CO_2 conversion in arrangements A and B dramatically dropped to 31% and 34%, respectively. In feed 7 with the highest steam content, CH_4 conversion in arrangement B dropped while it was totally consumed in arrangement A. Loss of active metallic sites due to oxidation of the Ni-Co bimetallic catalyst with steam in arrangement B could explain this phenomenon. In addition, more CO_2 was observed in the product gas than the feed in both arrangements for feed 7. This suggests that CO_2 was produced as a by-product with this feed. In both catalyst arrangements, it was observed that CO_2 and steam competed over CH_4 and increasing

steam content in a feed favoured more of both SRM and WGS reactions than CRM reaction. Therefore, with more steam content in the feed, a higher H_2/CO ratio in the product was obtained.

In summary, it was found that physical mixing of the Ni-Co catalysts with Co-Op reforming catalyst in both arrangements could not improve the overall performance for SCRM reaction using a biogas feed with high steam content. This further indicates that the steam content of the feed should be balanced to avoid the Ni-Co catalyst deactivation. However, literature suggest that addition of noble metals (Rh, Ru and Ir) as promoters could enhance the durability of Ni-based catalysts for feeds with high steam content. It is reported that these promoters along with Ni could form an alloy which could improve the catalyst resistance and stability in high steam content conditions (Moales-Cano et al., 2015; Sehested, 2006). Thus, addition of such promoters could be one possible solution to enhance the Ni-Co catalyst durability in high steam content feed, which needs to be further studied.

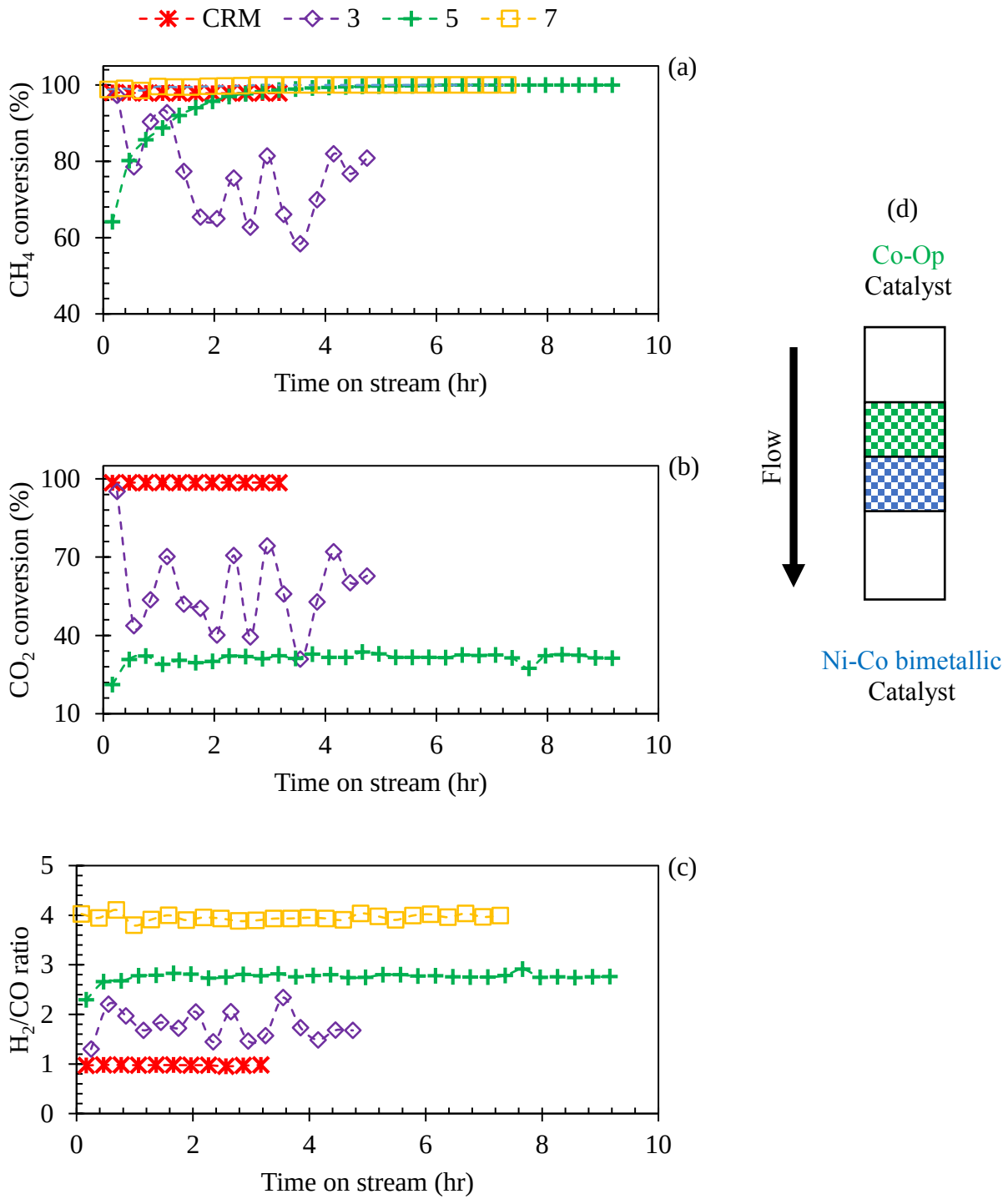

Figure 6.9 (a) CH_4 conversion, (b) CO_2 conversion, and (c) H_2/CO ratio of SCRM over (d) simultaneous Co-Op and Ni-Co catalysts in arrangement A. Reaction conditions: 850 °C, GHSV of 110 L g^{-1} hr^{-1}, and various biogas feed compositions. Legend shows the feed numbers

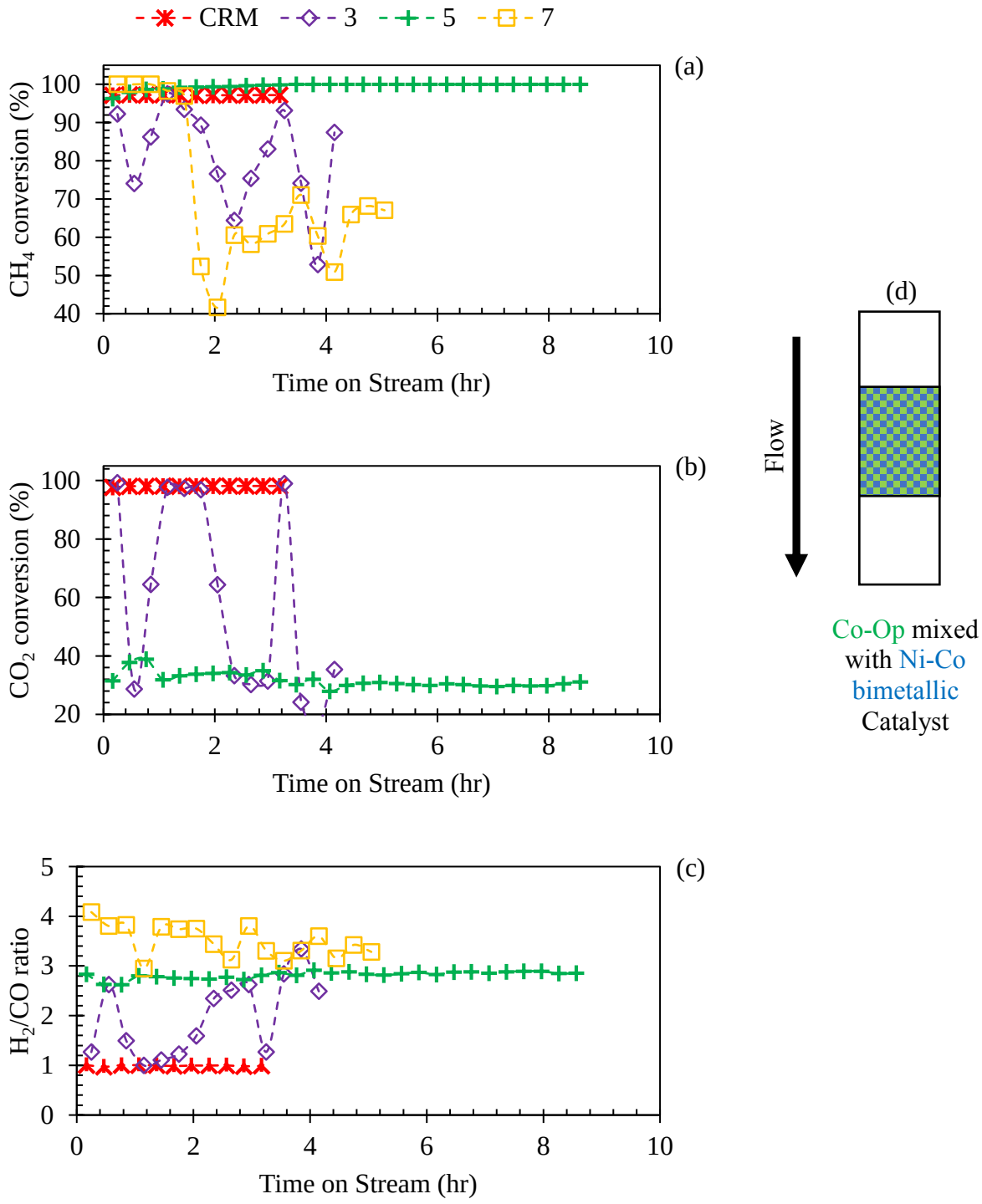

Figure 6.10 (a) CH_4 conversion, (b) CO_2 conversion, and (c) H_2/CO ratio of SCRM over (d) mixture of Co-Op and Ni-Co catalysts in arrangement B. Reaction conditions: 850 °C, GHSV of 110 L g^{-1} hr^{-1}, and various biogas feed compositions. Legend shows the feed numbers

6.4 Deactivation Mechanism of Ni and/or Co Catalysts in SCRM

The Ni-Co bimetallic, Ni monometallic and Co monometallic catalysts deactivated quickly with the biogas feed with high steam content. Researchers studying steam reforming reactions over Ni and Co catalysts, attributed the loss of catalyst activity to two major reasons: (a) carbon deposition and (b) metal sintering which could lead to metal oxidation (Argyle & Bartholomew, 2015; Morales-Cano et al., 2015; Sehested, 2006). The first one is more expected at low steam/methane ratios while the second one is more likely at the high steam contents and high reaction temperatures (above 500 °C). Moreover, catalysts with small metal particles are more resistant to both carbon deposition and sintering (Iglesias et al., 2017). Our earlier work showed that the reduced catalysts have small metal nanoparticles (less than 10 nm) and could facilitate CRM reaction without significant amount of carbon formation (Shakouri, 2012; Wang et al., 2013). Thus, it seems that the catalyst deactivations in SCRM reaction at 850 °C and high steam contents were more likely initiated due to sintering.

To investigate the effect of steam on the catalysts' activity, their performance for SRM reaction was studied. In each experiment, 0.1 g of catalyst (Ni-Co bimetallic and Ni and Co monometallic) was reduced at 900 °C in an Inconel reactor in a mixture of H_2 (50%) and N_2 (50%) for 4 hours. Then SRM reaction was carried out at 850 °C with an equimolar reactant ratio balanced with N_2 and GHSV of 110 L g^{-1} hr^{-1}. Reaction results, as shown in Figure 6.11, indicates that the catalysts could initially activate SRM reaction, however they were rapidly deactivated within 1 hour TOS. Sehested (2006) reported that this rapid deactivation in SRM is due to the sintering of the catalyst's metallic sites, while the deactivation because of carbon deposition is more like a gradual decay in the catalyst activity. He found that in the presence of excess amount of steam, the catalyst metal particles could grow larger sizes than their sizes in the reduced state. These large metal sites are more likely to be re-oxidized resulting in a rapid catalyst deactivation.

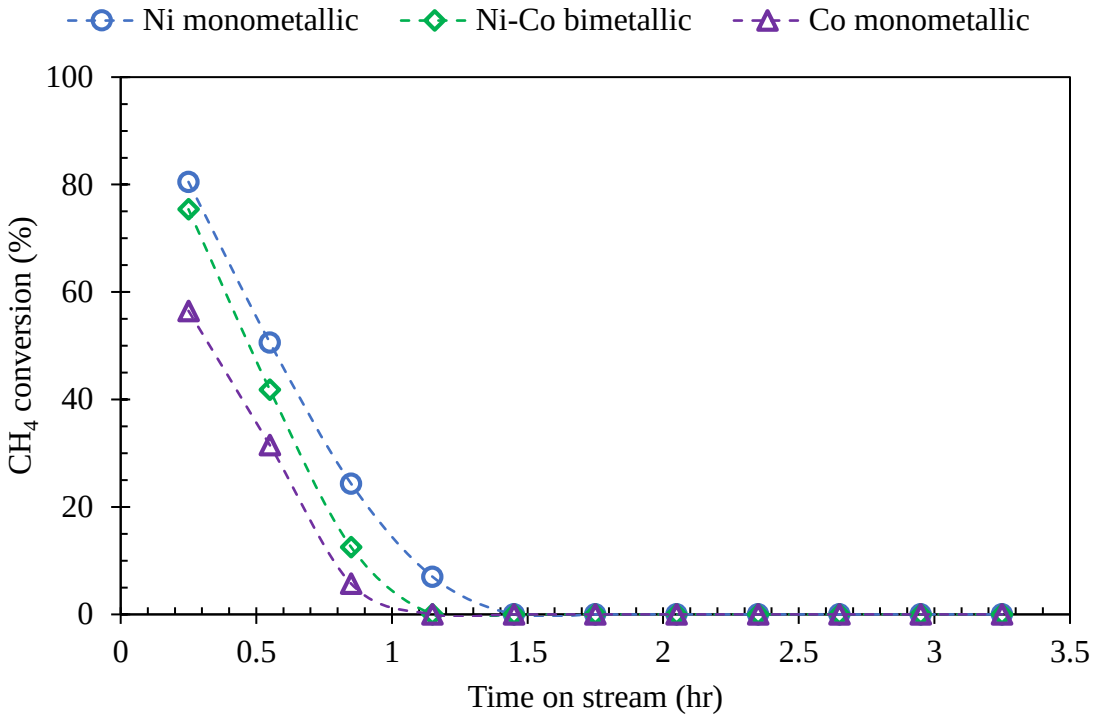

Figure 6.11 Activity of Ni-Co bimetallic as well as Ni and Co monometallic catalysts for SRM reaction. Reaction conditions: 0.10 g catalyst, temperatures: 850 °C, 1atm, GHSV of 110 L g^{-1} hr^{-1}, $CH_4/H_2O/N_2$ = 1/1/1

Although different reaction pathways have been proposed for steam reforming of methane reaction on Ni and Co catalysts, the following reactions on the surface of the catalysts are believed to play the main roles:

$$CH_4 + S \rightleftharpoons C{\cdot}S + 2H_2 \quad (6.8)$$

$$H_2O + S \rightleftharpoons O{\cdot}S + H_2 \quad (6.9)$$

$$C{\cdot}S + O{\cdot}S \rightleftharpoons CO + 2S \quad (6.10)$$

where S represents a catalyst surface site (Rakass et al., 2006; Rostrup-Nielsen et al., 2002; Xu & Froment, 1989). Reaction 6.10 indicates that if there are excess number of O·S intermediates in the reaction system, catalyst could be deactivated from re-oxidization.

To further investigate the deactivation mechanism, an XAS analysis was conducted in the SXRMB beamline at the Canadian Light Source. 10 mg of each catalyst (Ni-Co bimetallic, Ni monometallic and Co monometallic) were loaded in the 6-hole shooter and were reduced at 900 °C in a quartz reactor in a mixture of H_2 (50%) and N_2 (50%) for 4 hours. A feed containing 33% CH_4, 33% steam (which is more than the amount that each catalyst could tolerate in biogas feed) and 34% N_2 was next introduced to the reduced catalysts at 850 °C for 6 hours. To compare, another set of catalysts were reduced in a mixture of H_2 (50%) and N_2 (50%) for 4 hours. Both sets of catalysts were cooled down to room temperature in the presence of N_2. Then the catalysts used for SRM reaction, reduced catalysts and catalysts before reduction were taken to the SXRMB beamline at CLS for XAS analysis. Figure 6.12 compares the Ni and Co K-edges XANES spectra of the catalysts at the three reaction stages, before reduction, after reduction and after used for SRM reaction. Moreover, to quantify the extent of Ni and Co reduction in the catalysts, the linear combination fitting (LCF) module in Athena software was used. K-edge XANES spectra of Ni and Co of the catalysts in the range of -20 eV to +30 eV of the edge jumps were fitted with their respective metal foil and metal oxide standard spectra. Fitting results are given in Table 6.2.

Figure 6.12 reveals that both Ni and Co spectra of the catalysts after SRM reaction were more like their spectra before reduction (oxide forms) than the reduced ones. This indicates that in the presence of steam, the metallic sites in the reduced catalysts were likely altered to their initial state before reduction (metal oxides). The LCF results, as summarized in Table 6.2, also reveal that more than 90% of Ni and 50% of Co sites in the reduced catalysts were in metallic forms while after SRM reaction, both Ni and Co sites were 100% in their oxide forms. This further proves that

there are not any metal sites left on the catalysts after SRM reaction. It seems that in the harsh reaction environment (high temperature and high steam content), the metallic sites have grown larger particles due to sintering. These large metal sites were more likely to react with the excess O·S intermediates from seam dissociation resulting in re-oxidization of the metallic sites. On the other hand, our earlier research proves that CH_4 could only be activated on the metallic sites. Thus, the catalysts lost their ability to activate CH_4, resulting in a rapid deactivation of the catalysts in feeds with high steam content.

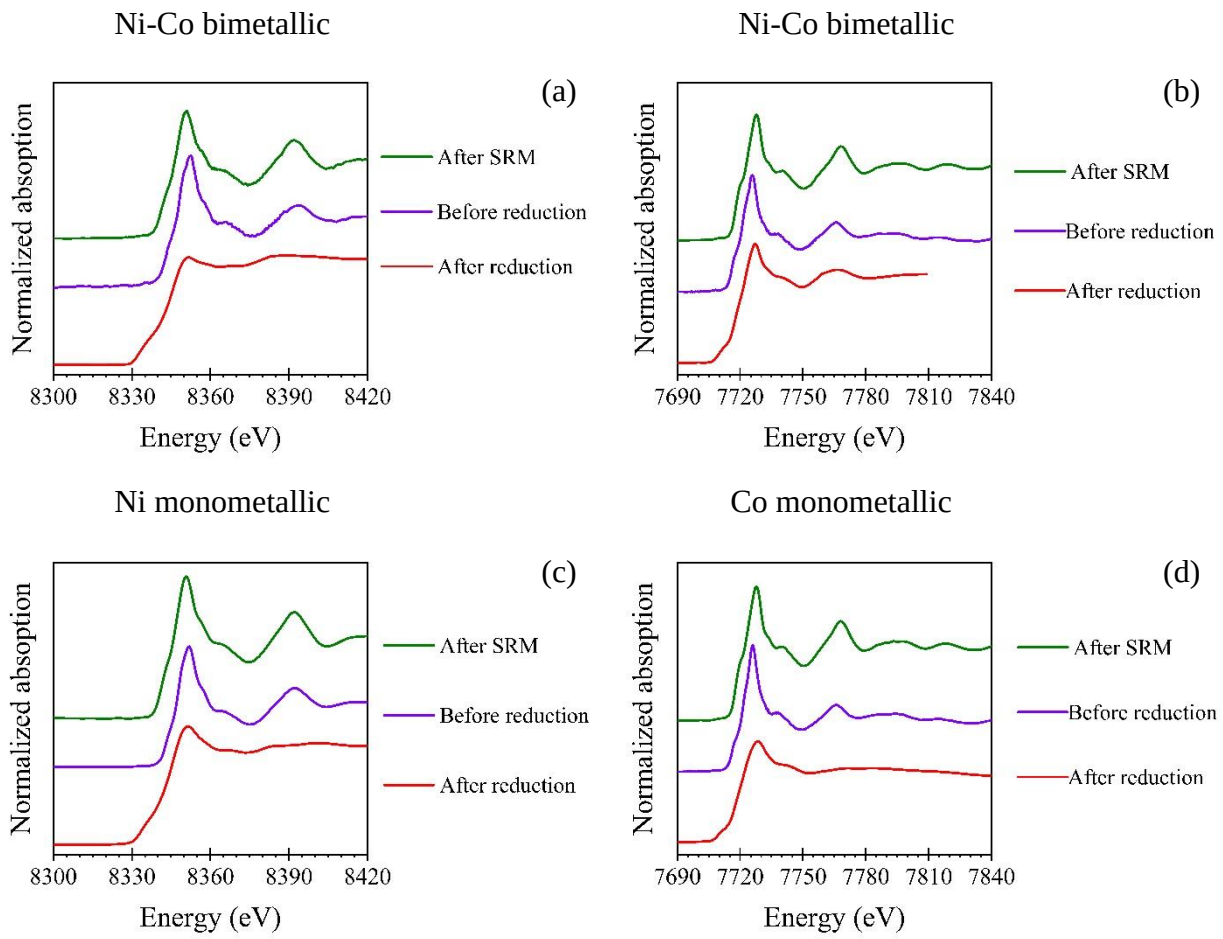

Figure 6.12 XANES spectra of catalysts after reduction (red line), before reduction (purple line), and after SRM (green line). (a) Ni K-edge of Ni-Co bimetallic, (b) Co K-edge of Ni-Co bimetallic, (c) Ni K-edge of Ni monometallic, and (d) Co K-edge of Co monometallic catalysts. Reduction conditions: 4 hr, 900 °C, 20% H_2 and 80% N_2. Reaction conditions: 6 hr, 850 °C, $CH_4/H_2O/N_2$ = 1/1/1

Table 6.2 Ni and Co species content in the reduced catalysts as well as the catalysts used for SRM reaction calculated by linear combination fitting. Reduction conditions: 900°C, 20% H_2 and 80% N_2 mixture for 4 hr. Reaction conditions: temperatures 850 °C, 1atm, GHSV of 110 L g^{-1} hr^{-1}, $CH_4/H_2O/N_2$ = 1/1/1

	Reduced				Used for SRM reaction			
	Ni	NiO	Co	CoO	Ni	NiO	Co	CoO
Catalyst	%				%			
Ni monometallic	89	11	-	-	0	100	-	-
Ni-Co bimetallic	91	9	51	49	0	100	0	100
Co monometallic	-	-	52	48	-	-	0	100

6.5 Ni-Co Catalyst Performance in Feeds Rich of CO and H_2

Produced syngas from various applications could contain a few percentages of CH_4 and CO_2. Purity of a syngas as feed for some industrial applications could be critical to avoid any unwanted side reactions such as CO-methanation (reaction 6.11) or reverse CRM reaction. One possible method to purify the syngas, is to remove the excess CH_4 and CO_2 through catalytic CRM reaction. Therefore, the catalyst should not only be able to facilitate CRM reaction, but it should not enable methane formation.

$$CO + 3H_2 \rightleftharpoons CH_4 + H_2O \text{ (CO methanation)} \quad (6.11)$$

It was found that the Ni-Co bimetallic catalyst could facilitate CRM reaction close to its equilibrium compositions. Thus, the catalyst has the potential to be used in industrial applications where purification of a syngas containing a little amount of CH_4 and CO_2 is required. In addition, industrial partner of this research has requested to investigate the performance of Ni-Co bimetallic catalyst in a syngas mixture with H_2/CO ratio of 2.

6.5.1 Performance of Ni-Co Catalyst in Pure Syngas

Methanation over Ni-Co catalyst using a pure syngas feed was initially investigated. A 0.05 g of Ni-Co powdered catalyst was reduced at 800 °C in a mixture of H_2 (20%) and N_2 (80%) for 4 hr. Then a mixture of N_2 and syngas (N_2/CO/H_2 = 1/1/2) was fed to the reactor at 800 °C and a GHSV of 110 L g^{-1} hr^{-1}. The product gas was analyzed using an online GC every 18 min. To compare, the equilibrium conversions of H_2 and CO as well as CH_4 equilibrium composition, with an identical feed, at various temperatures were calculated using the HSC Chemistry software. The experimental and theoretical results are shown in Figure 6.13 (a) and (b), respectively.

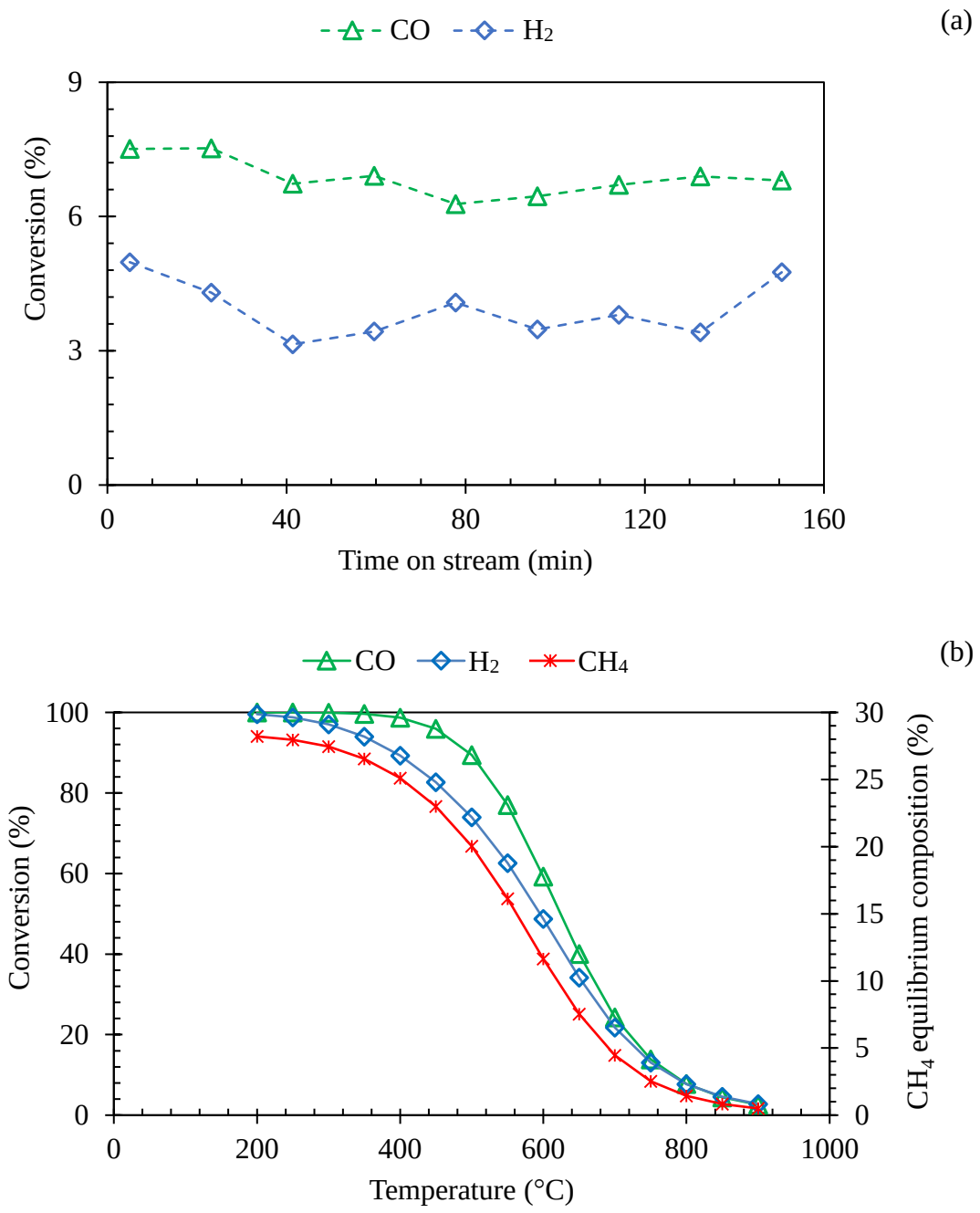

Figure 6.13 (a) CO and H_2 conversions using syngas feed over Ni-Co bimetallic powder catalyst. Reaction condition: 0.05 g catalyst, $N_2/CO/H_2$ = 1/1/2, reaction temperature: 800 °C, 1atm, GHSV of 110 L g^{-1} hr^{-1}; (b) theoretical calculation of methanation using syngas feed ($N_2/CO/H_2$ = 1/1/2) at various temperatures. Left vertical axis shows CO and H_2 conversions. Right vertical axis shows the equilibrium composition of CH_4.

Figure 6.13 (a) shows that about 7% (±0.2%) and 4% (±0.3%) of CO and H_2 were consumed in the reaction environment, respectively. However, the GC could not detect either CH_4 or CO_2 in the product gas. The low activity of Ni-Co catalyst for methanation is due to the thermodynamics barrier of methane formation. Figure 6.13 (b) reveals that formation of CH_4 from H_2 and CO is thermodynamically favourable at low reaction temperatures (200 to 600 °C). Therefore, the high experimental reaction temperature (800 °C) could explain the low activity of Ni-Co bimetallic catalyst toward CO-methanation and reverse CRM reaction using a pure syngas feed.

6.5.2 Ni-Co Catalyst Performance in Syngas-Rich Feed

This section tests the impact of H_2 and CO on CRM over the Ni-Co bimetallic catalyst in a syngas-rich feed containing only a small amount of CO_2 and CH_4. Syngas-rich feed composition is given in Table 6.3. A 0.15 g Ni-Co catalyst was reduced at 800 °C in a mixture of H_2 (20%) and Ar (80%) for 4 hr. The syngas-rich feed, with GHSV of 110 L g^{-1} hr^{-1}, was then introduced to the reactor at 800 °C and 850 °C. The product gas was analyzed using an online GC every 18 min. The reaction results are shown in Figure 6.14. Equilibrium compositions of reaction system for the syngas-rich feed at various temperatures were calculated using the HSC chemistry software. Then, CO_2 and CH_4 conversions as well as H_2/CO ratio were calculated using the equilibrium compositions and compared with the experimental results as shown in Figure 6.15.

Figure 6.14 reveals that the overall conversions of CH_4 and CO_2 at 800 °C were 68.2% (±1.9%) and 86.8% (±0.6%) during 15 hr TOS at 800 °C, respectively. Increasing the temperature to 850°C raised the overall conversions of CH_4 and CO_2 to 80.3% (±0.3%) and 89.1% (±0.3%), respectively. Occurrence of RWGS reaction can explain higher conversion of CO_2 than CH_4. It was also observed that the difference between CH_4 and CO_2 conversions at 800 °C was greater than their difference at 850 °C. It seems that the RWGS reaction affected the catalytic performance more at the lower temperature. Callaghan (2006) reported that the equilibrium constant for the WGS reaction reaches close to one at 850 °C, which could explain the lower effect of RWGS at 850 °C. A closer look at the results indicate that CH_4 and CO_2 conversions were oscillating at 800 °C while the oscillations were not significant at 850 °C. Cyclical deposition and removal of carbon from the catalyst's surface at the lower reaction temperature could be the possible explanation for

this phenomenon. Moreover, the H_2/CO ratio was slightly increased from 1.66 (±0.01) at 800 °C to 1.68 (±0.01) at 850 °C.

Figure 6.15 indicates that regardless of reaction temperature, the Ni-Co catalyst could facilitate CH_4 conversion close to the equilibrium value. However, both experimental CO_2 conversion and H_2/CO ratio were lower than the thermodynamic calculated values. This further supports the occurrence of RWGS over the Ni-Co bimetallic catalyst.

To summarize, in a syngas-rich feed, Ni-Co catalyst could not activate CO and H_2 toward methanation. However, water gas shift (WGS) reaction and its reverse (RWGS) could take place simultaneously along with dry reforming reaction. The catalyst could facilitate CH_4 and CO_2 conversions close to the possible theoretical values in the syngas-rich feed through a CRM reaction (81% conversion of CH_4, 89% conversion of CO_2 at 850 °C). Therefore, purified syngas contains much lower CH_4 and CO_2 content than the syngas-rich feed which could be further used for industrial applications.

Table 6.3 Composition of a syngas rich feed

Feed composition	mol %
Ar	8
CH_4	6
CO_2	6
H_2	53.5
CO	26.5

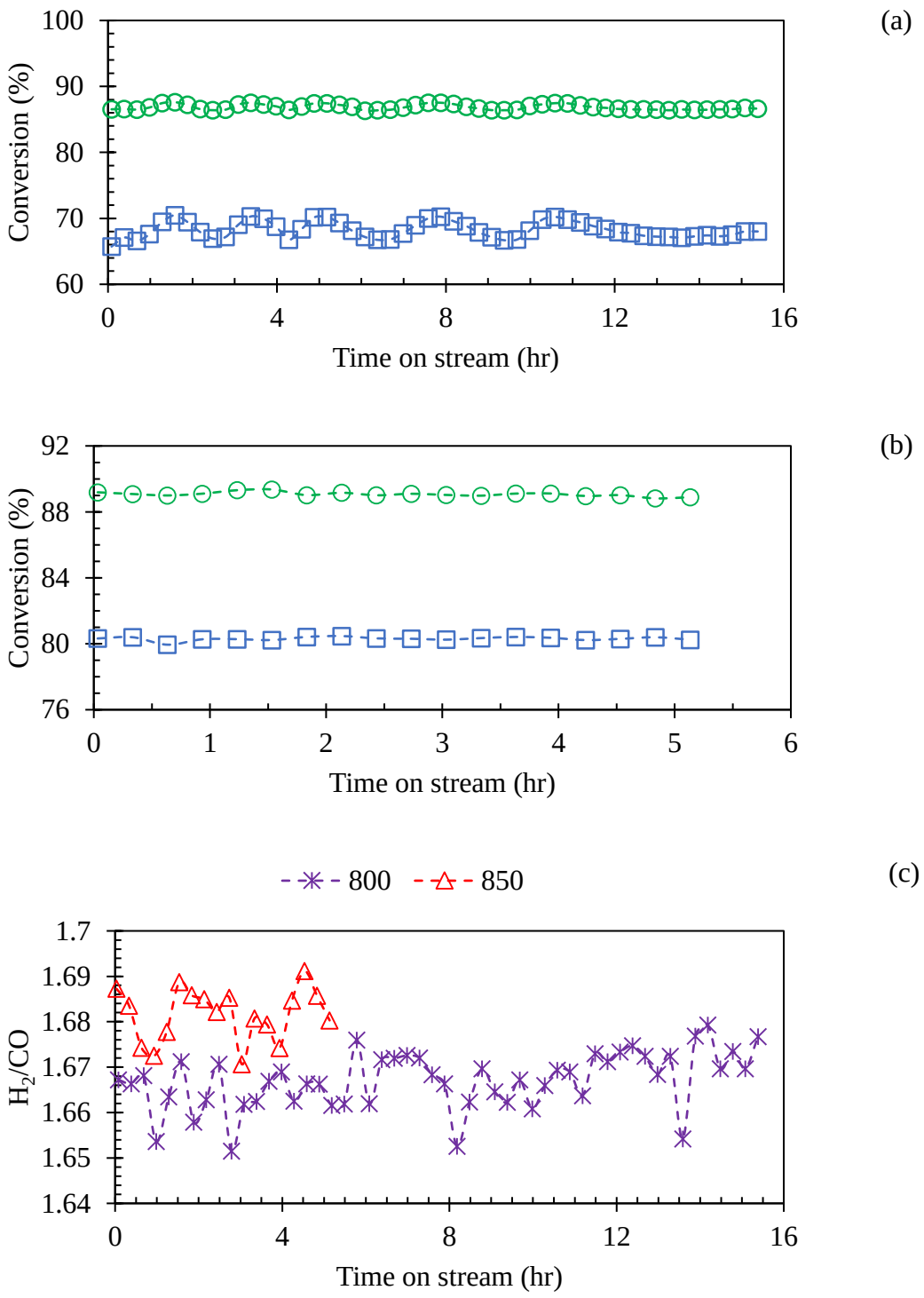

Figure 6.14 CO_2 (○) and CH_4 (□) conversions using syngas rich feed over Ni-Co bimetallic powder catalyst at (a) 800 °C, (b) 850 °C. (c) H_2/CO ratio at 800 °C and 850 °C. Reaction condition: 0.15 g catalyst, reaction temperature: 800 °C, 850 °C, 1atm, GHSV of 110 L g^{-1} hr^{-1}

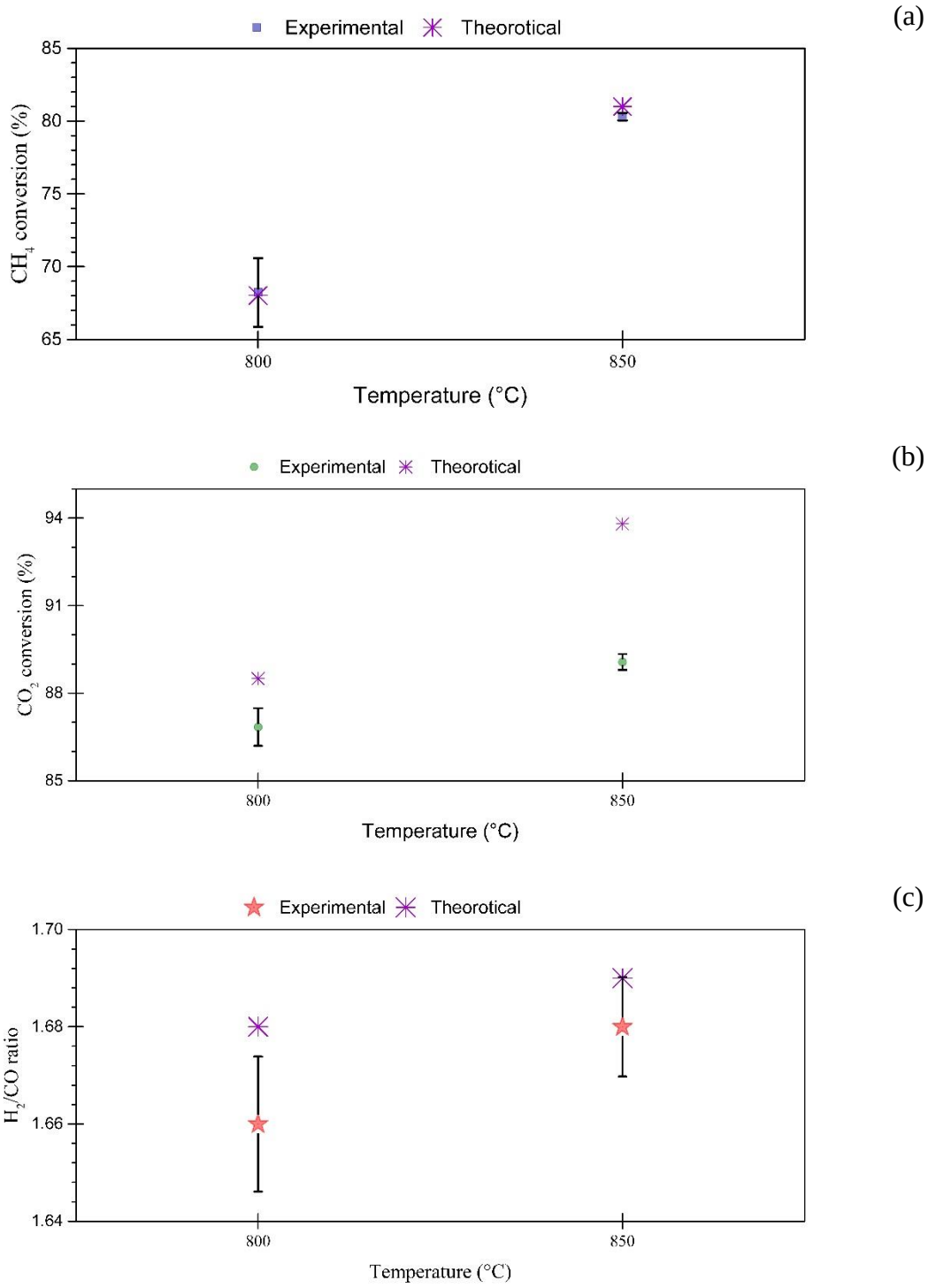

Figure 6.15 Experimental and theoretical (a) CH_4 conversion, (b) CO_2 conversion, and (c) H_2/CO ratio of CRM using syngas-rich feed over Ni-Co catalyst. Reaction condition: 0.15 g catalyst, reaction temperature: 800 °C, 850 °C, 1atm, GHSV of 110 L g^{-1} hr^{-1}. Error bars shows the 95% confidence intervals.

6.6 Conclusions

The steam content of the biogas feed is the key factor which affects the catalytic performance the SCRM reaction. The Ni-Co bimetallic, Ni monometallic and Co monometallic catalysts could not handle a biogas feed containing more than 12, 15, and 6 % mol of steam. On the other hand, CO_2 was produced as a by-product during SCRM reactions over catalyst X, catalyst Y and the Co-Op commercial reforming catalyst using a biogas feed containing more than 20, 17, and 15% mol of steam, respectively. Ni-Co bimetallic catalyst and biogas feed composition 5 (about 33% of CH_4, 21.5 mol% of CO_2, 12 mol% of H_2O, 3.5 mol% of H_2 and 30 mol% of N_2) represent the optimum combination, not only to produce syngas with the desired H_2/CO ratio (1.8 to 2) but also to convert more than 70 % of CO_2 of the biogas feed. Ni and Co K-edges XANES spectra of Ni-Co bimetallic, Ni monometallic and Co monometallic catalysts catalyst after SRM reaction with equimolar reactants (CH_4 = H_2O) revealed that steam could oxidize the active metallic sites leading to deactivation of the catalysts. Sintering of the metal active sites due to the harsh condition of the reaction environment (high temperature and high steam content) more likely initiated the catalyst deactivation. The excess amount of steam oxidized these metallic active sites resulting in deactivation of the catalysts. It was also found that the Ni-Co bimetallic catalyst (a) could not activate H_2 and CO, and (b) could convert CH_4 and CO_2 (impurities) in a syngas-rich feed through CRM reaction close to the possible theoretical values (81% conversion of CH_4, 89% conversion of CO_2 at 850 °C).

CHAPTER 7

Sulfur Poisoning Mechanism of Ni and Co Catalysts for CRM with SO_2

Methane gas from landfills, shale or coal-delivered gas may contain sulfur compounds such as H_2S, SO_2, COS, etc., which could deactivate the reforming catalysts. To understand the sulfur poisoning mechanism, the performance of Ni and Co catalysts for CRM reaction in the presence of SO_2 was studied. To monitor and investigate the effect of SO_2 on catalytic performance, a high concentration of SO_2, 500 ppm, was intentionally chosen.

7.1 Performance of Catalyst Support for CRM with SO_2

$AlMgO_x$ catalyst support was prepared using the co-precipitation method described in section 3.1.1. A 0.1 g sample of support was reduced in a quartz reactor in a mixture of H_2 (20%) and N_2 (80%) at 800 °C for 4 hr followed by a CRM reaction with a gas feed containing an equimolar ratio of CH_4, CO_2, and N_2 and GHSV of 60 L g^{-1} hr^{-1} at 800 °C for 1 hr. Then, 500 ppm of SO_2 was introduced to the feed and the reaction continued for 3 hr. The SO_2 was stopped and the CRM reaction continued for another 2 hr. The product gas was analyzed using an on-line GC equipped with TCD and PFPD detectors. The test results for the support are shown in Figure 7.1.

Figure 7.1 (a) indicates that the support was not active for the CRM reaction (negligible conversion of CH_4). However, the support could activate CO_2 to some extent (about 7% CO_2 conversion). When SO_2 was added to the feed of CRM, the conversion of CH_4 and CO_2 increased, H_2S was produced and both water and elemental sulfur were observed in the outlet of quartz

reactor. When the SO_2 was stopped, H_2S was not detected in product gas and the performance of the support for CRM became negligible. This implies that during the SO_2 poisoning period, unlike the CRM period, an interaction between SO_2 and catalyst support could have formed active intermediate which could facilitate the CH_4 dissociation. Consequently, the dissociated CH_4 intermediates could have reacted with the activated CO_2 intermediates producing H_2 and CO. As shown in Figure 7.1 (b), during the poisoning period, H_2 and CO were observed in the product supporting the occurrence of CRM reaction in the presence of SO_2. However, the observed H_2/CO ratio (0.38±0.02) in the product was much lower than its theoretical value at 800 °C (H_2/CO ratio of 0.95). The occurrence of RWGS reaction in the presence of SO_2 could be a possible explanation for this phenomenon. Figure 7.1 (c) shows that H_2S was produced as soon as SO_2 was introduced to CRM reaction. These observations agree with literatures stating SO_2 could be reduced by methane over alumina-based catalysts at temperatures higher than 550 °C through reactions 7.1 and 7.2 to produce H_2S, elemental sulfur and water (Bobrin et al., 1989; Hilli et al., 2015; Sarlis et al., 1988; Yu et al., 1997; Zhu et al., 1999).

$$CH_4 + 2SO_2 \rightleftharpoons 2[S] + CO_2 + 2H_2O \quad (7.1)$$

$$CH_4 + SO_2 \rightleftharpoons H_2S + CO + H_2O \quad (7.2)$$

To further investigate Raman Spectroscopy was conducted on the spent support using a Renishaw 2000 micro-Raman system operated at an argon laser wavelength of 514.5 nm (Saskatchewan Structural Science Centre, University of Saskatchewan). Figure 7.2 exhibits Raman spectra of the spent support for CRM reaction in the presence of SO_2. The Raman spectrum reveals peaks at about 1345, 1590, 2690 and 2950 cm^{-1}. The peaks at 1345 and 1590 cm^{-1} are respectively known as D-band (disorder-induced mode) and G-band (graphite-like mode), as the key features of carbon species. Moreover, peaks at 2690 and 2950 are attributed to the second order of the D peak and (D+G) peak, respectively (Barahuie et al., 2017; Ferrari, 2007). Thus, the Raman spectrum shown in Figure 7.2 clearly reveals the presence of carbon on the spent $AlMgO_x$ support, which further proves dissociation of CH_4 on the support in the presence of SO_2. CH_4 was more likely dissociated on the sulfur-support species to produce H_2 and H_2S gases as well as C-support intermediates. Some of the carbon intermediates from CH_4 dissociation could not react with O intermediates from CO_2 dissociation leading to carbon deposition on the surface.

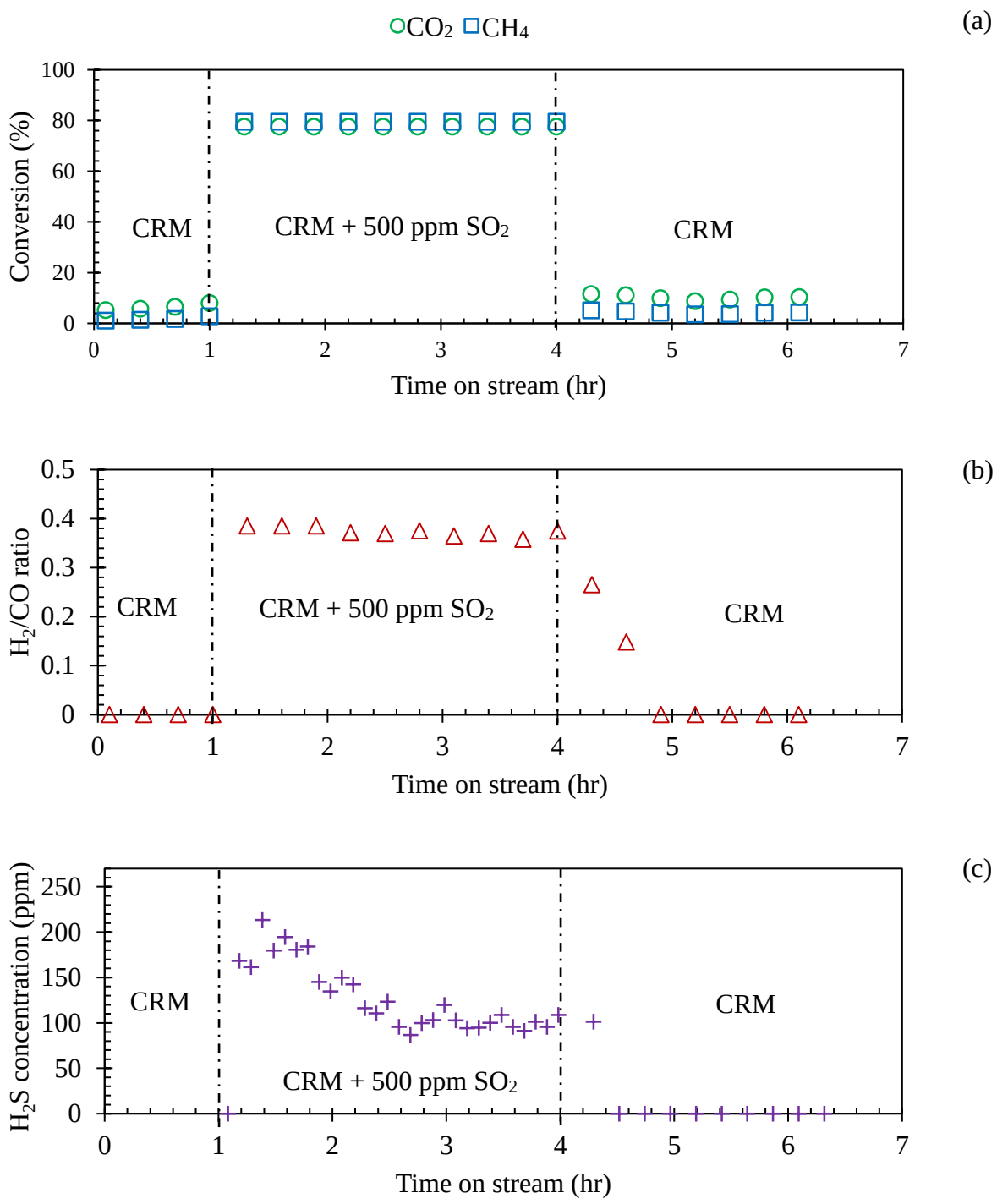

Figure 7.1 (a) CO_2 (○) and CH_4 (□) conversions, (b) H_2/CO (Δ) ratio in the product gas, and (c) H_2S (+) concentration in the product gas for CRM reaction in the presence of 500 ppm SO_2 over $AlMgO_x$. Reaction conditions: 0.10 g catalyst support, temperature: 800 °C, 1 atm, GHSV of 60 L g^{-1} hr^{-1}, $CH_4/CO_2/N_2$ = 1/1/1, 500 ppm SO_2 during the poisoning period

Putting the parcels together, the presence of SO_2 during the CRM reaction improved both CH_4 and CO_2 conversions over $AlMgO_x$ catalyst support. However, the production of H_2S, the low ratio of produced H_2/CO, deposited carbon on the support, and the appearance of both elemental sulfur and water in the outlet of the reactor indicate that the presence of SO_2 did not mainly facilitate CH_4 and CO_2 conversions through CRM reaction. H_2S and elemental sulfur were more likely produced from reduction of SO_2 by CH_4. Moreover, production of water and enchantment of CO_2 conversion were more likely because of the occurrence of RWGS reaction which resulted in low value of H_2/CO ratio in the product gas as well. Deposited carbon could also explain the enhancement of CH_4 conversion and decay of H_2 production in the presence of SO_2.

7.2 Performance of Catalysts for CRM with SO_2

Two groups of Ni-Co/$AlMgO_x$ catalysts were prepared with either the co-precipitation method, denoted as CC (or CopCat), or the impregnation method, denoted as IC (or ImpCat), with various Ni and/or Co loadings. For the IC group, $AlMgO_x$ support was synthesized by the co-precipitation of Al and Mg from their nitrate solutions. The catalysts' descriptions as well as their metal content, obtained from ICP analysis, are summarized in Table 7.1 (Wang et al., 2013).

The catalytic performance of each sample for CRM reaction in the presence of SO_2 was investigated with conditions identical to those described for testing the support in section 7.1. Reaction results in terms of CH_4 and CO_2 conversions are shown in Figure 7.3. In addition, in all the experiments, water and elemental sulfur were observed in the outlet of the quartz reactor and H_2S was detected as a by-product in the product gas.

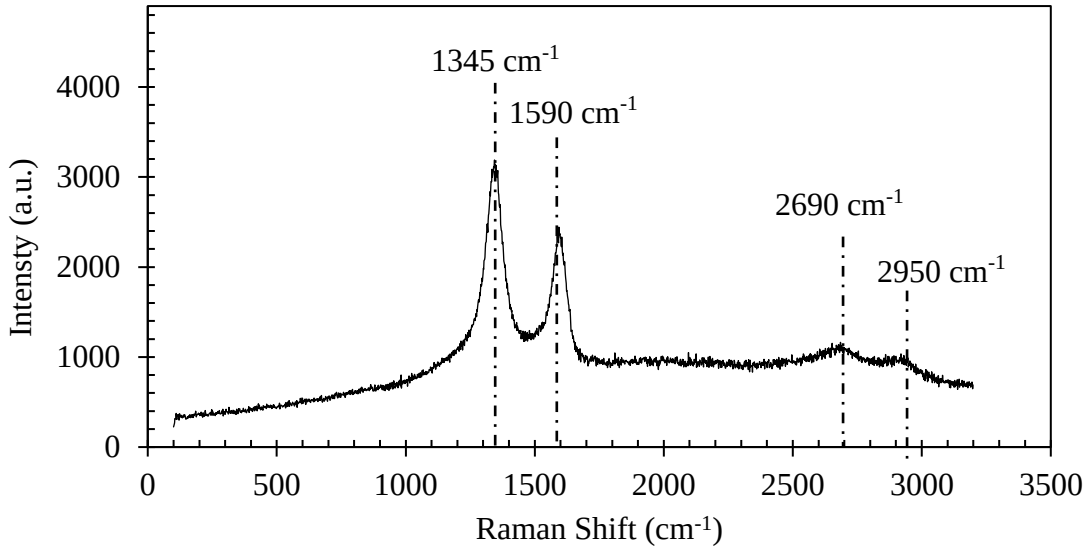

Figure 7.2 Raman spectrum of the spent support used for CRM reaction in the presence of 500 ppm SO_2. Reaction conditions: 0.10 g catalyst support, temperature: 800 °C, 1 atm, GHSV of 60 L g^{-1} hr^{-1}, $CH_4/CO_2/N_2$ = 1/1/1, 500 ppm SO_2 during the poisoning period

Figure 7.3 shows that both CO_2 and CH_4 conversions were increased as soon as SO_2 was added to the feed, while after the SO_2 was stopped, the conversions dropped to their values prior to the poisoning. Combining the results of Figures 7.1 and 7.3 indicates that the increase in CH_4 and CO_2 conversions over the catalysts in the presence of SO_2 was similar to the performance of the catalyst support shown ($AlMgO_x$). Because of $AlMgO_x$ was the dominant part of all the prepared catalysts (shown in Table 7.1), these results imply that the catalyst support plays the key role in the performance of the catalysts for CRM reaction in the presence of SO_2. Thus, a performance trend similar to that of the catalyst support alone was observed for both CH_4 and CO_2 conversions for all the catalysts regardless of their metal content and preparation procedure. On the other hand, the decomposition of SO_2 with CH_4 into elemental sulfur and water over support of catalysts ($AlMgO_x$) through reactions 7.1 and 7.2 could explain their appearance in the outlet of the reactor.

Figure 7.3 also indicates that both CH_4 and CO_2 conversions generally followed the order of Ni monometallic > Ni-Co bimetallic > Co monometallic during 10 hr TOS. However, IC-Co5 catalyst was the only exception to this trend in the presence of SO_2. Over IC-Co5 catalyst, the highest enhancement of CH_4 and CO_2 conversions was observed (about 54 % for CH_4 and 51 % for CO_2). It is reported that cobalt is thought to be an active phase for reduction of SO_2 by CH_4 (Yu et al., 1997). Since the IC-Co5 had the highest reduced cobalt content among the catalysts (Wang et al., 2013) then it likely had the highest cobalt sulfide content during the poisoning period, which could have led to higher CH_4 and CO_2 conversions than the other catalysts.

The selectivity results in terms of H_2/CO ratios as well as H_2 and CO yields are shown in Figure 7.4. Results clearly reveal that H_2/CO ratio decreased when SO_2 was introduced to CRM reaction. This suggests that in the presence of SO_2, catalysts were more selective toward CO production than H_2 production. Figure 7.4 (b) and (c) clearly show the higher production of CO and lower production of H_2 during the poisoning period. The occurrence of RWGS reaction could explain higher production of CO than H_2 and the increase of CO_2 conversion in presence of SO_2 during CRM reaction.

Table 7.1 Metal composition of the catalysts measured by ICP

Catalyst	Preparation method	Ni	Co	Mg	Al	Ni/Co	Mg/Al
		%					
CC-Co6	Co-precipitation	0	6	68	26	-	2.7
CC-Ni2Co4		2	4	68	26	0.6	2.6
CC-Ni4		4	0	69	27	-	2.6
$AlMgO_x$ support		-	-	69	31	-	2.2
IC-Co5	Impregnation	0	5	65	30	-	2.1
IC-Ni2Co3		2	3	68	27	0.5	2.5
IC-Ni5		5	0	65	30	-	2.2

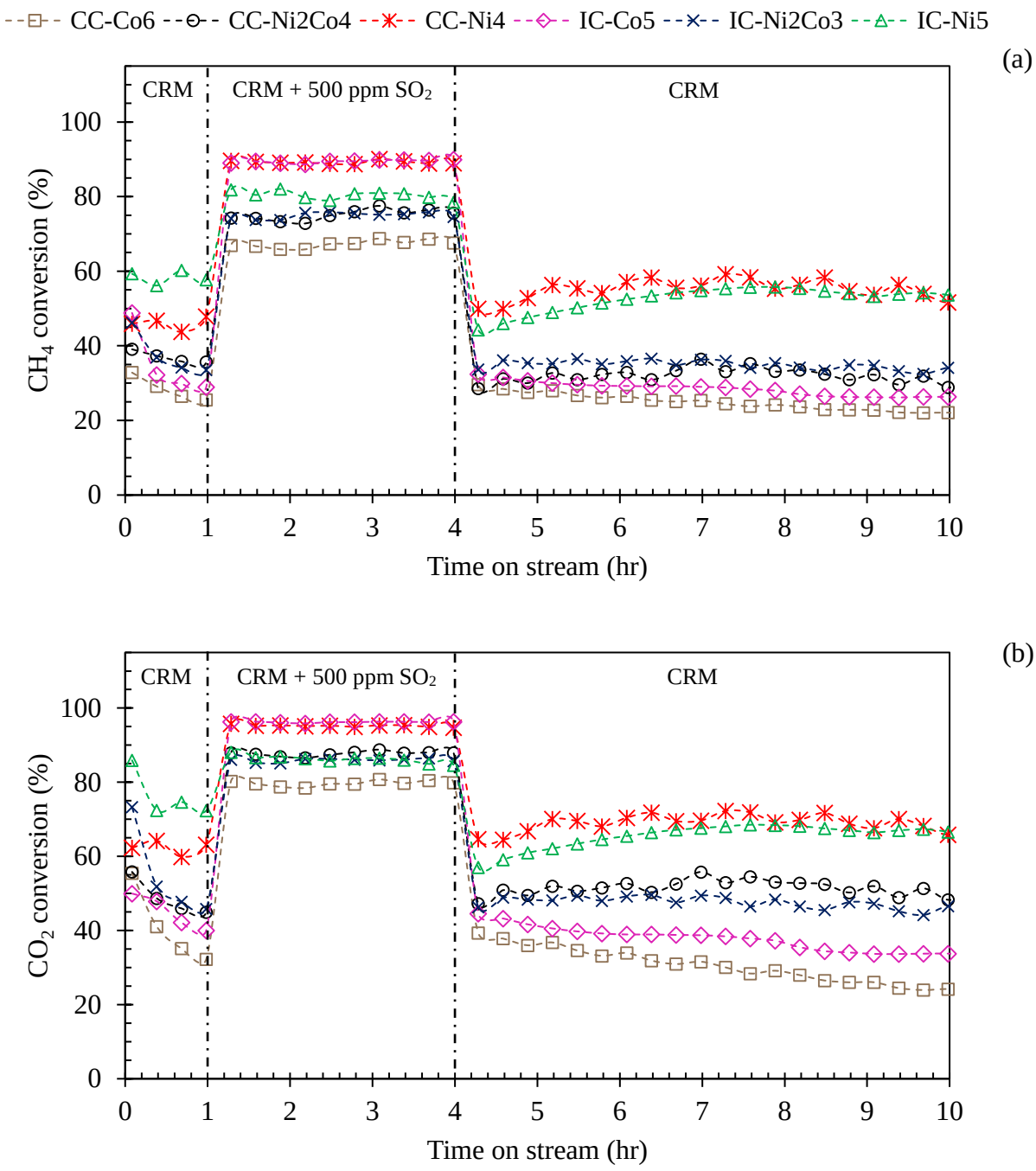

Figure 7.3 (a) CH_4 conversion and (b) CO_2 conversion from CRM reaction over Ni and Co monometallic and Ni-Co bimetallic catalysts before, during, and after the presence of SO_2. Reaction conditions: 0.10 g of catalyst, temperature: 800 °C, 1 atm, GHSV of 60 L g^{-1} hr^{-1}, $CH_4/CO_2/N_2$ = 1/1/1, 500 ppm SO_2 during the poisoning period

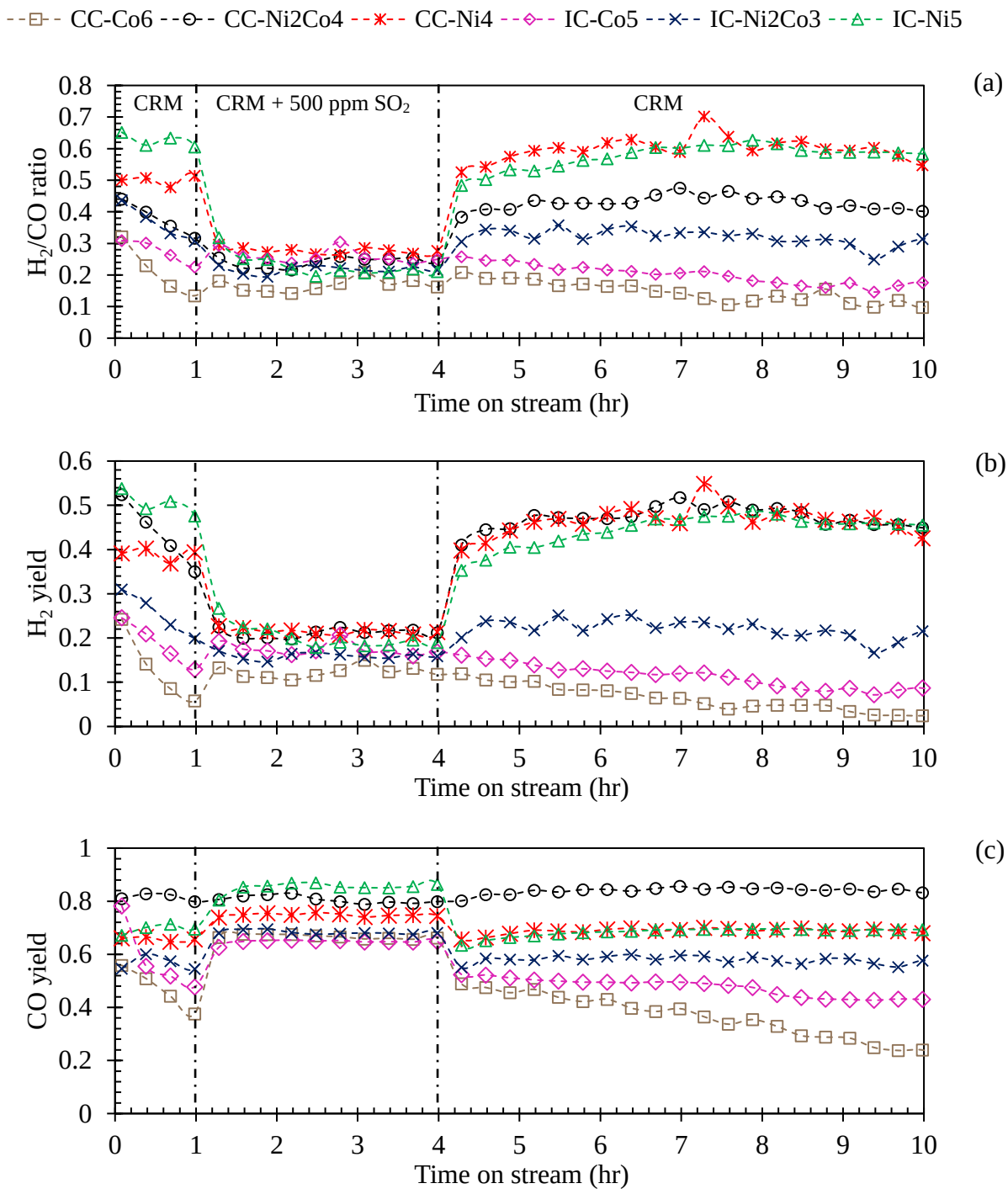

Figure 7.4 (a) H_2/CO ratio, (b) H_2 yield, and (c) CO yield for CRM over Ni and Co monometallic and Ni-Co bimetallic catalysts during 10 hr TOS. Reaction condition: 0.1 g of catalyst, temperature: 800 °C, 1 atm, GHSV of 60 L g^{-1} hr^{-1}, $CH_4/CO_2/N_2$ = 1/1/1, 500 ppm SO_2 during the poisoning period

Higher conversion of CH_4 (Figure 7.3(a)) and lower H_2 yields (Figure 7.4 (b)) over the catalysts during the poisoning period than the CRM period may imply that carbon was deposited on the catalysts during the poisoning period. However, the comparable activity of the catalysts before and after the presence of SO_2 in the CRM feed suggests that the catalyst-active sites (metallic Ni and/or Co sites) had not been deactivated by sintering or carbon deposition during the SO_2 poisoning period. Therefore, unreacted carbon intermediates from CH_4 dissociation were more likely deposited on the catalyst support (as discussed in section 7.1) than the active sites.

Figure 7.5 shows the produced H_2S when SO_2 was added to the CRM feed. Over Co monometallic catalysts (CC-Co6 and IC-Co5) and the IC-Ni2Co3 bimetallic catalyst, where isolated Co sites might have been present, H_2S was observed in the product gas as soon as SO_2 was introduced; while over Ni monometallic catalysts (CC-Ni4, IC-Ni5) and the CC-Ni2Co4 bimetallic catalyst, there was a delay before H_2S production. It seems that Co species facilitated immediate formation of H_2S and Ni species delayed it. In addition, the lowest and highest H_2S formation were observed over CC-Co6 and IC-Co5, respectively. Poor activity of CC-Co6 compared to IC-Co5 for CRM reaction could be a possible explanation (Wang et al., 2013). It was also observed that the catalysts made by impregnation (IC) facilitated more H_2S formation than those made by co-precipitation (CC). Shakouri (2013) reported that the content of active sites (Ni and/or Co) on the surface of impregnated catalysts was higher than on the precipitated ones. This appears to be an explanation for this phenomenon, which merits further investigation.

Figure 7.5 also shows that over IC catalysts, H_2S was still produced to some extent up to one hour of TOS after disconnecting the SO_2. It was found in our earlier study that more active sites (Ni and Co metallic sites) were found on the surface of the catalysts prepared by impregnation method than the co-precipitation method (Shakouri, 2012; Wang et al., 2013). Thus, the chance of formation of S-catalyst intermediates in the IC catalysts could be more than those in the CC one. The IC catalysts could still have S-catalysts intermediates on the surface that could still react with H_2 intermediates even when SO_2 was stopped. This could be the reason that H_2S production period was extended in case of IC catalysts than the CC ones.

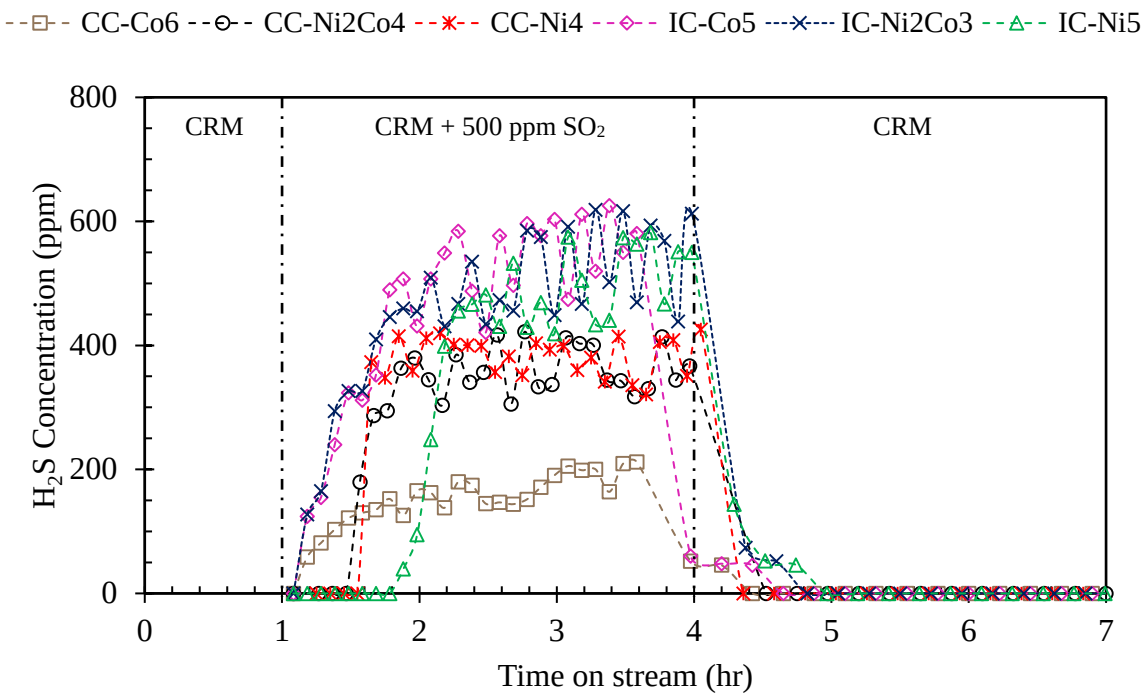

Figure 7.5 Produced H_2S content from SO_2 poisoning during CRM reaction over Ni-Co/$AlMgO_x$ catalysts. Reaction conditions: 0.10 g catalyst support, temperature: 800 °C, 1 atm, GHSV of 60 L g^{-1} hr^{-1}, $CH_4/CO_2/N_2$ = 1/1/1, 500 ppm SO_2 during the poisoning period

7.3 XAS Analysis of the Catalysts Used for CRM with SO_2

To further understand the mechanism of sulfur poisoning during CRM reaction in the presence of SO_2 over the Ni-Co/$AlMgO_x$ catalysts, an X-ray Absorption Spectroscopy (XAS) technique was used. Three sets of experiments were performed over the catalysts (Table 7.1) using the six hole shooter set-up and procedure described in section 3.2.3. The first set of catalysts were reduced in a H_2 (20%) and N_2 (80%) mixture at 800°C for 4 hr (reduction experiment). For the second set of catalysts, direct reaction between SO_2 and the reduced catalysts was conducted by introducing 500 ppm of SO_2 into the reduced catalysts at 800°C for 1hr. The third set were treated for CRM reaction in the presence of SO_2 as described in section 7.1. At the end of each treatment, the catalysts were cooled down in the presence of N_2 to room temperature and then collected for XAS analysis of Ni, Co, and S (if SO_2 was introduced) K-edge.

7.3.1 Ni and Co Reduction Extent

Ni and Co K-edge XAS spectra of the reduced catalysts were collected at the Canadian Light Source (CLS) in the SXRMB beamline. XAS spectra were also obtained for standard samples of Ni foil, Co foil, NiO and CoO which were then used as the references. It should be mentioned that only CoO was used as the cobalt oxide standard. Co_3O_4 was not considered because Co_2O_3, one component in Co_3O_4, reduces to CoO at a much lower temperature than 800 °C (Wang et al., 2013). As an example, normalized absorption of Ni and Co K-edge XANES spectra of reduced CC-Ni2Co4 compared with the respective metal foils and metal oxide standards are shown in Figure 7.6. It clearly shows that, after reduction, The XANES spectra for both Ni and Co fall between XANES for the respective metal foils and metal oxide standards, indicating that both Ni and Co sites in the CC-Ni2Co4 catalyst sample were partially reduced.

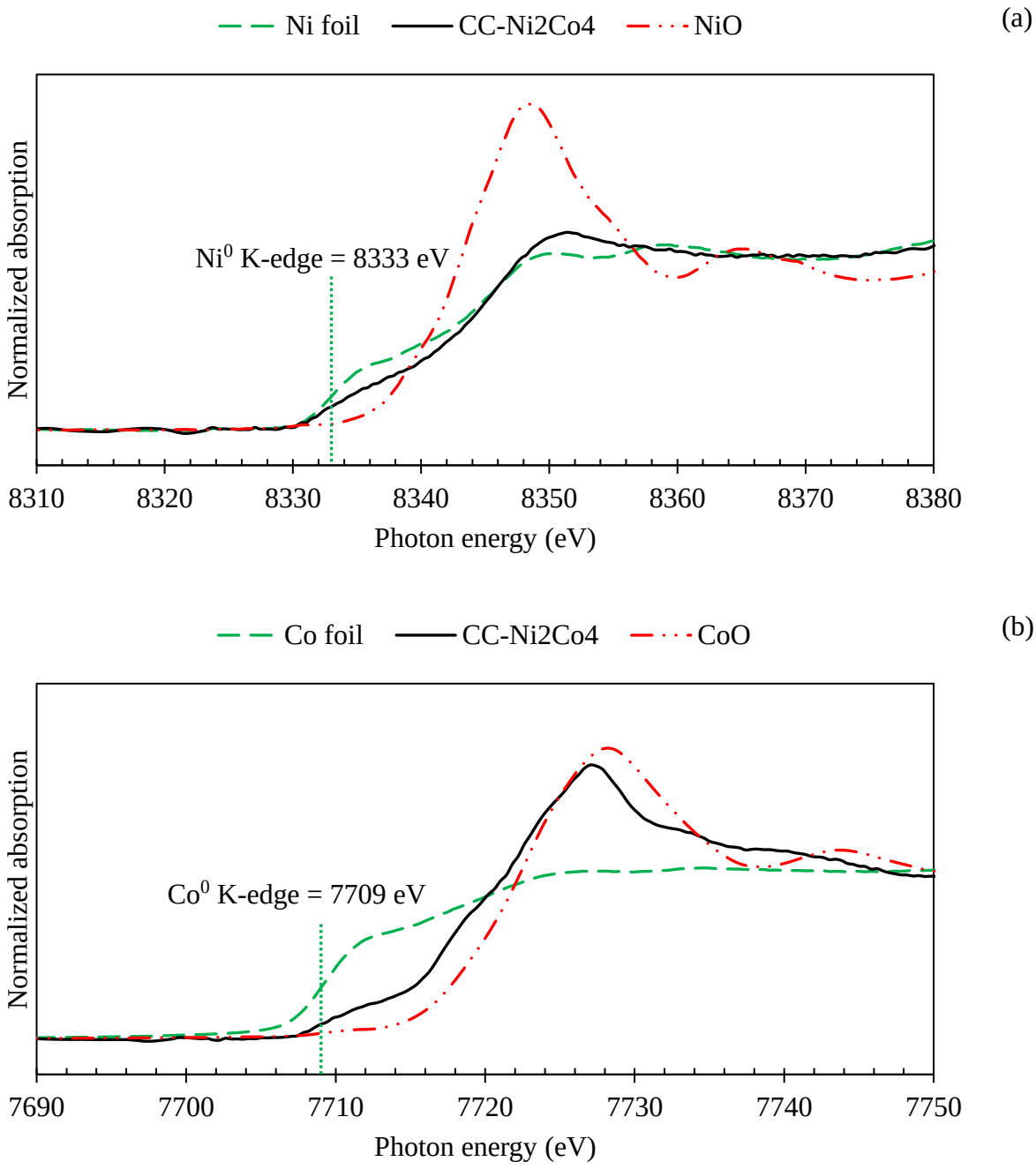

Figure 7.6 Normalized absorption for (a) Ni K-edge XANES from 8310 to 8380 eV of CC-Ni2Co4 catalyst reduced at 800 °C for 4hr (black), Ni foil (green) and NiO (red), and (b) Co K-edge XANES from 7690 to 7750 eV of CC-Ni2Co4 catalyst reduced at 800 °C for 4hr (black), Co foil (green) and CoO (red)

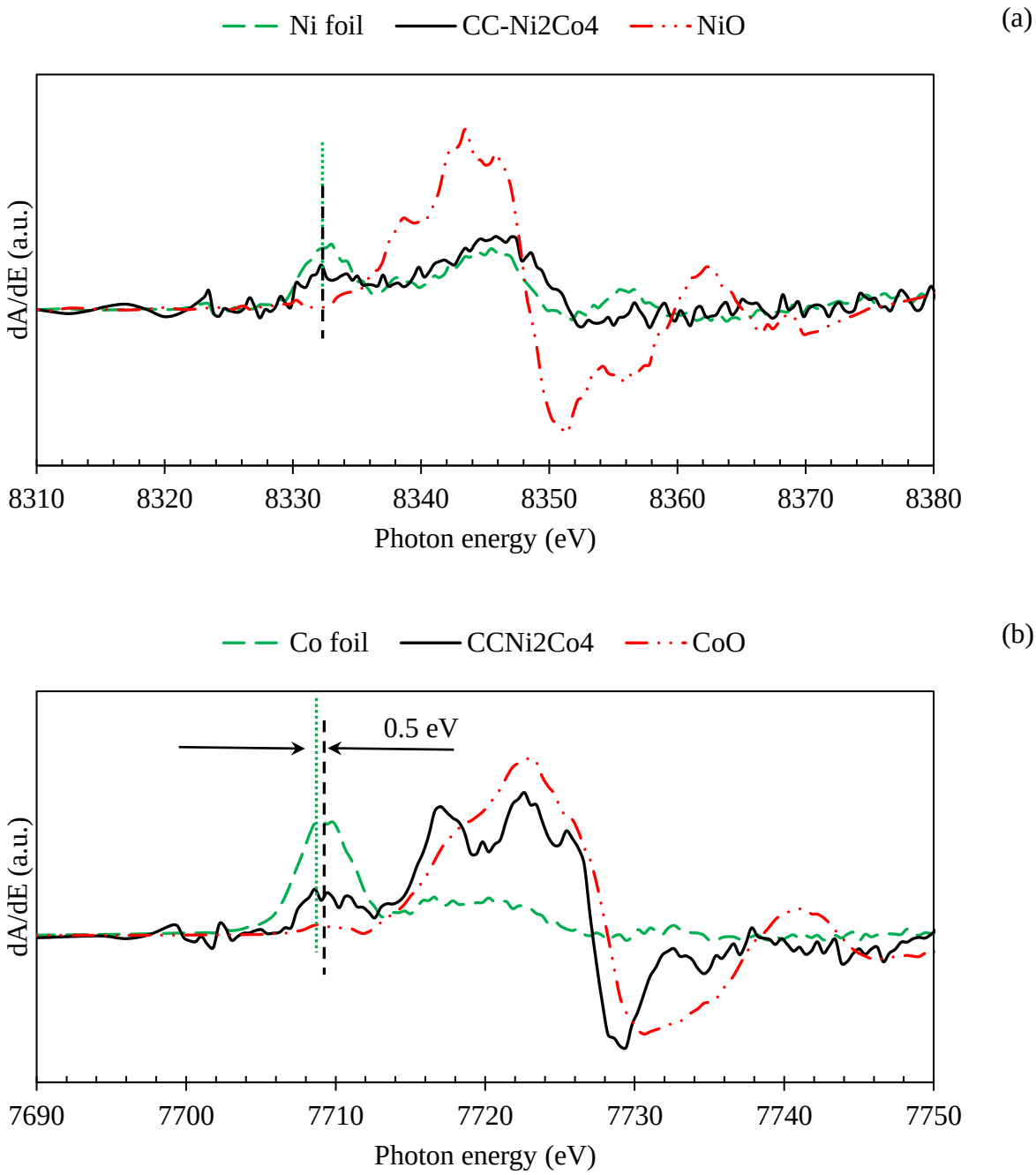

Figure 7.7 First derivative of normalized absorption for (a) Ni K-edge XANES from 8310 to 8380 eV of CC-Ni2Co4 catalyst reduced at 800 °C for 4hr (black), Ni foil (green) and NiO (red), and (b) Co K-edge XANES from 7690 to 7750 eV of CC-Ni2Co4 catalyst reduced at 800 °C for 4hr (black), Co foil (green) and CoO (red)

Figure 7.7 compares the first derivative of Ni and Co XANES for the Ni-Co catalyst with the references. It is clear that the Co spectra of the catalyst was shifted to an energy higher than the Co foil (~ 0.5 eV). However, such a shift was not significant for the Ni spectrum. In other words, the first derivative Ni spectrum of CC-Ni2Co4 was more comparable with the Ni foil standard than NiO while the Co spectrum was more like a mixture of both Co foil and CoO standards. This suggests that Ni could have been more reduced than Co in CC-NiCo4.

To quantify the extent of Ni and Co reduction in the catalysts, the linear combination fitting module in Athena software was used. K-edge XANES spectra of Ni and Co in the reduced catalysts in the range of -20 eV to +30 eV of the edge jumps were fitted with their respective metal foil and metal oxide standard spectra. The curve-fitting results for all the catalysts are summarized in Table 7.2. Results show that the extent of Ni reduction was very close: in a range of 89–92% in all catalyst samples. On the other hand, the extent of Co reduction was much lower than Ni and was in a range of 38–52%. Lee et al. (2005) and Wang et al. (2016) also found that reduction of Co cations were much harder than the Ni cations. Table 7.2 also reveals that reduction extent of Co monometallic catalyst prepared by the co-precipitation method (CC-Co6) was slightly less than the others. The highest Co content of all the catalysts (shown in Table 7.1) as well as the presence of Co in the inner porous due to its preparation method, could be the possible explanations. Moreover, the lowest Co reduction extent in CC-Co6 agrees with the poor performance of CC-Co6 for the CRM reaction, and therefore the lowest production of H_2S in the presence of SO_2 during CRM reaction (Figures 7.3, 7.4, and 7.5).

Table 7.2 Ni and Co species content in the reduced catalysts calculated by linear combination fitting. Reduction conditions: 800°C, 20% H_2 and 80% N_2 mixture for 4 hr

Catalyst	Ni	NiO	Co	CoO
	%			
CC-Co6	-	-	38	62
CC-Ni2Co4	91	9	51	49
CC-Ni4	92	8	-	-
IC-Co5	-	-	52	48
IC-Ni2Co3	90	10	47	53
IC-Ni5	89	11	-	-

7.3.2 Direct Reaction between SO_2 and Reduced Catalysts

Ni, Co, and S K-edge XAS spectra of the reduced catalysts after reacting with 500 ppm SO_2 for 1 hr at 800 °C were collected at the Canadian Light Source (CLS) in the SXRMB beamline. XAS spectra were also obtained for standard samples of Ni foil, Co foil, NiO, CoO, NiS and CoS, which were then used as the references. As an example, Figure 7.8 shows the Ni and Co XANES spectra of the CC-Ni2C4 catalyst as well as the standards. Comparing the Ni and Co K-edge XANES spectra with the standard spectra, suggests that nickel and cobalt sulfides could have been formed on the catalysts after reacting with SO_2.

The linear combination fitting of Ni and Co XANES delivers more quantitative results to compare the sulfide, oxide and metallic contents of the samples. Table 7.3 shows the fitting results for all the catalysts within -20 eV to +30 eV of the edge jump (8333 eV for Ni, and 7709 eV for Co). The results confirm that both NiS and CoS could be found to some extent on the reduced catalysts that reacted with SO_2. The reaction between S (from reduction of SO_2) and the metallic sites (Ni and/or Co) available on the surface of the reduced catalysts could have been the possible pathway towards sulfide formation. It was also observed that more NiS and CoS were formed on the IC group catalysts than the CC ones, possibly due to higher content of surface metallic sites than the CC catalysts. Comparing results in Table 7.2 with Table 7.3 further indicates that more than half of the Ni and almost all the Co metallic sites became metal sulfide. This suggests that Co metallic sites were less stable than the Ni ones which, is in agreement with the observed lower extent of reduction of Co than Ni as well.

Figure 7.9 (b) shows S K-edge XANES of the reduced catalysts that reacted with SO_2. Comparing them with the reference spectra (Figure 7.9 (a)) reveals that sulfide compounds (the peak at E_0 ~ 2470.5 eV) were formed on all the reduced catalysts when contacted with SO_2 alone, which could support the formation of NiS and/or CoS. The area under the sulfide peak of each spectrum was calculated using the Origin Lab software as an estimate of the amount of sulfide. Figure 7.9 (c), which shows the estimated area for each catalyst, clearly depicts that the amount of sulfide follows the order of Co monometallic > Ni-Co bimetallic > Ni monometallic. Wang et al. (2013) reported that Co are harder to reduce than Ni. Therefore, a lower stability of the Co metallic sites than the Ni ones could be a possible explanation for higher sulfide formation on the Co containing catalysts than mono Ni catalysts.

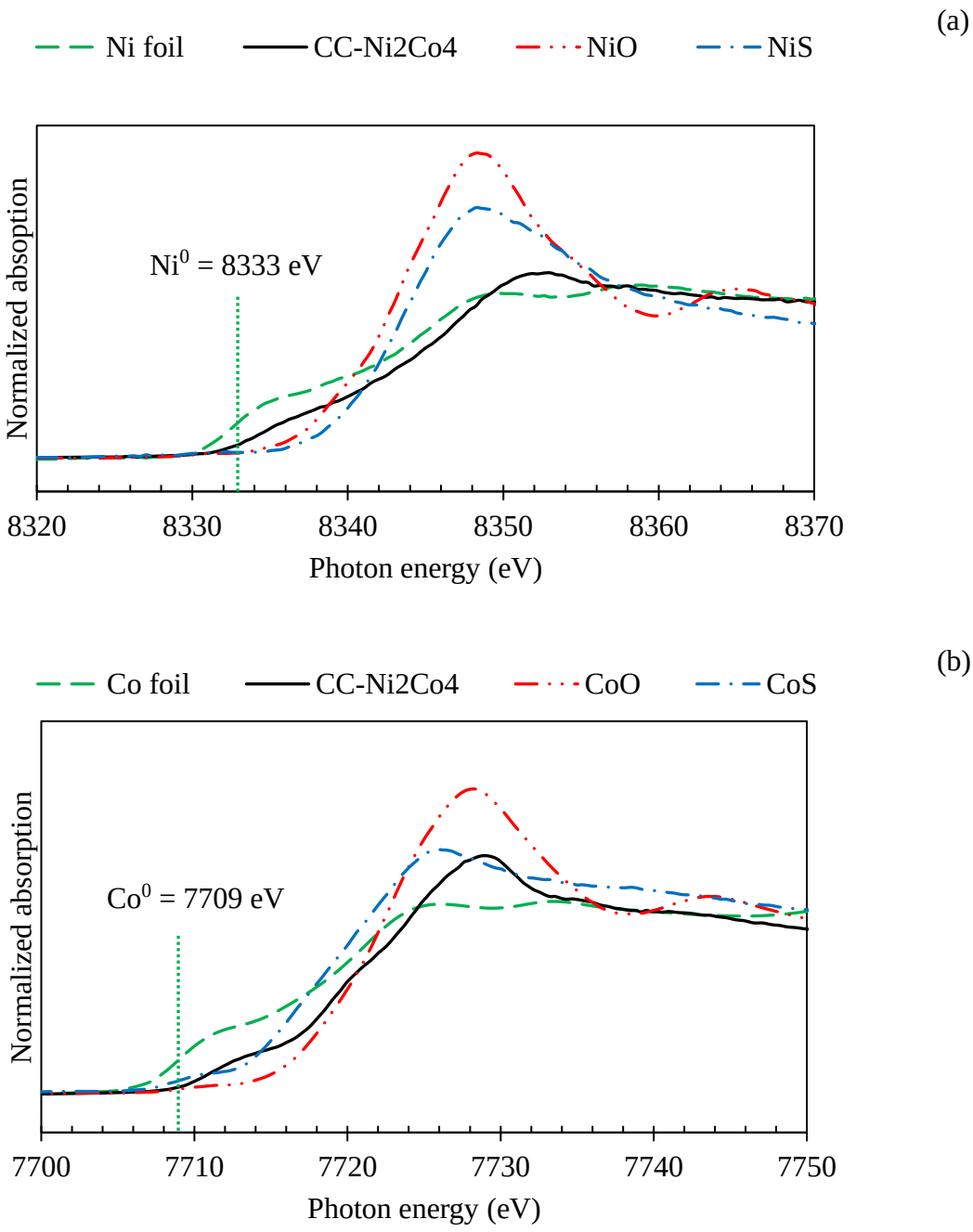

Figure 7.8 Normalized absorption of (a) Ni K-edge XANES spectra from 8320 to 8370 eV and (b) Co K-edge XANES spectra from 7700 to 7750 eV of reduced CC-Ni2Co4 catalyst reacted with 500 ppm SO_2 at 800 °C for 1 hr

Table 7.3 Linear combination fitting results for Ni and Co species content in the reduced catalysts reacted with SO_2. Reduction condition: 800 °C, 20% H_2 and 80% N_2 mixture for 4 h. Reaction condition: 800 °C, 1 h, 500 ppm SO_2.

Catalyst	NiS	Ni	NiO	CoS	Co	CoO
	%					
CC-Co6	-	-	-	51	0	49
CC-Ni2Co4	51	49	0	44	10	46
CC-Ni4	53	47	0	-	-	-
IC-Co5	-	-	-	56	3	41
IC-Ni2Co3	62	38	0	62	0	38
IC-Ni5	63	37	0	-	-	-

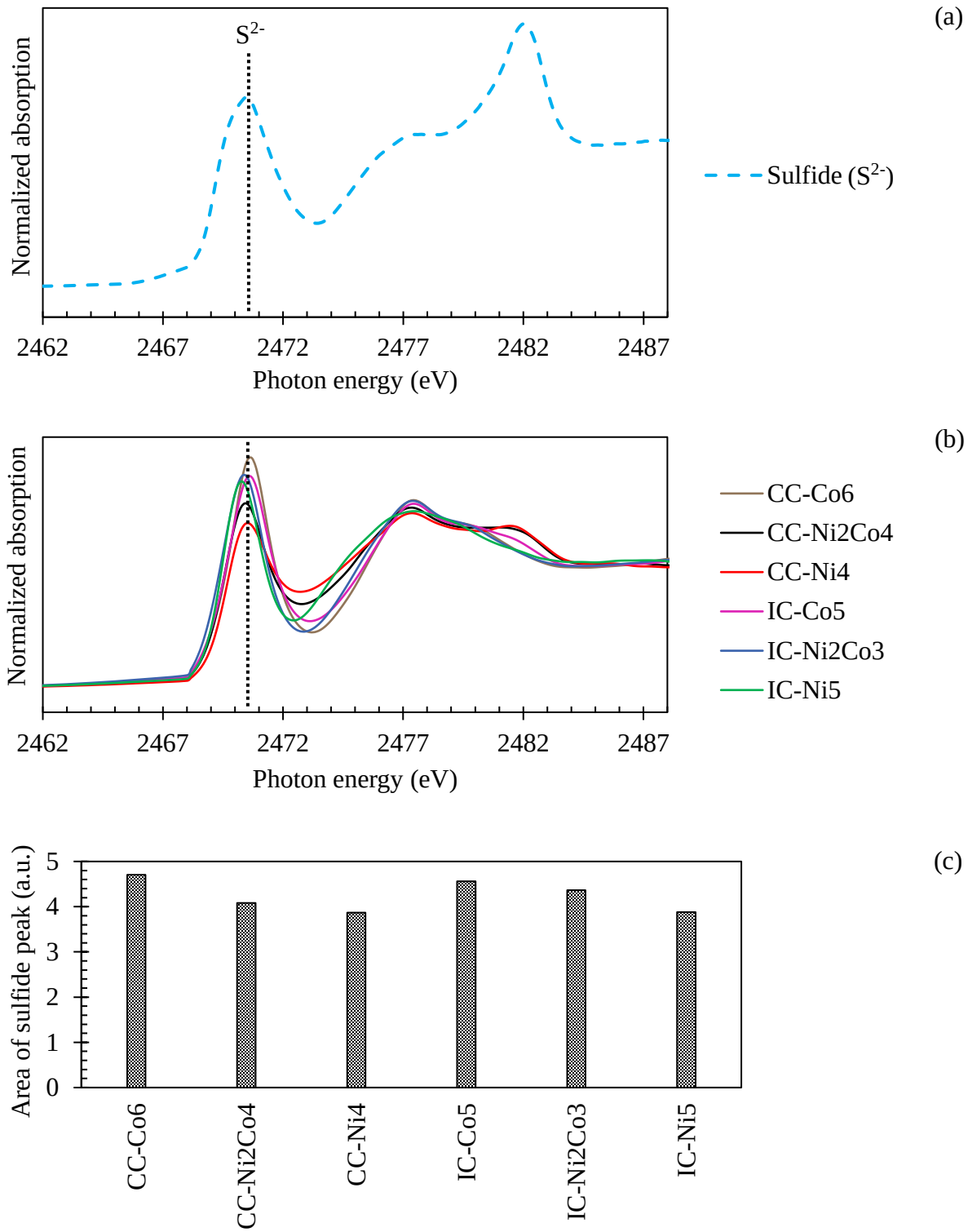

Figure 7.9 Normalized absorption of S K-edge XANES spectra from 2462 to 2488 eV for (a) sulfide (S^{2-}) and sulfate (S^{4+}) standard samples, and (b) reduced catalysts reacted with 500 ppm SO_2 at 800 °C for 1 hr; (c) correlation between area under the main sulfide peak and the catalysts

7.3.3 Catalyst Used for CRM in the Presence of SO_2 (Poisoning Experiment)

Ni, Co, and S K-edge XAS spectra of the reduced catalysts as well as $AlMgO_x$ (catalyst support) for CRM reaction in the presence of SO_2 were collected at the Canadian Light Source (CLS) in SXRMB beamline. Figure 7.10 compares the first derivative of the Ni K-edge XANES of the reduced catalysts used for direct reaction with SO_2 and the poisoning experiment. Similar comparison for the Co K-edge spectra are shown in Figure 7.11.

Figures 7.10 and 7.11 show that Ni and Co spectra moved to lower energy in the poisoning experiment than in direct reaction with SO_2 while such a shift was more significant in terms of Co K-edge than the Ni-Kedge. This reveals that Co have lower oxidation states after the poisoning experiment and therefore less CoS could have formed when SO_2 was introduced during CRM reaction. Production of H_2S in the poisoning experiment intends that sulfur was removed from the catalyst's surface. One possible conclusion is that H_2 from CH_4 dissociation could have reacted with sulfide on the Ni and/or Co sites to produce H_2S. Hence, a lower amount of NiS and CoS would have remained on the catalyst used for the poisoning experiment than the one reacted directly with SO_2 alone, which is in agreement with the Ni and Co K-edge results as well.

S K-edge XANES spectra of catalyst support ($AlMgO_x$) after CRM reaction in the presence of SO_2 as well as sulfide (S^{2-}) and sulfate (S^{4+}) reference spectra are shown in Figure 7.12. Figure 7.13 also compares the S- Kedge of the catalysts used for the poisoning experiment with those of reduced catalyst reacted with SO_2.

Referring to the standard spectra of S K-edge XANES (Pickering et al., 1998; Struis et al., 2009) indicates that the XANES spectra of the catalysts and catalyst support, which were used for the poisoning experiment, cannot adhere to those of a single sulfur compound. The results suggest that sulfide (S^{2-}; peak at 2470.5 eV), sulfite (S^{4+}; peak at 2477.5 eV) and sulfate (S^{6+}; peak at 2480 eV) compounds could have formed on all the samples. In addition, elemental sulfur (S^0; peak at 2472 eV) was only found on the catalyst support. Formation of sulfide as well as elemental sulfur suggest reduction of S^{4+} in SO_2 to either S^0 or S^{2-}. Decomposition of SO_2 in the presence of CH_4 on alumina-based catalysts (Yu et al., 1997), the appearance of elemental sulfur in the outlet of the reactor (reaction 7.1), and formation of H_2S (reaction 7.2) during CRM in the presence of SO_2 could be the possible explanations for this phenomenon.

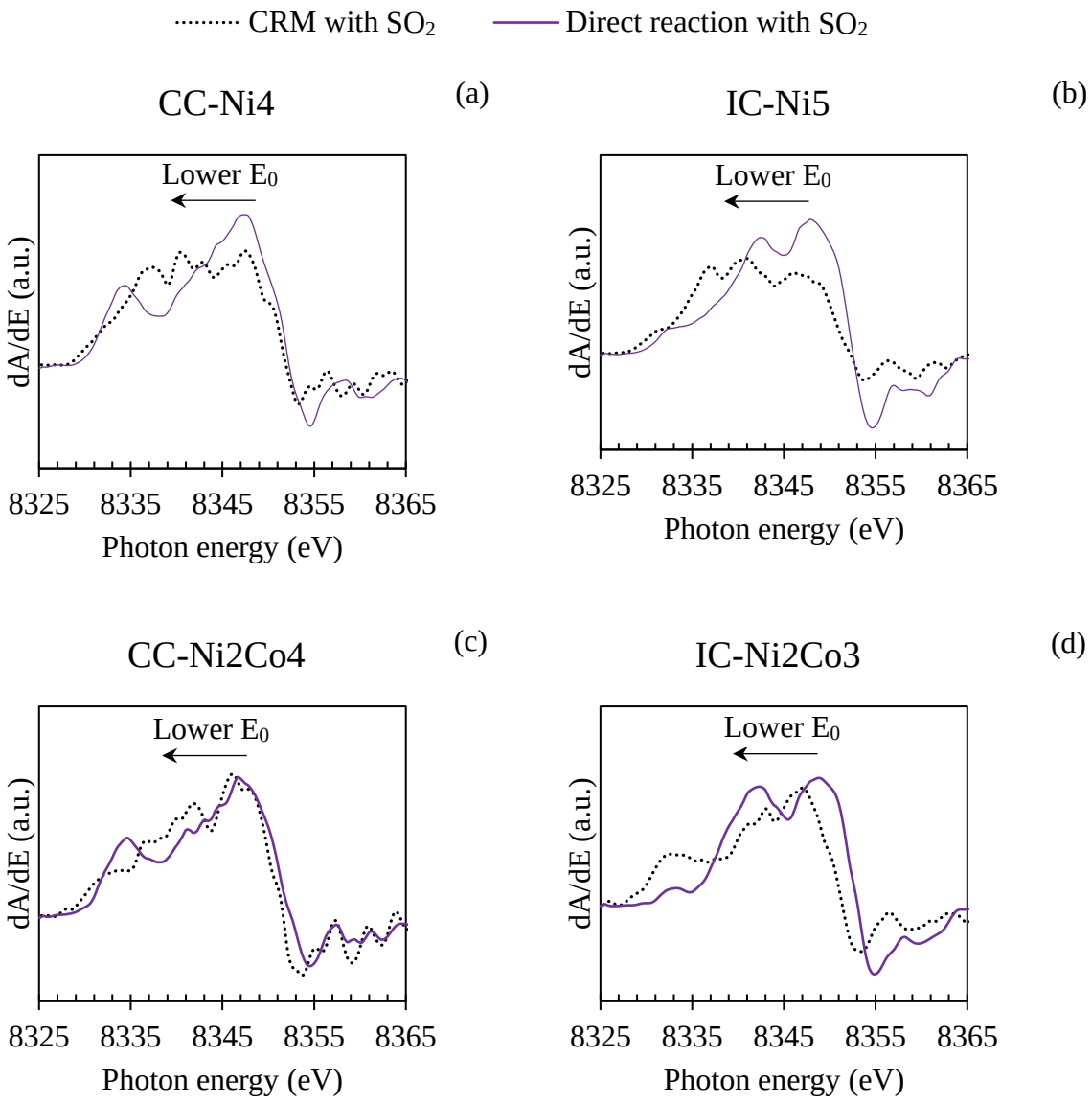

Figure 7.10 First derivative normalized absorption of Ni K-edge XANES spectra from 8325 to 8365 eV for (a) CC-Ni4, (b) CC-Ni2Co4, (c) IC-Ni5, and (d) IC-Ni2Co3 catalysts used for direct reaction with SO_2 (black, dotted line) and CRM in the presence of SO_2 (purple, solid line).

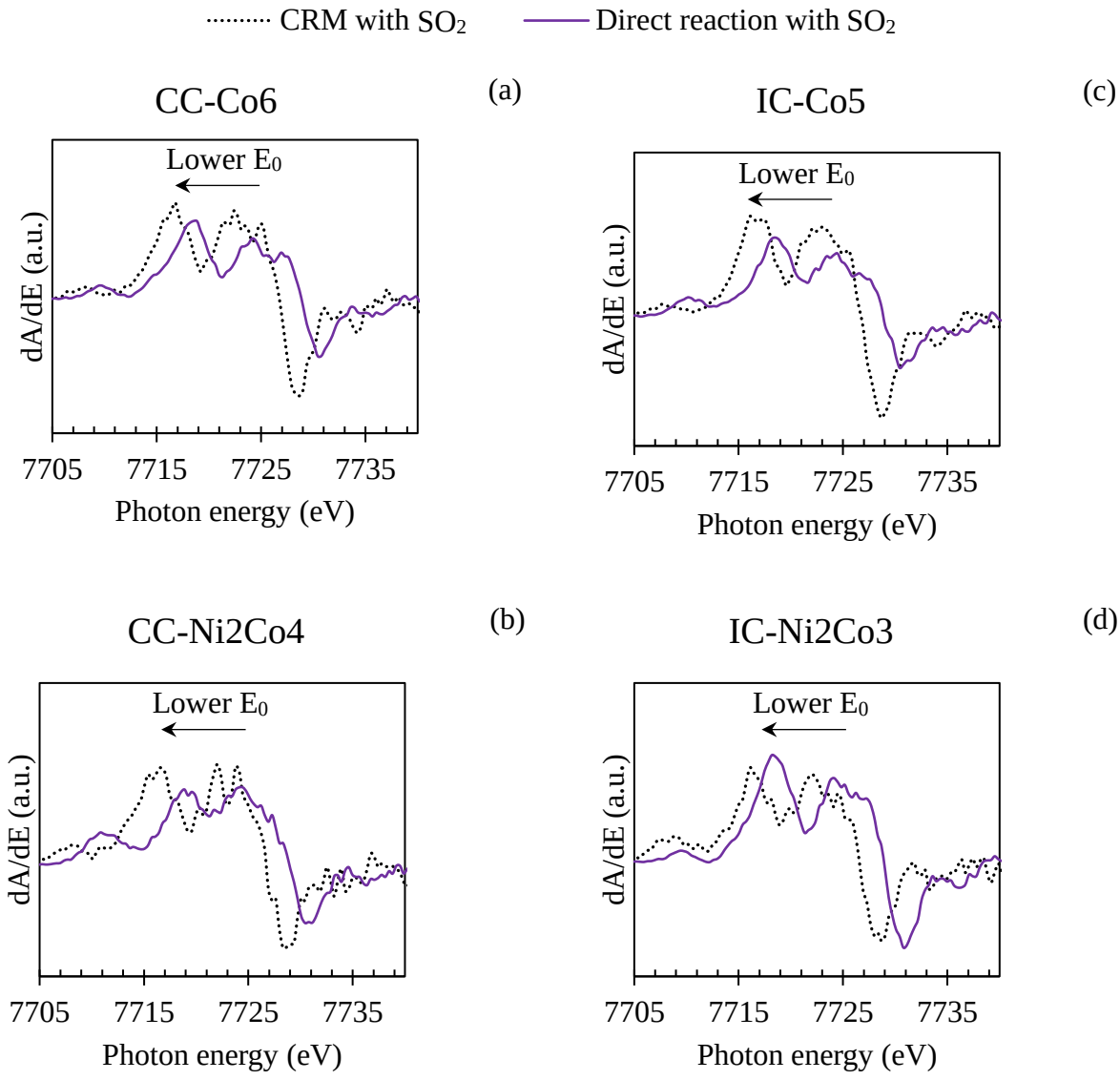

Figure 7.11 First derivative normalized absorption of Co K-edge XANES spectra from 7705 to 7740 eV for (a) CC-Ni4, (b) CC-Ni2Co4, (c) IC-Ni5, and (d) IC-Ni2Co3 catalysts used for CRM in the presence of SO_2 (black, dotted line) and direct reaction with SO_2 (purple, solid line).

Sulfite (S^{4+}) and sulfate (S^{6+}) could be formed from adsorption of SO_2 to the oxygen species on the sample's surface. The most likely oxygen species that could have interacted with SO_2 were: (a) the oxygen vacancies that were available within the catalyst's structure (either in the $AlMgO_x$ support or Ni/Co oxides); (b) O-intermediates that formed from the decomposition of CO_2 (Zhang et al., 2008). On the other hand, Figure 7.13 reveals that sulfate and sulfite were only found on the catalysts used for the poisoning experiment. Thus, sulfate and sulfite were more likely formed from interaction between SO_2 and O-intermediates formed from the CO_2 decomposition.

Figure 7.13 also indicates when SO_2 was fed during CRM, Co-containing catalysts facilitated sulfate formation while Ni-monometallic catalysts facilitated sulfide formation. In our previous studies for performance of these catalysts for CRM reaction, it was observed that Ni sites could facilitate CRM reaction more than Co ones (Shakouri, 2013; Wang et al., 2013). It means that the O-intermediates from CO_2 dissociation could have reacted more with C-Ni intermediates from CH_4 dissociation than C-Co intermediates. In other words, there are more O-Support intermediates available to react with SO_2 in Co containing catalysts than Ni monometallic catalysts. Hence, more sulfate could be formed in the Co-containing catalysts than the Ni monometallic ones.

Putting the parcels together, SO_2 was reduced by metallic sites or support on the catalyst's surface to form sulfide. When CH_4 also dissociated on the metallic sites or sulfur-support intermediates, hydrogen-intermediates (from CH_4 dissociation) reacted with sulfide to produce H_2S. On the other hand, when CO_2 dissociated on the support, the produced O-intermediate could have reacted with SO_2 to form sulfate.

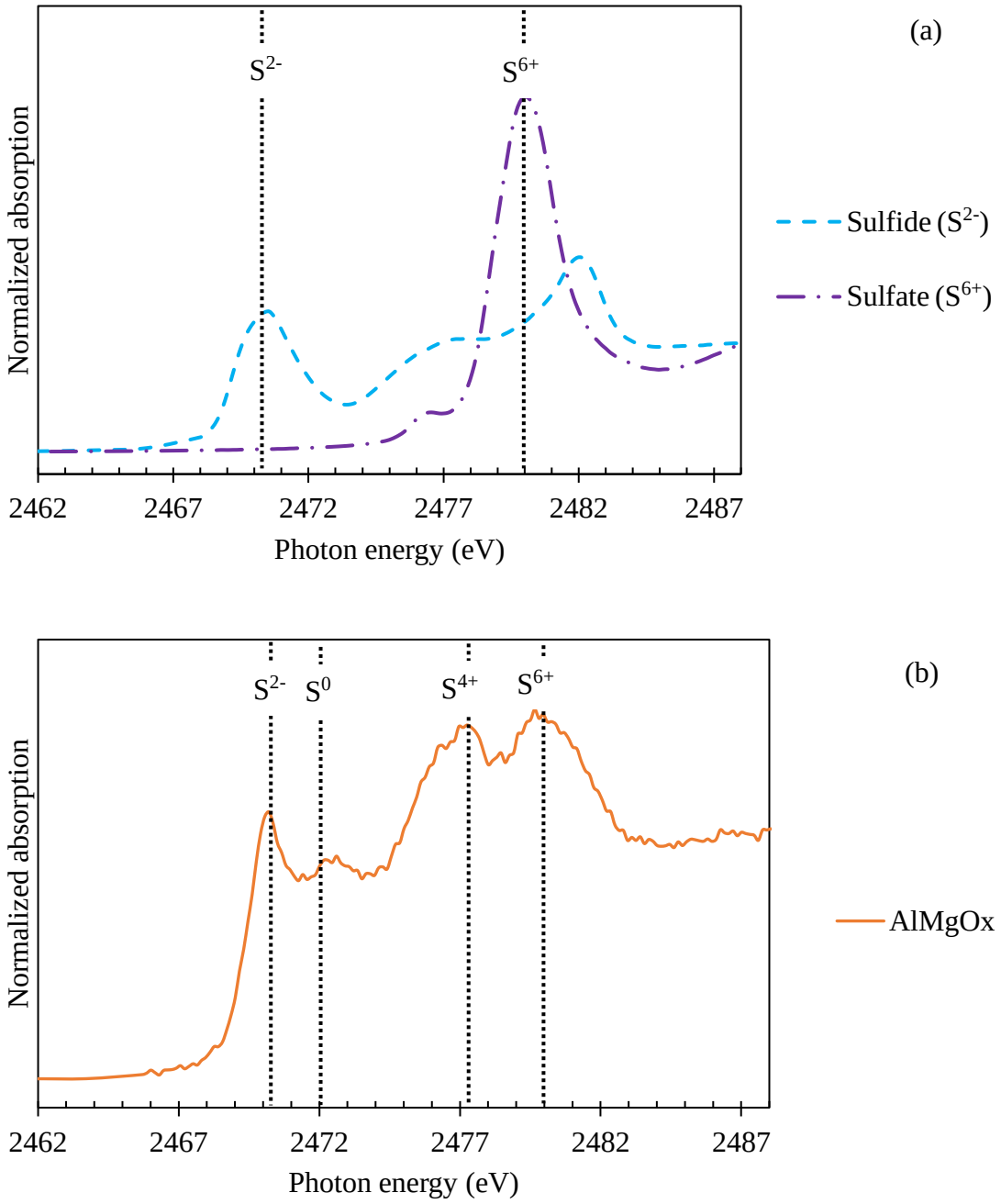

Figure 7.12 Normalized absorption of S K-edge XANES spectra from 2462 to 2488 eV for (a) sulfide (S^{2-}) and (b) $AlMgO_x$ catalyst support used for CRM reaction in thepresence of SO_2

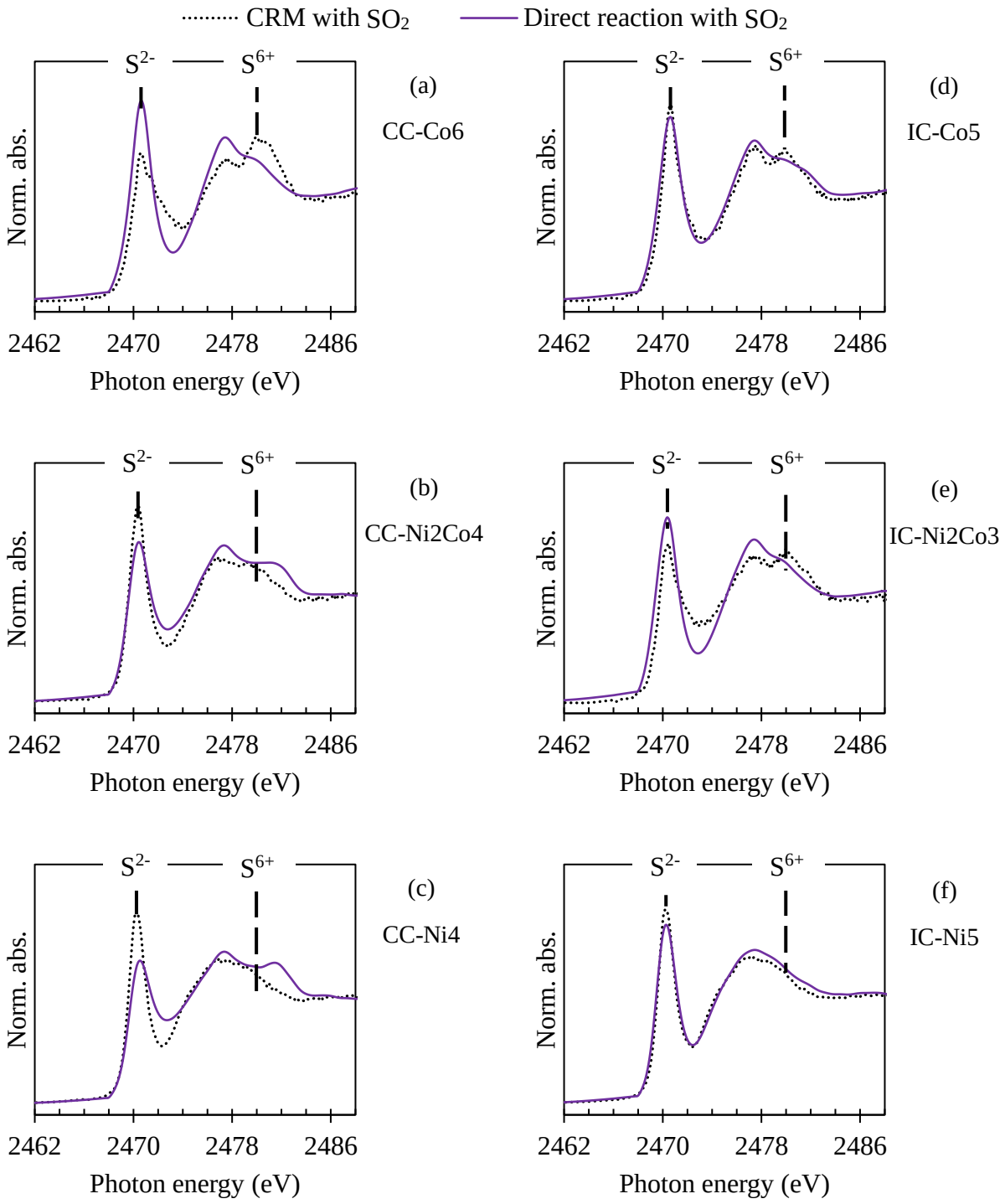

Figure 7.13 Normalize absorption of S K-edge XANES spectra from 2462 to 2488 eV for catalysts used for CRM reaction in the presence of SO_2 (purple solid line) and direct reaction with SO_2 (black dotted line); (a) CC-Co6, (b) CC-Ni2Co4, (c) CC-Ni4, (d) IC-Co5, (e) IC-Ni2Co3, (f) IC-Ni5.

7.4 Conclusions

In conclusion, the formation of H_2S and an increase of CH_4 and CO_2 conversions during the SO_2 poisoning of CRM reaction over the catalysts contributed to better understanding the sulfur poisoning mechanism. It was observed that the catalysts' support material ($AlMgO_x$) played a key role in the SO_2 poisoning period by providing additional active sites for methane dissociation. Over alumina-based catalysts, SO_2 could be reduced by methane to elemental sulfur (S) and water. Since alumina was the dominant phase in the synthesized catalysts, thus the enhancement of CH_4 conversions and production of S over the catalysts are more likely because of the support. Besides, occurrence of Water Gas Shift reaction could explain the enhancement of CO_2 conversions in presence of SO_2. S, Ni, and Co K-edge XANES revealed that sulfide, in the forms of CoS and NiS, was formed on the reduced catalysts reacted with SO_2. In the case of CRM in the presence of SO_2, sulfide (S^{2-}), sulfite (S^{4+}) and sulfate (S^{6+}) compounds were found on the catalysts as well as the support. SO_2 was likely reduced by metallic sites or support on the catalyst's surface to form sulfide. When CH_4 also dissociated on the metallic sites or sulfur-support intermediates, hydrogen-intermediates (from CH_4 dissociation) reacted with sulfide to produce H_2S and C-intermediates (from CH_4 dissociation) were deposited on the support, which was confirmed with Raman spectroscopy. On the other hand, when CO_2 dissociated on the support, the produced O-intermediate could have reacted with SO_2 to form sulfite or sulfate. Co-containing catalysts facilitated sulfate formation while Ni-monometallic catalysts facilitated sulfide formation.

CHAPTER 8

Conclusions and Recommendations

8.1 Conclusions

The following conclusions can be drawn from the work in Phase I;

The prepared shaped catalysts were comparably as strong as the commercial ones. Pore volume of the shaped catalysts with the addition of Boehmite (as the binding material) was larger than that of the Ni-Co bimetallic powder catalyst. However, the BET surface area (~160 m^2/g) was not significantly changed. The shaped catalysts had XRD patterns similar to the powdered Ni-Co bimetallic catalyst. However, the addition of Boehmite to shape the catalysts increased the spinel phase and reduced the MgO phase. The cylindrical catalysts, with or without addition of Boehmite, similarly facilitated CRM reactions at 800 °C. However, due to mass transfer limitations, the CH_4 and CO_2 conversions were around 10% lower than those for the Ni-Co bimetallic powdered catalyst. In spherical catalysts, both internal and external mass transfer severely affected their performance for CRM reaction. It was found that increasing the superficial velocity, to values greater than 129 m/s, could avoid the external mass transfer effect, while the internal mass transfer still limited the catalyst's performance. The temperature gradient within the radius of the spherical catalysts was negligible and therefore heat transfer limitation was not affecting the spherical catalyst performance for CRM reaction.

The work in Phase II can draw conclusions as follows:

Steam content of the biogas feed was the key factor affecting the catalytic performance during SCRM reactions. The Ni-Co bimetallic, Ni monometallic and Co monometallic catalysts could not handle a feed containing more than 12%, 15%, and 6% mol of steam, respectively. Ni

and Co K-edges XANES spectra of the catalyst reveal that steam could oxidize the metallic active sites leading to deactivation of the catalysts. Compared with the commercial catalyst performances, the Ni-Co bimetallic catalyst was more stable in a certain range of the steam content. It was found that Ni-Co bimetallic catalyst and biogas feed composition 5 (composed of 33 mol% CH_4, 3.5 mol% H_2, 30 mol% N_2, 12 mol% H_2O, and 21.5 mol% CO_2) represent the most effective combination, not only to produce syngas with the desired H_2/CO ratio (1.8 to 2) but also to convert more than 70% of CO_2 in the biogas feed. It was also found that the Ni-Co bimetallic catalyst (a) could not activate H_2 and CO, and (b) could convert significant amounts of CH_4 and CO_2 (impurities) in a syngas-rich feed through CRM reaction (90 % conversion of CH_4, 95 % conversion of CO_2 at 850 °C).

We can also reach the following conclusions from the work in Phase III:

H_2S, water and elemental sulphur were produced, and CH_4 and CO_2 conversions were increased when 500 ppm SO_2 was added to the feed for CRM reactions over the Ni and Co catalysts and Mg-Al-O_x catalyst support. Mg-Al-O_x support plays a key role in SO_2 poisoning period by providing additional active sites for methane dissociation. Over alumina-based catalysts, SO_2 could be reduced by methane to elemental sulfur (S) and water. Since alumina was the dominant phase in the synthesized catalysts, thus the enhancement of CH_4 conversions and production of S over the catalysts are more likely because of the Mg-Al-O_x support. Besides, occurrence of Water Gas Shift reaction could explain the enhancement of CO_2 conversions in presence of SO_2. S, Ni, and Co K-edges of the catalysts used for SO_2 poisoning experiments indicate that species such as sulfide (S^{2-}), sulfite (S^{4+}) and sulfate (S^{6+}) can be formed during the SO_2 poisoning. Produced H_2S during CRM in the presence of SO_2, is likely from the reaction between S^{2-} and H^+ intermediates on the catalysts' surface. When CH_4 also dissociated on the metallic sites or sulfur-support intermediates, hydrogen-intermediates reacted with sulfide to produce H_2S. Also, when CO_2 dissociated on the support, the produced O-intermediate could have reacted with SO_2 to form sulfite or sulfate. Over Co monometallic catalysts, H_2S was observed in the product gas as soon as SO_2 was introduced; over Ni monometallic catalysts, there was a delay for H_2S production. Monometallic and bimetallic sites and catalyst preparation methods had different impacts on the poisoning mechanism. Co-containing catalysts facilitated sulfate (SO_4^{2-}) formation while Ni-monometallic catalysts facilitated sulfide (S^{2-}) formation.

8.2 Recommendations

The following recommendations could be of interest for future work:

- Efforts could be made to investigate whether the effect of mass transfer on performance of shaped catalysts for CRM reaction could be reduced. As an example, shaped catalysts similar to the monolith structure could be prepared from the Ni-Co/AlMgO_x catalyst.
- Ni-Co catalyst could be further modified by addition of a promoter (noble metals such as Rh, Ru and Ir) to enhance the catalyst durability in feeds with high steam content.
- The performance of powdered and shaped Ni-Co catalyst for CRM reaction could be studied in different type of reactors. Fluidized bed reactors to reduce the mass transfer effect and membrane reactors to enhance the product yields have an exciting potential in CRM technology developments.
- Pilot-scale performance testing of the Ni-Co catalyst using real biogas and natural gas feed for methane-reforming reactions could be investigated. These steps would be beneficial in commercialization of the catalyst.
- The mechanism of sulfate and sulfite formations on the catalysts used for CRM in the presence of SO_2 needs to be further investigated. In-situ XAS analysis of Ni and Co catalysts as well as Mg-Al-O_x catalyst support for CRM reaction in the presence of various SO_2 concentrations could also lead to a better understanding of the catalyst environment during the poisoning period.

References

- Abatzoglou, N.; Fauteux-Lefebvre C., Review of Catalytic Syngas Production through Steam or Dry Reforming and Partial Oxidation of Studied Liquid Compounds, *Wiley Interdesip. Rev.: Energy Environ.* **2016**, *5*, 169.
- Adoption of the Paris Agreement, FCCC/CP/2015/L.9/Rev.1, United Nations, France, 2015.
- Adris, M.; Pruden, B.B.; Lim, C.J.; Grace, J.R., On the Reported Attempts to Radically Improve the Performance of the Steam Methane Reforming Reactor, *Can. J. Chem. Eng.* **1996**, *74(2)*, 177.
- Al-Nakoua, M.A.; El-Nass, M.H., Combined Steam and Dry Reforming of Methane in Narrow Channel Reactors, *Int. J. Hydrogen Energy* **2012**, *37*, 7538.
- Alvarez-Galvan, M.C.; Navarro, R.M.; Rosa, F.; Briceno, Y.; Alvarez, F.G.; Fierro, J.L.G., Performance of La, Ce-Modified Alumina-Supported Pt and Ni Catalysts for the Oxidative Reforming of Diesel Hydrocarbons, *Int. J. Hydro. Energy* **2008**, *33(2)*, 652.
- Amin, N.A.S.; Yaw, T.C., Thermodynamic Equilibrium Analysis of Combined Carbon Dioxide Reforming with Partial Oxidation of Methane to Syngas, *Int. J. Hydro. Energy*, **2007**, *32(12)*, 1789.
- Annesini, M.C.; Piemonte, V.; Turchetti, L., Carbon Formation in the Steam Reforming Process: a Thermodynamic Analysis Based on the Elemental Composition, *Chem. Eng. Trans.* **2007**, *11*, 21.
- Aparicio, P.,F.; Ramos, I.,R.; Ruiz,A.,G., On the Applicability of Membrane Technology to the Catalysed Dry Reforming of Methane, *Appl. Catal., A* **2002**, *237(1-2)*, 239.
- Aramouni, N.A. K.; Touma, J. G.; Abu Tarboush, B.; Zeaiter, J.; Ahmad, M. N., Catalyst design for dry reforming of methane: Analysis review, *Renewable Sustainable Energy Rev.* **2018**, *82(3)*, 2570.
- Arbag, H.; Yasyerli, S.; Yasyerli, N.; Dogu, G., Activity and Stability Enhancement of Ni-MCM-41 Catalysts by Rh Incorporation for Hydrogen from Dry Reforming of Methane, *Int. J. Hydro. Energy* **2010**, *35(6)*, 2296.
- Ashcroft, A. T.; Cheetham, A. K.; Green, M. L. H.; Vernon, P. D. F., Partial Oxidation of Methane to Synthesis gas using Carbon dioxide, *Nature* **1991**, *352*, 225.

- Aydinoglu, S.O.; Aksoylu, A.E., CO_2 Reforming of Methane over Pt−Ni/Al_2O_3 Catalysts: Effects of Catalyst Composition, and Water and Oxygen Addition to the Feed, *Int. J. Hydro. Energy* **2011**, *36(4)*, 2950.
- Barahuie, F.; Saifullah, B.; Dorniani, D.; Fakurazi, S.; Karthivashan, G.; Hussein, M.Z.; Elfghi, F.M., Graphene Oxide as a Nanocarrier for Controlled Release and Targeted Delivery of an Anticancer Active Agent, Chlorogenic Acid, *Mater. Sci. Eng., C* **2017**, *74*, 177.
- Barelli, L.; Bidini, G.; Gallorini, F.; Servili, S., Hydrogen Production through Sorption-Enhanced Steam Methane Reforming and Membrane Technology: A Review, *Energy* **2008**, *33*, 554.
- Barrett, E.P.; Joyner, L.G.; Halenda, P.H., The Determination of Pore Volume and Area Distributions in Porous Substances. I. Computations from Nitrogen Isotherms, *J. Am. Chem. Soc.* **1951**, *73(1)*, 373.
- Bitter, J.; Seshan, K.; Lercher, A., The State of Zirconia Supported Platinum Catalysts for CO_2/CH_4 Reforming, *J. Catal.* **1997**, *171*, 279.
- Bobrin, A.S.; Anikeev, V.I.; Yermakova, A.; Kirillov, V.A., High-Temperature Reduction of SO_2 by Methane at Various CH_4/SO_2 Ratios, *React. Kinet. Catal. Lette.* **1989**, *40(2)*, 363.
- Boger, T.; Heibel, A.K.; Sorensen. C.M., Monolithic Catalysts for the Chemical Industry, *Ind. Eng. Chem. Res.* **2004**, *43*, 4602.
- Borowiecki, T.; Denis, A.; Rawski, M.; Golebiowski, A.; Stolecki, K.; Dmytrzyk, J.; Kotarba, A., Studies of potassium-promoted nickel catalysts for methane steam reforming: Effect of surface potassium location, *Appl. Surf. Sci.* **2014**, *300*, 191.
- Bradford, M.C.J.; Vannice, M.A., Catalytic Reforming of Methane with Carbon Dioxide over Nickel Catalysts II. Reaction Kinetics, *Appl. Catal., A* **1996**, *142*, 97.
- Bradford, M.C.J.; Vannice, M.A., CO_2 Reforming of CH_4 Over Supported Pt Catalysts, J. Catal. **1998**, *173*, 151.
- Bradford, M.C.J.; Vannice, M.A., CO_2 Reforming of CH_4 Over Supported Ru Catalysts, *J. Catal.* **1999**, *183*, 69.
- Bradford, M.C.J.; Vannice, M.A., CO_2 Reforming of CH_4, *Catal. Rev.: Sci. Eng.* **1999**, *41(1)*, 1.
- Brunauer, S.; Emmett, P. H.; Teller, E., Adsorption of Gases in Multimolecular Layers, *J. Am. Chem. Soc.* **1938**, *60*, 309.

- Callaghan, C.A., Kinetics and Catalysis of the Water-Gas-Shift Reaction, Ph.D. Thesis, Worcester Polytechnic Institute, Worcester, MA, 2006.
- Chai, R.; Li, Y.; Zhang, Q.; Zhao, G.; Liu, Y.; Lu, Y., Monolithic Ni–MO_x/Ni-Foam (M = Al, Zr or Y) Catalysts with Enhanced Heat/Mass Transfer for Energy-Efficient Catalytic Oxy-Methane Reforming, *Catal. Commun.* **2015**, *70*, 1.
- Coq, B.; Tichit, D.; Rihet, S., Co/Ni/Mg/Al Layered Double Hydroxides as Precursors of Catalysts for the Hydrogenation of Nitriles: Hydrogenation of Acetonitrile, *J. Catal.* **2000**, *189(1)*, 117.
- Cybulski, A.; Moulijn, J.A., Monoliths in Heterogeneous Catalysis, *Catal. Rev.: Sci. Eng.* **1994**, *36(2)*, 179.
- Dahdah, E.; Abou Rached, J.; Aouad, S.; Gennequin, C.; Tidahy, H.L.; Estephane, J.; Aboukaïs, A.; Abi Aad, E., CO_2 Reforming of Methane over $Ni_xMg_{6-x}Al_2$ Catalysts: Effect of Lanthanum Doping on Catalytic Activity and Stability, *Int. J. Hydro. Energy* **2017**, *42(17)*, 12808.
- Demidov, D.V.; Mishin, I.V.; Mikhailov, M.N., Gibbs Free Energy Minimization as a Way to Optimize the Combined Steam and Carbon Dioxide Reforming of Methane, *Int. J. Hydro. Energy* **2011**, *36(10)*, 5941.
- Duan, Y.; Shang, R.; Zhong, X.; Xie, W.; Wang, X.; Huang, L., In-Situ Synthesis of Ni–Mo_2C/Al_2O_3 Catalysts for Dry Reforming of Methane, *Int. J. Hydro. Energy* **2016**, *41(47)*, 21955.
- Enger, B., C.; Lødeng, R.; Holmen, A., A Review of Catalytic Partial Oxidation of Methane to Synthesis Gas with Emphasis on Reaction Mechanisms Over Transition Metal Catalysts, *Appl. Catal., A* **2008**, *346*, 1.
- Ertl, G.; Knözinger, H.; Schüth, F.; Weitkamp, J., Handbook of Heterogeneous Catalysis, WILEY-VCH Verlag GmbH & Co. KGaA, 2008.
- Fang, X.; Lian, J.; Nie, K.; Zhang, X.; Dai, Y.; Xu, X.; Wang, X.; Liu, W.; Li, C.; Zhou, W., Dry Reforming of Methane on Active and Coke Resistant Ni/$Y_2Zr_2O_7$ Catalysts Treated by Dielectric Barrier Discharge Plasma, *J. Energy Chem.* **2016**, *25(5)*, 825.

- Fang, X.; Zhang, X.; Guo, Y.; Chen, M.; Liu, W.; Xu, X.; Peng, H.; Gao, Z.; Wang, X.; Li, C., Highly Active and Stable Ni/$Y_2Zr_2O_7$ Catalysts for Methane Steam Reforming: on the Nature and Effective Preparation Method of the Pyrochlore Support, *Int. J. Hydro. Energy* **2016**, *41(26)*, 11141.
- Faure, R.; Basile, F.; Bersani, I.; Chartier, T.; Cuni, A.; Cornillac, M.; Del Gallo, P.; Etchegoyen, G.; Gary, D.; Rossignol, F.; Vaccari, A., Foam-Supported Catalysts Tailored for Industrial Steam Reforming Processes, *Stud. Surf. Sci. Catal.* **2010**, *175*, 241.
- Faure, R.; Rossignol, F.; Chartier, T.; Bonhomme, C.; Maitre, A.; Etchegoyen, G.; Del Gallo, P.; Gary, D., Alumina Foam Catalyst Supports for Industrial Steam Reforming Processes, *J. Eur. Ceram. Soc.* **2011**, *31(3)*, 303.
- Ferrari, A.C., Raman Spectroscopy of Graphene and Graphite: Disorder, Electron–Phonon Coupling, Doping and Nonadiabatic Effects, *Solid State Commun.* **2007**, *143(1-2)*, 47.
- Froment, G.F., Production of Synthesis Gas by Steam-and-CO_2 Reforming of Natural Gas, *J. Mol. Catal. A: Chem.* **2000**, *163(1)*, 147.
- Fulton, J.W., Selecting the Catalyst Configuration, *Chem. Eng.* **1986**, *93*, 97.
- Gallei E.; Schwab E., Development of Technical Catalysts, *Catal. Today* **1999**, *51(3-4)*, 535.
- Ghoneim, S.A.; El-Salamony R.A.; El-Temtamy, S.A., Review on Innovative Catalytic Reforming of Natural Gas to Syngas, *World J. Eng. Technol.* **2016**, *4(1)*, 116.
- Gibson, L.J.; Ashby, M.F., Cellular Solids: Structure and Properties, Oxford, Pergamon Press., 1988.
- Gil, A.G.; Wu, Z.; Chadwick, D.; Li, K., Ni/SBA-15 Catalysts for Combined Steam Methane Reforming and Water Gas Shift—Prepared For Use In Catalytic Membrane Reactors, *Appl. Catal., A* **2015**, *506*, 188.
- Gomez, F.J.P., Mechanism of Sulfur Poisoning by H_2S And SO_2 of Nickel and Cobalt Based Catalysts for Dry Reforming of Methane, M.Sc. Thesis, University of Saskatchewan, Saskatoon, SK, 2016.
- Hansen, T.W.; DeLaRiva, A.T.; Challa, S.R.; Datye, A.K., Sintering of Catalytic Nanoparticles: Particle Migration or Ostwald Ripening, *Acc. Che. Res.* **2013**, *46(8)*, 1720.
- Heffner, L.E.; Pfost, H.B., Gelatinization during Pelleting, *Feedstuffs* **1973**, *45(23)*, 32.

- Hilli, Y.; Kinnunen, N., M.; Suvanto, M.; Savimaki, A.; Kallinen, K.; Pakkanen, T., A., Sulfur Adsorption and Release Properties of Bimetallic Pd–Ni Supported Catalysts, *J. Mol. Catal. A: Chem.* **2015**, *408*, 161.
- Horváth, A.; Guczi, L.; Kocsonya, A.; Sáfrán, G.; La Parola, V.; Liotta, L.F.; Pantaleo, G.; Venezia, A.M., Sol-Derived AuNi/$MgAl_2O_4$ Catalysts: Formation, Structure and Activity in Dry Reforming of Methane, *Appl. Catal., A* **2013**, *468*, 250.
- Hossain, M. A.; Ayodele, B.V.; Cheng, C.K.; Khan, M.R., Artificial Neural Network Modeling of Hydrogen-Rich Syngas Production from Methane Dry Reforming over Novel Ni/$CaFe_2O_4$ Catalysts, *Int. J. Hydro. Energy* **2016**, *41(26)*, 11119.
- Hu, E.L.; Davis, S.M.; Davis, R.; Scher, E.: Nanotechnology Research Directions for Societal Needs, Springer, 2010.
- Huang C; T-Raissi A., Thermodynamic Analyses of Hydrogen Production from Sub-Quality Natural Gas. Part II: Steam Reforming and Autothermal Steam Reforming, *J. Power Sources* **2007**, *163*, 637.
- Iglesias, I.; Baronetti, G.; Mariño, F., Ni/$Ce_{0.95}M_{0.05}O_{2-d}$ (M = Zr, Pr, La) for Methane Steam Reforming at Mild Conditions, *Int. J. Hydro. Energy* **2017**, *42(50)*, 29735.
- Intergovernmental Panel on Climate Change (IPCC), Synthesis Report: Summary for Policymakers, **2014**.
- Irandoust, S.; Andersson, B., Monolithic Catalysts for Nonautomobile Applications, *Catal. Rev.: Sci. Eng.* **1988**, *30(3)*, 314.
- Jenness, L.G., Catalyst Pellet and Process of Making, U.S. Patent No. 2136509, 1938**.**
- Zhu, J.; Peng, X.; Yao, L.; Deng, X.; Dong, H.; Tong, D.; Hu, C., Synthesis Gas Production from CO_2 Reforming of Methane over Ni–Ce/SiO_2 Catalyst: the Effect of Calcination Ambience, *Int. J. Hydro. Energy*, **2013**, *38(1)*, 117.
- Jin, L.; Xie, T.; Ma, B.; Li, Y.; Hu, H., Preparation of Carbon-Ni/MgO-Al_2O_3 Composite Catalysts for CO_2 Reforming Of Methane, *Int. J. Hydro. Energy* **2017**, *42(8)*, 5047.
- Kapteijn, F.; Nijhuis, T. A.; Heiszwolf, J. J.; Moulijn, J. A., New Nontraditional Multiphase Catalytic Reactors Based on Monolithic Structures, *Catal. Today* **2001**, *66*, 133.
- Károlyi, J.; Németh, M.; Evangelisti, C.; Sáfrán, G.; Schay, Z.; Horváth, A.; Somodi, F., Carbon Dioxide Reforming of Methane over Ni–In/SiO_2 Catalyst without Coke Formation, *Ind. Eng. Chem.* **2018**, *58*, 189.

- Kohn, M.P.; Castaldi, M.J.; Farrauto, R.J., Auto-Thermal and Dry Reforming of Landfill Gas over a Rh/γAl_2O_3 Monolith Catalyst, *Appl. Catal., B* **2010**, *94(1-2)*, 125.
- Lange, F.F.; Miller, K.T., Open-Cell, Low-Density Ceramics Fabricated from Reticulated Polymer Substrates, *Adv. Ceram. Mater.* **1987**, *2(4)*, 827.
- Lavoie, J., M., Review on Dry Reforming Of Methane, a Potentially More Environmentally-Friendly Approach to the Increasing Natural Gas Exploitation, *Front. Chem.* **2014**, *2*, 81.
- Lee, Y.; Kim, M.G.; Kim, J.; Kim, Y.; Cho, J., Phase Transition of Bare and Coated $LixCoO_2$ (x = 0.4 and 0.24) at 300 °C, *J. Electrochem. Soc.* **2005**, *152(9)*, 1824.
- Li, C.; Fu, S.; Zhang, H.; Xin, Q., An Infrared Spectroscopic Study on the Lewis Base Properties of Metal Oxides by Using a Novel Probe Molecule: Boric Acid Trimethyl Ester, *J. Chem. Soc., Chem. Commun.* **1994**, *1*, 17.
- Li, Y.; Wang, Y.; Zhang, X.; Mi, Z., Thermodynamic Analysis of Autothermal Steam and CO_2 Reforming of Methane, *Int. J. Hydro. Energy* **2008**, *33(10)*, 2507.
- Liang, M.; Tian, L.; Shakouri, M.; Hu, Y.; Wang, H., Development of Shaped NiCoMg/γ–Al_2O_3 Catalyst with Commercial Support for CO_2 Reforming of CH_4, *Catal. Today* **2017**, *291*, 76.
- Liang, Y.; Wang, P.; Dai, H.-B., Hydrogen Bubbles Dynamic Template Preparation of a Porous Fe–Co–B/Ni Foam Catalyst for Hydrogen Generation from Hydrolysis of Alkaline Sodium Borohydride Solution, *J. Alloys Comd.* **2010**, *491(1-2)*, 359.
- Lide, D.R.: CRC Handbook of Chemistry and Physics; CRC: Boca Raton, FL, 2005.
- Ma, R.; Hu, Z.; Zhang, J.; Ma, H.; Jiang, L.; Ru, D., Reduction of Greenhouse Gases Emissions During Anoxic Wastewater Treatment by Strengthening Nitrite-Dependent Anaerobic Methane Oxidation Process, *Bioresour. Technol.* **2017**, *235*, 211.
- Motay, M.T.D.; Marechal, M., Preparation indusrille de I'lhydrogene, *Bulletin de la Société Chimique de France* **1868**, *9*, 334.
- Morales-Cano, F.; Lundegaard, L.F.; Tiruvalam, R.R.; Falsig, H.; Skjoth-Rasmussen, M.S., Improving the Sintering Resistance of Ni/Al2O3 Steam-Reforming Catalysts by Promotion with Noble Metals, *Appl. Catal., A* **2015**, *498*, 117.
- Nandini, A.: Pant, K.K.; Dhingra, S.C., Kinetic Study of the Catalytic Carbon Dioxide Reforming of Methane to Synthesis Gas over Ni-K/Ceo_2-Al_2O_3 Catalyst, *Appl. Catal., A* **2006**, *308*, 119.

- National Centers for Environmental Information, NOAA: Global Climate Report, April 2017, https://www.ncdc.noaa.gov/sotc/global/201704, Oct 2017.
- Ocsachoque, M.; Pompeo, F.; Gonzalez, G., Rh–Ni/CeO_2–Al_2O_3 Catalysts for Methane Dry Reforming, *Catal. Today* **2011**, *172*, 226.
- Ozkara-Aydınoglu, S., Thermodynamic Equilibrium Analysis of Combined Carbon Dioxide Reforming With Steam Reforming of Methane to Synthesis Gas, *Int. J. Hydro. Energy* **2010**, *35(23)*, 12821.
- Pacurariu, C.; Lazau, I.; Ecsedi, Z.; Lazau, R.; Barvinschi, P.; Marginean, G., New Synthesis Methods of $MgAl_2O_4$ Spinel, *J. Eur. Ceram. Soc.* **2007**, *27(2-3)*, 707.
- Palma, S.; Bobadilla, L.F.; Corrales, A.; Ivanova, S.; Romero-Sarria, F.; Centeno, M.A.; Odriozola, J.A., Effect of Gold on a $NiLaO_3$ Perovskite Catalyst for Methane Steam Reforming, *Appl. Catal., B* **2014**, *144*, 846.
- Park, D.; Moon, D.J.; Kim, T., Preparation and Evaluation of a Metallic Foam Catalyst for Steam-CO_2 Reforming of Methane in GTL-FPSO Process, *Fuel Process. Technol.* **2014**, *124*, 97.
- Pena, M.A.; Gomez, J.P.; Fierro, J.L.G., New Catalytic Routes for Syngas and Hydrogen Production, *Appl. Catal., A* **1996**, *144*, 7.
- Perego, C.; Peratello, S., Experimental Methods in Catalytic Kinetics, *Catal. Today* **1999**, *52(2-3)*, 133.
- Pickering, I.J.; Princeb, R.C.; Diversc, T.; George, G.N., Sulfur K-edge X-ray Absorption Spectroscopy for Determining the Chemical Speciation of Sulfur in Biological Systems, *FEBS Lett.* **1998**, *441 (1)*, 11.
- Pino, L.; Italiano, C.; Vita, A.; Laganà, M.; Recupero, V., $Ce_{0.70}La_{0.20}Ni_{0.10}O_{2-\delta}$ Catalyst for Methane Dry Reforming: Influence of Reduction Temperature on the Catalytic Activity and Stability, *Appl. Catal., B* **2017**, *218*, 779.
- Quiros, D.C.; Smith, J.; Thiruvengadam, A.; Huai, T.; Hu, S., Greenhouse Gas Emissions from Heavy-Duty Natural Gas, Hybrid, and Conventional Diesel on-Road Trucks during Freight Transport, *Atmos. Environ.* **2017**, *168*, 36.
- Rakass, S.; Oughiri-Hassani, H.; Rowntree, P.; Abatzoglou, N., Steam Reforming of Methane over Unsupported Nickel Catalysts, *J. Power Sources* **2006**, *158(1)*, 485.
- Richardson, J.T., Principles of catalyst development, Plenum Press, New York, 1989.

- Rostrup-Nielsen, J. R.; Anderson, J.R.; Boudart, M., Catalysis, Science and Technology, vol 5, Springer-Verlag, Berlin, 1984.
- Rostrup-Nielsen, J. R., Industrial Relevance of Coking, *Catal. Today* **1997**, *37(3)*, 225.
- Rostrup-Nielsen, J.R.; Hansen, J.H., CO_2 Reforming of Methane over Transition Metals, *J. Catal.* **1993**, *144(1)*, 38.
- Rostrup-Nielsen, J.R.; Sehested, J.; Norskov, J.K., Hydrogen and Synthesis Gas by Steam- and CO_2 Reforming, *Adv. Catal.* **2002**. *47*, 65.
- Sadykov, V.; Mezentseva, N.; Alikina, G.; Bunina, R.; Pelipenko, V.; Lukashevich, A.; Tikhov, S.; Usoltsev, V.; Vostrikov, Z.; Bobrenok, O.; Smirnova, A.; Ross, J.; Smorygo, O.; Rietveld, B., Nanocomposite Catalysts for Internal Steam Reforming of Methane And Biofuels in Solid Oxide Fuel Cells: Design and Performance, *Catal. Today* **2009**, *146(1-2)*, 132.
- San-Jose-Alonso, D.; Juan-Juan, J.; Illan-Gomez, M.J., Roman-Martinez, M.C., Ni, Co and Bimetallic Ni–Co Catalysts for the Dry Reforming of Methane, *Appl. Catal., A* **2009**, *371*, 54.
- Sarlis, J.; Berk, D., Reduction of Sulfur Dioxide with Methane over Activated Alumina, *Ind. Eng. Chem. Res.* **1988**, *27*, 1951.
- Sehested, J., Four Challenges for Nickel Steam-Reforming Catalysts, *Catal. Today* **2006**, *111(1-2)*, 103.
- Shakouri, M., Effect of Preparation, Ni/Co Ratio, and Sulfur Poisoning of Ni-Co Bimetallic Catalyst for Dry Reforming Reaction, M.Sc. Thesis, University of Saskatchewan, Saskatoon, SK, 2012.
- Siang, T. J.; Pham, T.L.M.; Cuong, N.V.C.; Phuong, P.T.T.; Phuc, N.H.H.; Troung, Q.C.; Vo, D.V.N., Combined Steam and CO_2 Reforming of Methane for Syngas Production over Carbon-Resistant Boron-Promoted Ni/SBA-15 Catalysts, *Microporous and Mesoporous Mater.* **2018**, *262*, 122.
- Silva, J. M.; Soria, M.A.; Madeira, L. M., Thermodynamic Analysis of Glycerol Steam Reforming for Hydrogen Production with in Situ Hydrogen and Carbon Dioxide Separation, *J. Power Sources* **2015**, *273*, 423.
- Silveira, E. B.; Rabelo-Neto, R.C.; Noronha, F.B., Steam Reforming of Toluene, Methane and Mixtures over Ni/ZrO_2 Catalysts, *Catal. Today* **2017**, *289*, 289.

- Simakov, D.S.A.; Wright, M.M.; Ahmed, S.; Mokheimer, E.M.A.; Roman-Leshkov, Y., Solar Thermal Catalytic Reforming of Natural Gas: A Review on Chemistry, Catalysis and System Design, *Catal.: Sci. Technol.* **2015**, *5*, 1991.
- Slagtern, A.; Olsbye, U.; Blom, R.; Dahl, I.M., The Influence of Rare Earth Oxides on Ni/Al_2O_3 Catalyst During CO_2 Reforming of CH_4, *Stud. Surf. Sci. Catal.* **1997**, *107*, 497.
- Snoeck, J.W.; Froment, F.; Fowles, M., Steam/CO_2 Reforming of Methane. Carbon Filament Formation by the Boudouard Reaction and Gasification by CO_2, by H_2, and by Steam: Kinetic Study, *Ind. Eng. Chem. Res.* **2002**, *41(17)*, 4252.
- Solomon, S.; Plattner, G.K.; Knutti, R.; Friedlingstein,P., Irreversible Climate Change due to Carbon Dioxide Emissions, *Proc. Natl. Acad. Sci. U. S. A.* **2009**, *106(6)*, 1704.
- Somorjai, G.A., Introduction to Surface Chemistry and Catalysis, Wiley-Inter science, New York, 1994.
- Song, X.; Dong, X.; Yin, S.; Wang, M.; Li, M.; Wang, H., Effects of Fe Partial Substitution of $La_2NiO_4/LaNiO_3$ Catalyst Precursors Prepared by Wet Impregnation Method for the Dry Reforming of Methane, *Appl. Catal., A* **2016**, *526*, 132.
- Standard test method for determination of bulk crush strength of catalysts and catalyst carriers, ASTM D7084- 04.
- Standard test method for single pellet crush strength of formed catalysts and catalyst carriers, ASTM D4179- 11.
- Standard test method for splitting tensile strength of cylindrical concrete specimens, ASTM C496-96.
- Staub, D.; Meille, S.; Le Corre V.; Chevalier, J.; Rouleau, L., Revisiting the Side Crushing Test Using the Three-Point Bending Test for the Strength Measurement of Catalyst Supports, *Oil Gas Sci. Technol.* **2014**, *70(3)*, 475.
- Struis, R.P.W.J.; Schildhauer, T.J.; Czekaj, I.; Janousch, M.; Biollaz, S.M.A.; Ludwig, C., Sulphur Poisoning of Ni Catalysts in the SNG Production from Biomass: A TPO/XPS/XAS Study, *Appl. Catal., A* **2009**, *362*, 121.
- Sugiura, Y.; Mukai, D.; Murai, Y.; Tochiya, S., Oxidation Resistance of $Ni/La_{0.7}Sr_{0.3}AlO_{3-\delta}$ Catalyst for Steam Reforming of Model Aromatic Hydrocarbon, *Int. J. Hydro. Energy* **2013**, *38(19)*, 7822.

- Tabrizi, F.F.; Mousavi, S.A.HS.; Atashi, H., Thermodynamic Analysis of Steam Reforming of Methane with Statistical Approaches, *Energy Convers. Manage.* **2015**, *103*, 1065.
- Tian, L., Development of Spherical Ni-Co/MgAlO Bimetallic Catalyst for CO_2 Reforming of CH_4, M.Sc. Thesis, University of Saskatchewan, Saskatoon, SK, 2013.
- Tichit, D.; Medina, F.; Coq, B.; Dutartre, R., Activation under Oxidizing and Reducing Atmospheres of Ni-containing Layered Double Hydroxides, *Appl. Catal., A* **1997**, *159(1-2)*, 241.
- Tronconi, E.; Groppi, G.; Visconti, C.G., Structured catalysts for non-adiabatic applications, *Curr. Opin. Chem. Eng.* **2014**, *5*, 55.
- Tsai, H.L.; Wang, C.S., Thermodynamic Equilibrium Prediction for Natural Gas Dry Reforming in Thermal Plasma Reformer, *J. Chin. Inst. Eng.* **2008**, *31(5)*, 891.
- Tsang, S.C.; Claridge, J.B.; Green, M.L.H., Recent Advances in the Conversion of Methane to Synthesis Gas, *Catal. Today* **1995**, *23(1)*, 3.
- Tsipouriari, V.A.; Verykios, X.E., Kinetic Study of the Catalytic Reforming of Methane with Carbon Dioxide to Synthesis Gas over Ni/La_2O_3 Catalyst, *Catal. Today* **2001**, *64(1-2)*, 83.
- Twigg, M.V.; Sengelow, W.M., Preparation and Properties of Ceramic Foam Catalyst Supports, *Stud. Surf. Sci. Catal.* **1995**, *91*, 345.
- Twigg, M.V.; Sengelow, W.M.: Foam Catalysts, Method of Manufacture and Method of Using, U. S. Patent 4810685 A, 1989.
- Udengaard, N.R.; Hansen, J.H. B.; Hanson, D. C.; Stal, J. A., Sulfur Passivated Reforming Process Lowers Syngas H_2/CO Ratio, *Oil Gas J.* **1992**, *90(10)*, 62.
- Usman, M.; Daud, W.W.M.A.; Abbas, H.F., Dry Reforming of Methane: Influence of Process Parameters—A Review, *Renewable Sustainable Energy Rev.* **2015**, *45*, 710.
- Varga, D.D.L.; Ruiz, I.; Álvarez, J.A.; Soto, M., Methane and Carbon Dioxide Emissions from Constructed Wetlands Receiving Anaerobically Pretreated Sewage, *Sci. Total Environ.* **2015**, *538*, 824.
- Vasiliades, M.A.; Makri, M.M.; Djinović, P.; Erjavec, B.; Pintar, A.; Efstathiou, A.M., Dry Reforming of Methane over 5 Wt% $Ni/Ce_{1-x}Pr_xO_{2-\delta}$ Catalysts: Performance and Characterisation of Active and Inactive Carbon by Transient Isotopic Techniques, *Appl. Catal., B* **2016**, *197*, 168.

- Vita, A.; Cristiano, G.; Italiano, C.; Pino, L.; Specchia, S., Syngas Production by Methane Oxy-Steam Reforming on Me/CeO_2 (Me = Rh, Pt, Ni) Catalyst Lined on Cordierite Monoliths, *Appl. Catal., B* **2015**, *162*, 551.
- Vita, A.; Cristiano, G.; Italiano, C.; Specchia, S.; Cipiti, F.; Specchia, V., Methane Oxy-Steam Reforming Reaction: Performances of Ru/γ-Al_2O_3 Catalysts Loaded on Structured Cordierite Monoliths, *Int. J. Hydro. Energy* **2014**, *39(32)*, 18592.
- Wang, C.; Sun, N.; Zhao, N.; Wei, W.; Sun, Y.; Sun, C.; Liu, H.; Snape, C.E., Coking and Deactivation of a Mesoporous Ni–CaO–ZrO_2 Catalyst in Dry Reforming of Methane: A Study under Different Feeding Compositions, *Fuel* **2015**, *143*, 527.
- Wang, C.Z.; Si, L.J.; Li, H.; Wen, X.; Sun, N.N.; Zhao, N.; Wei, W.; Sun, Y.H., Template-Free One-Pot Synthesis of Mesoporous Ni-CaO-ZrO_2 Catalyst and Its Application in CH_4-CO_2 Reforming, *J. Fuel Chem. Technol.* **2013**, *41(10)*, 1204.
- Wang, F.; Tan, J.; Shuai, Y.; Gong, L.; Tam, H., Numerical Analysis of Hydrogen Production via Methane Steam Reforming in Porous Media Solar Thermochemical Reactor Using Concentrated Solar Irradiation as Heat Source, *Energy Convers. Manage.* **2014**, *8*, 956.
- Wang, H.; Miller, J.T.; Shakouri, M.; Xi, C.; Wu, T.; Zhao, H.; Akatey, M.C., XANES and EXAFS Studies on Metal Nanoparticle Growth and Bimetallic Interaction of Ni-Based Catalysts for CO_2 Reforming of CH_4, *Catal. Today* **2013**, *207*, 3.
- Wang, H.; Zaidi, S.: Catalyst Development for Carbon Dioxide Activation to Produce Syn-Gas through CO_2 Reforming of CH_4: Mitigation of Carbon Formation on Ni-based Catalysts, Activation of Carbon Dioxide, Chapter 15, Elsevier B.V., Amsterdam, 2013.
- Wang, S.; Lu, G.Q. (Max); Millar, G.J., Carbon Dioxide Reforming of Methane to Produce Synthesis Gas over Metal-Supported Catalysts: State of the Art, *Energy Fuels* **1996**, *10(4)*, 896.
- Wang, T.; Porosoff, M.D.; Chen, J.G., Effects of Oxide Supports on the Water-Gas Shift Reaction over Pt–Ni Bimetallic Catalysts: Activity and Methanation Inhibition, *Catal. Today* **2014**, *233*, 61.
- Wang, Y.; Peng, J.; Zhou, C.; Lim, Z.Y.; Wu, C.; Ye, S.; Wang, W.G., Effect of Pr Addition on the Properties of Ni/Al_2O_3 Catalysts with an Application in the Autothermal Reforming of Methane, *Int. J. Hydro. Energy* **2014**, *39(2)*, 778.

- Wu, D.F.; Zhou, J.C.; Li, Y.D., Statistical Analysis of Pellet Size Variation in Commercial Catalyst, *Part. Part. Syst. Charact.* **2005**, *22(1)*, 63.
- Wu, D.F.; Zhou, J.C.; Li, Y.D., Distribution of the Mechanical Strength of Solid Catalysts, *Chem. Eng. Res. Des.* **2006**, *84(12)*, 1152.
- Wu, H.; Pantaleo, G.; La Parola, V.; Venezia, A.M.; Collard, X.; Aprile, C.; Liotta, L.F., Bi- and Trimetallic Ni Catalysts over Al_2O3 and Al_2O_3-MO_x (M = Ce or Mg) Oxides for Methane Dry Reforming: Au and Pt Additive Effects, *Appl. Catal., B* **2014**, *156-157*, 350.
- Xi, C.; Hu, Y.; Wang, H., A Study of Poisoning of Ni-Co/AlMgO Bimetallic Catalyst for CO_2 Reforming of CH_4 in Presence of Sulfur-Containing Gases, 21st CSC, Banff, AB, May 9-12, 2010.
- Xi, C.; Wang, H., Effects of Preparation Conditions and Ni/Co Ratio on Ni-Co Bimetallic Catalyst Performance for CO_2 Reforming of CH_4, 21st NAM, San Francisco, CA, June 7-12, 2009.
- Xu, J.; Froment, G.F., Methane Steam Reforming, Methanation and Water-Gas Shift: I. Intrinsic Kinetics, *AIChE J.* **1989**, *35(1)*, 88.
- Yadav, T.P.; Mukhopadhyay, N.K.; Tiwari, N.K.; Srivastava, O.S.; Nanosci, J., Synthesis of Nanocrystalline (Co,Ni)Al_2O_4 Spinel Powder by Mechanical Milling of Quasicrystal line Materials, *J. Nanosci. Nanotechnol.* **2007**, *7(2)*, 575.
- Yao, L.; Wang, Y.; Shi, J.; Xu, H.; Shen, W.; Hu, Ch., The Influence of Reduction Temperature on The Performance of ZrO_x/Ni-MnO_x/SiO_2 Catalyst for Low-Temperature CO_2 Reforming Of Methane, *Catal. Today* **2017**, *281(2)*, 259.
- Yaw, T.C., Saidina Amin, N.A., Analysis of Carbon Dioxide Reforming of Methane via Thermodynamic Equilibrium Approach, *Jurnal Teknologi* **2005**, *43(1)*, 31.
- York, A.P.E.; Xiao, T.; Green, M.L.H., Brief Overview of the Partial Oxidation of Methane to Synthesis Gas, *Top. Catal.* **2003**, *22(3-4)*, 345.
- Yu, J.-J.; Yu, Q.; Jin, Y.; Chang, S.-G., Reduction of Sulfur Dioxide by Methane to Elemental Sulfur over Supported Cobalt Catalysts, *Ind. Eng. Chem. Res.* **1997**, *36*, 2128.
- Zhang, J., Research and Development of Nickel Based Catalysts for Carbon Dioxide Reforming of Methane, Ph.D. Thesis, University of Saskatchewan, Saskatoon, SK, 2008.
- Zhang, J.; Wang, H.; Dalai, A.K., Development of Stable Bimetallic Catalysts for Carbon Dioxide Reforming of Methane, *J. Catal.* **2007**, *249(2)*, 300.

- Zhang, J.; Wang, H.; Dalai, A.K., Effects of Metal Content on Activity and Stability of Ni-Co Bimetallic Catalysts for CO_2 Reforming of CH_4, *Appl. Catal., A* **2008**, *339(2)*, 121.
- Zhang, J.; Wang, H.; Dalai, A.K., Kinetic Studies of CO_2 Reforming of CH_4 over Ni-Co/Al-Mg-O Bimetallic Catalyst, *Ind. Eng. Chem. Res.* **2009**, *48*, 677.
- Zhang, J.; Wang, H.; Xi, C.; Shakouri, M.; Hu, Y.; Dalai, A.K.: Nanocatalysis for Fuels and Chemicals, American Chemistry Society, Washington DC, 2012.
- Zhao, C.Y., Review on Thermal Transport in High Porosity Cellular Metal Foams with Open Cells, *Int. J. Heat Mass Transfer* **2012**, *55(13-14)*, 3618.
- Zhu, J.; Peng, X.; Yao, L.; Deng, X.; Dong, H.; Tong, D.; Hu, C., Synthesis Gas Production from CO_2 Reforming of Methane Over Ni–Ce/SiO_2 Catalyst: the Effect of Calcination Ambience, *Int. J. Hydro. Energy* **2013**, *38(1)*, 117.
- Zhu, Q.; Zhao, X.; Deng, Y., Advances in the Partial Oxidation of Methane to Synthesis Gas, *J. Nat. Gas. Chem.* **2004**, *13*, 191.
- Zhu, T.; Dreher, A.; Flytzani-Stephanopoulos, M., Direct Reduction of SO_2 to Elemental Sulfur by Methane over Ceria-Based Catalysts, *Appl. Catal., B* **1999**, *21(2)*, 103.

Appendix A: Reproducibility of the Experimental Results

N_2 Chemisorption: at least of the catalysts was characterized twice, to investigate whether the characterization results are reproducible. The percent difference of two values (x_1 and x_2) is calculated using equation A.1.

$$\text{Diff.} = \left|\frac{(x_1 - x_2)}{(x_1 + x_2)/2}\right| \times 100, \% \quad \text{(A.1)}$$

BET surface area, pore sizes and pore volumes for Sph-C were measured twice and results as well as Diff. % are shown in Table A.1 which reveals that the test results were reproducible (about 3% difference).

XAS analysis: For each set of 6-hole shooter, three XAS spectra for at least one of the samples were collected. As an example, Ni and Co K-edge spectra for the reduced CC-Ni2Co4 sample reacted with SO_2 are shown in Figure A.1. The results clearly show that the spectra are almost identical, and no significant difference could be observed.

Catalyst activity test: The catalyst CRM activity test over CC-Ni2Co4 powdered catalyst was repeated. Figures 4.1 and 4.2 show reactant conversions ratio during 10 hr TOS. Both CH_4 and CO_2 conversions are in the range of ± 1% which indicate that the catalyst activity tests were reproducible.

Table A.1 Repeatability results for N_2-chemisorption analysis

	X_1	X_2	Diff. %
BET surface area (m^2/g)	166.01	161.10	3.00
Pore volume (cm^3/g)	0.267	0.259	3.04
Average pore size (Å)	65.60	64.80	2.78

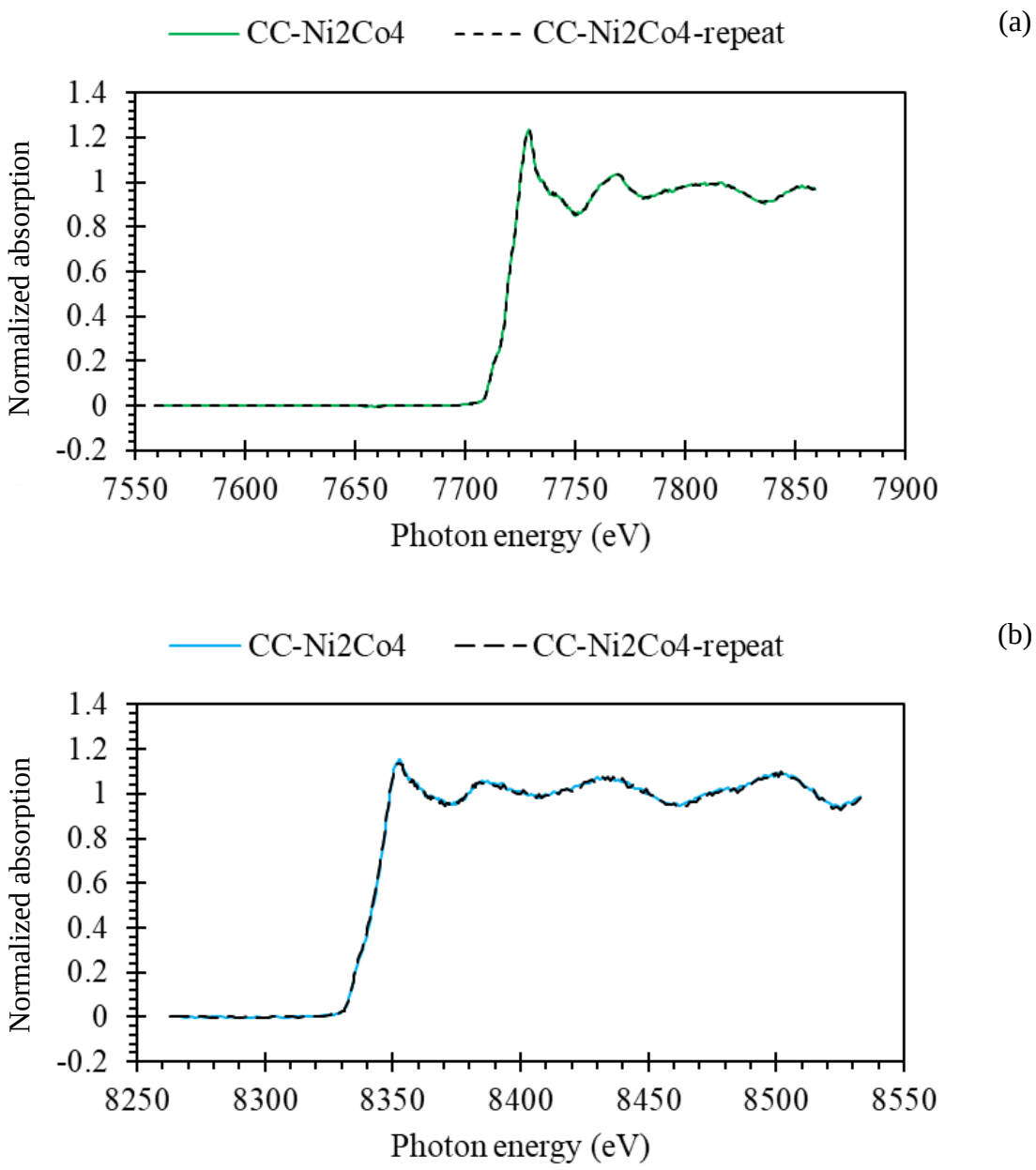

Figure A.1 Reproducibility of normalized absorption of (a) Ni K-edge and (b) Co K-edge XANES spectra of reduced CC-Ni2Co4 catalyst reacted with 500 ppm SO_2 at 800 °C for 1 hr

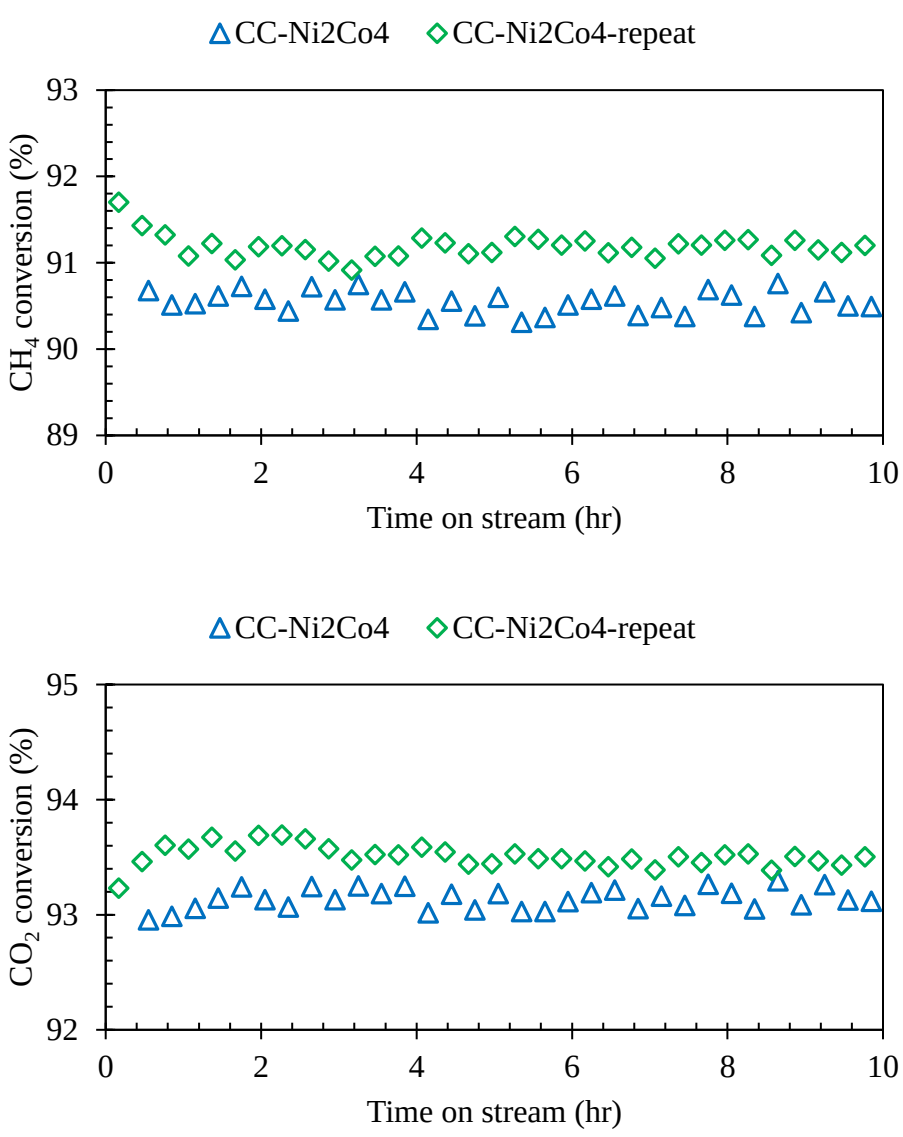

Figure A.2 (a) CH_4 and (b) CO_2 conversions using Ni-Co bimetallic powder catalyst for CRM reaction (repeated catalyst performance evaluation experiments). Reaction conditions: 0.10 g catalyst, temperatures: 850 °C, 1atm, GHSV of 110 L g^{-1} hr^{-1}, $CH_4/CO_2/N_2$ = 1/1/1

Appendix B: Calibration of Mass Flow Controller (MFC)

To calibrate the MFC, N_2 was used as the reference gas. Then for any gas other than N_2 as well as gas mixtures, the correction factor (CF) was used to convert the flow rate of N_2 to the corresponding gas flow rate. The correction factors were calculated using heat capacity (C_p) of gases, shown in Table A.1, at constant pressure. Equation B.1 was used to convert the flow rates.

$$F_j = F_{N_2} \times CF \tag{B.1}$$

where, FN_2 is flowrate of N_2, Fj are flowrates of gas j and CF is the correction factor. CF for a single gas and gas mixture were calculated using equations B.2 and B.3, respectively.

$$CF_j = \frac{C_p of\ N_2\ at\ 21\ °C, cal/L/°C}{C_p of\ gas\ "j"\ at\ 21\ °C, cal/L/°C} \tag{B.2}$$

$$CF_{mix.} = \sum CF_j \times \frac{V_j}{V_{total}} \tag{B.3}$$

where j is any gas in the mixture.

Figure B.1 shows the calibration curves of mass flow controllers for N_2 gas. Each point stands as the average of 10 measured flow rates at the same set-point. Using the MFC calibration curves (with R^2 more than 0.9998) and correction factors, the set-pint for any gas or mixture to achieve the actual flow rate, which were required for the activity tests, could be precisely calculated.

Table B.1 Heat capacity of gases at 21 °C

Gas	C_p at 21 °C (cal/L/°C)
Ar	0.2066
CH_4	0.3547
CO	0.2892
CO_2	0.3749
H_2	0.2847
H_2S	0.3521
He	0.2058
N_2	0.2885
SO_2	0.4035

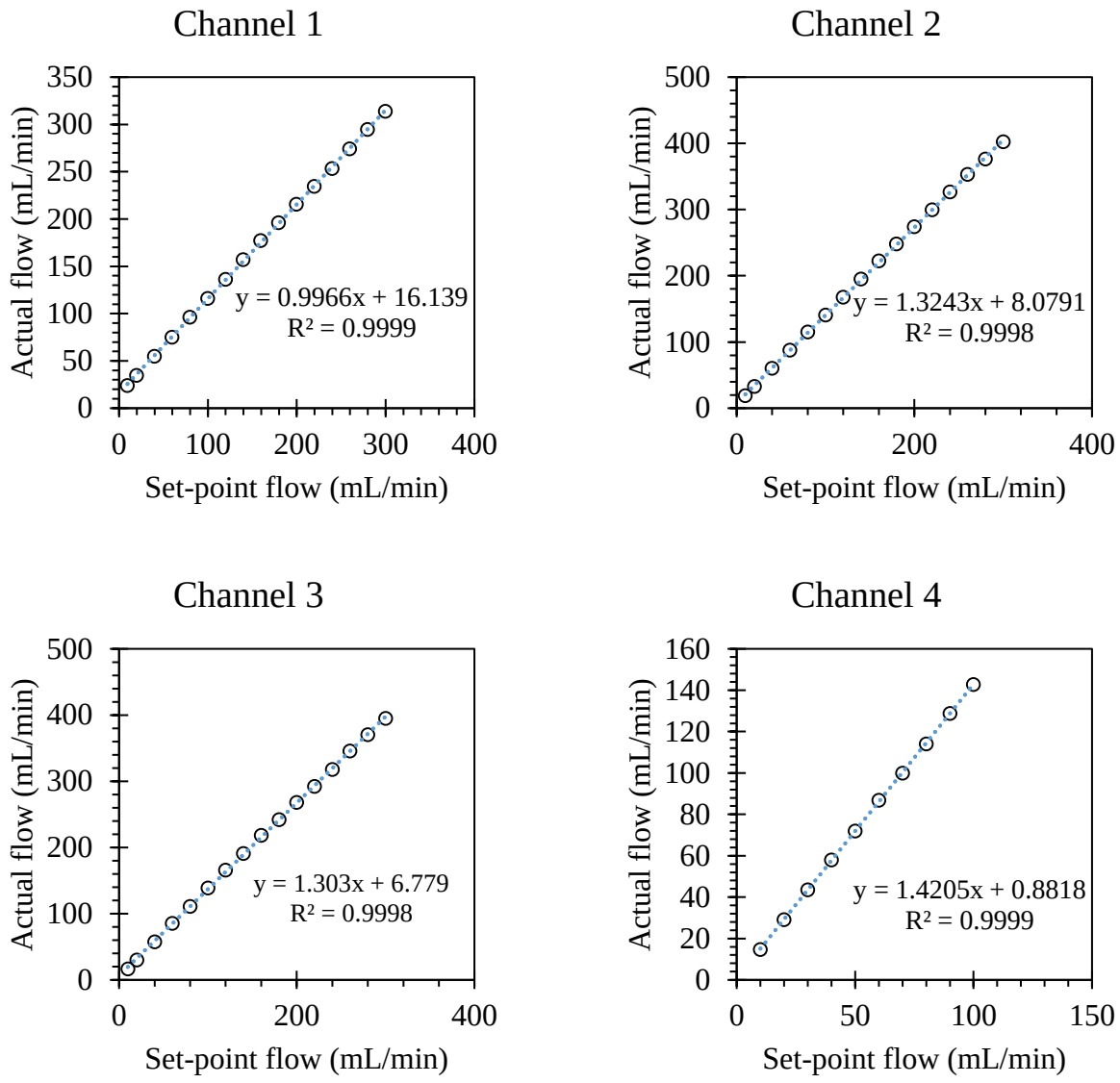

Figure B.1 MFC calibration curves of each channel for N_2 gas.

Appendix C: Calibration of Gas Chromatography (GC)

Gas Chromatography (GC) was calibrated using at least three concentrations, where at least three times injections at each concentration was conducted. Then the average area was calculated to use in the calibration curve. Also the Standard Deviation of the obtained data is calculated using equation C.1.

$$STD = \sqrt{\frac{1}{N}\sum_{i=1}^{N}(x_i - \bar{x})^2} \quad \text{(C.1)}$$

where,

STD: standard deviation of the obtained areas at each concentration

N: total number of experiments at each concentration

x_i: are under the detected peak by GC at each concentration

$\bar{x}$: average of areas (x_i) for the same concentration

The calibration was repeated until STD < 0.5 at each concentration and $R^2 > 0.9990$ for the fitted line were obtained. Calibration curves for Ar, N_2 and permanent gases (CO, H_2, CH_4, and CO_2) are shown in Figure C.1, and curves for H_2S and SO_2 are shown in Figure C.2.

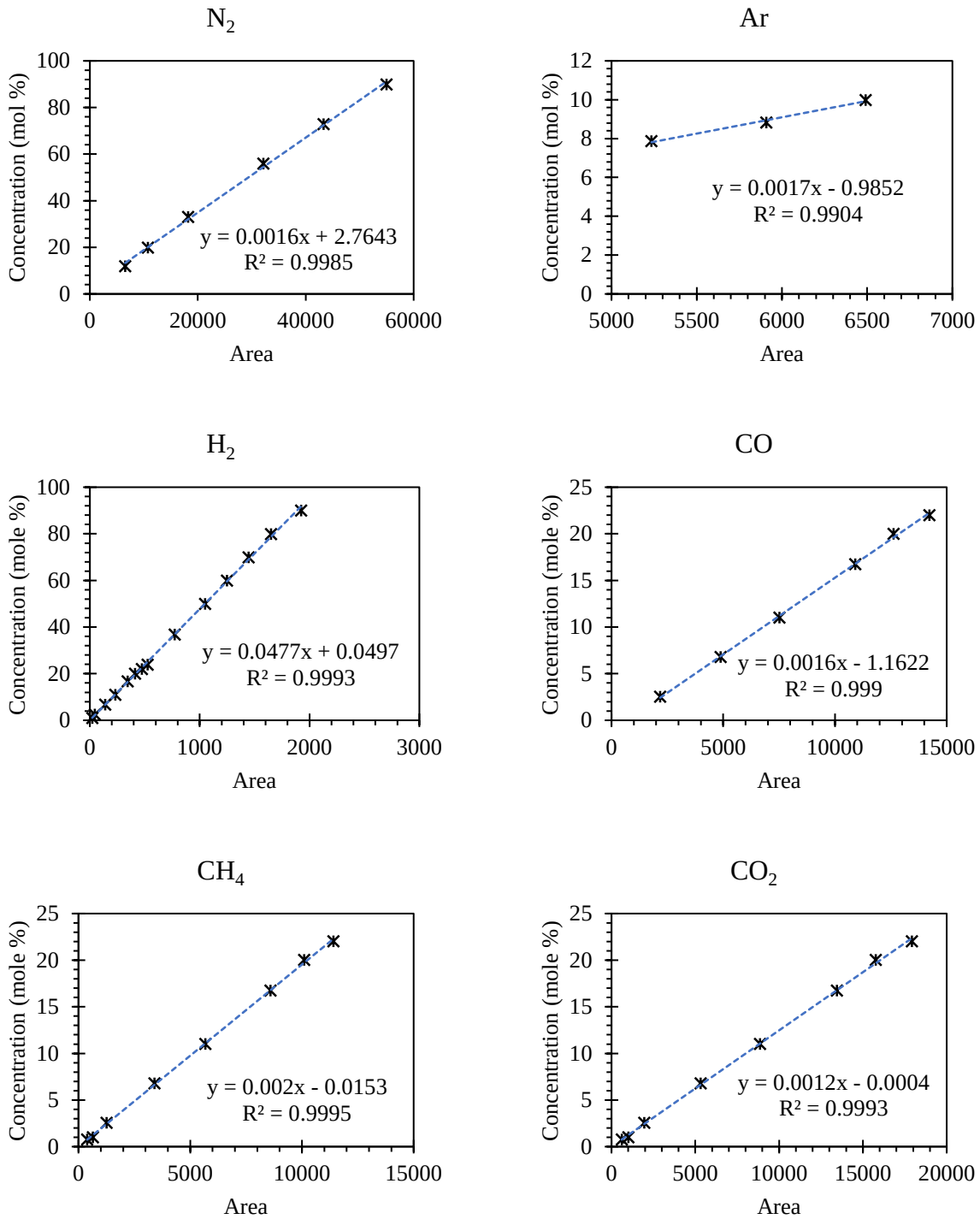

Figure C.1 Calibration curves for the Agilent 6890N GC equipped with a TCD detector

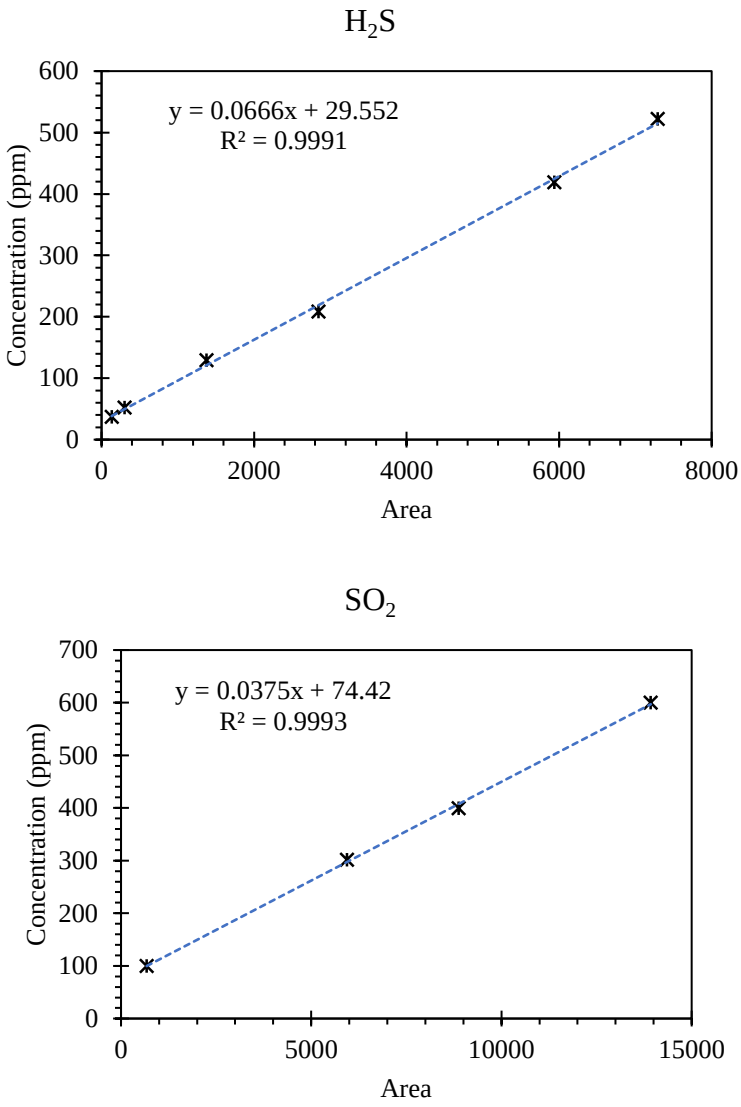

Figure C.2 Calibration curves for the Varian 3800 equipped with a PFPD detector

Appendix D: Temperature Profile of Reactor

To obtain the temperature profile inside the reactor, various temperatures were set on the furnace while N2 gas was passing through the reactor. The inside temperature was measured a recorded at various position using a K-type thermocouple. Figure D.1 shows the schematic of the reactor temperature measurements set-up. Temperature at each position were recorded three times and then the average value was used to (1) calibrate the set-point of furnace vs actual temperature, and (b) obtain the profile within the reactor length, as shown in Figure D.2.

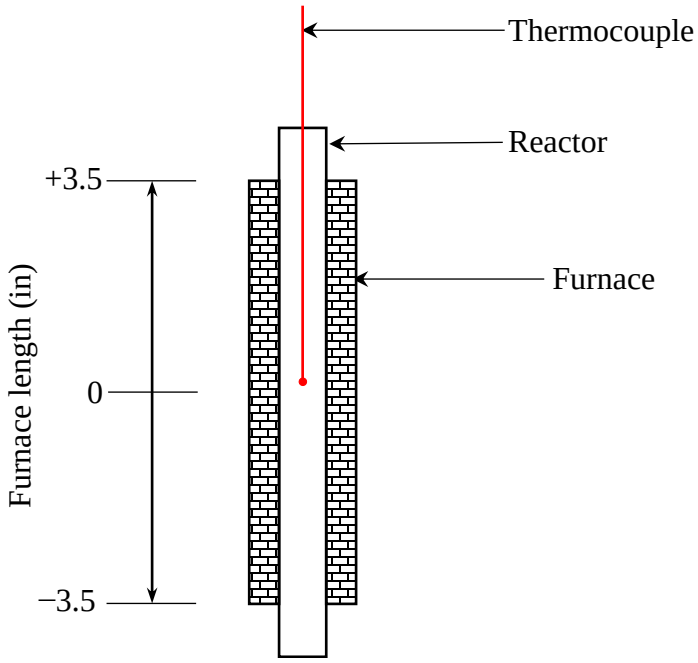

Figure D.1 Schematic for the reactor temperature measurements

(a)

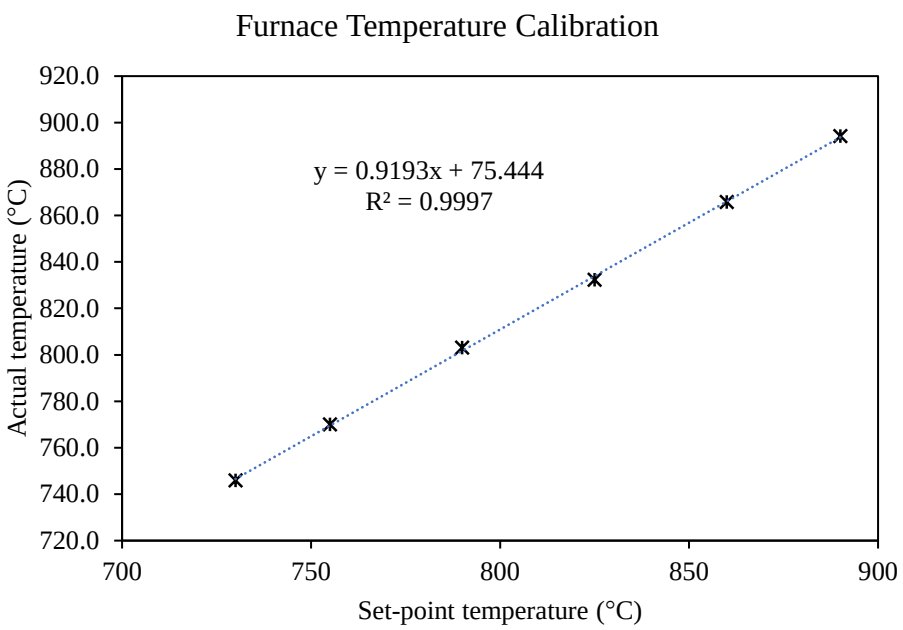

(b)

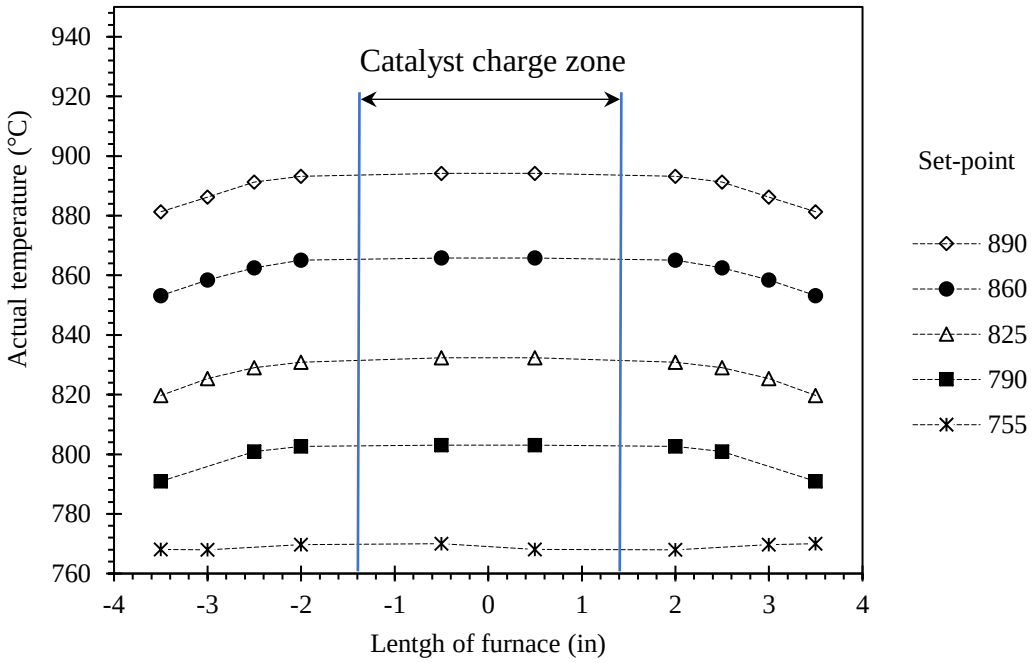

Figure D.2 (a) Furnace temperature calibration curve, and (b) reactor temperature profile within the furnace length

Appendix E: Carbon and Hydrogen Balance

Carbon and hydrogen balance could be calculated using equations E.1 to E.6.

$$C\big|_{in} = (CH_4 + CO_2)\big|_{in}, \text{ mole} \quad \text{(E.1)}$$

$$C\big|_{out} = (CH_4 + CO_2 + 2\times CO)\big|_{out}, \text{ mole} \quad \text{(E.2)}$$

$$\triangle C = C\big|_{in} - C\big|_{out}, \text{ mole} \quad \text{(E.3)}$$

$$H\big|in = 4\times CH_4\big|_{in}, \text{ mole} \quad \text{(E.4)}$$

$$H\big|out = (4\times CH4 + 2\times H_2)\big|_{out}, \text{ mole} \quad \text{(E.5)}$$

$$\triangle H = H\big|_{in} - H\big|_{out}, \text{ mole} \quad \text{(E.6)}$$

As an example, Carbon and Hydrogen in both inlet and outlet streams of the reactor were calculated from CRM results over Sph-C catalyst for 10 hr TOS and are shown in Figure E.1. Also, the Carbon and Hydrogen balance and Diff. %, within 10hr TOS, were calculated using Equations E.3, E.6, and A.1, respectively and are summarized in Table E.1.

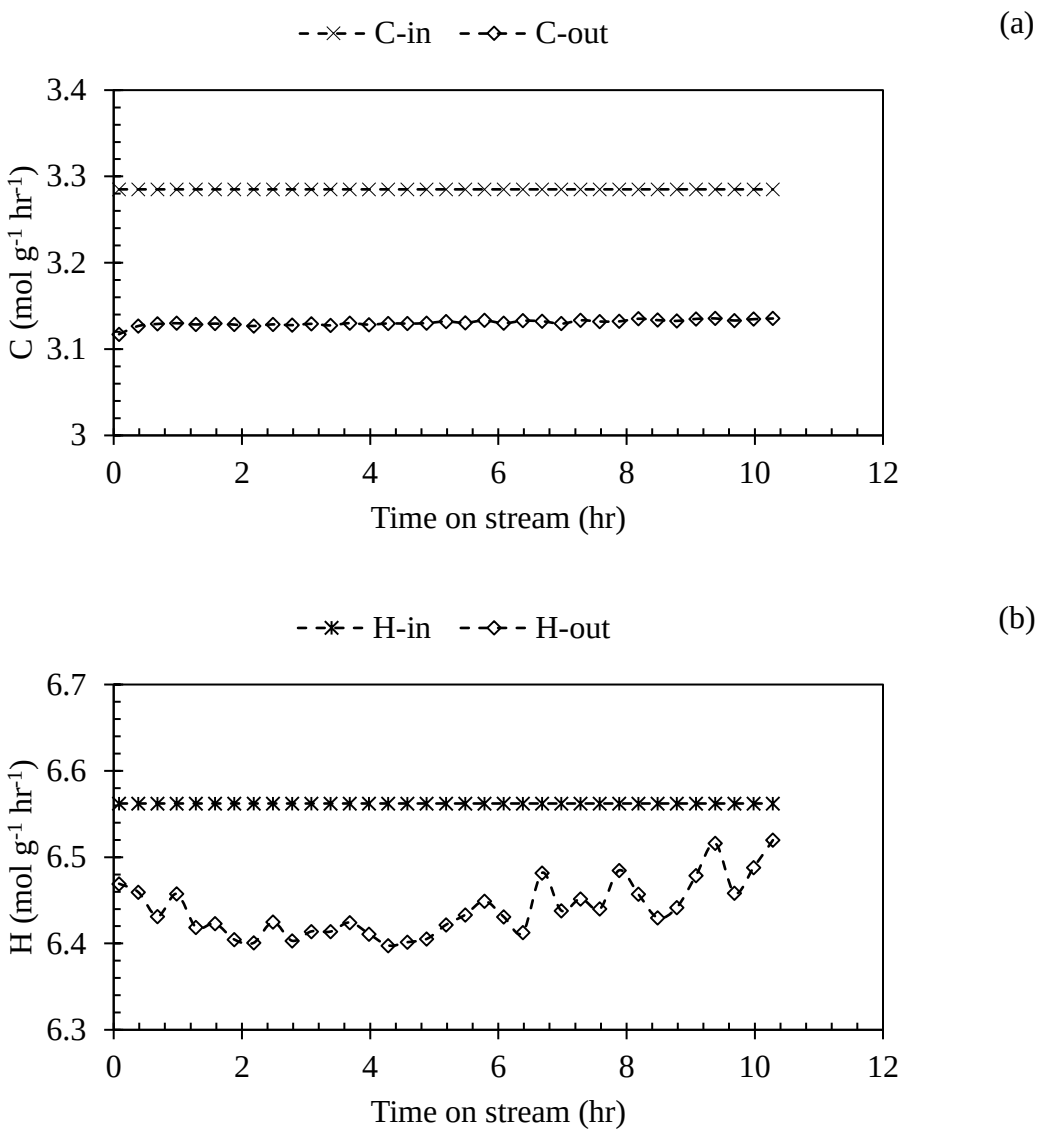

Figure E.1 (a) Carbon and (b) Hydrogen flow in inlet and outlet streams of the reactor using Sph-C catalyst for CRM reaction. Reaction conditions: 0.15 g catalyst, temperatures: 800 °C, 1atm, GHSV of 110 L g^{-1} hr^{-1}, $CH_4/CO_2/N_2$ = 1/1/1

Table E.1 Carbon and Hydrogen balance for CRM over Sph-C within 10 hr TOS. Reaction conditions: 0.15 g catalyst, temperatures: 800 °C, 1atm, GHSV of 110 L g^{-1} hr^{-1}, $CH_4/CO_2/N_2$ = 1/1/1

TOS (hr)	Carbon				Hydrogen			
	In (mole)	Out (mole)	Balance (mole)	Diff. %	In (mole)	Out (mole)	Balance (mole)	Diff. %
10	4.93	4.70	0.23	4.78	9.84	9.66	0.18	1.85

Appendix F: Oven Temperature Profile of GC

The oven temperature profile of the GC for the methods which have been used to analyze the product stream of the reactions using TCD and PFPD detectors are summarized in Tables F.1 and F.2. Table F.3 also shows the retention time of the detected gases using TCD and PFPD detectors.

Table F.1 Oven temperature profile of the Agilent 6890N GC equipped with a TCD detector used to detect and separate N_2, Ar and permanent gases (H_2, CO, CH_4, and CO_2)

Oven ramp	Ramp rate (°C/min)	Next T (°C)	Hold time (min)	Run time (min)
Initial	-	40	3.00	3.00
Ramp 1	10.00	60	1.00	6.00
Ramp 2	35.00	125	5.50	13.36
Post run	-	40	0.00	13.36

Table F.2 Oven temperature profile of the Varian 3800 GC equipped with a PFPD detector used to detect and separate H_2S, and SO_2

Oven ramp	Ramp rate (°C/min)	Next T (°C)	Hold time (min)	Run time (min)
Initial	-	40	5.50	5.50

Table F.3 Retention time of gases using Agilent 6890N (TCD detector) and Varian 3800 GC (PFPD detector)

Gas	Detector	Retention time (min)
H_2	TCD	1.5
N_2		3.4
CO		4.5
CH_4		7.5
CO_2		12.2
H_2S	PFPD	4.2
SO_2		4.7